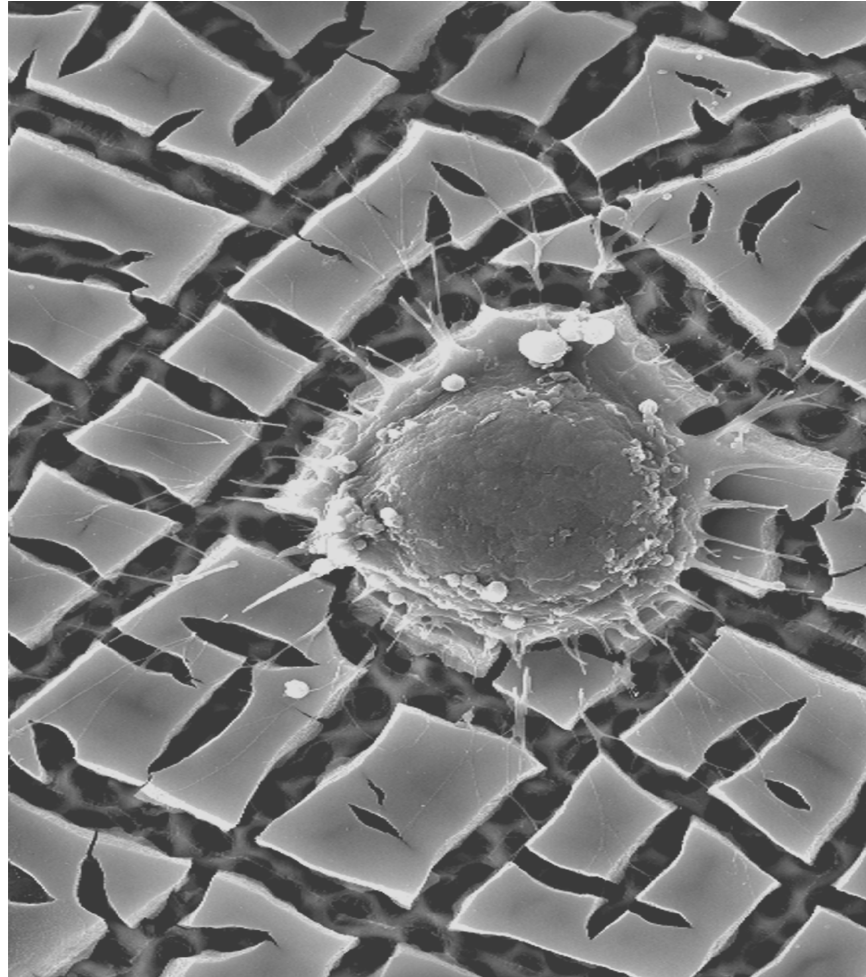


## **Development of porous silicon as a scaffold for the delivery of cells into ocular tissue**



*Scanning electron micrograph of a human lens epithelial cell cultured on macroporous silicon*

**Suet Peng Low**

**School of Chemistry, Physics and Earth Sciences  
Faculty of Science and Engineering  
Flinders University**

**March 2008**

## Table of Contents

Summary .....	v
Declaration .....	vii
Acknowledgements .....	viii
Publications Arising From This Thesis .....	ix
List of Abbreviations.....	x

### Chapter 1

<b>Introduction to biomaterials, porous silicon production and the human cornea</b> .....	1
<b>Thesis Overview</b> .....	2
1.1. Biomaterials.....	2
1.1.1. Current ocular biomaterials .....	5
1.2. Porous Silicon.....	8
1.2.1. Fabrication of porous silicon .....	12
1.2.2. Degradation mechanism of porous silicon.....	16
1.2.3. Porous silicon as a biomaterial .....	17
1.2.4. Porous silicon as a substrate for delivering cells into the eye .....	18
1.3. The Cornea .....	20
1.3.1. Corneal transplantation .....	22
1.3.2. The limbus .....	23
1.3.3. Limbal transplantation .....	27
1.4. Current Support Substrates in Limbal Tissue Engineering .....	29

### Chapter 2

<b>Evaluation of mammalian cell adhesion on surface-modified porous silicon</b> .....	34
<b>Introduction</b> .....	35
<b>Methods and Materials</b> .....	38
2.1. Chemicals .....	38
2.2. Preparation of Porous Silicon.....	38
2.3. Preparation of Surface-Modified Porous Silicon.....	39
2.3.1. Ozone oxidised samples.....	39
2.3.2. Amine functionalised samples (APTMS).....	40
2.3.3. Polyethylene glycol functionalised samples (PEGs).....	41
2.3.4. Collagen coated samples (Collagen).....	41
2.3.5. Foetal bovine serum coated samples (FBS).....	41
2.3.6. Thermally oxidised samples .....	41
2.4. Surface Characterisation.....	42
2.4.1. Atomic force microscopy and scanning electron microscopy .....	42
2.4.2. Porosity studies .....	42
2.4.3. Contact angle measurements .....	43
2.4.4. Interferometric reflectance spectroscopy .....	43
2.4.5. Transmission FTIR .....	43
2.5. Cell Experiments .....	44

2.5.1. Cell lines .....	44
2.5.2. Cell attachment .....	44
2.5.3. Alamar Blue cell viability assay .....	44
2.5.4. Neutral red cell viability assay .....	46
2.5.5. Cell counts .....	46
2.5.6. Statistical analysis on cell counts .....	47
<b>Results &amp; Discussion</b> .....	48
2.6. Characterisation of Surface-Modified pSi .....	48
2.6.1. AFM and contact angle measurements .....	48
2.6.2. Transmission FTIR spectroscopy .....	51
2.6.3. Degradation studies .....	52
2.7. Cell Attachment and Morphology .....	55
2.8. Cell Viability Assays .....	60
2.8.1. Alamar Blue .....	60
2.8.2. Neutral red .....	69
2.9. Cell Counts .....	73
<b>Conclusions</b> .....	77
<b>Chapter 3</b>	
<b>Porous silicon powder and pellets</b> .....	78
<b>Introduction</b> .....	79
<b>Methods and Materials</b> .....	85
3.1. Chemicals .....	85
3.2. Porous Silicon Powder .....	86
3.3. Pellet Formation .....	86
3.3.1. Leaching agents .....	86
3.3.2. Binding agent and lubricating agents .....	87
3.4. Die Cast and Press .....	87
3.5. Pellet Compositions .....	88
3.5.1. Pellet fabrication from silicon powder .....	89
3.5.2. Pellet fabrication from oxidised porous silicon powder .....	89
3.5.3. Pellet fabrication from silanised porous silicon powder .....	90
3.6. Cell Culture Studies .....	90
3.6.1. Pellet composition used for cell culture studies .....	90
3.6.2. Pellet stabilisation after pressing .....	91
3.6.3. Cell culture on pellet .....	92
3.7. Indirect Cell Viability Assay .....	92
3.7.1. Indirect viability assay of pellet components .....	92
3.8. Statistical Analysis .....	93
<b>Results and Discussion</b> .....	94
3.9. Silicon Powder .....	94
3.10. Pellets Made From Oxidised Porous Silicon Powder .....	95
3.11. Use of Lubricants During Pellet Fabrication .....	96
3.11.1. Stearic acid as a lubricating agent .....	96
3.12. Pellet Production from Aminosilanised Porous Silicon Powder .....	98
3.12.1. Use of starch as a binding agent during pellet formation .....	99

3.13. Increasing Pellet Wettability .....	101
3.13.1. Glucose as a wetting agent.....	101
3.13.2. Glycine as a wetting agent.....	102
3.14. Effect of Compaction Force on Pellet Stability.....	104
3.15. Heat Treatment of Pellets .....	105
3.16. Cell Culture Studies.....	108
3.16.1. Stability of pellets in cell culture medium.....	109
3.16.2. Cell culture on pellets .....	111
3.17. Indirect Cell Viability Assay .....	112
3.17.1. Indirect cell viability assay on pellet components.....	112
<b>Conclusions</b> .....	116

## Chapter 4

### Primary cell culture and *in vivo* studies on porous silicon membranes.....

<b>Introduction</b> .....	117
<b>Introduction</b> .....	118
<b>Methods and Materials</b> .....	120
4.1. Chemicals and Antibodies.....	120
4.2. Membrane Preparation .....	120
4.3. Pore Size and Surface Roughness .....	121
4.4. Energy Dispersive X-Ray Spectroscopy (EDX) .....	121
4.5. Degradation Studies.....	121
4.5.1. Ammonium molybdate assay in Tris-HCl.....	121
4.5.2. Silicic acid assay in artificial tear fluid (ATF) .....	123
4.6. Human Lens Epithelial Cells.....	124
4.6.1. Human lens epithelial cell growth on porous silicon membranes .....	124
4.6.2. Fluorescence imaging .....	125
4.6.3. SEM preparation.....	125
4.7. Human Corneal Rims .....	125
4.7.1. Expansion of human corneal cells on glass coverslips.....	126
4.7.2. Expansion of limbal tissue on membranes .....	126
4.8. Identification of Cell Populations.....	127
4.8.1. Immunohistochemistry .....	127
4.9. MicroCT (X-ray Micro Computerised Tomography) .....	128
4.10. Animal Studies .....	128
4.10.1. Surgical technique for the implantation of porous silicon membranes into the eye .....	129
4.10.2. Histology.....	129
4.10.3. Membranes with Corneal Cell Outgrowths .....	130
<b>Results and Discussion</b> .....	133
4.11. Characterisation of Porous Silicon Membranes .....	133
4.11.1. AFM analysis.....	133
4.11.2. Energy dispersive X-ray analysis .....	133
4.12. Degradation Studies.....	137
4.12.1. Ammonium molybdate assay.....	137
4.12.2. Calibration curve in Tris-HCl.....	138

4.12.3. Artificial tear fluid (ATF) .....	141
4.13. Cell Culture Studies.....	146
4.13.1. Immortalized cells.....	146
4.13.2. Primary cell culture.....	147
4.14. Animal Studies .....	154
4.14.1. Implantation of thermal APTMS membranes into the eye .....	154
4.14.2. Histology of eyes implanted with porous silicon membranes .....	158
4.15. Implantation of Membranes Containing Cultured Primary Cells.....	171
<b>Conclusions</b> .....	175
<b>Chapter 5</b>	
<b>Overall findings and conclusions</b> .....	177
<b>References</b> .....	189

*Scanning electron images presented on the title page and proceeding chapter title pages were all conducted on a Philips XL30 scanning electron microscope operating at 10 keV with a working distance of 10 mm. Samples shown on the title page and Chapter 1, 2 & 5 title pages, were all prepared as described on page 124. Samples shown on Chapter 3 & 4 title pages were prepared by coating with a thin layer of platinum.*

## Summary

Porous silicon has been shown to support the growth of cells and its capacity to fully degrade into harmless silicic acid, two properties that make porous silicon an appealing biomaterial. In this thesis, porous silicon was first tested in its suitability to support the growth of two different cell lines *in vitro*. The porous silicon surface was also surface-modified by oxidation, silanisation and by protein coatings to enhance its attachment properties. We found that silanisation with 3-aminopropyltrimethoxysilane (APTMS) was the simplest surface modification method that yielded the best cellular attachment characteristics and cellular morphology in comparison to the other surface modification methods tested. It was also discovered that surface modification was necessary to control the degradation rate of the porous silicon surface. APTMS-modified surfaces and thermally oxidised surfaces were both able to slow the degradation rate of the porous silicon surface and were thus used for subsequent experimentation.

Different forms of porous silicon were also tested, including membranes and particles. It was also discovered that certain colorimetric cell viability assays have the ability to interact with the redox-active porous silicon surface, thus yielding false positives. We focused upon assays such as Alamar Blue and the dye neutral red, both of which were able to generate a positive result with the porous silicon surface in the absence of cells.

We have shown that the porous silicon membranes were capable of supporting immortalised cells as well as primary cells isolated from human tissue. The biocompatibility of the porous silicon membranes was tested in a rat eye model, where the tissue response to the membrane could be observed macroscopically. It was noticed that there was a small inflammatory response around the membranes. Vascularisation and noticeable swelling was isolated to monofilament nylon sutures rather than the implanted membranes. The biocompatibility of porous silicon in the eye was also investigated through histological methods. The implanted porous silicon membranes only induced a small foreign body response which was noticeably smaller than the inflammatory response observed around commonly-used monofilament nylon sutures.

This is the first time that histological and microscopy evidence is given to show that porous silicon has good tissue biocompatibility. We offer evidence that the porous silicon membranes are able to degrade whilst implanted and the evidence also suggests that they are able to undergo full degradation.

Porous silicon was also investigated for its ability to act as a support scaffold for the delivery of cells into tissue. Primary cells were successfully cultured and implanted into eye of an animal. After one week, cells could be observed migrating away from the membrane into the surrounding tissue.

Therefore an enhanced porous silicon-based support has been developed that supports the attachment and growth of mammalian cells. This support is also biocompatible, biodegradable and can be used to deliver cells into tissue.

## **Declaration**

I certify that this thesis does not incorporate without acknowledgment any material previously submitted for a degree or diploma in any university; and that to the best of my knowledge and belief it does not contain any material previously published or written by another person except where due reference is made in the text.

Suet Peng Low

## **Acknowledgements**

This work would not have been possible without the supervision and guidance of my principal supervisor Associate Professor Nicolas Voelcker and I would like to thank my co-supervisor Associate Professor Keryn Williams for encouragement and advice during my PhD.

I gratefully acknowledge Professor Leigh Canham for his advice and discussions on different aspects of my project. I would also like to thank Dr Armando Loni and the members of pSiMedica for looking after me and making me feel welcome during my short stay in Malvern. I would also like to thank Dr Peter Self and the rest of the Adelaide Microscopy staff for assistance with the SEM and microCT examinations.

I especially thank Kirsty Marshall for conducting all animal surgery, histology work as well as teaching me animal handling techniques and tissue preparation for microscopy. I thank Margaret Philpott from the Eye Bank for her dedication in liaising with the Flinders Eye Centre in retaining human cornea rims from corneal graft surgery. I am also grateful for the help from members of the Ophthalmology department in helping me in the lab.

I thank all members of the SoCPES mechanical and electrical workshops for their constant dedication in maintaining equipment crucial to my work. I would also like to thank Dr Sean Graney and Rachel Lowe for stimulating discussions. I appreciate the work done by Evelyn Yap for the development of the silicic acid assay which was used in this thesis. Thanks must be extended to the members of the Voelcker group for helping in the maintenance of the lab, constant discussions and consultations.

I would not have been able to do this without the love and support from my family, Stimpy and friends for helping me throughout this period. Finally I would like to thank Endre for his love and encouragement for me.

## **Publications Arising From This Thesis**

Low, SP; Williams, KA; Canham, LT and Voelcker, NH (2006) Evaluation of mammalian cell adhesion on surface-modified porous silicon. *Biomaterials*, **27**:4538-4546.

Low, SP; Voelcker, NH; Canham, LT and Williams, KA. (2008) Porous silicon as a biomaterial for ophthalmic implants. *Biomaterials*. (Submitted October 2008)

Low, SP; Williams, KA; Canham, LT and Voelcker, NH (2008) Generation of reactive oxygen species from porous silicon particles in cell culture medium. (In preparation).

## List of Abbreviations

°C	Degrees Celsius
µg	Microgram
µm	Micrometre
µM	Micromolar
2-D	2- Dimensional
3-D	3- Dimensional
3T3	Mouse Fibroblast Cells
AFM	Atomic Force Microscopy
AM	Amniotic Membrane
APTMS	3-aminopropyltrimethoxysilane ( <i>modified surface</i> )
ARVO	Association for Research in Vision and Ophthalmology
ATF	Artificial Tear Fluid
CCD	Charge Coupled Device
CHO	Chinese Hamster Ovary cells
CK	Cytokeratin
C <sub>OX</sub>	Concentration of Oxidised Form (Alamar Blue)
C <sub>RED</sub>	Concentration of Reduced Form (Alamar Blue)
DCM	Dichloromethane
dH <sub>2</sub> O	Distilled Water
DMEM	Dullbecco's Modified Eagle's Medium
DMSO	Dimethyl Sulfoxide
ECM	Extra Cellular Matrix
EDTA	Ethylenediaminetetraacetic Acid
EDX	Energy Dispersive X-Ray
EOT	Effective Optical Thickness
F12	Cell Culture Medium Formulation by Ham <sup>[1]</sup>
FBS	Foetal Bovine Serum
FDA	Fluorescein diacetate

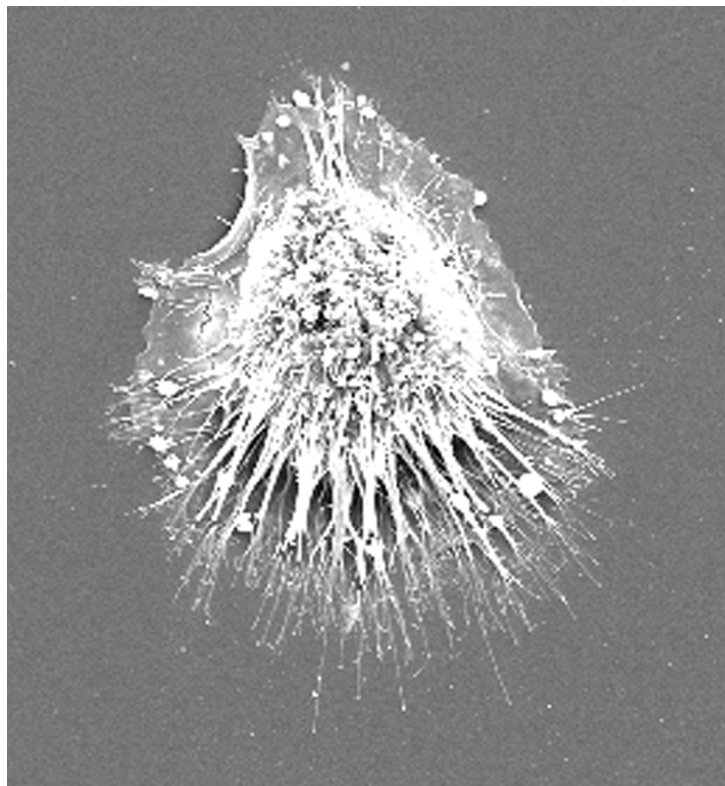
FITC	Fluorescein isothiocyanate
FTIR	Fourier Transform Infra-Red
g	Grams
H&E	Haematoxylin and Eosin
HEMA	hydroxyethyl methacrylate
HF	Hydrofluoric Acid
HLE	Human Lens Epithelial Cells
HO	Hoechst 33342 ( <i>cellular nuclear dye</i> )
IOL	Intraocular Lens
IU	International Units
kD	KiloDalton
keV	Kilo Electron Volt
kHz	KiloHertz
kN	Kilo Newton
m	Metre
M	Molar
mA	Milliamps
MicroCT	X-ray Micro Computerised Tomography
MilliQ	Purified Deionised Water ( <i>with a resistivity of 18.2 MΩ·cm at 25 °C</i> )
mins	Minutes
ml	Millilitre
mm	Millimetre
mM	Millimolar
mmol	Millimoles
MOPS	4-Morpholinepropanesulfonic Acid
MTT	3-(4, 5-Dimethylthiazol-2-yl)-2,5-Diphenyl Tetrazolium Bromide
MTS	3-(4,5-Dimethylthiazol-2-yl)-5-(3-Carboxymethoxyphenyl)-2-(4 Sulfophenyl)-2H-Tetrazolium Inner Salt
mV	Millivolts
NADH	Nicotinamide Adenine Dinucleotide Hydride

NADPH	Nicotinamide Adenine Dinucleotide Phosphate
PBS	Phosphate Buffered Saline (pH 7.4) <i>Containing: 8g/L NaCl + 0.2 g/L KCl + 2.68 g/L Na<sub>2</sub>HPO<sub>4</sub>.2H<sub>2</sub>O + 0.24 g/L KH<sub>2</sub>PO<sub>4</sub></i>
PC12	Rat Pheochromocytoma ( <i>cell line</i> )
PEG	Polyethylene glycol
PEGS	N-(triethoxysilylpropyl)-O-polyethylene glycol urethane ( <i>modified surface</i> )
PHEMA	poly(hydroxyethyl methacrylate)
PKH26	Cell Tracker Dye
PLGA	Poly(lactic- <i>co</i> -glycolic acid)
PMMA	Poly(methyl methacrylate)
ppm	Parts per Million
pSi	Porous Silicon ( <i>abbreviation used in figure captions</i> )
PTFE	Polytetrafluoroethylene
rms	Root Mean Square
SDS	Sodium Dodecyl Sulphate
SEM	Scanning Electron Microscopy
TAC	Transiently Amplifying Cells
TCPS	Tissue Culture Polystyrene
TRIS	Methacryloxypropyltris(trimethyl siloxy silane)
V	Volt
v/v	Volume per Volume
w/v	Weight per Volume
w/w	Weight per Weight
XTT	2,3-Bis(2-Methoxy-4-Nitro-5-Sulphophenyl)-5-Carboxanilide-2H-Tetrazolium, Monosodium Salt
Ω	Ohm

## Chapter 1

### Introduction to biomaterials, porous silicon production and the human cornea

A literature review including the aims of the thesis



*Scanning electron micrograph of human lens epithelial cell on APTMS surface-modified porous silicon membrane*

## **Thesis Overview**

The first chapter of this thesis presents a background to biomaterials in general and introduces porous silicon with a focus on its production and its properties. This section also gives information about the human cornea and materials currently used in this tissue.

The second chapter focuses upon the characterisation of porous silicon and surface-modified porous silicon as a biomaterial. The third chapter investigates the use of a different form of porous silicon; powdered porous silicon compressed into a pellet form and the subsequent investigation into the suitability of the pellet as an ocular biomaterial. The fourth chapter introduces porous silicon membranes and the observations and reactions of membranes being implanted into the eye. The fifth chapter concludes the findings and suggests future directions for the use of porous silicon as a biomaterial.

### **1.1. Biomaterials**

An often used definition of a biomaterial is “a material intended to interact with biological systems”<sup>[2]</sup>. This does not only include materials that are to be transplanted, but also materials that are in constant contact with biological tissues and fluids. Biomaterials tend to fall into two main categories, biologically derived and synthetic materials. Biologically derived materials include collagen, fibronectin, membranes, silk and cellulose, some of which are also biodegradable. Limitations of these biologically derived materials lie in their source and in their reproducibility, as often these materials are produced from animal or bacterial sources<sup>[3]</sup>, where each production batch can vary. An issue that has recently arisen from animal-derived materials is the transmission of prion proteins. When this bovine prion protein is transmitted to humans, it can lead to Creutzfeldt-Jakob disease<sup>[4]</sup>, a degenerative neurological diseases.

## *Chapter 1: Biomaterials*

Synthetic biomaterials can overcome some of the problems associated with biological materials. Further, synthetic materials can be tailored to have a desired surface chemistry or topography, controlled degradation or can even be loaded with certain drugs or proteins that can directly affect the cells surrounding the material. Synthetic materials can also be modified to suit a certain application. An example is the use of biodegradable materials for drug or cell delivery purposes. Once these materials are inserted into the body, there is no requirement for additional processes to remove the material. For other applications, the biodegradability of the material may not be of importance, such as materials used as bone support structures. In this case, a rigid material with good mechanical strength is of greater value.

The development and focus of synthetic biomaterials have changed over the years as requirements and scopes of uses broaden. Initially, most biomaterials developed were inert, such as gold being used to replace lost teeth. For transplantable materials it was initially desirable not to induce a host immune response and to have little or no toxic properties, hence the use of inert materials. The focus then shifted to bioactive materials, which can invoke a controlled physiological response, such as directing stem cells down a specific differentiation pathway. An example of this last application is the use of hydroxyapatite, a mineral component of bone. Materials that have a hydroxyapatite coating allow osteoblast cells to bind and differentiate and form new bone structures <sup>[5, 6]</sup>. This is particularly useful in dental implants, where bone regeneration in and around the implant helps its integration <sup>[7]</sup>.

The shape or overall structure of the material is also able to influence cell behaviour. For instance, bones have a three dimensional structure within which skeletal stem cells can migrate and differentiate to become bone marrow cells or osteogenic cells for bone formation <sup>[5]</sup>. Bioengineered synthetic bone would require a three dimensional scaffold to which the cells can adhere, rather than a flat structure, as the former mimics the normal environment on which the cells migrate and proliferate <sup>[8]</sup>. It has been shown that the surface on which the cells reside can greatly influence their activity and their movement across a surface. Topography of the surface (such as ridges or pores) or

## *Chapter 1: Biomaterials*

chemistry of the surface that cells reside upon all have an influence on cell behaviour<sup>[9]</sup>. The effect a surface can have on cells is also dependent upon cell type. Some cells can be sensitive to differences in heights as low as 30 nm, while other cells only react to heights greater than 100 nm<sup>[10, 11]</sup>.

Some three dimensional materials are also capable of incorporating of proteins, peptides, amino acids, and other products such as cell attachment factors or cell growth factors. These incorporated substances can direct specific cell attachment or migration<sup>[12]</sup>, and in the case of stem cells, proteins that direct their differentiation pathway or maintain their stem cell state<sup>[13]</sup>. In normal tissue, the extracellular matrix creates a 3-D environment for the cells. The extracellular matrix is comprised of a variety of proteins, including collagen, vitronectin and fibronectin, as well as glycosaminoglycans<sup>[14, 15]</sup>. The invasion of cells and degradation of the extracellular matrix is important in tissue formation. Cells can remodel the extracellular matrix to change their cellular orientation or migrate by direct interaction with proteins in the matrix, mainly through the release of proteases that degrade the extracellular matrix to allow the cells to move through a certain region<sup>[16]</sup>.

Biodegradability is an important factor for synthetic cell supports. A support that is capable of promoting cellular attachment and proliferation is not useful if the products that it degrades into are highly toxic, provided that the support is capable of degradation in the first place. Supports such as titanium have shown to be highly bioactive, where cells readily attach and grow on the surface<sup>[17]</sup>. However, titanium is incapable of degradation and is more useful as a large and rigid implantable device, such as a support for bone or tooth implants.

Biodegradable supports do exist. An example of this is the use of poly(lactic-*co*-glycolic acid) (PLGA), a polymer consisting of lactic and glycolic acid monomers that is commonly used in absorbable sutures. Studies into the use of this polymer have included embedding the PLGA structure with matrix metalloprotease cleavage sites. Matrix metalloprotease sites are peptide sequences which are targeted by specific

proteases. Cells secrete these proteases to cleave the matrix at these sites, enabling the cell to migrate through the structure <sup>[18]</sup>. The use of PLGA in this manner was to further mimic the natural cell environment. As an added bonus, the degradation products of PLGA have low toxicity and are easily excreted from the body.

### **1.1.1. Current ocular biomaterials**

Current ocular biomaterials include contact lenses, glaucoma filtration implants artificial corneas (keratoprosthesis) and intraocular lenses. Contact lenses are widely used by the public for the correction of vision and are in constant evolutionary development. The requirements for an optimum contact lens are comfort, oxygen permeability and low lipid fouling. Wettability is required for comfort and oxygen permeability is required for oxygen exchange with epithelial cells on the cornea to prevent hypoxia. A range of methacrylate based polymers have been used in the development of contact lenses. Rigid contact lenses were initially developed with poly(methyl methacrylate) (PMMA) <sup>[19]</sup>. PMMA lenses quickly fell out of favour due to its rigidity and low oxygen permeability <sup>[20]</sup> and were replaced with softer hydrogel lenses containing poly(hydroxyethyl methacrylate) (PHEMA). This material offered the wearer greater comfort, although oxygen permeability through this material was still low <sup>[21]</sup>. Other hydrogel lenses were soon developed with copolymers of hydroxyethyl methacrylate (HEMA) or hydrophilic monomers <sup>[19]</sup>. This improved oxygen permeability and the wettability of the lens, which offered greater comfort and extended use to the wearer. Long-term wear and use of lenses was an important aspect to the design of this biomaterial, as there was great demand for lenses that could be worn for long periods, including during sleep.

Silicone rubber contact lenses, made from polydimethylsiloxane, were used for a short time as they offered high gas permeability and were extremely durable. They are not commonly used now as they are known to dry out and adhere to the cornea <sup>[22]</sup>. The silicon-oxygen bonds (siloxanes) in silicone lenses were the main contributing factor to the high gas permeability. This led to the formation of methyl methacrylate polymers

## *Chapter 1: Porous silicon*

containing siloxanes, such as methacryloxypropyltris(trimethyl siloxy silane) (TRIS), with added methacrylic acid added to improve wettability. To improve upon wettability and gas permeability, these siloxane-based lenses were co-polymerised with fluoromethacrylate, along with other crosslinkers (for durability) and wetting agents <sup>[23]</sup>. This is a form of a rigid, high gas permeable contact lens in use today.

The newest form of soft contact lenses with high gas permeability are siloxane-hydrogels. These materials, known under the trade names of balafilcon A and lotrafilcon A and the exact components in each material is propriety information. Balafilcon A is thought to contain a TRIS component such as tris(trimethylsiloxy)silylpropylvinylcarbamate, to further improve gas permeability, whilst lotrafilcon A also contains a TRIS component along with hydrophilic monomers to improve wettability. The surfaces of both materials were still considered to be rather hydrophobic and were made more hydrophilic by introducing surface oxide groups by a plasma reaction (for balafilcon A) <sup>[23]</sup> or by the addition of a plasma deposited polymer containing trimethyl silane, oxygen and methane <sup>[24]</sup>.

Intraocular lenses (IOL) are widely implanted into the eyes of patients to replace lenses damaged by cataracts. The material requirements for an IOL include being bioinert, clear and have a high refractive index to reduce the size of the IOL. More recently, there is the requirement for more flexible materials, which allows the lens to be folded and inserted through a smaller incision, reducing the patient recovery time. Occasionally a secondary cataract can form after the insertion of the IOL due to the migration of epithelial cells across the lens. This can be easily removed by laser treatment, but a material is required that can withstand this treatment. The initial IOLs were developed with PMMA in 1949 <sup>[25]</sup>. PMMA is rigid but has shown to be fairly bioinert, especially after surface-modifications to reduce any inflammatory responses <sup>[26]</sup>. The inflexibility of PMMA led to the shift of more flexible materials such as PHEMA, soft acrylics and silicone IOLs, which can be folded and inserted through a smaller incision, although the soft acrylic lens is considered to be “sticky” and more liable to crack when folded and the silicone based lens are harder to handle as they

## *Chapter 1: Porous silicon*

become slippery when wet <sup>[27]</sup>. Although these materials are also more resistant than PMMA to laser treatment, PMMA is still widely used due to its low cost manufacture and long-term proven results.

Glaucoma shunts are used to relieve the intraocular pressure of the anterior chamber by draining fluid from the chamber into the subconjunctival space. The material used in the shunts is required to be bioinert and have low biofouling properties. Early materials included gold and silk, which induced a high degree of inflammation once implanted and blocked the flow of fluid <sup>[19]</sup>. Silicone is currently the material of choice to be used as a glaucoma shunt <sup>[28]</sup>.

An artificial cornea or keratoprosthesis is used in place of a corneal transplant when there is an underlying disorder that causes graft rejection. Such disorders include (but are not restricted to) patients exhibiting Stevens-Johnson syndrome (irritation of the mucous membranes which lead to corneal ulcerations) <sup>[29]</sup>, trachoma infections, severe-dry eye syndrome, vascularisation and mechanical and chemical injuries. The biomaterial that composes an artificial cornea has to be clear, permeable, invoke a low inflammatory response and be able to be sutured in place. A material that integrates into the surrounding tissue is now favoured, as the stromal cells that adhere to the material holds the prosthesis in place and reduces inflammation <sup>[30]</sup>. Currently, there are three corneal prosthesis approved for use today, AlphaCor, Boston and BioKPro. PMMA again is the main component of the Boston keratoprosthesis. Its limitations in its use are its rigidity, lack of gas and nutrient permeability, and as it is bioinert, it does not promote tissue integration. AlphaCor is made from PHEMA, the design of the prosthesis has a clear central lens with a porous skirt surrounding the lens for tissue integration. Despite good results, the durability of this material is low and in some cases, degradation of the PHEMA polymer has been reported <sup>[31]</sup>. In this situation, a biodegradable implant is not required and unwanted. The third prosthesis is BioKPro, this is made up of a central silicone lens coated with polyvinyl pyrrolidone and surrounded by a porous Teflon skirt <sup>[32]</sup>. The polyvinyl pyrrolidone coating on the silicone forms a hydrogel layer upon contact with water <sup>[33]</sup>. This material is more

## *Chapter 1: Porous silicon*

flexible and durable, whilst still being permeable and the Teflon skirt allows for tissue integration.

Each of these different ocular biomaterials has different properties to suit its purposes. It is preferred that contact lenses are bioinert, whereas keratoprosthesis should be biocompatible and encourage cellular infiltration to hold the material in place. Each of these materials have a requirement for being clear, not induce a large inflammatory response and more importantly for the implanted materials, not degrade over time.

This thesis focuses upon the development of a biomaterial to be implanted in the limbal region of the human cornea. Severe corneal injuries can lead to a loss of an adult stem cell population. Hence the damaged tissue would then require the implantation of a stem cell population to regenerate the corneal surface (discussed in greater detail in **Section 1.3**). A suitable biomaterial is needed as a support for the delivery of healthy cells into the cornea. This biomaterial is required to induce little inflammatory response, to be capable of supporting cell growth and to be biodegradable once transplanted into the eye. The above mentioned materials do not fit these criteria, a material that might have these properties is porous silicon.

### **1.2. Porous Silicon**

Silicon substrates have a controlled amount of dopants added to them to alter their electronic properties. During the formation of crystalline silicon, an atom of a different element is added, which has either one less or one more valence electron than a silicon atom. Hence, when the dopant takes the place of a silicon atom, there will either be an excess or a lack of electrons. The type of dopant employed will give rise to a particular type of silicon, n-type or p-type. In n-type silicon, the dopant used is often phosphorus, which has five valence electrons, in comparison to silicon which has four valence electrons. When phosphorus substitutes a silicon atom, one electron remains unbound generating an excess of electrons. These excess electrons are capable of independent movement the silicon crystal structure. In p-type silicon, the dopant often used is

## *Chapter 1: Porous silicon*

boron, which has three valence electrons. When boron substitutes a silicon atom, one bond will be missing an electron, leading to the formation of a positively charged hole, which is also capable of movement within the silicon wafer. The presence of the dopants makes silicon a semi-conductor and the greater the amount of dopant in the silicon, the better its conductivity. The amount of dopant in a silicon wafer is regularly described as the “resistivity” of the silicon, and is measured in  $\Omega\cdot\text{cm}$ . In this thesis the focus is upon the use of p-type, boron doped silicon.

In 1956, porous silicon was first discovered during the electropolishing of silicon and has since been used in various applications, such as its use in silicon based micromachines, optoelectronics, chemical and biological sensors <sup>[34-36]</sup>. The properties that make porous silicon useful for these applications include its high surface area, controllable pore sizes, its ability to degrade in aqueous solutions and its photoluminescent properties.

Porous silicon has been shown to be photoluminescent, an aspect that has been exploited for chemosensor applications. When excited by light at a certain wavelength, porous silicon exhibits visible photoluminescence at a different wavelength, which can shift in accordance with the porosity of the silicon <sup>[37, 38]</sup>. It has been shown that the photoluminescence of porous silicon can be quenched when exposed to hexane, toluene or methanol <sup>[39]</sup>. Quenching or a shift in the photoluminescence spectra allows porous silicon to be used as a sensor.

A concept that utilizes the photoluminescent property of porous silicon is an enzyme based biosensor. When porous silicon had an enzyme covalently bonded to its surface, little change in its photoluminescence emission was observed. When a substrate that the enzyme acts upon was added to the surface, a marked decrease in photoluminescence was detected. By washing off the substrate, photoluminescence was regained, demonstrating that it was a reusable biosensor. The unfortunate drawback to this biosensor was its inability to differentiate between different concentrations of

## *Chapter 1: Porous silicon*

substrate as the same amount of photoluminescence quenching was measured across all concentrations <sup>[40]</sup>.

Proteins can be loaded into the pores of porous silicon, and since there is a large surface area, it can hold a much larger amount of protein in comparison to flat silicon (a 1 cm<sup>2</sup> piece of porous silicon can have a surface area up to approximately 500 m<sup>2</sup>) <sup>[41]</sup>. Due to its ability to encapsulate molecules, porous silicon has also been considered as a drug delivery device, where the drug can be released in a controlled fashion through the pores <sup>[42]</sup>. Proteins and molecules can be covalently bound to the porous surface and can be released slowly as the pores degrade.

A different method in which porous silicon is used as a sensor, is the ability to obtain fringe patterns from porous silicon by shining light onto the surface. Light can be reflected off the top of the porous surface, the walls and the bottom of the pores, towards a detector (Figure 1). Reflection of the light from the different regions results in constructive and destructive interference effects resulting in a fringe pattern (termed Fabry-Perot fringes). Changes to the porous silicon surface, such as chemical or biological binding, result in changes to the thickness or refractive index of the porous layer. This results in wavelength shifts of the fringe pattern. Changes in the fringe patterns can be Fourier-transformed to give a representation the optical thickness of the porous layer (Figure 2). A wavelength shift towards the blue spectrum is a result of a decrease in thickness or refractive index, whilst a shift towards the red spectrum is due to an increase in thickness or refractive index <sup>[34]</sup>. If a protein is adsorbed to the porous surface, the fringe pattern shifts towards the red region, indicating an increase in thickness due to the protein. Removal of the protein or degradation of the porous surface, shifts the fringe pattern towards the blue region, indicating a decrease in thickness. Interferometric reflectance spectroscopy allows us to determine if a protein has bound to the surface or has been removed from the surface. In this thesis, we use interferometric reflectance spectroscopy to demonstrate degradation of the porous silicon layer.

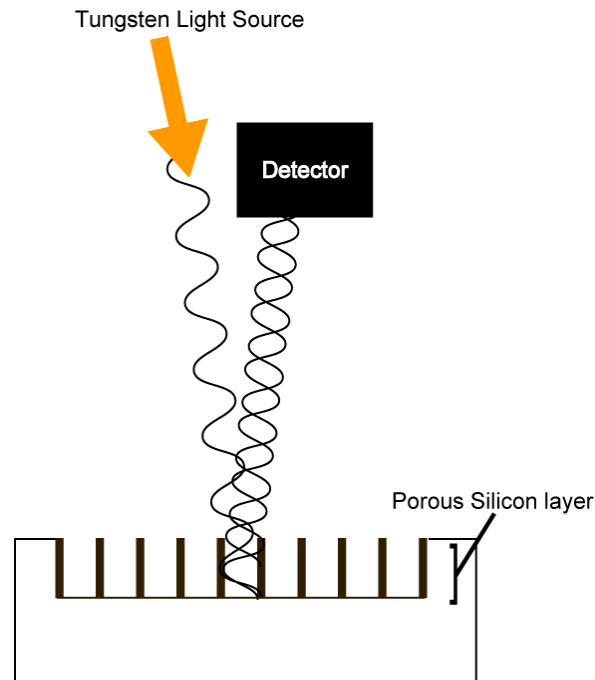


**Figure 1 – Schematic of an interferometric reflectance unit. Light is directed onto the porous silicon surface and is reflected back towards the detector. Light reflecting off the bottom, the sides and top of the pores results in constructive and destructive interference of the light.**

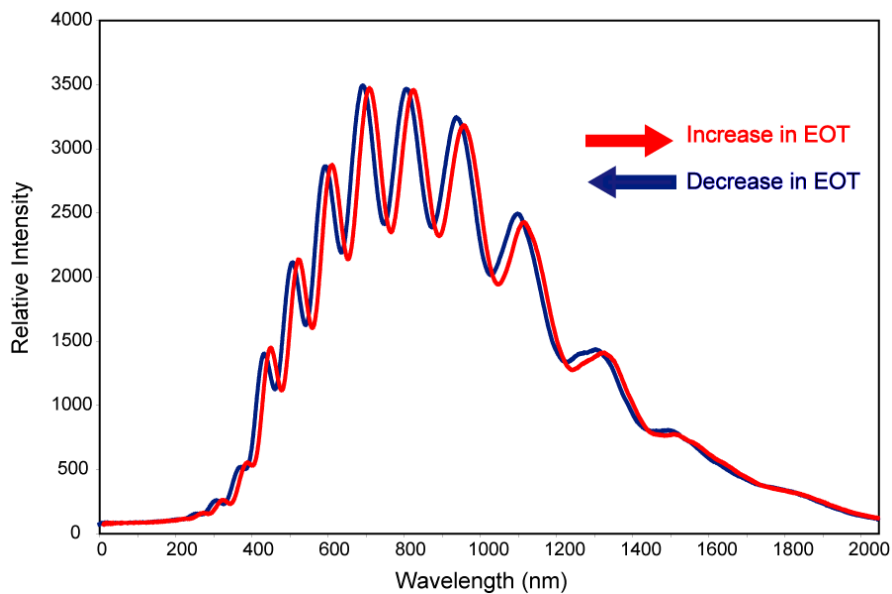


**Figure 2 – Fringe pattern created from the constructive and destructive interference of the light on a porous silicon layer. Shifts in the pattern towards the red region indicate an increase in effective optical thickness (EOT), whereas shifts in the blue region represent a decrease in EOT.**

### **1.2.1. Fabrication of porous silicon**

Pores can be formed on silicon either chemically <sup>[43]</sup> or electrochemically. The electrochemical method affords greater control over porosity and pore size. Electrochemical etching of porous silicon is conducted in a cell (usually Teflon) where a mixture of electrolyte (usually aqueous hydrofluoric acid) and an organic solvent acting as a surfactant can be contained on the silicon wafer by an O-ring that seals the cell. In the cell, only the region of silicon in contact with the electrolyte will be able to form porous silicon.

In this thesis, porous silicon is formed using an anodic reaction <sup>[44]</sup>, which allows us to control pore sizes and pore depth. An increase in the anodic potential leads to the increase in pore diameters. By further increasing the anodic potential to beyond the “current peak”, electropolishing occurs (Figure 3). Electropolishing is described as when the pore diameters increase to the extent in which they start to overlap, resulting in the removal of silicon material from the surface (described in greater detail in **Chapter 3**). The anodic potential at which electropolishing occurs is dependent upon the electrolyte concentration, the composition of solution and on the dopant of the silicon <sup>[44]</sup>.

Pore sizes can be controlled by the current value (anodic potential), such that an increased current results in an increased pore diameter. Three different pore regimes are distinguished: macroporous, with pore diameters in excess of 50 nm; mesoporous, pore diameters ranging from 2 nm-50 nm; and microporous, having pore diameters smaller than 2 nm <sup>[45]</sup>. The depth of the pores can be controlled by time; a longer etch time results in deeper pores.

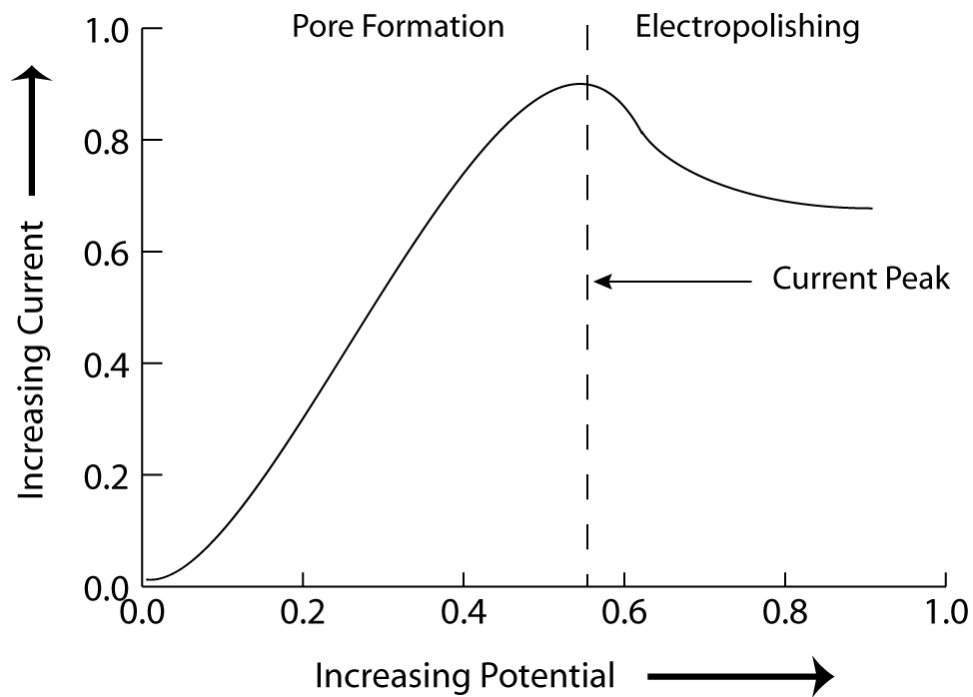


**Figure 3 - Current-voltage relationship for the formation of porous silicon. At low potentials, porous silicon is formed. Beyond the current peak, electropolishing of the silicon occurs.**

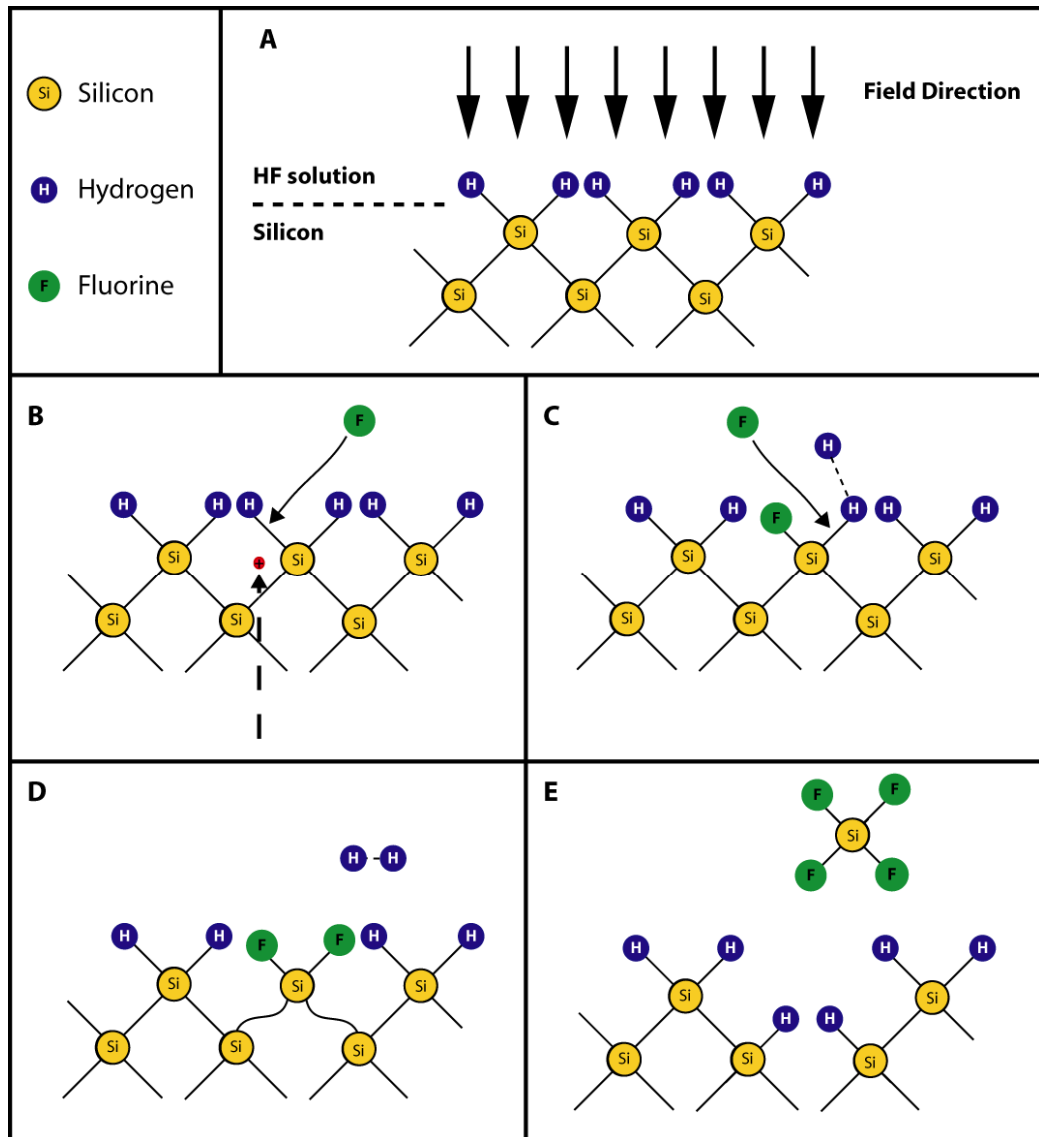


**Figure 4 - Formation mechanism of p-type porous silicon using a HF electrolyte: Panel A:** at the silicon-HF interface. **Panel B:** when a current potential is applied, positively charged holes move to the surface and weakens surface Si-H bonds. **Panel C:** fluoride atoms replace the hydrogen in the weakened bonds. **Panel D:** the presence of the fluorine atoms polarises the back bonds of the silicon atom. **Panel E:** A  $\text{SiF}_2$  molecule is released which quickly becomes  $\text{SiF}_4$  in the presence of the HF solution. Adapted from Lehman and Gösele (1991) <sup>[46]</sup>.

The exact chemistry for the dissolution of silicon is still not fully elucidated, though the generally accepted method is based on that of Lehman & Gösele <sup>[46]</sup>. In the presence of HF, the silicon atoms at the surface become hydride terminated (Figure 4A) <sup>[47]</sup>. Under anodic conditions, positively charged holes can reach the hydride terminated surface

and can attack the surface Si-H bonds (Figure 4B). By attacking this bond, fluoride ions in the electrolyte can form a Si-F bond (Figure 4C). This strongly polarises the silicon back bonds and allows another fluoride ion to attack the remaining Si-H bond forming a SiF<sub>2</sub> group and releasing a hydrogen molecule (Figure 4D). The Si-F bonds at the surface polarise and stress the remaining silicon back bonds therefore releasing the SiF<sub>2</sub> group (Figure 4E), which reacts with the HF in the solution forming SiF<sub>4</sub> and leaving the silicon substrate as Si-H groups. This results in an atomic size dip in the surface of the silicon and the start of a pore. The newly formed corrugations on the surface allow the current flow to focus on the dips, generating a slightly stronger field in that region. Additionally, the holes reach the bottom of these dips faster than the top surface. This process causes dissolution to occur preferentially in the dips, which grow into pores<sup>[48, 49]</sup>. There is also a slight current change at the tips of the pores, with the field being more focused and thus stronger at the tips.

After etching, the porous surface is silicon hydride (Si-H) terminated. The hydride groups are unstable and can quickly oxidise when exposed to air<sup>[38]</sup>. Different surface modifications such as oxidation, hydrosilylation or silanisations can be employed to stabilise the surface or to modify the surface thus introducing desired functional groups<sup>[36]</sup>. In some instances, the stability of the porous surface is not important, such as its use in drug delivery, as the aim is to exploit the degradation properties of the porous silicon to release the drug. As a substrate for biosensing, it is more important that the surface should be very stable, to allow for multiple uses and extend its time of use<sup>[50]</sup>. When used as a substrate for cell culture, extending the stability of the surface will allow time for cells to grow on the surface, though in most instances, it is desired that the porous silicon will dissolve eventually.

### 1.2.2. Degradation mechanism of porous silicon

Porous silicon is known to degrade in aqueous solutions. The accepted mechanism in which porous silicon undergoes chemical dissolution follows the model proposed by Allongue, Costa-Kieling and Gerisher<sup>[51]</sup>. A schematic of this model is shown in Figure 5.

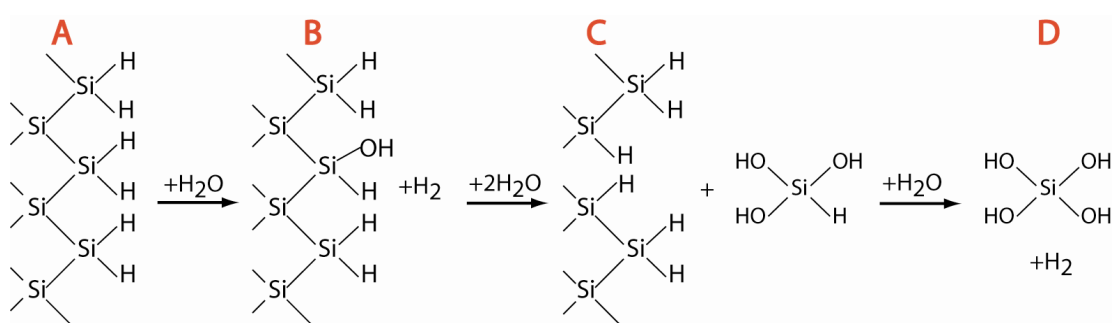


**Figure 5 – Proposed mechanism for porous silicon degradation in aqueous solutions by Allongue, Costa-Kieling and Gerisher<sup>[51]</sup>. A: A Si-H terminated surface immersed in H<sub>2</sub>O. B: The Si-H bond undergoes hydrolytic attack and is converted to Si-OH and producing a hydrogen molecule. C: The Si-OH at the surface polarises and weakens the Si-Si backbones, which are then attacked by H<sub>2</sub>O, producing HSi(OH)<sub>3</sub>. D: In solution the HSi(OH)<sub>3</sub> molecule is quickly converted to Si(OH)<sub>4</sub> and releases a hydrogen molecule.**

In this model, hydrolysis of a Si-H bond at the surface occurs (Figure 5A). The Si-H bond is converted to Si-OH and releases a hydrogen molecule (Figure 5B). The presence of the Si-OH polarises the silicon backbones allowing another OH to bind to the Si-OH molecule. This further destabilises the backbones and releases the silicon molecule from the surface as HSi(OH)<sub>3</sub>. The new silicon surface is left as Si-H and is susceptible to further hydrolytic attack (Figure 5C). In aqueous solution, water decomposes HSi(OH)<sub>3</sub> to Si(OH)<sub>4</sub> and produces another hydrogen molecule (Figure 5D). The main product from degradation is orthosilicic acid Si(OH)<sub>4</sub>.

Hydrolysis occurs preferentially at Si-H bonds since the polarisation of the Si-H bond renders it vulnerable to nucleophilic attack by water<sup>[51]</sup>. Hydrolytic attack by H<sub>2</sub>O on the Si-Si backbones is unlikely due to the lack of polarisation<sup>[52]</sup>. Converting surface Si-H groups to Si-OH by oxidation will slow down this hydrolysis significantly.

### **1.2.3. Porous silicon as a biomaterial**

The use of porous silicon as a biomaterial has not been studied extensively, as the focus for its use has resided mainly in its optical and optoelectronic properties. In recent years, interest has grown for its use as a substrate for cell growth. The first experiments of the use of porous silicon in a biological environment focused on the formation of hydroxyapatite crystals, a precursor to bone formation, on porous silicon when placed into a simulated body fluid. This gave an indication for the use of porous silicon in biological situations<sup>[53]</sup>. In those studies, it was also demonstrated that porous silicon was capable of degradation in simulated biological fluids, and interest was generated in the possible use of porous silicon as a biodegradable scaffold for cell growth<sup>[53, 54]</sup>.

In biological fluids, porous silicon degrades into orthosilicic acid,  $\text{Si}(\text{OH})_4$  (as shown in **Section 1.2.2**), which is present in drinking water, human blood plasma and beer<sup>[55]</sup>. The results of silicic acid deficiencies have been demonstrated by withholding silicon supplements from chicks. The chicks showed retarded growth and formation, indicating that silicic acid is an important molecule for development<sup>[56]</sup>. In the adult, it has been speculated that orthosilicic acid aids in the prevention of aluminium ion toxicity by preventing metal uptake in the gastrointestinal tract and regulating aluminium uptake into cells<sup>[57, 58]</sup>. Orthosilicic acid is also readily absorbed from the gastrointestinal tract of humans and the majority is excreted from the urinary tract swiftly, demonstrating that it does not accumulate within the body<sup>[59]</sup>. Therefore if porous silicon is implanted into the body, the degradation product, silicic acid, will be readily excreted.

Mammalian cells have been cultured onto porous silicon and the cells were still shown to be viable after a 4 day incubation period<sup>[60, 61]</sup>. In trying to establish a silicon-neuronal biosensor, *Aplysia* (a sea-snail) neurons have been cultured onto porous silicon, where it was reported that cell membrane integrity was maintained and the neurons were capable of producing action potentials, indicating normal function of the

## *Chapter 1: Porous silicon*

cells. The authors were able to demonstrate neuron survival on porous silicon for up to one week <sup>[62]</sup>.

Porous silicon has also been implanted into the abdominal wall of rats, and the inflammatory response to the porous silicon was compared with that of titanium, another well known (and tested) biomaterial. The inflammatory response observed around the porous was mentioned to be similar to titanium. The formation of collagen capsules were reported around both implants although the thickness of the capsule was recorded to be smaller around the porous silicon than around titanium. When the cell-surface interface of porous silicon was studied, a smaller amount of necrosis was observed in comparison to the titanium implant <sup>[63]</sup>. This is significant since necrosis of cells around an implant can lead to spontaneous rejection of the implant <sup>[64]</sup>.

In summary, the available literature strongly suggests that it is possible to utilise porous silicon as an implantable biomaterial and as a support the growth of cells.

### ***1.2.4. Porous silicon as a substrate for delivering cells into the eye***

Porous silicon is a substrate that is easily manufactured, with pore sizes and porosity that can be controlled, from nm to  $\mu\text{m}$  and 20% - 80%, respectively, making it a substrate that is flexible in terms of production. It has a large surface area (a  $1\text{ cm}^2$  piece of porous silicon can have a surface area up to  $500\text{ m}^2$ ) with a surface chemistry that can be modified to change the surface properties. These pores can be filled with large amounts of bioactive molecules, whilst on planar substrates, the smaller surface area would hold a much smaller amount. Porous silicon is also capable of degradation in biological fluids into orthosilicic acid, which is readily excreted from the body, indicating that porous silicon will not degrade into toxic products that can potentially remain in the body. Cell growth of both immortalised and primary cells on porous silicon have been recorded with no adverse effect on the cells and implantation experiments have indicated that porous silicon does not illicit an immune response any

*Chapter 1: Porous silicon*

different to other inert implantable materials, but shows less scar tissue forming around the implant. Given these previous findings, a biodegradable porous silicon scaffold for the culture of cells can be envisaged where upon implantation into the eye, cells can migrate from the porous silicon surface into the surrounding tissue.

### 1.3. The Cornea

The cornea is situated at the front surface of the eye (Figure 6). It forms a transparent barrier against foreign bodies whilst still allowing the entry of light through the pupil and the lens which focuses the light on the retina. At the periphery of the cornea lies the limbus, which separates the cornea from the sclera and conjunctiva, the white section of the eye.

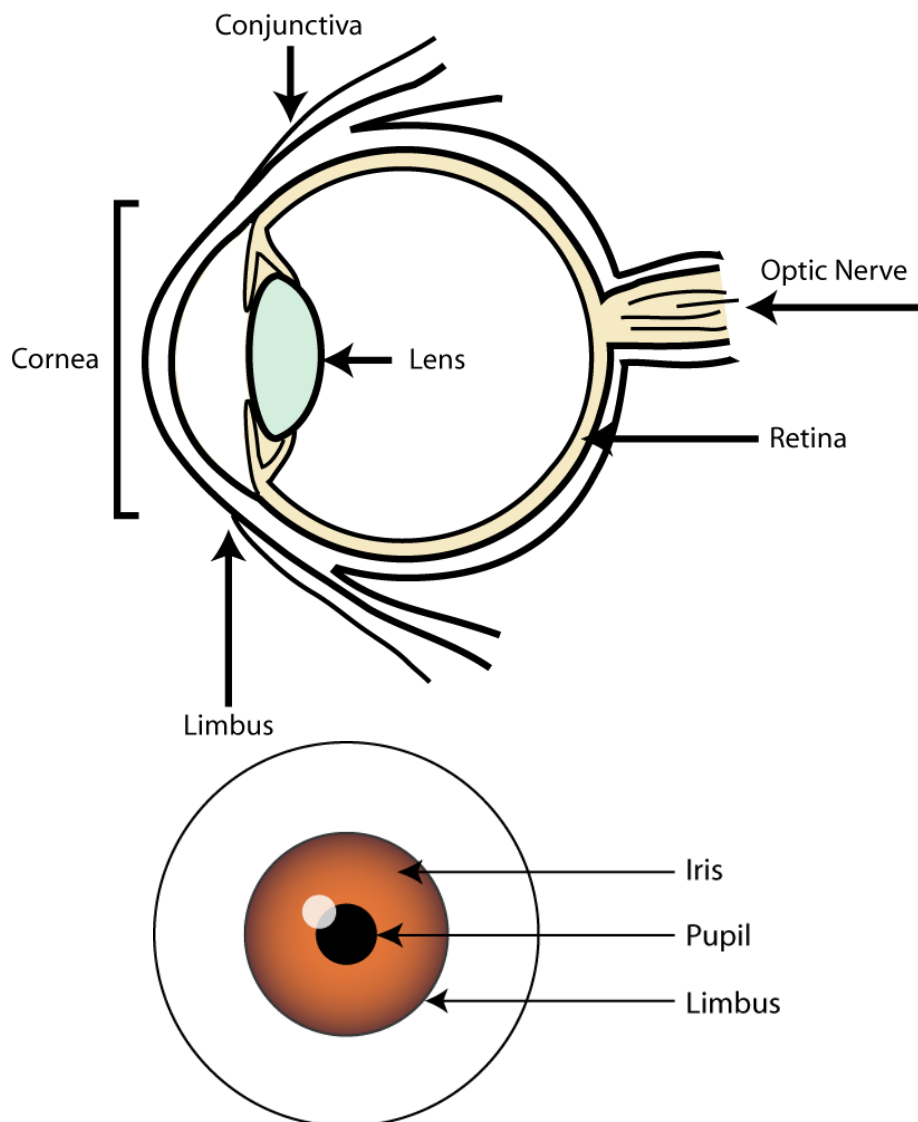


**Figure 6 - Cross section (top panel) and front diagrammatic view (lower panel) of the human eye.**

*Chapter 1: The Cornea*

The cornea is made up of six different layers of cells and proteins (Figure 7). The outermost layer of the cornea is the epithelium, consisting of cells that are constantly shed and regenerated from cells residing on the basement membrane. The epithelium itself is composed of several layers of non-pigmented epithelial cells; basal cells, polyhedral cells and squamous cells. Basal cells, with columnar shapes, are attached to the basement membrane and are continually undergoing mitosis. There is a vertical movement of cells from the basement membrane towards the surface. In the process cells become flattened and finally result in squamous cells at the surface. In turn, squamous cells are shed on a daily basis, where the tear film and movement from the eyelids continuously abrade the outermost layer of epithelial cells [65]. The basement membrane is attached to Bowman's layer, an acellular area densely packed with collagen fibrils which allows for a strong and resilient surface for the basement membrane to attach.

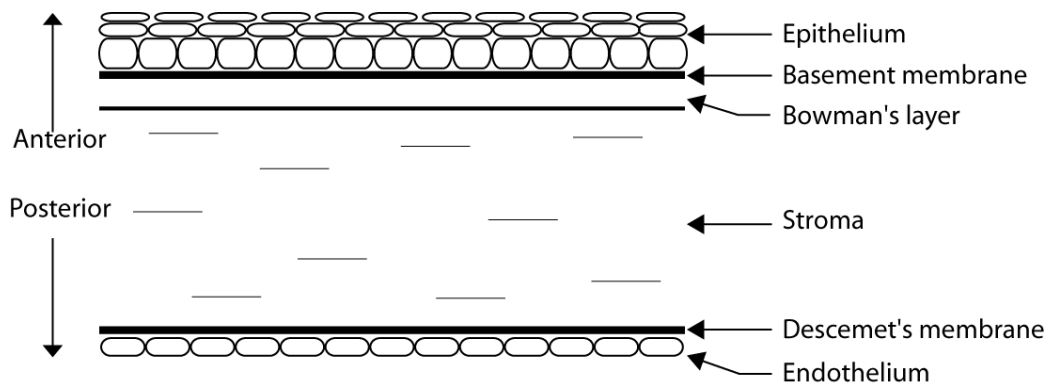


**Figure 7 - The six layers of the cornea. The epithelium is the outermost layer of the cornea. In the epithelium, squamous cells at the surface are sloughed off daily by eyelid movement. Basal cells migrate vertically to the surface to replace these cells and in the process become flattened. Basal cells reside on the basement membrane which is attached to the Bowman's layer. The collagen-filled stroma is attached to Descemet's membrane. A thin endothelial layer is also attached to Descemet's membrane.**

The next layer is the stroma, which makes up about 90% of the corneal thickness. Here collagen fibrils are arranged in transparent layers that are important in allowing the passage of light with minimal diffraction occurring. The stromal layer also contains

## *Chapter 1: The Cornea*

water, proteoglycans, glycosaminoglycans and a few keratocytes. The stroma rests on Descemet's membrane, another collagenous region that acts as the basement membrane for the endothelium, which pumps excess water out of the stroma.

The purpose of the epithelial layer is to absorb nutrients and allow the diffusion of oxygen into the interior layers of the cornea. Nutrients are mainly absorbed from the tear film, but also from capillaries in the conjunctival area, which diffuse across the cornea. The glucose supply for the cornea is gained from the aqueous humour. The cornea, being transparent, allows light to travel towards the lens, which focuses the light upon the retina. The health and clarity of the cornea is essential for effective visual function.

### **1.3.1. Corneal transplantation**

As the cornea is the most exposed region of the eye, the integrity of the cornea can be easily compromised by external factors or by a variety of disorders, such as keratoconus, the thinning of the cornea <sup>[66]</sup> and Fuch's dystrophy, a progressive deterioration of endothelial cells <sup>[67]</sup>. The cornea can also be damaged by mechanical and chemical injuries or through infection. In severe injuries or disorders, a corneal transplant is required to restore visual acuity. Corneal transplantation is a procedure in which a donor cornea is grafted in place of the damaged cornea. This procedure is also known as penetrating keratoplasty. Topical immunosuppressive drugs are often used in conjunction with transplantation to prevent graft rejection.

The first successful corneal allotransplantation was reputed to occur in 1905 and carried out by Eduard Zirm, on a patient with lime burns in both eyes <sup>[68]</sup>. Though no immunosuppressive drugs were used in conjunction, the transplantation procedure was regarded as a success as indicated by one of the grafted corneas remaining clear and transparent. This method is still in practice to this day and remains one of the most successful transplantation procedures of all organ transplants <sup>[69]</sup>.

Corneal transplantation will only succeed if the surrounding limbus remains intact and active. If the limbus is severely damaged, the graft will fail since reepithelialisation of the cornea cannot occur. In the case of total loss of the limbal stem cell population, a limbal graft is required.

### **1.3.2. The limbus**

The limbus lies at the periphery of the cornea and separates the cornea from the conjunctiva. In contrast to the cornea, which is avascular, the limbus is highly vascular and along with the termination of Bowman's layer, vessels are used as a marker in the identification of the transition between the cornea and the sclera. Davenger & Evensen (1971) were the first to hypothesize that the cells residing in the limbus were the source of cells that were capable of renewing the corneal epithelium. They conducted an experiment involving the removal of corneal epithelium in guinea-pigs and demonstrated that cells migrated from the limbus region to completely reepithelialise the corneal surface after a few days<sup>[70]</sup>. They also observed that limbal cells resided upon papillary structures, termed the Palisades of Vogt, a highly vascularised area that is suited to the demands of cells constantly undergoing mitosis for migration into the cornea ensuring the continuous renewal of the epithelial layer (Figure 8). This region is often pigmented with melanin, which is thought to provide the limbal cells with protection from ultraviolet radiation<sup>[71]</sup>.

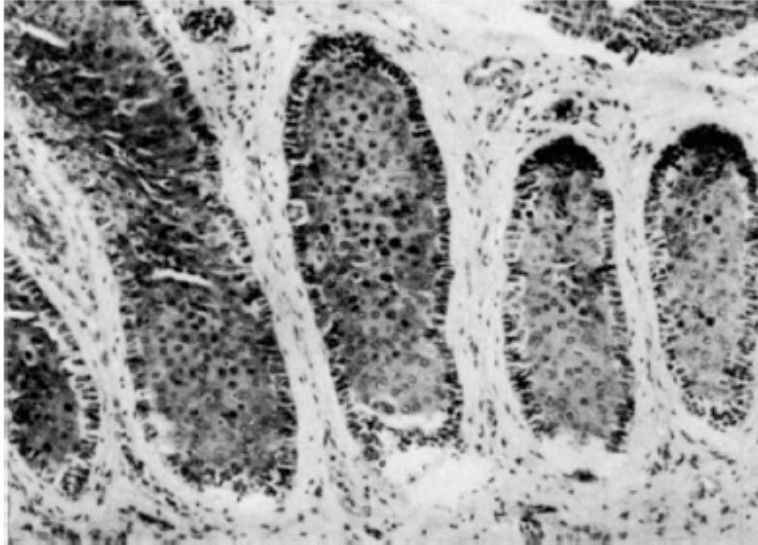


**Figure 8 – Histological section of the limbal region showing the pigmented palisades of Vogt Taken from Davenger and Evensen (1971) <sup>[70]</sup>.**

To further demonstrate that the limbus is the source of corneal epithelial cells, cells from the limbus have been used to generate epithelium *in vitro*. Cells from the limbus region were cultured to form a cell sheet. The cultured cells was compared with epithelial cells in tissue and were found to have similar morphology <sup>[72]</sup>.

Later studies showed that cells from the limbal area periodically migrate towards the centre of the cornea in horizontal and vertical directions as well as in a centripetal fashion (Figure 9), allowing for the regeneration of corneal epithelium <sup>[65, 73-75]</sup>. Cells from the limbus differentiate to form basal epithelial cells, which migrate along the basement membrane and eventually form the epithelial layer of the cornea.

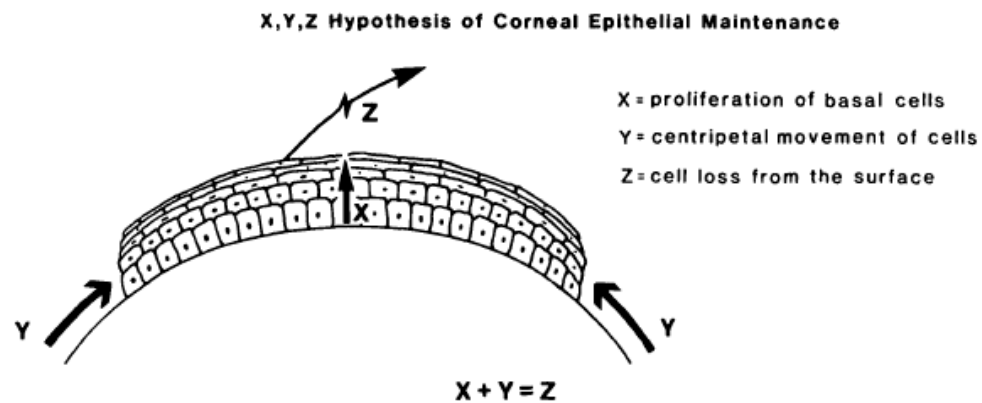


**Figure 9 –The x, y, z movement of cells in the cornea. Stem cells from the limbus differentiate into basal cells that migrate centripetally across the basement membrane in the y direction. The basal cells proliferate and migrate in the x direction and become squamous cells in the process. The cells on the surface are removed by the tear fluid and by the eyelid during blinking. Taken from Thoft and Friend (1983) <sup>[65]</sup>.**

By inducing a wound in the cornea it was shown that limbal basal cells could be stimulated to proliferate <sup>[76]</sup>. Limbal cells showed a nine-fold increase in proliferation activity in response to an injury, whereas peripheral corneal epithelial cells showed a two-fold increase and corneal epithelial cells only showed a slight increase. This proliferation activity in limbal cells would decrease 48 hours post-operatively indicating that this was a wound response activity <sup>[77]</sup>. The results indicated that limbal cells could be important in the process of healing and repair of the cornea.

Corneal wound healing was also observed to occur in two stages of cell proliferation, each intermitted by a stage of cell differentiation to form normal epithelia <sup>[78]</sup>. This was the first indication of basal limbal cells giving rise to transient amplifying cells (TAC). When the cornea is wounded, the slow dividing basal limbal stem cells proliferate to give rise to TAC, which differentiate further to give rise to terminally differentiated cells or to corneal epithelial cells <sup>[79-81]</sup>. The presence of TAC is supported by the ability of peripheral corneal cells to proliferate in response to corneal injury <sup>[76, 77]</sup>.

## *Chapter 1: The Cornea*

The population of basal cells in the limbus has a slow proliferation rate. Limbal basal cells take over two weeks to divide, as indicated by the use of a tritiated thymidine label, which is only taken up by cells about to enter mitosis<sup>[77]</sup>. The difference between corneal epithelial cells and limbal cells was demonstrated by the expression of a particular 64 kD keratin protein<sup>[82]</sup>, now known as cytokeratin 3 (CK3)<sup>[83]</sup>. All epithelial cells are classified by their expression of keratin proteins and subfamilies can be identified by their specific keratin protein expression and hence their differentiation pathway<sup>[82]</sup>. In an early study, basal limbal cells were shown not to express CK3, whereas corneal epithelial cells did, indicating that limbal basal cells did not possess the same degree of differentiation as corneal basal epithelial cells and were more primitive<sup>[82]</sup>. This was the first evidence of a population of adult stem cells residing in the limbus area. Another cytokeratin, CK19, was found to be expressed only in cells found in the basal layer of the limbus<sup>[79, 84]</sup>. Importantly, these cells did express CK3. This suggested that CK19 could be used as a protein marker to identify limbal stem cells or at least transiently amplifying cells. There is great interest in finding a marker for limbal stem cells, which would aid research in the culture of limbal stem cells.

Literature has shown that  $\alpha$ -enolase, a glycolytic enzyme, is expressed in high amounts in limbal basal cells<sup>[85]</sup>, and was tentatively speculated to be a marker for limbal stem cells. It is unlikely that  $\alpha$ -enolase is a specific marker for limbal stem cells as it now been reported to also be found in migrating basal epithelial cells but not in corneal epithelial cells<sup>[86]</sup>, indicating that  $\alpha$ -enolase expression can also be present in transiently amplifying cells.

The transcription factor p63, found in many stem cells, is also suggested to be a marker for limbal stem cells<sup>[87]</sup>. Recently a membrane associated protein called ATP-binding cassette of the G-subfamily (ABCG2), has also been associated with cells found in the limbal region of the eye<sup>[83]</sup>. Immunohistochemical and reverse-transcriptase polymerase chain reaction results have shown that both p63 and ABCG2 are expressed

## *Chapter 1: The Cornea*

in cells found in the basal layer of the limbus<sup>[83]</sup>, again indicating that these protein may be used as markers to identify a stem cell-like population.

The evidence for the existence of limbal stem cells was further demonstrated by the transplantation of limbus tissue into human patients with severe injury to the corneal epithelium and limbal basal cells, in the expectation of corneal reepithelialisation<sup>[88]</sup>. Autografts of limbal and conjunctival tissue from the healthy eye into the damaged eye resulted in regeneration of the corneal epithelium within two weeks of the operation. Though not all patients reported an improvement in visual acuity, impression cytology performed on selected patients showed the presence of normal corneal epithelium in the previously injured eye.

Thus, research has established that limbal stem cells are required for the continued health of the corneal surface. Limbal stem cell deficiency can lead to vascularisation, invasion of conjunctival cells, inflammation and corneal opacification<sup>[89, 90]</sup>. In such cases a limbal transplant may be required to restore visual acuity.

### **1.3.3. Limbal transplantation**

In 1977 conjunctival tissue was transplanted into eyes of patients with chemical burns. At that time, this method of transplantation was considered a success, as small sources of conjunctival tissue could be obtained from the patient's uninjured eye to be transplanted into the injured eye to repair the cornea. Although vascularisation into the central cornea was observed in the implanted eye, vision was markedly improved<sup>[91]</sup>. The main aim is always to improve vision and comfort in the diseased eye.

The interest in the limbus grew when it became evident that limbal cells were the source of corneal reepithelialisation. Allografts (transplantation of tissue from the same species but genetically non-identical person) of limbal rings from cadaveric donors have been transplanted into the damaged eye. A study on 43 recipients of such a graft showed that 22 out of 43 (51%) eyes showed corneal reepithelialisation and an

## *Chapter 1: The Cornea*

improvement of visual acuity, indications of a successful graft. However, in the same study 46% of the recipients showed graft rejection <sup>[92]</sup>. In another study, neovascularisation into the donor tissue occurred in some patients but regressed after a few months, even with the use of immunosuppressive drugs. Most patients however, reported an improvement in visual acuity <sup>[93]</sup>. Limbal allografts are prone to immune rejection since the limbal region contains many antigen presenting cells <sup>[94]</sup>. The central corneal epithelium on the other hand, has immature antigen presenting cells, and thus well tolerated by the host.

The first limbal autografts (tissue belonging to the patient transplanted to another region of the body) were performed on 26 patients <sup>[88]</sup>. In all cases, limbal tissue was taken from the patient's uninjured eye and transplanted into the eye with the damaged cornea and improvements were observed with most cases. The reason for the use of limbal cells instead of conjunctival cells was confirmed when an animal study using autografts from the conjunctiva and the limbus showed that corneas with transplanted limbal cells resulted in less vascularisation and conjunctivalisation (invasion of conjunctival cells) <sup>[89]</sup>. The use of an autograft removes the requirement for immunosuppressive drugs to prevent graft rejection, but patients with bilateral injuries would not benefit. Another obstacle in the use of autografts is the size of graft tissue removed. In some cases it is up to 10 mm in length and 2 mm in width (Figure 10). This in turn can cause limbal deficiency in the donor eye if a minor injury was inflicted on it <sup>[95]</sup>. Therefore it would be preferable to remove only a small amount of tissue for grafting.

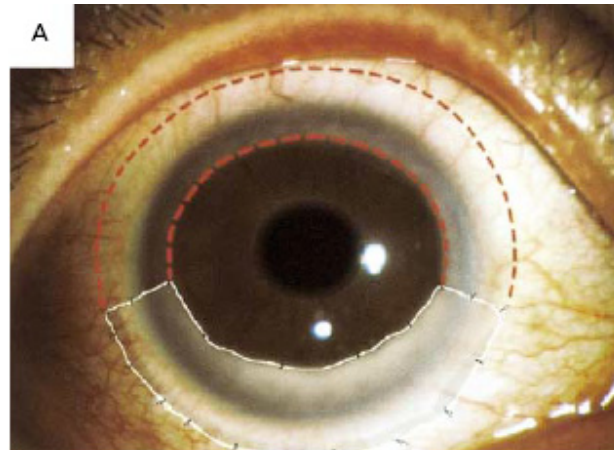


**Figure 10 – Limbal grafts can be conducted by either a sectorial graft (white lines) or a whole limbal transplant (red lines). Taken from Tsai *et al*, 2000 <sup>[90]</sup>.**

Current interest, and our aim, is to culture a small piece of limbal tissue *in vitro*. From the tissue, limbal stem cells can be propagated, which can then be transplanted into a damaged eye to replenish the stem cell niche, which in turn can heal the corneal surface. Therefore a suitable material is required to support the growth and proliferation of these cells.

#### **1.4. Current Support Substrates in Limbal Tissue Engineering**

To use only a small amount of limbal tissue for grafting into a damaged eye, it is desirable to expand the tissue to generate a larger graft for implantation, a typical tissue engineering approach. To be able to expand the limbal tissue, a material is required that will support the growth of cells to be implanted. When this cell-loaded material is implanted into the eye, it is expected that cells will migrate from the material into the surrounding tissue to repopulate the limbal cell niche. To prevent any further damage or so as not to disrupt the newly populated niche, it is desirable that the material degrade into non-toxic products, avoiding the need for explantation of the support.

Recently, amniotic membrane (AM) has been used in association with limbal grafts to facilitate the healing of the cornea. AM is the innermost layer of the placenta and was

## *Chapter 1: The Cornea*

reportedly used in 1940 to facilitate the healing of damaged conjunctiva <sup>[96]</sup>. AM consists of a basement membrane and an avascular stromal matrix, and its basement membrane is similar to that of the conjunctiva making it an ideal substrate to support the growth of corneal epithelial cells <sup>[96, 97]</sup>. When a sheet of AM was placed over mildly injured corneas, the membrane alone was able to support the growth of the few remaining limbal stem cell populations present in the eye, thus facilitating reepithelialisation, with the added bonus of the AM dissolving after 3-4 weeks of transplantation <sup>[98]</sup>. The membrane was able to facilitate wound healing in eyes which still maintained the limbal cell population. In severely injured corneas where there was total limbal deficiency, donor limbal cells had to be transplanted along with the AM to be able to restore the corneal surface.

AM has also been shown to be capable of expanding cells *in vitro*, reducing the amount of donor tissue required. Small pieces of limbal tissue containing the stem cells can be expanded on AM in culture before transplantation to the damaged corneal surface to restore or improve visual acuity (Figure 11) <sup>[90]</sup>. A study using rabbits demonstrated that when AM alone was placed over wounded corneas, it was not as effective as an AM containing cultured limbal cells in healing the injury <sup>[99]</sup>. The authors showed that corneas with only the AM sheet showed an epithelial layer with defects, but corneas with AM containing cultured limbal cells showed a continuous epithelial layer.

A later study involving the culture of limbal stem cells on AM showed that AM can suppress the differentiation of stem cells, most likely due to a component that suppresses signalling. When the cells were cultured on AM, immunohistochemical evidence showed that the limbal cells were proliferating and expressed p63, indicating that the cultured cells were not terminally differentiated <sup>[100]</sup>.

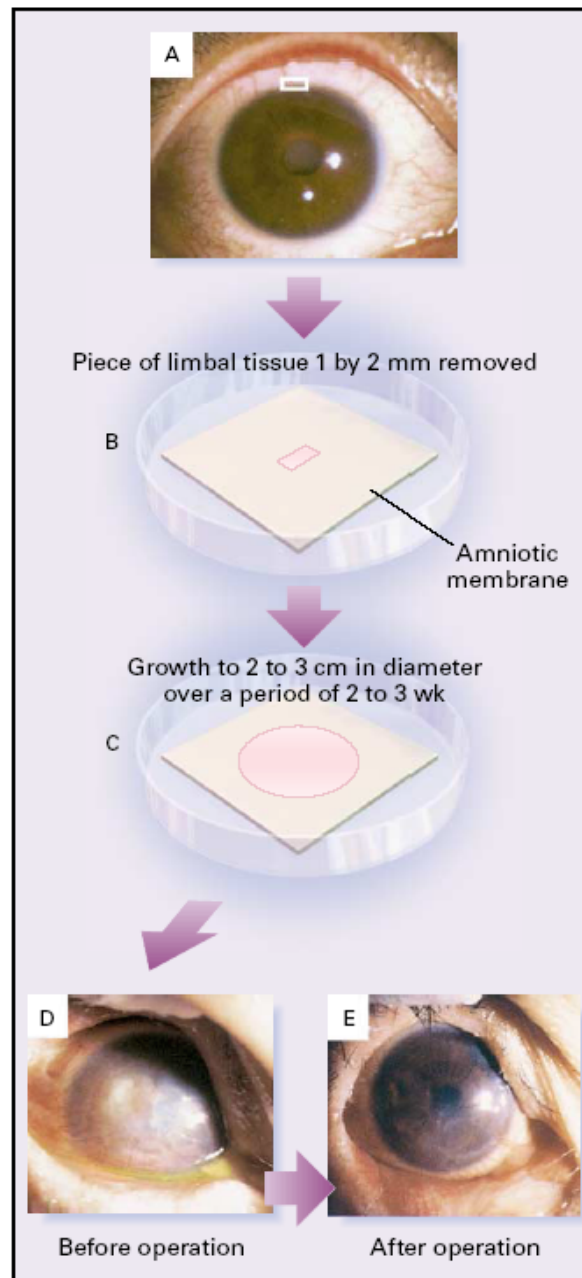


**Figure 11 – Procedure by which a small amount of limbal tissue is removed from a healthy eye and expanded on amniotic membrane. The expanded tissue can then be grafted onto the damaged eye for reepithelialisation of the cornea. Taken from Tsai *et al* (2000) <sup>[90]</sup>.**

## *Chapter 1: The Cornea*

For facilitating the repair of a wounded corneal epithelium, amniotic membrane has so far shown the most promising results, due to the amniotic membrane's similarity to the basement membrane of the corneal epithelium. Over a period of three weeks, the membrane becomes integrated with the corneal surface, allowing epithelial cells to grow over the membrane surface. In a sense, the amniotic membrane degrades whilst assisting the repair of the ocular surface.

Issues with AM include its harvesting from human placentas and the requirement for chemical processing. The latter entails the stripping of the native cell population off the AM surface to be able to support the culture of limbal cells <sup>[101]</sup>. Amniotic membranes also carry the risk of transmitting blood-borne diseases <sup>[102]</sup>. For these reasons, the Food and Drug administration (FDA) in the USA and the Therapeutic Goods Administration (TGA) in Australia, both medical regulatory bodies, are opposed to the use of human amniotic membrane but allow its use. As such, there is now a search for an alternative substrate.

Mouse 3T3 fibroblasts have also been used as a substrate upon which limbal cells have been cultured <sup>[87]</sup>. The 3T3 cells are often used as a “feeder layer”, where the cells are cultured into a confluent sheet and then chemically treated or irradiated to prevent the cells from continuing mitosis. 3T3 cells secrete a variety of matrix proteins into culture which promote cell growth <sup>[103]</sup>. A 1 mm<sup>2</sup> piece of limbal tissue has been cultured on this surface and the subsequent epithelial sheet grown was used to successfully treat a damaged human eye <sup>[104]</sup>. 3T3 cells have also been used in conjunction with AM, where the limbal tissue was cultured upon an AM surface that was suspended above a layer of 3T3 cells, but shared the same culture medium <sup>[105]</sup>. The cultured cells from the limbus were then transplanted into a human eye expressing limbal stem cell deficiency, which resulted in reepithelialisation of the diseased surface. Despite this success with 3T3 cells, they are of rodent origin, which makes it undesirable for use with tissue to be implanted into humans.

## Chapter 1: The Cornea

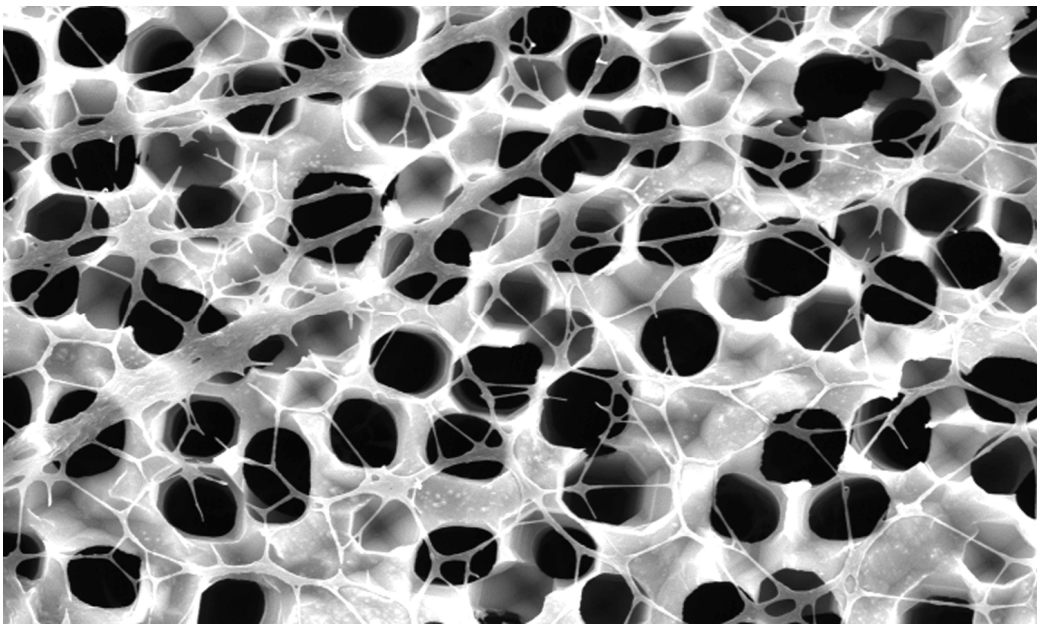
In 1985, an investigation into the use of collagen as a substrate was carried out by culturing epithelial cells onto a collagen layer. Epithelial cells that exhibit “normal” behaviour in culture are able to generate a basement membrane. When cultured on collagen, a basement membrane was established by the cultured epithelial cells in only one out of five experiments <sup>[106]</sup>. Fibrin has been suggested as a possible substrate to support the *in vitro* proliferation of limbal stem cells. Autologous cells cultured on fibrin were transplanted into an injured eye with the result of a “normal”-looking epithelium after one month. The drawback was that the cells were cultured on fibrin using a mouse 3T3 feeder layer <sup>[107]</sup>. It is desirable to create a scaffold that does not require the use of human or animal tissue. Therefore a synthetic scaffold that is capable of supporting cell growth from limbal tissue would be greatly beneficial.

As a material for the delivery of cells, it is preferable that the cell scaffold be degradable, to minimise invasive treatments to a recently operated and hence, delicate area. To reduce animal or human based products, a synthetic material is required that is biocompatible and will support the growth of cells. In the case of culturing limbal tissue for transplantation, the material is also required to be stable for the culture period *in vitro* but still be manageable for transplantation. The implanted material should be able to degrade into non-toxic components after a period of time. The biocompatibility of the material has to be tested in an *in vivo* environment to determine the host response to the implanted material. As the conjunctiva of the eye is not pigmented, the host response to materials implanted into that region can be easily observed without the need for intrusive actions. The eye can be used as a model to test the *in vivo* response to biomaterials.

We propose a material that is biocompatible, biodegradable and is able host a population of cells, to be porous silicon. In this thesis, we tested porous silicon for its ability to support the growth of cells using *in vitro* culture techniques and we examined the ability of porous silicon to degrade under different conditions. We also implanted porous silicon into the eyes of rats to elucidate the host response to the material and to determine if cells cultured on porous silicon can migrate into the surrounding tissue.

## Chapter 2

### Evaluation of mammalian cell adhesion on surface-modified porous silicon



*Scanning electron micrograph of the surface of macroporous silicon coated with collagen*

## **Introduction**

In this chapter the properties of porous silicon as a substrate for the culture of cells is investigated. The effect of surface-modified porous silicon on cells is also studied and the modified porous silicon is characterised through a variety of analytical techniques.

A variety of cells have been successfully cultured onto porous silicon (pSi) surfaces. For example, Chinese Hamster Ovary cells (CHO) and the neuronal cell line, B50, were cultured onto a porous silicon surface and the viability of the cells was determined by an MTT (3-[4, 5-dimethylthiazol-2-yl]-2,5-diphenyl tetrazolium bromide) and a neutral red uptake assay <sup>[60, 108-111]</sup>. These assays indicated that B50 cells had a preference for porous silicon surfaces in comparison to glass surfaces <sup>[61]</sup>. In comparison, the CHO cells showed a preference for bulk (non-etched) silicon over than porous silicon <sup>[61]</sup>.

Other researchers demonstrated that the attachment of primary rat hepatocytes was affected by the surface modification applied to porous silicon <sup>[112]</sup>. In this study, porous silicon was ozone oxidised, converting a hydride terminated surface into a hydroxy (OH) terminated surface. The porous silicon was then further surface-modified by a coating with collagen. Hepatocytes were cultured on the porous silicon surfaces and the viability was determined by protein release from the cells and through fluorescence microscope images. The results showed that hepatocytes had a preference for collagen coated porous silicon over an oxidised porous silicon surface. This indicates that the surface chemistry of porous silicon is an important parameter in promoting cell attachment.

Self assembled monolayers have recently been used to control the surface chemistry of biomaterials to better understand the interaction between a cell and a surface <sup>[113]</sup>. A type of self assembled monolayer is functional alkylsilane, which binds to a material by the alkoxy groups in the silane reacting with surface hydroxyl groups <sup>[114]</sup>. The process of depositing a silane onto the surface is called silanisation. 3-aminopropyltrimethoxysilane and N-(triethoxysilylpropyl)-O-polyethylene glycol

## *Chapter 2: Introduction*

urethane are two silanes used in this thesis. When deposited onto a surface, the functional group of the silane determines the surface chemistry. Silanisation can modify the surface properties of the material, such as wettability (hydrophobicity), charge repulsion and electrostatic interactions. These changes in surface properties are dependent upon the type of silane used.

Changes in hydrophobicity have long been known to affect the attachment and proliferation of anchorage-dependent cells, where cell attachment can be inhibited on very hydrophobic surfaces <sup>[115, 116]</sup>. This has been partly attributed to the amount and type of serum proteins (containing attachment factors) that can be adsorbed to the surface. Surface chemistry is a major factor in cell attachment and proliferation, and along with wettability, can influence the amount of protein adsorbed to the surface <sup>[113]</sup>. This in turn affects the number of cells that can attach to the material <sup>[117]</sup>.

Aminosilanes, such as 3-aminopropyltrimethoxysilane, are often used to coat surfaces to promote cell attachment. A substrate coated with an aminosilane generates an amine-terminated surface that promotes cell adhesion <sup>[115, 117]</sup>. Polyethylene glycol containing compounds, such as N-(triethoxysilylpropyl)-O-polyethylene oxide urethane, are commonly used in anti-biofouling coatings, where the poly ethylene glycol chains prevent the adsorption of proteins to the surface <sup>[118, 119]</sup>, which in turn can prevent cell attachment. We compared the effect that these two silanes had on the attachment of cells to porous silicon surfaces.

Cell adhesion is widely known to be dependent upon cell surface receptors interacting with proteins of the extracellular matrix <sup>[120]</sup>. Collagen is a well known component of the extracellular matrix and is commonly used to coat surfaces to increase their bioactivity. Collagen is also a main component of the cornea. We investigated the use of collagen and other serum proteins as a coating on porous silicon and the effect that it may have on cellular adhesion.

## *Chapter 2: Introduction*

The aims of the work to be presented in this chapter are:

- to generate porous silicon surfaces modified with different functional groups and different wettability;
- to characterise native and surface modified porous silicon chemistry and topography;
- to determine which surface modifications promote cell attachment;
- to investigate the suitability of different viability assays in conjunction with porous silicon surfaces.

## **Methods and Materials**

### **2.1. Chemicals**

Dulbecco's modified Eagle's medium (DMEM), horse serum, Type I rat tail collagen, fluorescein diacetate, 3-aminopropyltrimethoxysilane, neutral red and penicillin/streptomycin solution were obtained from Sigma Chemical Co. (St Louis, MO, USA). Foetal Bovine Serum (FBS) was purchased from Bovogen Biologicals Ltd (Essenden, Vic, Aus). L-glutamine and Hoechst 33342 were purchased from Invitrogen (Carlsbad, CA, USA). Alamar Blue was purchased from Biosource International, Camarillo, CA, USA. N-(triethoxysilylpropyl)-o-polyethylene oxide urethane was purchased from Gelest (Tullytown, PA, USA).

### **2.2. Preparation of Porous Silicon**

P-type wafers with <100> orientation and with 3-6 $\Omega$ cm resistivity were obtained from Silicon Quest (Santa Clara, CA, USA). Wafers were etched in a custom-made Teflon cell (Figure 12) at a constant current density of 44 mA/cm<sup>2</sup> for 2 mins in a 25% hydrofluoric acid (HF) solution in ethanol. The porous silicon piece was then rinsed consecutively with methanol, acetone and dichloromethane (DCM) and dried under a stream of nitrogen. This sample is termed "freshly etched" porous silicon.

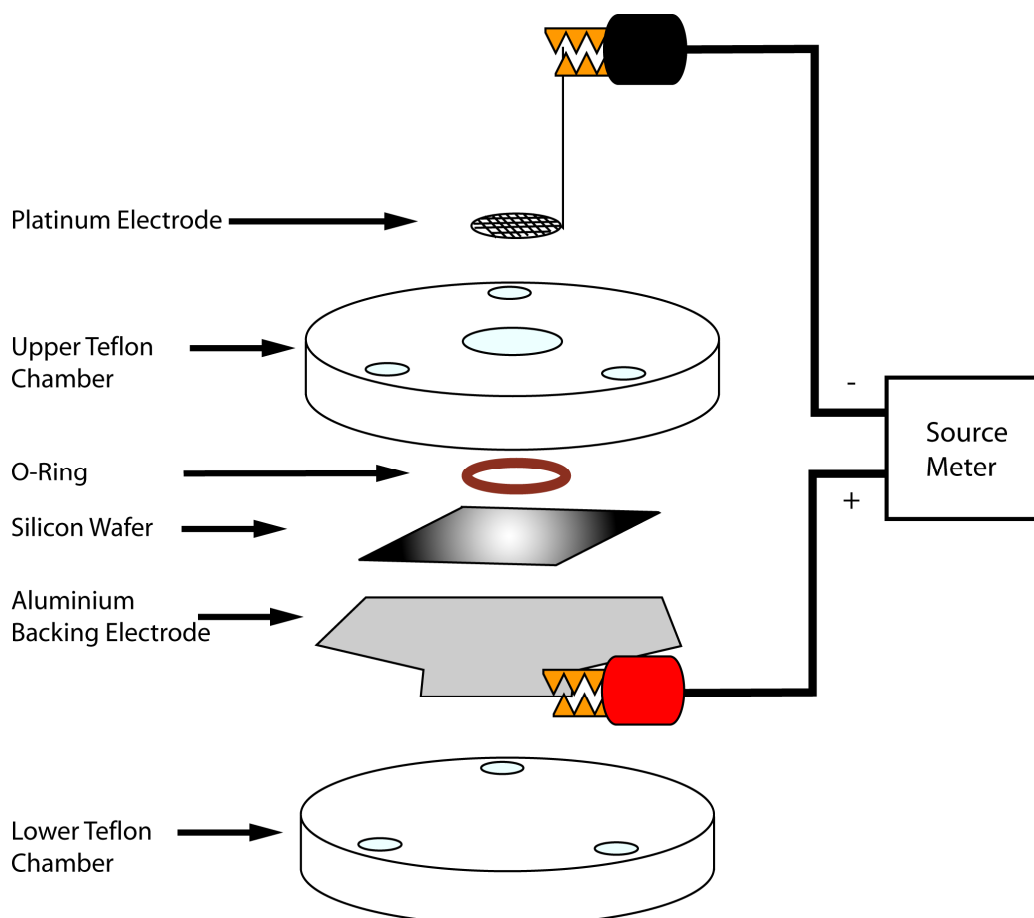


**Figure 12 – Illustration of the components used in the custom-made Teflon etching cell for the production of porous silicon wafers. After the chamber is assembled and held together by screws, hydrofluoric acid in ethanol is added to the upper Teflon chamber and a current is applied.**

## **2.3. Preparation of Surface-Modified Porous Silicon**

### **2.3.1. Ozone oxidised samples**

Etched wafers were ozone-oxidized in an ozone generator (Fischer America Inc, Houston, TX, USA) for 30 mins using an ozone flow rate of 8 g/hour. For use in cell culture, the wafers were sterilised by immersion in 70% (v/v) ethanol for 10 mins before drying under sterile air flow.

### 2.3.2. Amine functionalised samples (APTMS)

For the preparation of amine-functionalised surfaces, ozone oxidised porous silicon samples were placed into a 50 mM solution of 3-aminopropyltrimethoxysilane (APTMS, Figure 13A) in toluene for 5 minutes at room temperature, then washed in succession with DCM, acetone, methanol, then again in acetone and DCM, before being dried under a stream of nitrogen. For cell culture experiments, the surfaces were sterilised by immersion in 70% (v/v) ethanol for 10 mins and dried in sterile air.

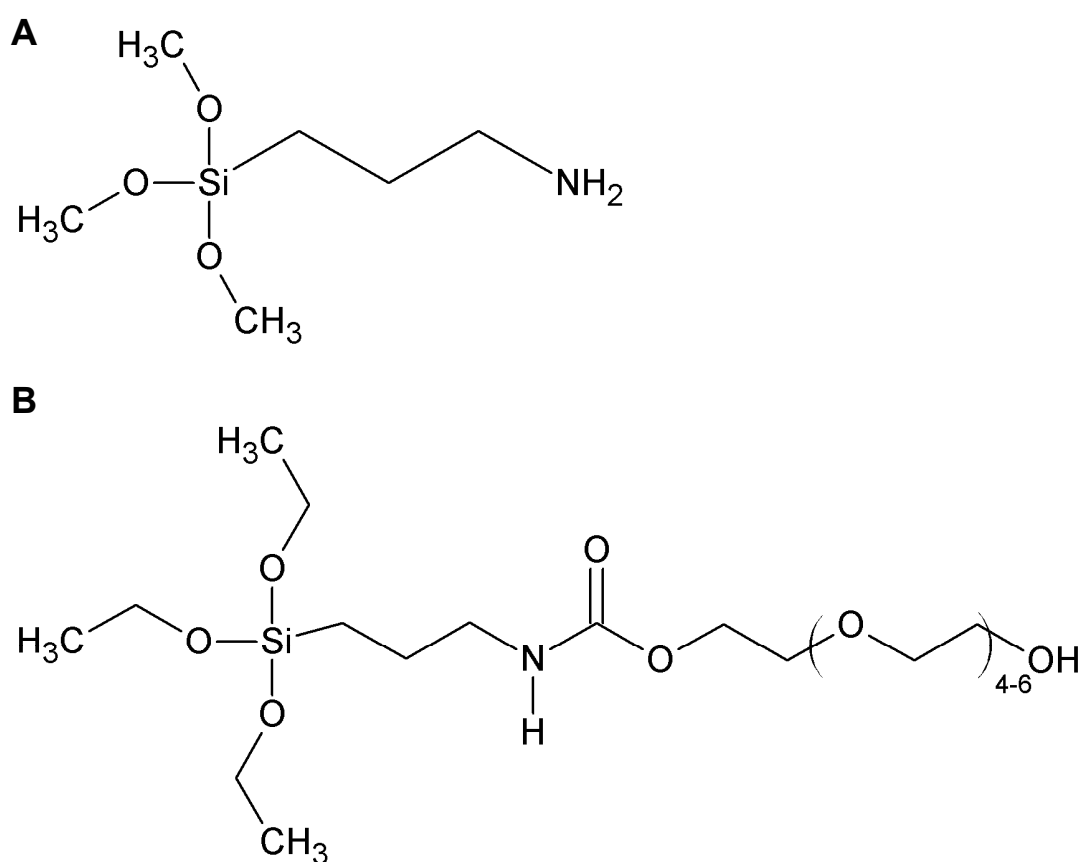


Figure 13 – Structures of A: 3-aminopropyltrimethoxysilane (APTMS) and B: N-(triethoxysilylpropyl)-O-polyethylene oxide urethane (PEGS).

### **2.3.3. Polyethylene glycol functionalised samples (PEGS)**

Polyethylene glycol terminated porous silicon was prepared by the immersion of ozone oxidised wafers in a 50 mM solution of N-(triethoxysilylpropyl)-O-polyethylene oxide urethane (PEGS, Figure 13B) in toluene for 10 minutes, before being washed and dried using the same method used for APTMS samples. For cell culture experiments, the surfaces were sterilised by immersion in 70% (v/v) ethanol for 10 minutes and dried in sterile air.

### **2.3.4. Collagen coated samples (Collagen)**

10 µg of Type I rat tail collagen in 0.1 M acetic acid was spread onto the surface of ozone oxidised porous silicon wafers using a plastic spreader. The collagen layer was allowed to air dry and was then sterilised via exposure to ultraviolet light overnight. These samples were used without further modification.

### **2.3.5. Foetal bovine serum coated samples (FBS)**

For foetal bovine serum (FBS) treatment of pSi, 50 µl of a 10% (v/v) solution of FBS in 10 mM phosphate buffered saline (PBS, pH 7.4) was spotted onto ethanol sterilised pieces of oxidised porous silicon and allowed to dry onto the surface. These samples were used without further modification.

### **2.3.6. Thermally oxidised samples**

Freshly etched porous silicon samples were heat treated in a furnace. Temperatures were raised to 600 °C and held for a minimum of 1 hour. For sterilisation, the samples were immersed in 70% (v/v) ethanol for 10 mins and allowed to air dry.

## **2.4. Surface Characterisation**

### **2.4.1. Atomic force microscopy and scanning electron microscopy**

The topography of surface modified porous silicon samples was analysed by means of atomic force microscopy (AFM) on a Multimode Nanoscope IV (Veeco Instruments Inc., Woodbury, NY, USA) operating in tapping mode in air. FESP (Force modulation, Etched Silicon Probes) cantilevers (Veeco Instruments Inc.) with a resonance frequency of ~75 kHz, were used at a free oscillation amplitude of 2V. For offline analysis of images, Nanoscope III 5.12r3 software was used. All scans were of a 1 µm x 1 µm area.

The thickness of the porous silicon layer was determined by scanning electron microscopy (SEM). Etched porous silicon wafers were snapped in half and the cross-section was examined on a Phillips XL30 SEM operating at 10 keV. Samples were coated in platinum prior to scanning to reduce sample charging.

### **2.4.2. Porosity studies**

To determine the porosity of porous silicon, a gravimetric analysis method was employed<sup>[121]</sup>. The mass of the silicon wafer was recorded before etching ( $m_1$ ), after etching ( $m_2$ ) and after the porous layer was removed ( $m_3$ ). The porous layer was removed by immersing the porous silicon in a 100 mM solution of NaOH diluted in water for 10 mins. The percentage porosity of the porous silicon was then determined by using this formula:

$$\text{Porosity (\%)} = (m_1 - m_2)/(m_1 - m_3) \times 100.$$

### **2.4.3. Contact angle measurements**

Sessile drop water contact angle measurements were conducted in a custom-made setup consisting of a sample stage, a macro lens and a CCD camera. At room temperature, 1  $\mu\text{l}$  of MilliQ water was spotted onto the surfaces, images of the drop profiles were captured and Scion Image 4.0.2 software (Scion Corp., Frederick, MD, USA) was used to measure contact angles on both sides of the droplet. A minimum of four replicates were measured for each sample surface.

### **2.4.4. Interferometric reflectance spectroscopy**

Degradation studies of porous silicon were conducted using interferometric reflectance spectroscopy (Ocean Optics S2000 with illumination by a tungsten halogen light source) to determine changes in the effective optical thickness of the porous silicon layer due to hydrolytic degradation in neutral phosphate buffered saline (PBS) pH 7.4. Effective optical thickness was calculated using a Fast-Fourier transformation of the fringe patterns created by reflections of the light source off the porous surface. Changes in effective optical thickness were measured in one minute intervals over a period of one hour.

### **2.4.5. Transmission FTIR**

Porous silicon surface chemistry was determined by Fourier-transform infrared (FTIR) spectroscopy collected on a Nicolet Avatar 370 spectrometer in transmission mode in air. A blank silicon wafer was used to obtain background spectra. 32 scans were averaged at a resolution of 4  $\text{cm}^{-1}$ .

## **2.5. Cell Experiments**

### **2.5.1. Cell lines**

PC12 is an immortalised rat pheochromocytoma cell line, with neuronal-like properties [122]. The cells were cultured in Dulbecco's modified Eagle's medium (DMEM) supplemented with 10% (v/v) horse serum, 5% (v/v) foetal bovine serum, 5 mM L-glutamine, 100 IU/ml penicillin and 100 µg/ml streptomycin sulphate. Human lens epithelial cells (HLE cells), an immortalised cell line designated SRA 01/04 [123], were used with permission from Professor Venkat Reddy from the Kellogg Eye Centre, USA. Cells were cultured in DMEM containing 5 mM L-glutamine, 100 IU/ml penicillin, 100 µg/ml streptomycin sulphate and 10% (v/v) FBS. Both cell lines were maintained at 37 °C with 5% CO<sub>2</sub> in air, in a humidified incubator.

### **2.5.2. Cell attachment**

PC12 and HLE cells were seeded onto surface modified porous silicon at a cell density of  $5 \times 10^4$  cells/ml. Glass coverslips were used as support for control cultures. All porous silicon samples were cut to 1 cm<sup>2</sup> size pieces with a diamond-edged cutter, prior to sterilisation and culture. Cultures were incubated for 4 hours at 37°C with 5% CO<sub>2</sub> in air, in a humidified incubator. To determine cellular morphology and viability on the surfaces, cells were stained with 75 µg/ml of fluorescein diacetate and incubated for 5 mins at 37 °C. Samples were subsequently washed with PBS to remove non-adherent cells before observation by fluorescence microscopy on a Leitz Laborlux II microscope at excitation wavelengths of 450-490 nm. Images were captured using a Nikon digital camera (DS-5M).

### **2.5.3. Alamar Blue cell viability assay**

To determine the effectiveness of the Alamar Blue solution in quantifying cell survival on porous silicon, HLE cells were initially cultured on glass coverslips and on silicon wafers at a density of  $1 \times 10^5$  cells/ml in a 24 well plate (Iwaki, Chiba, Japan). These

## Chapter 2: Methods and Materials

cells were our positive control. The cells were incubated overnight and the cell culture medium was replaced with 400  $\mu\text{l}$  of a 10% (v/v) Alamar Blue solution diluted in cell culture medium. As a negative control, tissue culture polystyrene (TCPS), silicon and ozone oxidised porous silicon were incubated in the presence of the Alamar Blue solution, but in the absence of cells. The assay was conducted for 2 hours at 37 °C.

After 2 hours, 100  $\mu\text{l}$  of the incubated Alamar Blue solution was placed into a 96 well plate and read at 600 nm and at 570 nm (Vmax, Molecular Devices, CA, USA). Concentration of the reduced form of Alamar Blue was calculated using this formula provided by the manufacturer, Biosource International:

$$C_{\text{RED}} = \frac{(\epsilon_{\text{OX}})\lambda_2 A\lambda_1 - (\epsilon_{\text{OX}})\lambda_1 A\lambda_2}{(\epsilon_{\text{RED}})\lambda_1 (\epsilon_{\text{OX}})\lambda_2 - (\epsilon_{\text{OX}})\lambda_1 (\epsilon_{\text{RED}})\lambda_2}$$

$C_{\text{RED}}$  = Concentration of reduced Alamar Blue (RED)

$C_{\text{OX}}$  = Concentration of oxidised Alamar Blue (OX)

$\epsilon_{\text{OX}}$  = Molar extinction coefficient of Alamar Blue oxidised form

$\epsilon_{\text{RED}}$  = Molar extinction coefficient of Alamar Blue reduced form

$A$  = Absorbance of test wells

$\lambda_1$  = 570nm

$\lambda_2$  = 600nm

Molar Extinction Coefficients		
Wavelength ( $\lambda$ )	$\epsilon_{\text{RED}}$	$\epsilon_{\text{OX}}$
570nm	155,677	80,586
600nm	14,652	117,216

An interferometric analysis of the porous silicon surface in the presence of Alamar Blue was conducted to study the effect of Alamar Blue on the porous silicon surface. Ozone oxidised porous silicon was used for this experiment. The effective optical thickness was determined using the same method as described in **Section 2.4.4**. A baseline degradation rate was obtained using pH 7.4 PBS, then a 50% Alamar Blue solution diluted in PBS was introduced into the chamber. To determine a change in the baseline degradation rate and hence a change in effective optical thickness, PBS was reintroduced into the chamber, followed by another injection of Alamar Blue solution.

#### **2.5.4. Neutral red cell viability assay**

The neutral red assay was conducted in a similar fashion to Alamar Blue. As positive controls, HLE cells were cultured on glass coverslips and on silicon at a density of  $1 \times 10^5$  cells/ml in a 24 well plate. The cells were incubated overnight before the cell solution was replaced with 500  $\mu$ l of a 50  $\mu$ g/ml neutral red solution, diluted in cell culture medium. As negative controls, silicon and oxidised porous silicon were cultured in the presence of the neutral red solution in the absence of cells. Assays were conducted for 2 hours at 37 °C.

After the 2 hour incubation, the wells were washed with PBS twice to remove any remaining unincorporated dye. The dye was then released from the cells using 400  $\mu$ l of lysis solution: 1% (v/v) acetic acid, 50% (v/v) ethanol and 49% (v/v) dH<sub>2</sub>O. The 24 well plate was agitated for 5 mins before 100  $\mu$ l of solution was transferred to a 96 well plate to be read at 570 nm in the spectrometer.

#### **2.5.5. Cell counts**

PC12 and SRA 01/04 cells were seeded onto the surface of sterilised, surface-modified porous silicon at a density of  $5 \times 10^4$  cells/ml. Cells were incubated on the samples at 37 °C for 4 hours or 24 hours in Ultra Low Adherence 24 well plates (Corning Enterprises, Corning, NY, USA) which inhibit cell attachment to the tissue culture

## *Chapter 2: Methods and Materials*

plate, allowing cells to attach only to the porous silicon. Cells were stained with 2 µg/ml of Hoechst 33342 dye for 30 mins before being washed with PBS to remove any non-adherent cells. Cells were observed under fluorescence microscopy at an excitation wavelength of 270 - 380 nm. Controls were cells cultured on glass coverslips cut into 1 cm<sup>2</sup> squares. Cell counts were conducted at five different locations on the surface of each sample (four peripheral and one central) in areas measuring 850 µm x 650 µm.

### **2.5.6. Statistical analysis on cell counts**

The statistical software package SPSS 12.0.1 for Windows (SPSS Inc, Chicago, IL, USA) was used for analysis. An independent t-test was performed for all samples against the positive control, considering  $p \leq 0.05$  as statistically significant.

## Results & Discussion

### 2.6. Characterisation of Surface-Modified pSi

Previous studies have focused upon p-type silicon wafers with low etching current densities for cell culture [62, 112]. For this investigation, we used p-type, boron doped silicon wafers containing moderate levels of dopant with a resistivity of 3-6  $\Omega\cdot\text{cm}$ . We chose an anodisation procedure that resulted in the formation of disordered mesopores of 10-20 nm in diameter, with a porous layer of approximately 2.2  $\mu\text{m}$  thickness (Figure 14) and an average porosity of 74%. Porous silicon was surface-modified by ozone oxidation, silanised with APTMS or PEGS, or coated with collagen or an FBS solution to improve surface stability and to impart functionalities to promote cell adhesion and proliferation.

#### 2.6.1. AFM and contact angle measurements

AFM studies showed little change to topographical characteristics amongst freshly etched, oxidised and silanised porous silicon (Figure 15A-D). Area statistical root mean square (rms) roughness values for freshly etched and oxidised were similar, 0.159 and 0.140 nm, respectively. Silanised samples were slightly rougher with rms values of 0.247 nm for APTMS and 0.173 nm for PEGS samples. Coating porous silicon with collagen resulted in the formation of collagen aggregates where individual fibres could be distinguished (Figure 15E, rms 0.828 nm). Pores were not easily discerned in FBS coated porous silicon, indicating deposition of proteins on the surface (Figure 15F, rms 0.271 nm). After 4 hours incubation in cell culture medium at 37 °C, oxidised porous silicon (Figure 15G) and APTMS (Figure 15H) showed significant surface degradation indicated by a significant increase in roughness. Surface roughness also increased significantly to 2.45 and 7.12 nm for ozone oxidised and APTMS porous silicon, respectively.

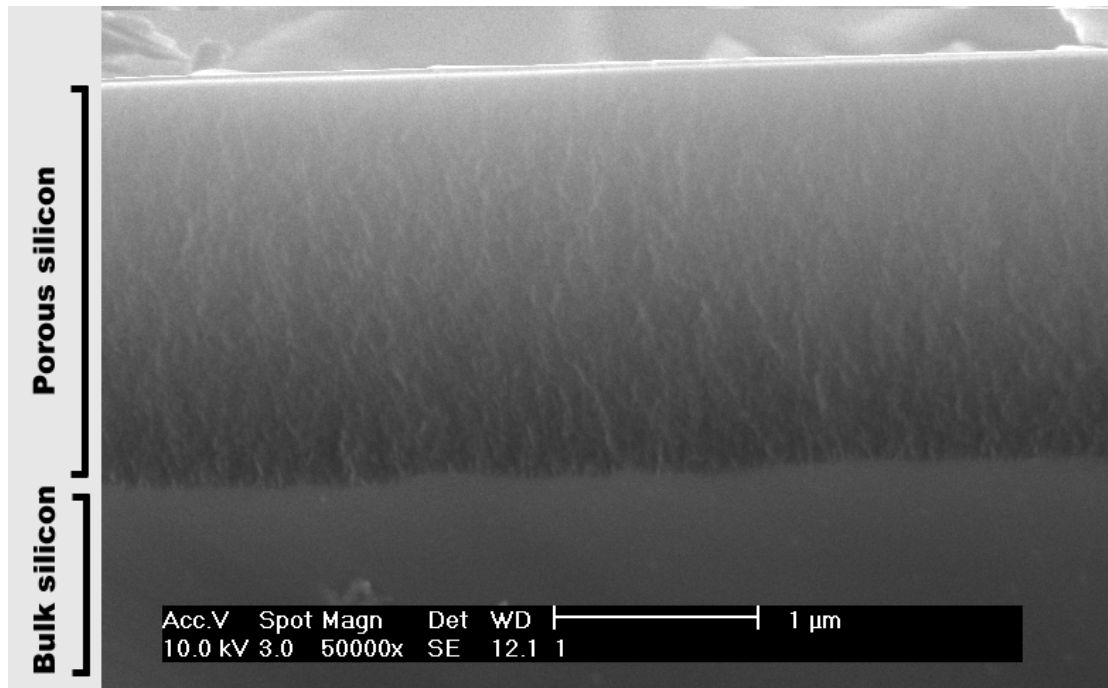
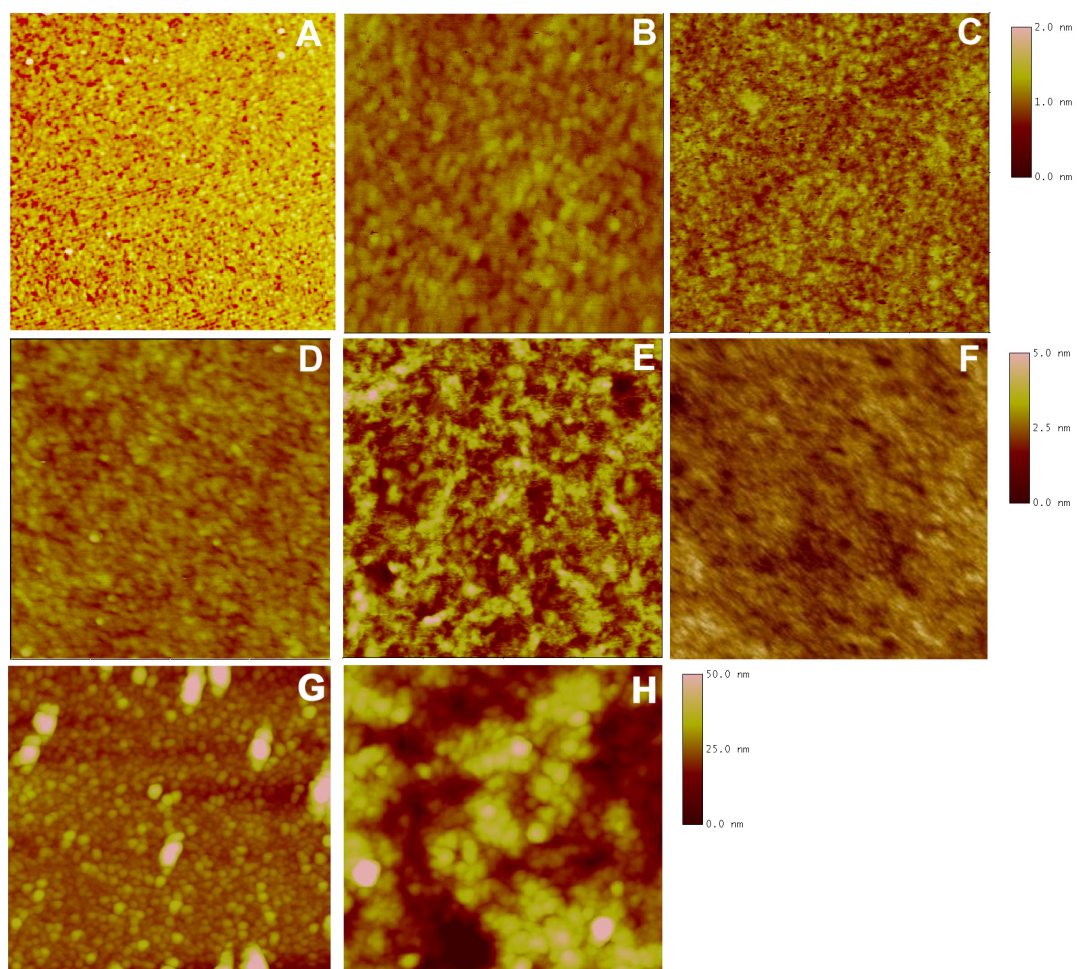


Figure 14 - SEM image of a cross-section of porous silicon etched at a current density of  $44 \text{ mA/cm}^2$  for 2 minutes in a 25% HF solution in ethanol. The porous layer is visible above the bulk silicon.



**Figure 15 – AFM images of surface-modified porous silicon: (A) freshly etched; (B) ozone oxidised; (C) PEGS; (D) APTMS; (E) collagen coated; (F) FBS coated; (G and H) ozone oxidised and APTMS functionalised pSi after 4 hr incubation in cell culture medium. All images are of a  $1 \mu\text{m}^2$  area and were obtained in tapping mode in air. Height scales: (A-C) 2 nm; (D-F) 5 nm and (G and H) 50 nm.**

Contact angle measurements on porous silicon cannot be directly compared with measurements taken on flat surfaces due to the influence of the topography of the porous surface with the contact angle measurements. Wettability of the surfaces was only compared amongst our different samples as a qualitative assessment of wettability. As expected, freshly etched porous silicon was hydrophobic ( $>99^\circ \pm 3^\circ$ ), and ozone oxidation resulted in a drop of the contact angle to below  $5^\circ$ . This was attributed to the formation of a polar Si-OH capped surface after oxidation. FBS coated surfaces were also very hydrophilic ( $10^\circ \pm 1^\circ$ ). Aminosilanised porous silicon had a contact angle of  $56^\circ \pm 3^\circ$  in accordance with published data <sup>[124, 125]</sup>, whilst PEGS modification of the surface decreased the angle to  $26^\circ \pm 2^\circ$  <sup>[113]</sup>. Collagen coating on oxidised porous silicon generated a contact angle of  $32^\circ \pm 8^\circ$ . Thus, the order of surface hydrophobicity was: freshly etched > APTMS > collagen-coated > PEGS > FBS-coated > ozone oxidised.

### **2.6.2. Transmission FTIR spectroscopy**

The surface chemistry of the surface-modified porous silicon was determined using transmission FTIR (Figure 16). Freshly etched porous silicon displayed absorption spectra consistent with a hydride-terminated surface. The stretching modes at  $2088\text{ cm}^{-1}$  for (Si-H),  $2116\text{ cm}^{-1}$  for (Si-H<sub>2</sub>) and  $2137\text{ cm}^{-1}$  for (Si-H<sub>3</sub>) were apparent <sup>[126, 127]</sup>. The spectrum further showed bending vibrations for a Si-H<sub>2</sub> scissor mode at  $910\text{ cm}^{-1}$  and Si-H<sub>x</sub> deformations at  $626\text{ cm}^{-1}$ . Upon ozone oxidation, the bands corresponding to Si-H<sub>x</sub> stretching and bending modes were removed and replaced with bands at  $1070\text{ cm}^{-1}$ . A broad band centred around  $3400\text{ cm}^{-1}$  was attributed to (SiO-H) stretching vibrations. There was also a (SiO-H) bending mode which gave rise to a peak at  $1640\text{ cm}^{-1}$  and a band at  $810\text{ cm}^{-1}$  that corresponded to a Si-O-Si stretching vibration <sup>[127]</sup>.

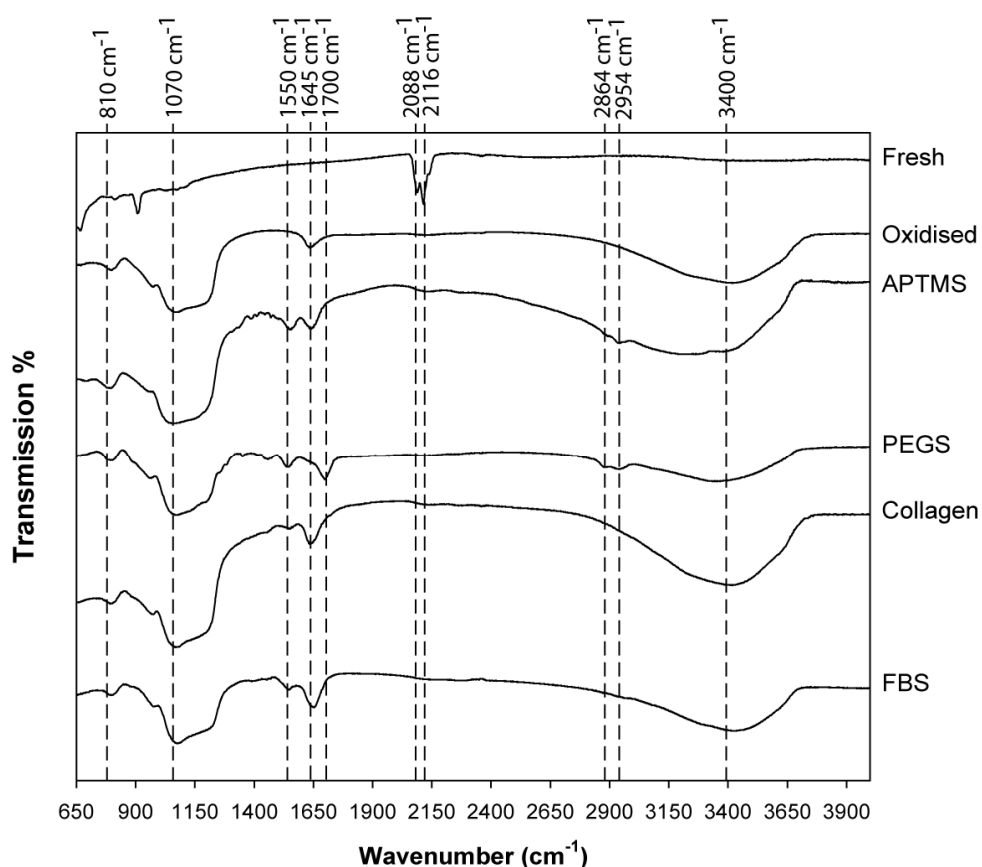


**Figure 16 - Transmission FTIR spectra of: freshly etched (Fresh); ozone oxidised (Ox); aminosilanised (APTMS); PEG functionalised (PEGS); collagen and FBS coated pSi.**

Two peaks at 2954 and 2864 cm<sup>-1</sup> correspond to aliphatic (C-H) stretches <sup>[125]</sup> in APTMS and PEGS functionalised surfaces. The peaks below 800cm<sup>-1</sup> were attributed to bending vibrations of Si-C. The PEGS functionalised surface also exhibited a peak at 1700 cm<sup>-1</sup> attributed to the urethane (C=O) vibration and a band at 1550 cm<sup>-1</sup> for the urethane (C-N) bond. IR spectra of collagen and FBS coated porous silicon both showed an amide I band at 1645 cm<sup>-1</sup> and an amide II band at 1550 cm<sup>-1</sup>.

### **2.6.3. Degradation studies**

Interferometric reflectance spectroscopy was used to measure the degradation rate of the various porous silicon samples in neutral pH PBS buffer. Freshly etched hydride terminated porous silicon hydrolyses and oxidises readily upon exposure to aqueous

## *Chapter 2: Results and Discussion*

solution, accompanied by the generation of  $H_2$  <sup>[51]</sup> (**Section 1.2.2**). This corrosion of the porous silicon surface can be measured by a decrease in effective optical thickness using interferometric reflectance spectroscopy <sup>[35, 128, 129]</sup> (**Section 1.2**). As shown in Figure 17, freshly etched porous silicon had the least stable surface; in 1 hour, a 20% decrease in effective optical thickness (relative to initial optical thickness) was recorded. We found that simple oxidation stabilised the porous silicon surface significantly in aqueous medium and functionalisation with silanes further reduced the rate of hydrolytic dissolution. FBS coated porous silicon had similar degradation rates to the silanised surfaces, indicating the presence of a protective protein layer on the surface. Collagen coating was less effective in protecting the porous silicon layer as indicated by the intermediate slope. We demonstrated that both silanisation and protein-coating of porous silicon could improve surface stability and reduce the rate of surface degradation, consistent with existing data <sup>[50, 62, 128, 130]</sup>.

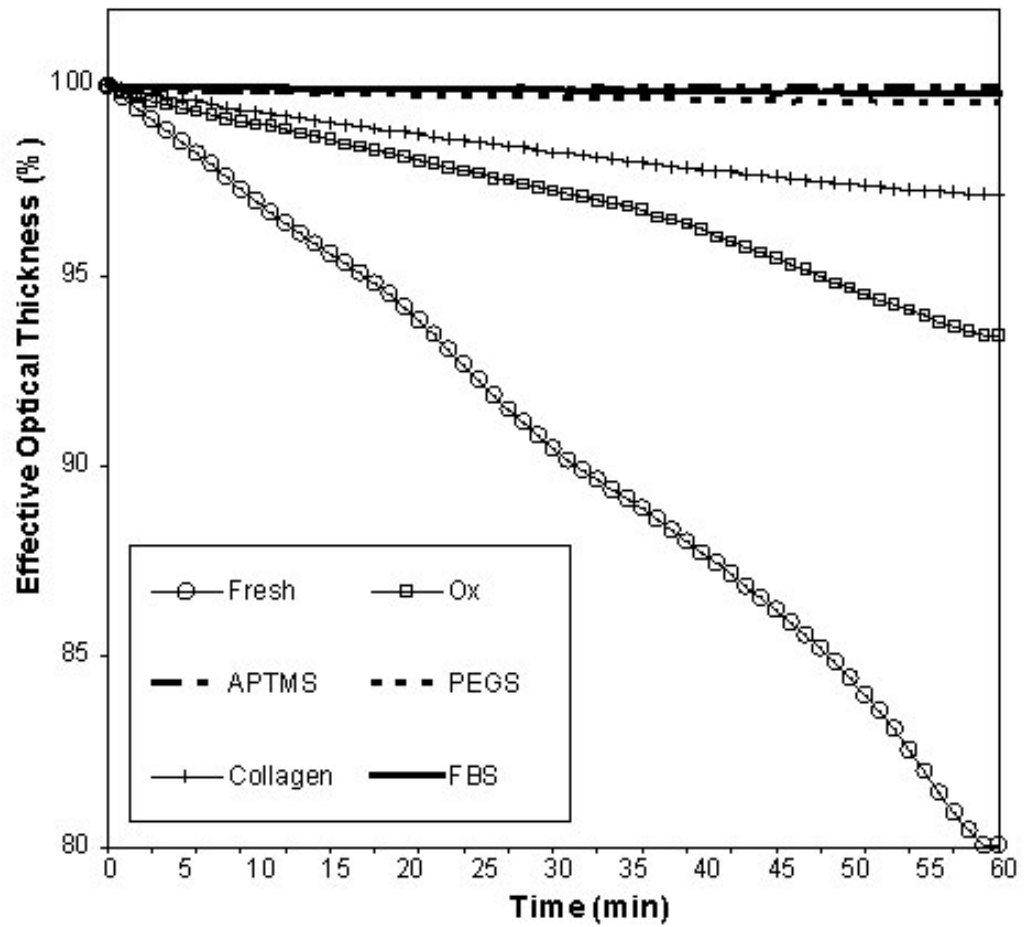
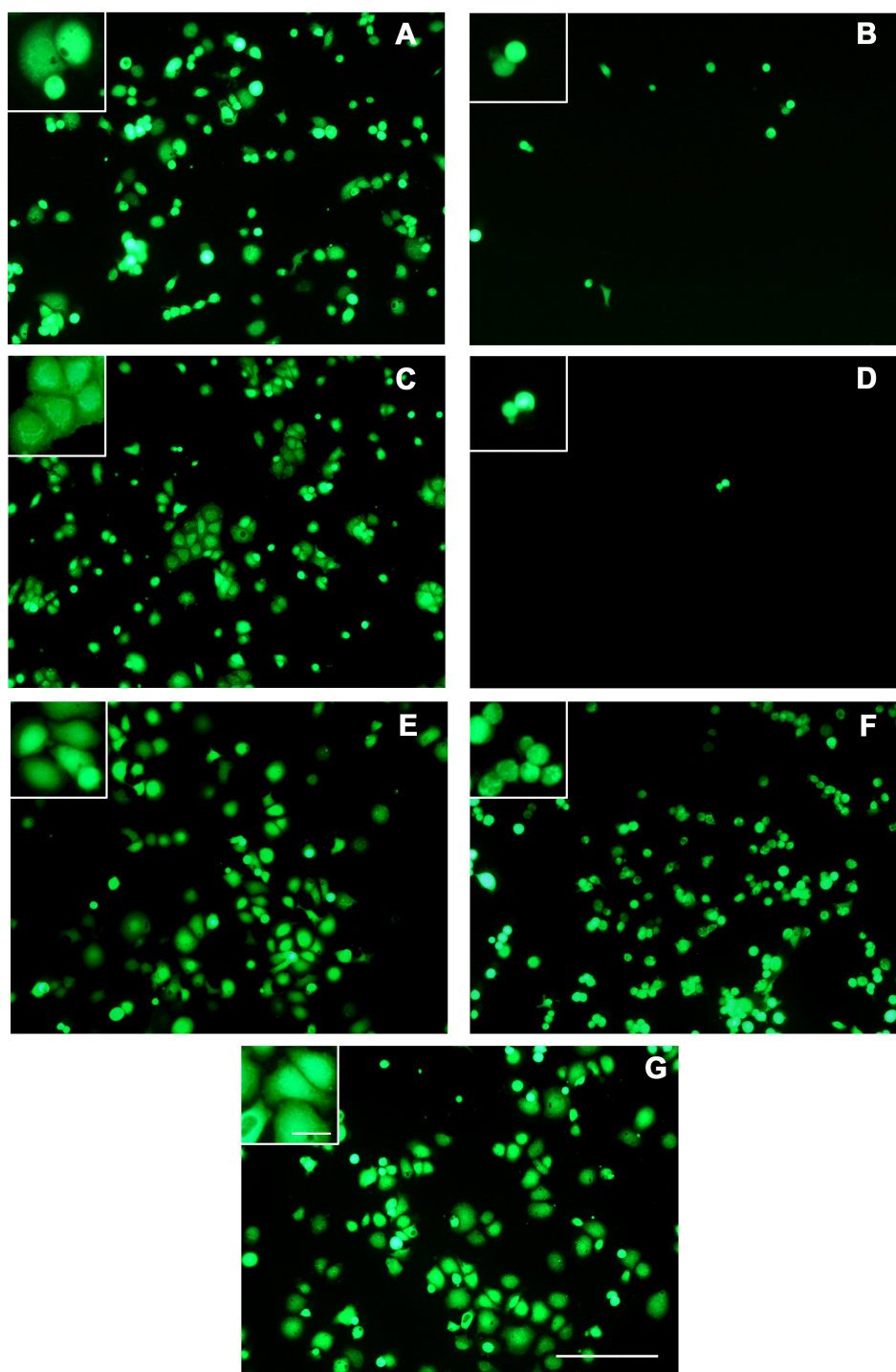


Figure 17 - Degradation slopes of freshly etched (Fresh), ozone oxidised (Ox), aminosilanised (APTMS), PEG functionalised (PEGs) porous silicon, collagen coated (collagen) and FBS coated (FBS) pSi in PBS (pH 7.4) using interferometric reflectance spectroscopy. Data were normalised to represent difference in effective optical thickness in reference to the initial effective optical thickness.

## **2.7. Cell Attachment and Morphology**

We used two mammalian cell lines, rat pheochromocytoma (PC12) and human lens epithelial (HLE) cells for comparative purposes. HLE cells are capable of completing cell attachment within 30 minutes of culture and can attach to ECM coated surfaces in the absence of serum <sup>[131]</sup>. PC12 cells, a neuronal-like cell line, are serum sensitive and have a longer attachment period, though this period can be reduced if surfaces are treated with ECM proteins <sup>[132]</sup>. We examined cell attachment to various surface-modified porous silicon substrates and compared the results with cells cultured on glass surfaces after a period of 4 hours. Cells were stained with the vital dye FDA to observe cell adherence and cytoplasmic spreading. The morphologies of PC12 and HLE cells on surface modified porous silicon are shown in Figure 18 and Figure 19 respectively.



**Figure 18 – Attachment studies showing PC12 cells cultured for 4 hours on surface modified pSi. Cells were stained with FDA. A: freshly etched, B: ozone oxidised, C: APTMS, D: PEGS, E: collagen coated, F: FBS coated and G: glass coverslip. Cells on APTMS and collagen coated surfaces have similar morphology to the glass surface. Scale: main image – 200 μm; inset – 30 μm.**

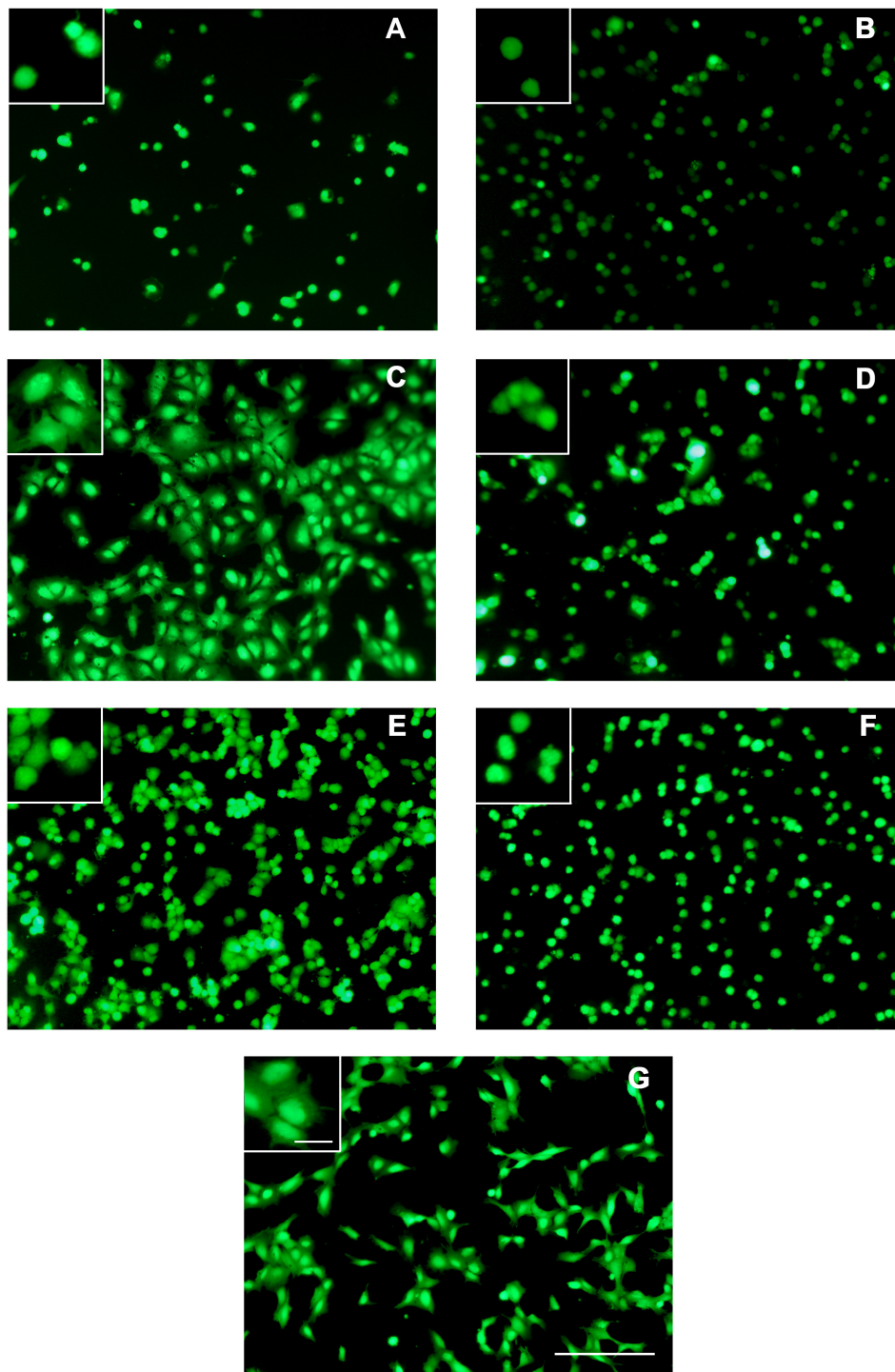


**Figure 19 - Human lens epithelial (HLE) cells cultured for 4 hours on surface modified pSi. Cells were stained with FDA. A: freshly etched, B: ozone oxidised, C: APTMS, D: PEGS, E: collagen coated, F: FBS coated and G: glass coverslip. Cells on APTMS and collagen coated surfaces have similar morphology to the glass surface. Scale: main image – 200  $\mu\text{m}$ ; inset – 30  $\mu\text{m}$ .**

## *Chapter 2: Results and Discussion*

On the glass surface, HLE cells were elongated and displayed cytoplasmic extensions that resulted in an overall polygonal shape, whereas PC12 cells exhibited smaller cytoplasmic projections (Figure 18G and Figure 19G). Few cells adhered to freshly etched porous silicon, but some cell spreading was observed, whereas PC12 cells formed aggregates on the surface. Although oxidation stabilised porous silicon films significantly, our results showed that the highly hydrophilic surface did not support PC12 cell attachment (Figure 18), in accordance with results reported by others <sup>[112]</sup>. Whilst the hydrophilic surface discourages protein adsorption of most serum proteins present in the cell culture medium <sup>[113]</sup>, HLE cells were found to attach to the oxidised surface to a certain extent (Figure 19). Published data have shown that HLE cells require only 1% serum present in the medium to attach <sup>[123]</sup>. Serum concentrations used in this study were at 10%.

Silanisation with 3-aminopropyltrimethoxysilane (APTMS) encouraged cell attachment, resulting in a significant number of PC12 and HLE cells attached to the APTMS porous silicon surface (Figure 18C and Figure 19C). These cells also showed morphology that was similar to cells cultured on a glass coverslip. This was in accordance with a published study showing amine capped surfaces promoting cell attachment <sup>[113]</sup>. The amine groups present on the surface produce a net positive charge. It has been demonstrated that positively charged surfaces enhance cell attachment, even in serum-free conditions <sup>[133]</sup>. There is also evidence that negatively charged surfaces, such as oxidised surfaces, also promote cell attachment <sup>[134]</sup>. Therefore surface charge alone does not influence cell attachment, it is a combination of increased wettability (hydrophilicity), positive surface charge of the APTMS surface and surface functional groups that result in increased cell attachment.

We also silanised oxidised porous silicon with N-(triethoxysilylpropyl)-O-polyethylene glycol urethane (PEGS) with 4-6 ethylene oxide repeating units, to introduce short polyethylene glycol (PEG) brushes on the surface. PEG is commonly used in biomaterials to present a non-fouling surface to prevent undesired reactions with the immune system, and has been shown to reduce cell attachment <sup>[113, 135]</sup>. Dense PEG

## *Chapter 2: Results and Discussion*

films are known to provide an interfacial barrier that prevents proteins from interacting with the underlying substrate due to steric exclusion and steric stabilisation effects <sup>[118]</sup>. When porous silicon was surface modified with PEGS, the result was a significant reduction of cell attachment for both cell lines. This was expected, though again, more HLE cells attached to this surface in comparison to PC12 cells. The few PC12 and HLE cells that did attach were rounded and little cytoplasmic spreading was observed. Although the presence of a PEG layer on porous silicon was confirmed by FTIR and contact angle analyses, we could not exclude the possibility of pinholes in this coating.

We showed that although oxidised porous silicon was more hydrophilic than PEGS porous silicon, the latter surfaces were more effective in preventing cell attachment. This implies that the non-fouling nature of PEG was not due to its hydrophilicity alone, but could also be attributed to the high surface mobility of PEG chains in the grafted film and to the entropic forces that prevented proteins and other biomolecules from attaching to the surface <sup>[136]</sup>.

Both PC12 and HLE cells have been reported to attach to collagen-coated surfaces faster than to tissue culture plastic <sup>[131, 132]</sup>. Although oxidised porous silicon suppresses protein adsorption from the cell culture medium, our results showed that both cell lines attached quickly to collagen-coated oxidised porous silicon in high numbers, with PC12 cells showing cell morphology that was comparable to the control sample (Figure 18E & G). This suggested that this method of protein deposition improved cell attachment to the oxidised porous silicon. Pre-coating porous silicon with an FBS solution improved cell attachment for PC12 cells in comparison to the oxidised surface (Figure 18B & F). A slight increase in cell numbers on this surface over the oxidised surface was also observed with HLE cells (Figure 19F). Collagen-coating was shown to improve cell attachment to porous silicon to a greater extent than FBS-coating (Figure 19E).

## **2.8. Cell Viability Assays**

### **2.8.1. Alamar Blue**

To quantify attachment and viability of cells grown on surface modified porous silicon, we made use of two standard vitality assays; Alamar Blue and neutral red. Alamar Blue is a colorimetric assay that operates via enzymatic reduction of the dye by the metabolic activity of cells, presumed to be by the oxygen consumption of the cells. The neutral red assay is based upon the incorporation of the neutral red dye into the cell and subsequent trapping in lysosomes<sup>[137]</sup>.

Alamar Blue (resazurin, a phenoxazin-3-one dye) is commonly used in cell vitality assays as it is less toxic than tetrazolium salts, and hence allows for continuous culture after the addition of the dye. The cells reduce the Alamar Blue reagent (resazurin, a blue solution) into resorufin, a pink solution (Figure 20). The solution is read at two wavelengths to determine the concentration of the reduced form.

To determine the effect of the porous matrix alone in Alamar Blue solution, oxidised porous silicon wafers were incubated with Alamar Blue in the absence of cells (Figure 21). This resulted in absorbance readings that were greater than values obtained with cells grown on glass, the positive control. This effect was not seen on flat silicon, where absorbance readings were similar to the negative controls (cell culture medium in the absence of cells).

Cellular enzymatic reactions reduce blue resazurin to pink resorufin, which is completely reduced into colourless hydroresorufin by the action of intercellular dehydrogenases<sup>[138]</sup>. Resazurin ( $E_o = +380$  mV) is a known electron acceptor and can be reduced by metabolic intermediates of NADPH or NADH coenzymes. Therefore, it should be obvious that resazurin is sensitive to the redox status of the chemical environment, for instance it has been shown to be reduced in the presence of other dyes<sup>[138]</sup>. Our results showed that in the presence of porous silicon and in the absence of cells, resazurin was reduced, as indicated by colorimetric detection of resorufin.

## *Chapter 2: Results and Discussion*

Porous silicon is easily oxidised and hydrolysed in aqueous solutions resulting in the formation of silicic acid <sup>[54]</sup>. The degradation mechanism of porous silicon, shown in **Section 1.2.2**, features the intermediate product of  $\text{HSi(OH)}_3$ , a reactive species which could reduce Alamar Blue. To determine if the reactive species released into solution was involved in reducing Alamar Blue, rather than a direct redox reaction between the porous silicon surface and Alamar Blue, an interferometric analysis was carried out.

In interferometric reflectance analysis, a baseline degradation slope was obtained using PBS. Once the slope was ascertained, Alamar Blue was introduced into the chamber. We observed a decrease in effective optical thickness immediately after Alamar Blue was added (Figure 22). This was attributed to the colour of the Alamar Blue solution causing a change in the refractive index. To demonstrate that Alamar Blue did not react directly with the porous silicon surface, a PBS solution was introduced into the chamber. If the porous silicon surface was being degraded by Alamar Blue, a shift in the baseline degradation slope would be expected. The results show that Alamar Blue did not cause an increase in the rate of porous silicon dissolution, and hence was not reacting with surface molecules. This result suggests that Alamar Blue was being reduced by a reactive species in solution, which we suspect is  $\text{HSi(OH)}_3$ . Substituted silane molecules such as trichlorosilane or triethylsilane are well known reducing agents <sup>[139, 140]</sup>, where the substituted species can lower the Si-H bond energy <sup>[141]</sup>.  $\text{HSi(OH)}_3$  might also act as a reducing agent.

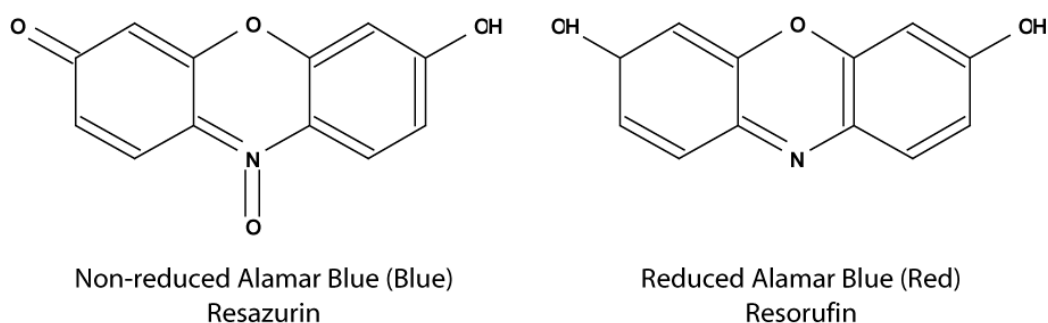


Figure 20 – Structure of Alamar Blue in its non-reduced and its reduced form

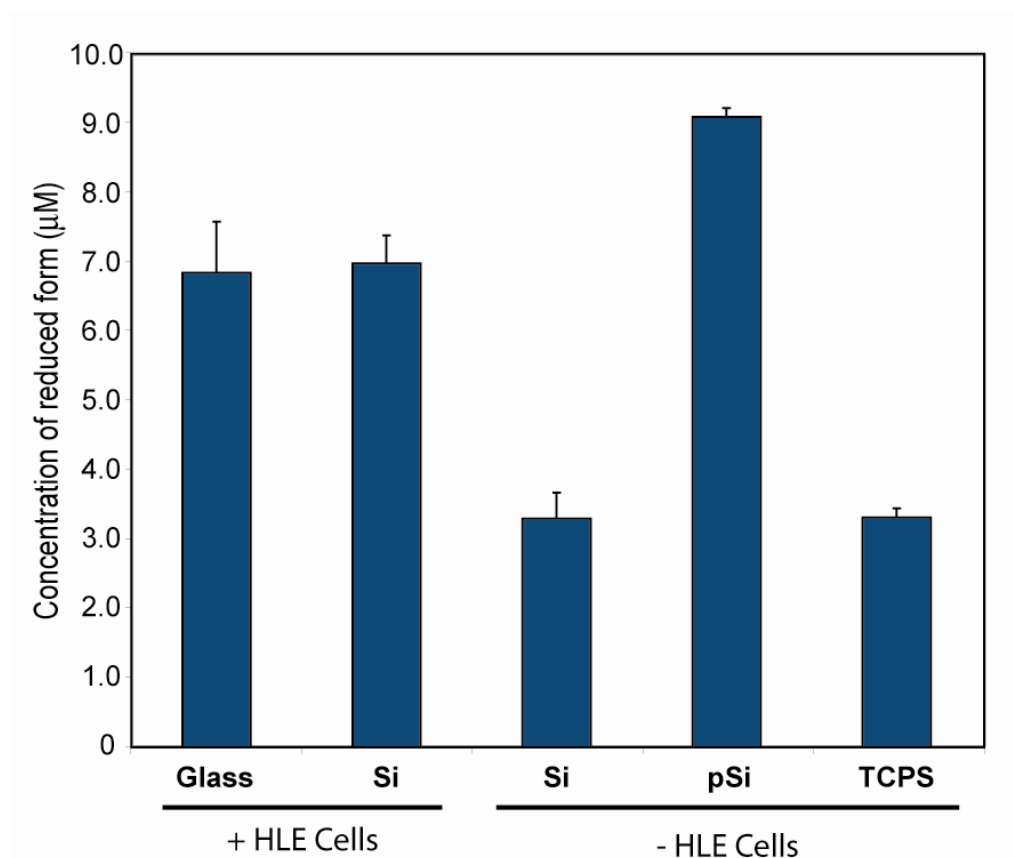
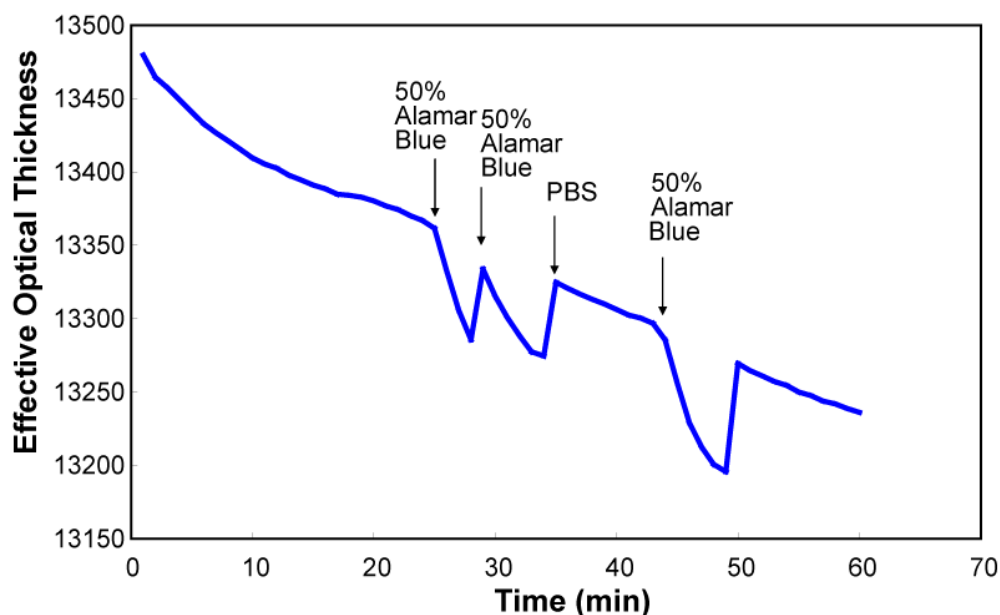


Figure 21 – Alamar Blue concentration of the reduced form after a 2 hour culture on various surfaces. As positive controls, HLE cells were cultured on glass and on flat silicon (Si), respectively in the presence of Alamar Blue. Flat silicon (Si), oxidised porous silicon (pSi) and tissue culture polystyrene (TCPS) represent surfaces incubated with Alamar Blue in the absence of cells. Bars represent standard deviation of the mean,  $n=2$ .



**Figure 22 – Interferometric reflectance spectroscopy of a 50% Alamar Blue solution in PBS with an ozone oxidised porous silicon sample. After the introduction of Alamar Blue, sharp drops in the effective optical thickness was observed and were attributed to the change in refractive index due to the colour of the Alamar Blue solution. Re-introduction of a PBS solution demonstrated that the baseline degradation rate had not changed, demonstrating that the Alamar Blue solution was not being reduced by surface molecules.**

If the products of porous silicon dissolution are able to reduce Alamar Blue, then forms of porous silicon that are protected against hydrolytic attack should not reduce Alamar Blue. This was tested by comparing the effect of a highly oxidised sample of porous silicon against a freshly etched sample with Alamar Blue. Freshly etched porous silicon would release more redox active species than an oxidised piece of porous silicon. Therefore a freshly etched piece of porous silicon should reduce the Alamar Blue solution faster than an oxidised piece of porous silicon due to the Si-H surface species making it susceptible to hydrolytic attack. A thick oxide layer on the porous silicon will prevent or reduce the rate of dissolution.

Ozone oxidation creates Si-OH surfaces, demonstrated by transmission FTIR analysis (Figure 23) and is represented by a broad band at  $3400\text{ cm}^{-1}$ , a SiO-H bending mode at  $1640\text{ cm}^{-1}$  and a Si-OH stretching mode at  $950$  and  $887\text{ cm}^{-1}$ . Oxidising porous silicon thermally increases the extent of oxidation for the porous silicon sample. Transmission

## *Chapter 2: Results and Discussion*

FTIR analysis showed a broad peak around  $1070\text{ cm}^{-1}$ , evident in both samples, which we attributed to the stretching modes of  $\text{SiO}_x$  species, in particular Si-O-Si <sup>[142, 143]</sup>. The appearance of a OSi-H stretching mode at  $2256\text{ cm}^{-1}$  is a characteristic of a thermally oxidised porous silicon surface <sup>[127]</sup>. The optical properties of thermally oxidised porous silicon had also changed. Whereas an ozone oxidised sample exhibited a dark brown surface, a thermally oxidised porous silicon surface was almost transparent.

Furthermore, we used interferometric reflectance spectroscopy to investigate the rate of change in the effective optical thickness (degradation rate) of the thermally oxidised porous silicon in comparison to an oxidised sample (Figure 24). The method to determine rate of change in effective optical thickness was stated in **Section 2.4.4**. The degradation rate of the thermally oxidised sample was reduced dramatically, indicating that a protective layer was indeed present on the surface of the porous silicon. In comparison to an APTMS sample of porous silicon, the thermally oxidised porous silicon had a similar rate of degradation over the 60 minute time period.

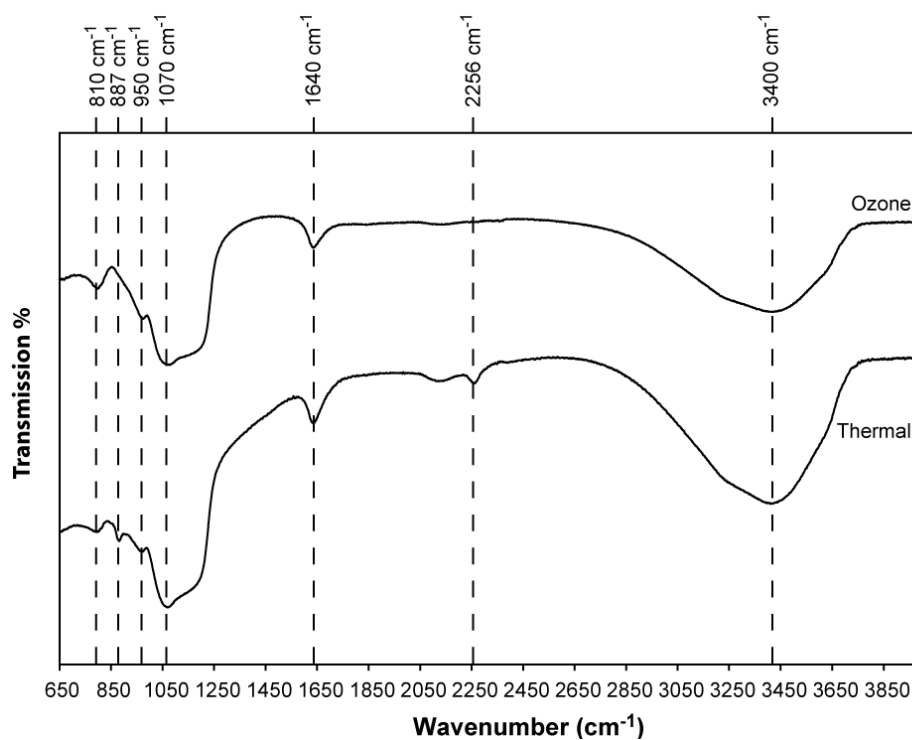
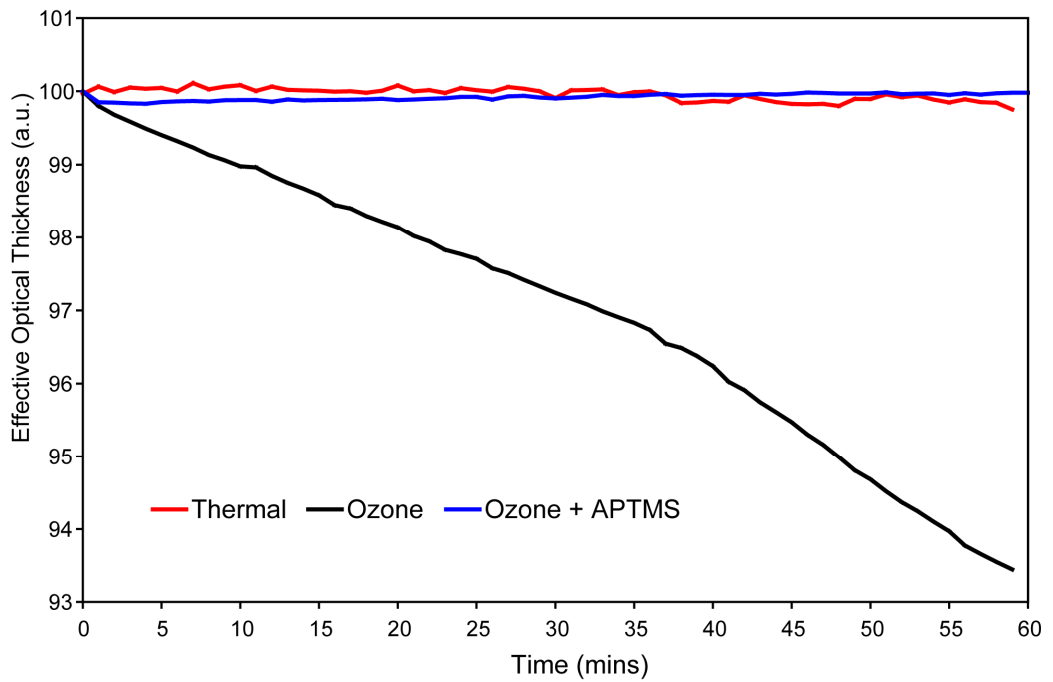


Figure 23 - Transmission FTIR spectra of ozone oxidised and thermally oxidised pSi.



**Figure 24 – Interferometric reflectance spectroscopy study comparing the rate of change in the effective optical thickness of a 600 °C thermally oxidised sample of porous silicon against an ozone oxidised and an ozone oxidised + APTMS sample of porous silicon. Data were normalised to show effective optical thickness in reference to the initial optical thickness.**

## *Chapter 2: Results and Discussion*

These results indicated that a thermally oxidised sample is less likely to undergo further oxidation in aqueous solution than an ozone oxidised sample, and this has also been shown in literature <sup>[128, 129, 144]</sup>. We further verified these results by culturing human lens epithelial cells on an ozone oxidised and a thermally oxidised sample of porous silicon. The cells were cultured on the porous silicon samples at a concentration of  $1 \times 10^5$  cells/well and were allowed to incubate for 24 hours. The cells were then stained with FDA for observation. The results (Figure 25) showed that cells did not attach to ozone oxidised porous silicon, in accordance with previous results of cells cultured on ozone oxidised surfaces (Figure 19). On the other hand, large numbers of cells were observed on thermally oxidised porous silicon. The cells on this surface had spread and showed morphology similar to the control sample (glass coverslip).

In light of these results, we expected a thermally oxidised sample of porous silicon to be less redox active, and hence, when a piece of thermally oxidised porous silicon was incubated with Alamar Blue, the Alamar Blue solution should not be reduced, or should be reduced to a lesser extent than a solution incubated with an ozone oxidised piece of porous silicon. To demonstrate this, an experiment was carried out using freshly etched, ozone oxidised and thermally oxidised pieces of porous silicon. Controls used were a piece of silicon dipped in HF (which removed the native oxide layer and creates a Si-H surface <sup>[145-147]</sup>), a piece of untreated silicon, a glass coverslip and tissue culture polystyrene (TCPS), as the experiment was conducted in a cell culture grade 24-well plate. All samples were sterilised by immersion in 70% (v/v) ethanol and allowed to air dry. The samples were then incubated with a 10% (v/v) solution of Alamar Blue in PBS in a 37 °C humidified incubator. Samples were incubated for 2 hours. 100 µl of solution was removed to be read on the plate reader (spectrophotometer).

The result of this experiment is shown in Figure 26. As expected, the freshly etched and ozone oxidised sample reduced the Alamar Blue solution, whereas the thermally oxidised porous silicon behaved similarly to the control samples (glass, silicon and TCPS). The silicon wafer dipped in HF only showed a small amount of Alamar Blue

## Chapter 2: Results and Discussion

reduction. Interestingly, the ozone oxidised sample showed a greater reduction of the Alamar Blue reagent. We attributed this to the increased hydrophilicity of the ozone oxidised sample, allowing rapid diffusion of fluid into the pores. Ozone oxidised porous silicon is still capable of degradation (Figure 24) and therefore is able to generate the reactive species that reduces Alamar Blue. As the ozone oxidised sample is more rapidly wetted, more redox active species might be produced initially in comparison to the freshly etched sample. In contrast, the thermally oxidised sample, which has a thick oxide layer, is well protected against hydrolytic attack and hence did not produce many reactive species and thus did not display a large reduction of the Alamar Blue product.

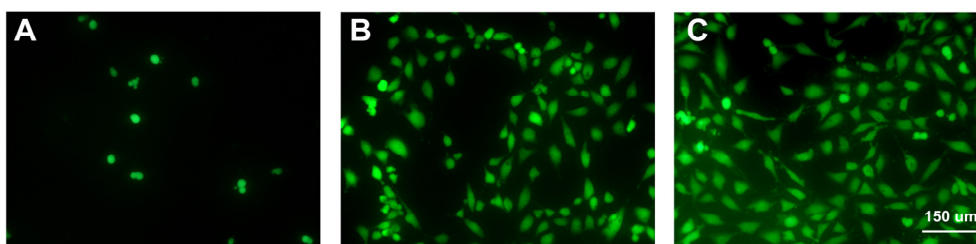


**Figure 25 – Human lens epithelial cells cultured on porous silicon for 24 hours and stained with FDA. A - Ozone oxidised, B - Thermally oxidised at 600 °C for 1 hour and C - glass control substrate. Scale represents 150 μm.**

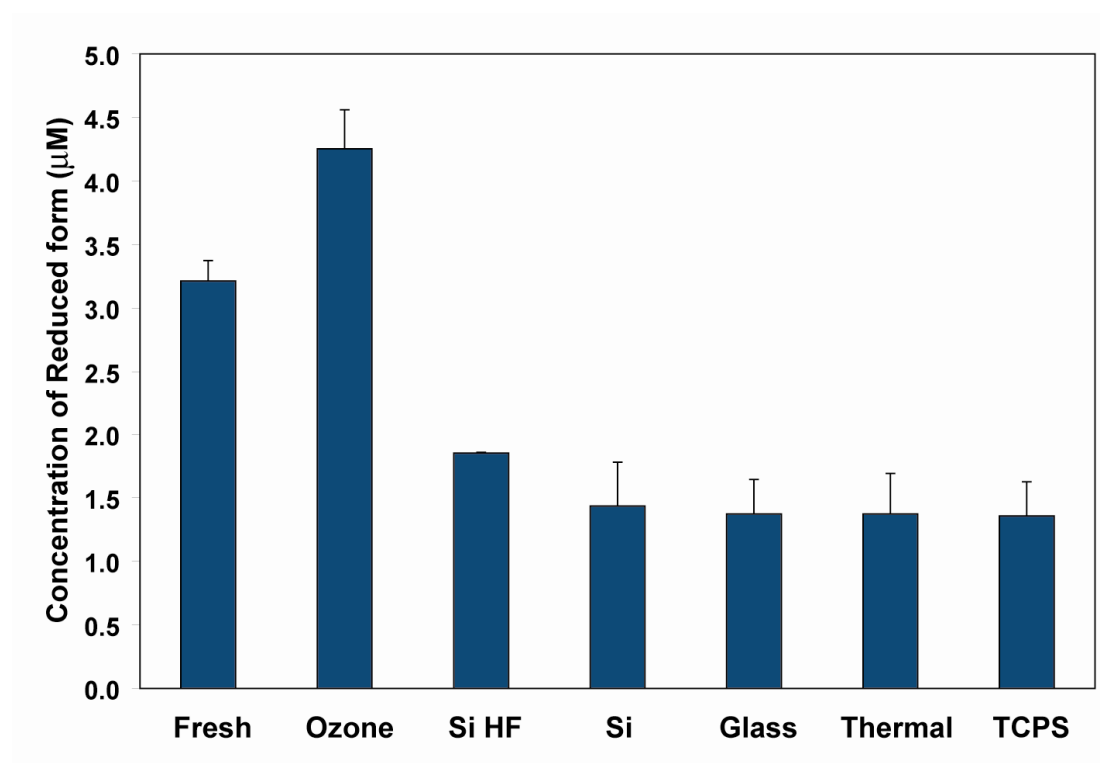


**Figure 26 – Alamar Blue incubated with freshly etched pSi (Fresh), ozone oxidised pSi (Ozone), silicon dipped in 25% HF (Si HF), silicon (Si), glass coverslip (Glass), 600 °C thermally oxidised pSi (Thermal) and tissue culture polystyrene (TCPS). A 10% Alamar Blue solution in PBS was incubated with the samples for 2 hours before a sample was taken for absorbance readings. Bars represent standard deviation of the mean.**

### **2.8.2. Neutral red**

Neutral red is a dye that is mainly taken up by cells by diffusion and becomes trapped within lysosomes. The accumulated dye can reach concentrations that are much higher than extracellular concentrations. The neutral red dye is a weak base, and is able to diffuse through membranes easily. When the dye enters the acidic environment of a lysosome, it becomes protonated and is then unable to diffuse through membranes<sup>[137]</sup>. Dead cells have lost membrane integrity and the dye is able to freely diffuse through the membranes, hence the dye does not accumulate within the lysosomes. This permits live/dead cell discrimination. The dye can subsequently be released from the cell by the use of a lysis solution and the absorbance of the released dye is then read

## *Chapter 2: Results and Discussion*

spectrophotometrically. We used a lysis solution recommended by the supplier, an aqueous acetic acid/ethanol mixture. We found high absorbance readings with the porous silicon surface in the absence of cells, even though extensive washing with PBS was performed (Figure 27). It is therefore likely that substantial amounts of the dye remained entrapped within the porous layer and could only be desorbed by the lysis solution, due to the ethanol in the lysis solution having a low surface tension<sup>[148]</sup>. The ethanol in the lysis solution was able to permeate the pores better than the PBS solution. The use of other known cell lysis solutions, for example, PBS containing 1% (v/v) Triton X-100 and PBS containing 1% (v/v) Triton X-100 and 0.5% (w/v) SDS, were not successful in dissolving the neutral red dye effectively, as crystal aggregates could still be observed.

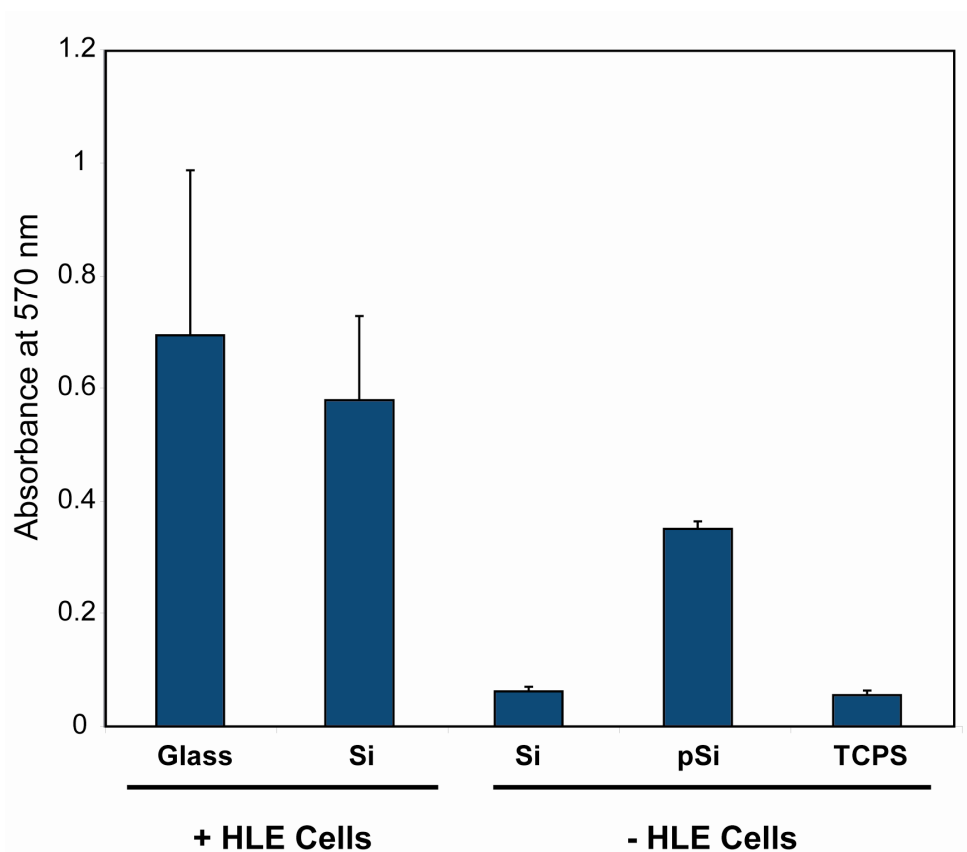


**Figure 27 - Neutral red absorbance readings after the addition of acidic alcohol lysis solution after a 2 hour culture on various surfaces. As positive controls, HLE cells were cultured on glass and on flat silicon (Si), respectively in the presence of neutral red. Flat silicon (Si), oxidised porous silicon (pSi) and tissue culture polystyrene (TCPS) represent surfaces incubated with neutral red in the absence of cells. Bars represent standard deviation of the mean,  $n=2$ .**

Whilst it might be possible to obtain background readings for the porous silicon surface in the absence of cells, which could be subtracted from samples cultured with cells, this does not seem an appropriate strategy, as the amount of dye trapped and incorporated in the pores will depend on several factors, such as surface area, wettability, charge and cell density, all of which can vary depending upon the surface modification used. An alternative, but relatively cumbersome method would be to use trypsin to remove and transfer the cells from the surface into a new vessel prior to the addition of the lysis solution.

## Chapter 2: Results and Discussion

Porous silicon has been shown to act as a reducing agent <sup>[149]</sup> and recently, porous silicon was demonstrated to reduce other viability reagents such as MTT (3-(4,5-dimethylthiazol-2-yl)-2,5-diphenyl-tetrazolium bromide) <sup>[150]</sup>. MTT also operates via enzymatic reduction <sup>[151]</sup>, and can be reduced by similar enzymes as Alamar Blue <sup>[152]</sup>. The tetrazolium salt is reduced to insoluble formazan crystals. The crystals require a solvent, such as DMSO (dimethyl sulphoxide), for spectrophotometric measurement <sup>[153]</sup>. XTT (2,3-bis(2-methoxy-4-nitro-5-sulphophenyl)-5-carboxanilide-2H-tetrazolium monosodium salt) and MTS (3-(4,5-dimethylthiazol-2-yl)-5-(3-carboxymethoxyphenyl)-2-(4-sulphophenyl)-2H-tetrazolium inner salt) are alternative assays that are reduced to a soluble formazan product, dismissing the requirement for a solubilisation step <sup>[154, 155]</sup>.

Bayliss *et al.* previously utilised the MTT and neutral red assays to quantify the viability of B50 and CHO cells on porous silicon after a 4 day culture <sup>[61]</sup>. They compared cell attachment between porous silicon, bulk silicon and a nano crystalline silicon surface. They also conducted cell counts on each of these surfaces using SEM. Their MTT and neutral red assay results did not correlate with their SEM results (Figure 28), where MTT and neutral red assays showed high cell viability results on porous silicon and low cell viability on bulk and nano crystalline silicon.

Their SEM counting results showed high cell numbers on bulk and nano crystalline silicon and low numbers found on porous silicon. The data indicated that the MTT and neutral red solution might react with the porous silicon surfaces and provide false positives, similar to the Alamar Blue results that we have presented here.

Table 1. Cell counts and standard deviation (SD) using MTT and NRU assays for B50 cells, and SEM for CHO and B50 cells, cultured on bulk silicon (wafer), mesoporous silicon (~10 nm pore size) and PECVD nanocrystalline polysilicon (annealed at 350°C) substrates.

B50					
Semiconductor material	MTT	MTT SD	NRU	NRU SD	
Porous silicon	119	5	141	3	
Bulk silicon	48	14	74	2	
Poly silicon	20	2	70	5	
		SEM cells mm <sup>-2</sup>			
Sample	B50	SD	CHO	SD	
Poly silicon	625	188	3000	515	
Bulk silicon	469	157	2140	368	
Porous silicon	260	63	1320	262	

Figure 28 – MTT, neutral red (NRU) and SEM counting results from Bayliss *et al.* (2000) [109].

## 2.9. Cell Counts

Since standard colorimetric vitality assays could not be used in conjunction with porous silicon, we resorted to cell counting as a means to quantify the number of cells on each surface. Cells were incubated on surface modified porous silicon for a period of 4 and 24 hours, stained with Hoechst 33342 and counted after both time intervals (Table 1). For PC12 cells, collagen-coated, freshly etched and APTMS surfaces had cell numbers that were similar to the control. FBS, oxidised and PEGS functionalised surfaces had cells counts that were significantly different to the control surface ( $p < 0.05$ ), indicating that cells adhered poorly to the surfaces. This applied to both 4 and 24 hour culture periods.

For HLE cells, at 4 hours, cell numbers were similar on all surfaces except for the PEGS functionalised surface (Table 1). At 24 hours, cell numbers were lower in comparison to the control except for the freshly etched surface, which was considered to be statistically similar. At 24 hours, significant degradation was evident on all surfaces, but especially on the freshly etched surface. Evidence of degradation was marked by the loss of colour in the porous region and the characteristic band

*Chapter 2: Results and Discussion*

formations (Figure 29), leaving only the base silicon remaining. Some colour was still present on the silanised surfaces.

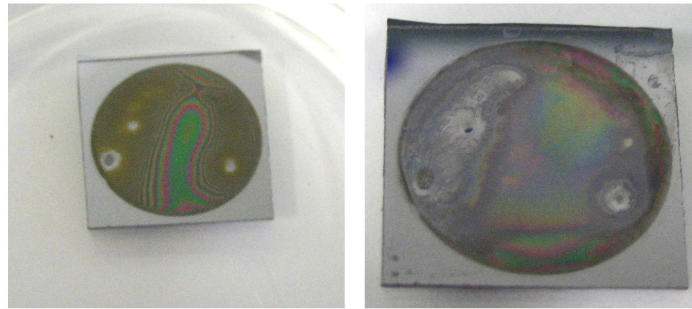


**Figure 29 – Images of a porous silicon wafer. Left: intact porous silicon layer, with characteristic bands of colour across the surface. Right: porous silicon layer has degraded, evident by loss of the bands and the loss of colour from the porous silicon layer.**

<b>4 hour</b>	<b>PC12 Cell Counts</b>	<b>Mean <math>\pm</math> SD</b>	<b>HLE Cell Counts</b>	<b>Mean <math>\pm</math> SD</b>
Fresh	548, 633, 600	<b>594 <math>\pm</math>43</b>	396, 349, 458	<b>401 <math>\pm</math>55</b>
Ox	9, 9, 19	<b>12 <math>\pm</math>6</b>	401, 400, 360	<b>387 <math>\pm</math>23</b>
APTMS	599, 680, 799	<b>693 <math>\pm</math>101</b>	497, 712, 528	<b>579 <math>\pm</math>116</b>
PEG	27, 24, 15	<b>22 <math>\pm</math>6</b>	140, 313, 347	<b>267 <math>\pm</math>111</b>
Collagen	836, 745, 738	<b>773 <math>\pm</math>55</b>	500, 634, 591	<b>575 <math>\pm</math>68</b>
FBS	259, 205, 83	<b>182 <math>\pm</math>90</b>	436, 475, 437	<b>449 <math>\pm</math>22</b>
Control	540, 575, 313	<b>476 <math>\pm</math>142</b>	504, 422, 566	<b>497 <math>\pm</math>72</b>

<b>24 hour</b>	<b>PC12 Cell Counts</b>	<b>Mean <math>\pm</math> SD</b>	<b>HLE Cell Counts</b>	<b>Mean <math>\pm</math> SD</b>
Fresh	555, 178, 1266	<b>666 <math>\pm</math>552</b>	75, 329, 386	<b>263 <math>\pm</math>166</b>
Ox	72, 27, 31	<b>43 <math>\pm</math>25</b>	187, 164, 41	<b>131 <math>\pm</math>79</b>
APTMS	987, 571, 1373	<b>977 <math>\pm</math>401</b>	300, 405, 421	<b>375 <math>\pm</math>66</b>
PEG	29,7,1	<b>12 <math>\pm</math>15</b>	100, 53, 26	<b>60 <math>\pm</math>37</b>
Collagen	1191, 1263, 911	<b>1122 <math>\pm</math>186</b>	149, 160, 302	<b>204 <math>\pm</math>85</b>
FBS	417, 290, 323	<b>343 <math>\pm</math>66</b>	188, 178, 121	<b>162 <math>\pm</math>36</b>
Control	1411, 1996, 1711	<b>1706 <math>\pm</math>293</b>	545, 615, 502	<b>554 <math>\pm</math>57</b>

**Table 1 - Cell counts of PC12 and HLE cells cultured on various surface-modified porous silicon surfaces for 4 and 24 hours. The cell counts are the sum of cells counted in 5 fields, each measuring 850  $\mu$ m x 650  $\mu$ m. Three replicates of each sample surface at each time point were conducted.**

## *Chapter 2: Results and Discussion*

Only on PEGS functionalised porous silicon were cell counts statistically different in comparison to the controls for both PC12 and HLE cells. Results from the fluorescence microscopy images of FDA stained cells were consistent with cell count data of both PC12 (Figure 18) and HLE (Figure 19) cells at 4 hours (Table 1) and at 24 hours.

Although cell counts for HLE cells incubated on the surfaces decreased after 24 hours, FDA images showed that on collagen and APTMS surfaces, cells displayed morphology similar to the control after a 4 hour incubation period. This demonstrated that collagen and APTMS can promote cell attachment and spreading, but do not necessarily support the growth and proliferation of HLE cells over time <sup>[131]</sup>. The results also demonstrated that different cell lines have different adhesion and growth characteristics. It may also be possible that the quick rate of degradation of the porous silicon may have had a detrimental effect on the adhesion of the cells, as cells were unable to form strong adherent bonds to a surface that is rapidly degrading.

## **Conclusions**

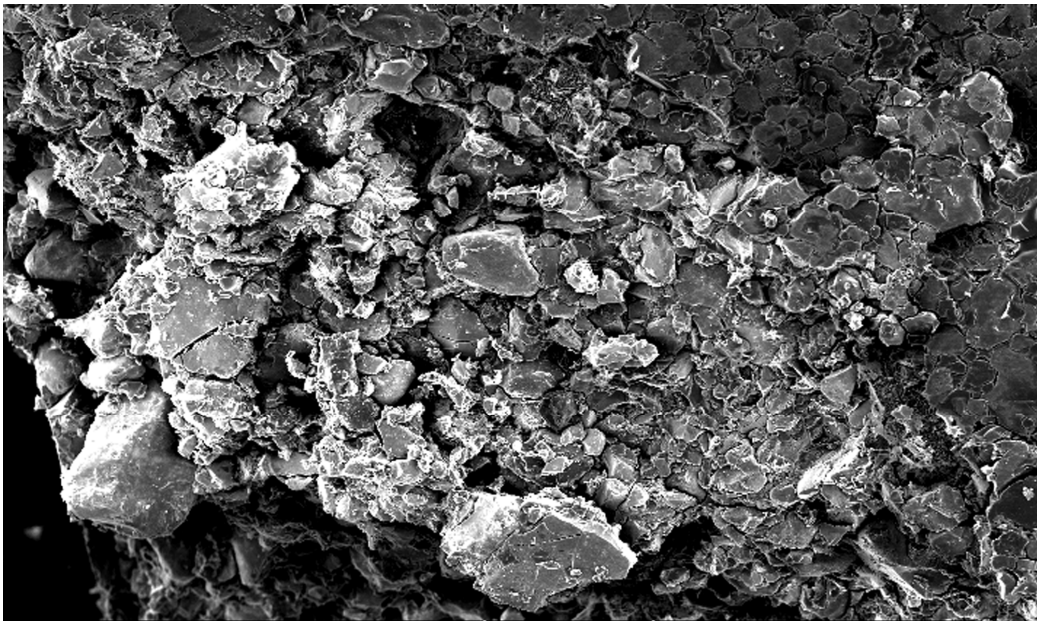
We have demonstrated that mammalian cells are capable of adhering to porous silicon surfaces. Silanisation of porous silicon stabilised the surface significantly and reduced its degradation in aqueous solutions. Aminosilanisation and coating the porous silicon surface with collagen enhanced cell attachment and spreading.

We showed that porous silicon is capable of acting as a reducing agent, therefore when redox based assays are used in conjunction with porous silicon, caution should be employed. The open pore structure of porous silicon also allows for the absorption of dyes over time. Hence dye based assays can be compromised when used with porous silicon. We have yet to investigate whether alternative assays, such as  $^3\text{H}$  thymidine or BrdU incorporation, are suitable for use with porous silicon.

The main result from this study was the determination of the surface modification that led to enhanced cell attachment. This was shown to be an aminosilanised or APTMS surface. This surface permitted the best cell attachment over a short and longer term period. A pressing issue is the stability of these surfaces. APTMS surfaces were shown to be stable for at least 24 hours, but considerable degradation was visible after this time period (marked by the loss of colour in the porous region).

## Chapter 3

### Porous silicon powder and pellets



*Scanning electron micrograph of the edge of a porous silicon pellet*

## Introduction

In the previous chapter, we described the evaluation of mammalian cell adhesion to porous silicon. This porous silicon was generated by etching a silicon wafer that was approximately 380 $\mu\text{m}$  thick, with hydrofluoric acid. The etching conditions used created a 2.2  $\mu\text{m}$  porous silicon layer above the silicon (Figure 30).

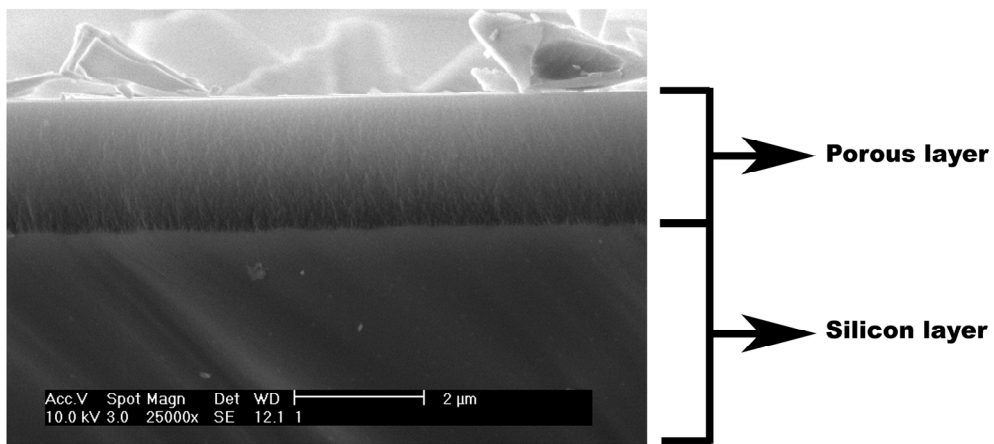


**Figure 30 – SEM image of porous silicon generated by anodic etching of silicon in hydrofluoric acid. Under these etching conditions, a porous layer can be clearly seen above a silicon layer.**

Production of porous silicon by this method creates a degradable layer (porous silicon) on top of a non-degradable layer (silicon). As a potential biomaterial, it is desirable that the whole material be able to undergo degradation. Therefore, a biomaterial consisting of only the porous silicon layer would be more suitable for many applications.

Free-standing porous silicon layers, from here on termed porous silicon membranes or membranes, were generated by pSiMedica, Malvern, Worcestershire, UK. These membranes were generated by anodic etching of silicon wafers in hydrofluoric acid to create a porous silicon layer over 150  $\mu\text{m}$  thick.

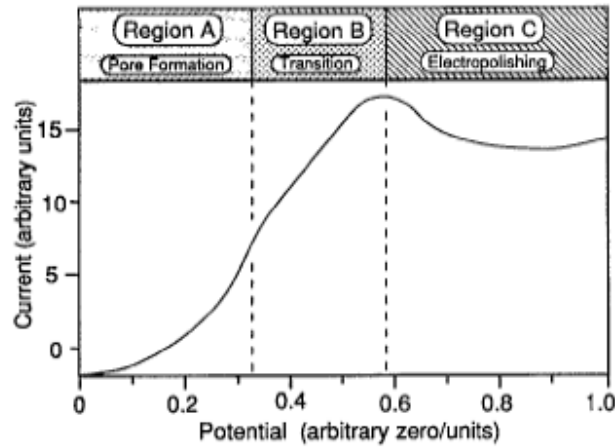


**Figure 31 – Typical current-voltage characteristics of p-type silicon in a HF solution. Region A: pore formation occurs at the chosen current density whilst in Region C, electropolishing occurs. Region B: is the transition between pore formation and electropolishing. Scale and units are arbitrary and depend upon the dopant density of the silicon and the concentration of HF. Taken from Smith and Collins (1992) <sup>[44]</sup>.**

This porous layer was then lifted off by increasing the current density beyond an electropolishing point, shown in Figure 31. At the electropolishing point, pore diameter increases at a faster rate than the pore depth evolution. This high current density creates pores that are so large that they start overlapping with each other, which allows the porous layer to be lifted off. A schematic of this procedure is shown in Figure 32.

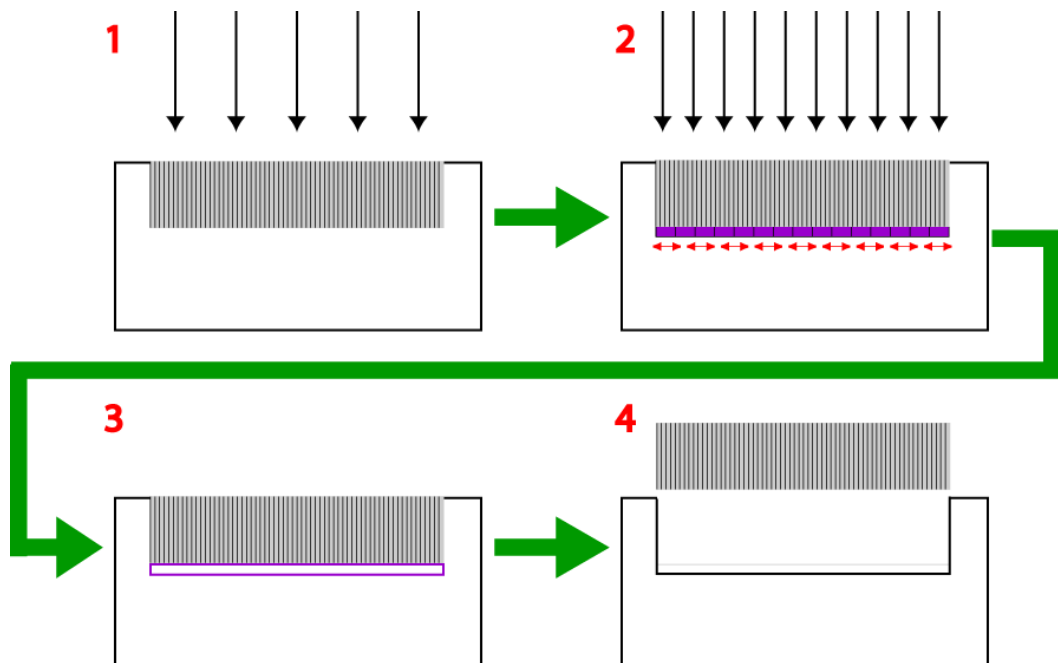


**Figure 32 – Generation of porous membranes. 1: A constant current is applied to generate the porous layer. 2: The current is increased to the electropolishing range, where the pore sizes become so large they overlap. 3: Electropolishing creates a gap between the porous layer and the bulk silicon below. 4: The porous layer can then be lifted off the silicon layer.**

The porous silicon membrane is capable of complete degradation into silicic acid and is therefore considered a more desirable substrate for biomaterial purposes than porous silicon on bulk silicon. The membrane can of course be surface-modified using a similar approach to that described in the last chapter in order to enhance cell attachment and to maintain the stability of the membrane in aqueous solutions.

The pores generated on the pSiMedica membranes were very small, approximately 40-60 nm in diameter. The diameter of a single mammalian cell is generally between 10 – 20  $\mu\text{m}$  or greater. When cultured on porous silicon, the material can almost be considered to be a 2-dimensional (2-D) substrate, where cells can only grow on the surface of the porous silicon. This is very different to the 3-dimensional (3-D) scaffold that cells are exposed to within the body, where the cells can grow and proliferate in the  $x$ ,  $y$  and  $z$  direction. Mimicking such a matrix would allow the cells to behave in a “normal” manner, where cell-cell contact and communication are important in determining cell polarity and differentiation <sup>[15]</sup>. Cells display different morphology

### *Chapter 3: Introduction*

within a 3-D scaffold and are known to align with and migrate along the scaffold structure <sup>[156]</sup>. In comparison to a 2-D scaffold, the cells are forced to utilise different migration strategies within a 3-D structure. In a 2-D environment, cells migrate using a succession of adhesion, contraction of the cell body towards the adhesion site, and de-adhesion of the lagging edge. In a 3-D environment, cells have to contend with matrix interactions, where they have to change their shape or even degrade the matrix in order to migrate or proliferate <sup>[16]</sup>, for example cells express matrix metalloproteinase proteins (which degrades matrix proteins) at higher levels when in a 3-D environment in comparison to a 2-D environment <sup>[15]</sup>. This in turn requires different cell signaling responses. Cells within a 3-D matrix are also known to have upregulated or downregulated signaling pathways in comparison to a 2-D matrix, such as the focal adhesion kinase signaling pathway <sup>[15]</sup>. Focal adhesions are found at the cellular surface and interact with extracellular matrix proteins. The focal adhesion kinase pathway is downregulated in 3-D matrices <sup>[15]</sup>. Along with extracellular matrix proteins, the 3-D micro- and nano-structure can have a profound effect upon directing the differentiation of immature cells down a certain pathway <sup>[14]</sup>. An example of this are collagen gels, where “stressed” and “relaxed” formations of the gels have different effects upon cell behaviour <sup>[15]</sup>. Creating such a biodegradable 3-D scaffold would more closely mimic the natural organisation of tissue, where we would be able to culture cells without inducing a directional bias through the presentation of planar surfaces.

Our goal was to generate porous silicon particles produced from porous silicon membranes, and to bind the particles together, forming a 3-D scaffold. During the binding of the particles, a leachant (such as sugar) would be added, and large void spaces would be left between the porous silicon particles upon extraction of the leachant. Hence, we would obtain a scaffold that is degradable, due to its porous silicon component, and is able to accommodate the in-growth of cells into the structure.

In 2006, an article by Barraclough *et al* reported the construction of a silicon pellet without the need for a binding agent <sup>[157]</sup>. The authors used “activated” silicon particles which were placed in a cast and pressed at pressures ranging from 100 -1000 MPa,

### Chapter 3: Introduction

resulting in a stable pellet (Figure 33). “Activated” silicon was made by adding a 20% (w/w) hydrofluoric acid solution in ethanol to the silicon particles. The hydrofluoric acid stripped the native oxide ( $\text{SiO}_2$ ) layer off the silicon particles, leaving a more chemically reactive hydride terminated surface. During the compaction process,  $\text{SiH}_4$  gas was detected, indicating that the pressures used for the compaction were sufficient to break Si-H bonds and forming Si-Si bonds in the silicon particles. This process resulted in strong particle bonding. If, on the other hand, an untreated powder was used (silicon not exposed to hydrofluoric acid), then the main binding interaction was attributed to the formation of crosslinking Si-O bonds from the native  $\text{SiO}_2$  layer on the particle surfaces. This was confirmed by exposing the pellet made from untreated silicon particles to hydrofluoric acid, which resulted in the immediate breakdown of the pellet structure since the hydrofluoric acid dissolves the  $\text{SiO}_2$  layer. In contrast, a pellet made from “activated” silicon particles was able to withstand the acid solution for a longer period <sup>[157]</sup>.

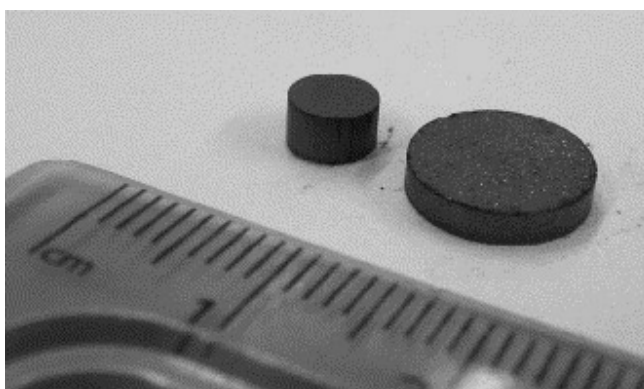


**Figure 33 – Pellets made from silicon particles that had been pretreated with HF. Reproduced from Barraclough *et al*, 2007 <sup>[157]</sup>**

If a pellet can be constructed using silicon, it should be possible to construct a pellet using porous silicon. This would enable us to create a 3-dimensional substrate that is degradable. Leaching agents such as glucose and glycine, common components of cell culture medium could be added to the pellet to generate the 3-D environment.

### *Chapter 3: Introduction*

The aims of the work to be presented in the following chapter are:

- to generate stable pellets from powdered porous silicon using various biocompatible binding agents and lubricants;
- to investigate the potential of a porous silicon pellet as a biomaterial;
- to investigate the bioactivity of different derivatives of porous silicon powder.

## **Porous Silicon Powder**

The experiments relating to the production of porous silicon pellets were conducted at pSiMedica in Malvern, Worcestershire, UK, under the supervision of Dr. Armando Loni and Professor Leigh Canham.

The pellets were taken to Australia to conduct investigations into the stability of the porous silicon pellets in cell culture medium. Preparation of individual starch, glycine, stearic acid, thermally oxidised and aminosilanised porous silicon powders were prepared at Flinders University, South Australia. Subsequent cell culture studies were also conducted at Flinders University.

## **Methods and Materials**

### **3.1. Chemicals**

Glycine, D+/- glucose and stearic acid were purchased from Sigma Chemical Company, St Louis, MO, USA. Starch 1500 was purchased from Colorcon Ltd, Dartford, Kent, UK. Silicon powder (~325  $\mu\text{m}$  mesh) was purchased from Sigma Chemical Co. Pure cod liver oil was obtained from local sources.

Dulbecco's modified Eagle's medium (DMEM), fluorescein diacetate and penicillin/streptomycin solution were obtained from Sigma Chemical Company, St Louis, MO, USA. Foetal Bovine Serum (FBS) was purchased from Bovogen Biologicals Ltd, Essenden, Vic, Australia. L-glutamine and Hoechst 33342 were purchased from Invitrogen, Carlsbad, CA, USA. Alamar Blue was purchased from Biosource International, Camarillo, CA,

### **3.2. Porous Silicon Powder**

Porous silicon membranes (BioSilicon™) were prepared by Dr Armando Loni at pSiMedica, Malvern, Worcestershire, UK. Membrane thickness was approximately 150 µm with porosity of approximately 68 – 70%.

Porous silicon powder was prepared by crushing the membranes using a ball mill. The powder was subsequently classified by High Force Research (Bowburn, Durham, UK), as containing microparticles with 20 – 60 µm dimensions.

### **3.3. Pellet Formation**

For the pellet production, porous silicon powder was thermally oxidised at temperatures above 300 °C (our facilities enabled us to only measure temperatures up to 300 °C). Thermal oxidation was shown in **Section 2.8.1** to stabilise the surface of porous silicon for cell adhesion and attachment. The oxidised powder was then silanised using a 50 mM solution of 3-aminopropyltrimethoxysilane in toluene for 5 minutes with occasional agitation. This surface modification was shown in **Section 2.7** to promote cell attachment. The powder was then filtered through a PTFE (polytetrafluoroethylene) filter and washed several times with toluene to remove excess silane. The powder was finally allowed to air dry.

#### **3.3.1. Leaching agents**

D+/- glucose was hand milled using a pestle and mortar, and was then sieved to a range of sizes; from >150 µm, >150 µm <75 µm, <75 µm. Glucose was mixed with the aminosilanised porous silicon particles at concentrations ranging from 10% (w/w) to 50% (w/w).

Glycine, electrophoresis grade, was hand milled and sieved to a range of sizes; from >150 µm, >150 µm <75 µm, <75 µm. Glycine was mixed with the aminosilanised porous silicon particles at concentrations ranging from 10% (w/w) to 50% (w/w).

### **3.3.2. Binding agent and lubricating agents**

Starch 1500 was added to the porous silicon powder between concentrations of 10% (w/w) and 25% (w/w) of the total pellet volume.

Lubricating agents were required to assist with the ejection of the pellet from the cast. Cod liver oil and stearic acid were both tested. Cod liver oil was used to coat the interior of the chamber and stearic acid was added to the porous silicon powder at concentrations ranging from 1% (w/w) to 10% (w/w).

### **3.4. Die Cast and Press**

The die cast consists of 5 components: the base, the chamber, the lower end cap, the upper end cap and the plunger (Figure 34). All components are thoroughly cleaned with ethanol before each press. The chamber is inserted into the base before the lower end cap is inserted into the chamber; this is then followed with 100 mg of powdered material. The upper end cap is then inserted followed by the plunger. The plunger provides an even pressure across the pellet when inserted into the press.



**Figure 34 – Left Panel: The die cast and its components. From top to bottom: Plunger, chamber, upper end cap, lower end cap and the base. Centre Panel: The assembled die cast. Right Panel: The base is removed and the cast inverted to push the pellet out of the chamber.**

The press (Rondol Technology Ltd., UK) is a hand operated hydraulic press. The cast was inserted into the centre of the press and forces between 20 kN to 45 kN were applied for a minimum of 5 mins. To eject the pellet, the base was removed and the cast was inverted (so the plunger is at the bottom) and placed back into the press to eject the pellet (Figure 34, Right Panel).

### **3.5. Pellet Compositions**

Each pellet consisted of 100 mg of powdered material. Studies were conducted on different combinations of aminosilanised porous silicon, leaching agents, binding agents and lubricating agents. The combined powder was then mixed in a rotary mixer for a minimum of 30 minutes to ensure a homogeneous composition. This mixed powder material was then loaded into the press.

### **3.5.1. Pellet fabrication from silicon powder**

Initially, the aim was to be able to repeat the experiment conducted by Barraclough *et al* <sup>[157]</sup> by producing a silicon powder pellet. Silicon powder with a particle diameter of 325  $\mu\text{m}$  was used for this experiment. To facilitate better compaction, some of the silicon powder was micronised (ball-milled to a smaller size) and mixed with the larger powder size at a ratio of 90% (w/w) micronised powder to 10% (w/w) non-micronised silicon powder in a rotary mixer for 30 mins.

Before compaction, the native oxide layer of the silicon powder was removed by immersion in 50% (vol/vol) HF with ethanol added as a surfactant. This created a silicon hydride-terminated surface layer which is known to assist in the binding of the silicon powder <sup>[157]</sup>. After the immersion in HF for 5 mins, the powder was filtered through a PTFE membrane and washed with ethanol and methanol to remove residual HF. The powder was then allowed to air dry. 100 mg of the silicon powder was used for each pellet and was compacted at 20 kN, 30 kN, 35 kN and 40 kN, with the force being held for 5 mins.

### **3.5.2. Pellet fabrication from oxidised porous silicon powder**

Porous silicon membranes were ball milled into a powdered form and classified by High Force Research Ltd (Bowburn, Durham, UK) to sizes ranging from 20  $\mu\text{m}$  to 60  $\mu\text{m}$ . The porous silicon had an approximate porosity of 70% and an average diameter of 35  $\mu\text{m}$  (Figure 35).

The porous silicon powder was thermally oxidised at temperatures above 300 °C on a hotplate for 1 hour. We investigated the compaction ability of oxidised porous silicon powder. Some lubrication was required as the pellet could not be ejected easily. Cod liver oil was tested as a lubricating agent and used to lubricate the walls of the chamber before loading the oxidised porous silicon powder into the chamber. Cod liver oil was applied to the inner surface of the cast and the end caps using a cotton bud. Stearic acid

was also tested as a lubricating agent and was added to the powder composition at 1% (w/w).

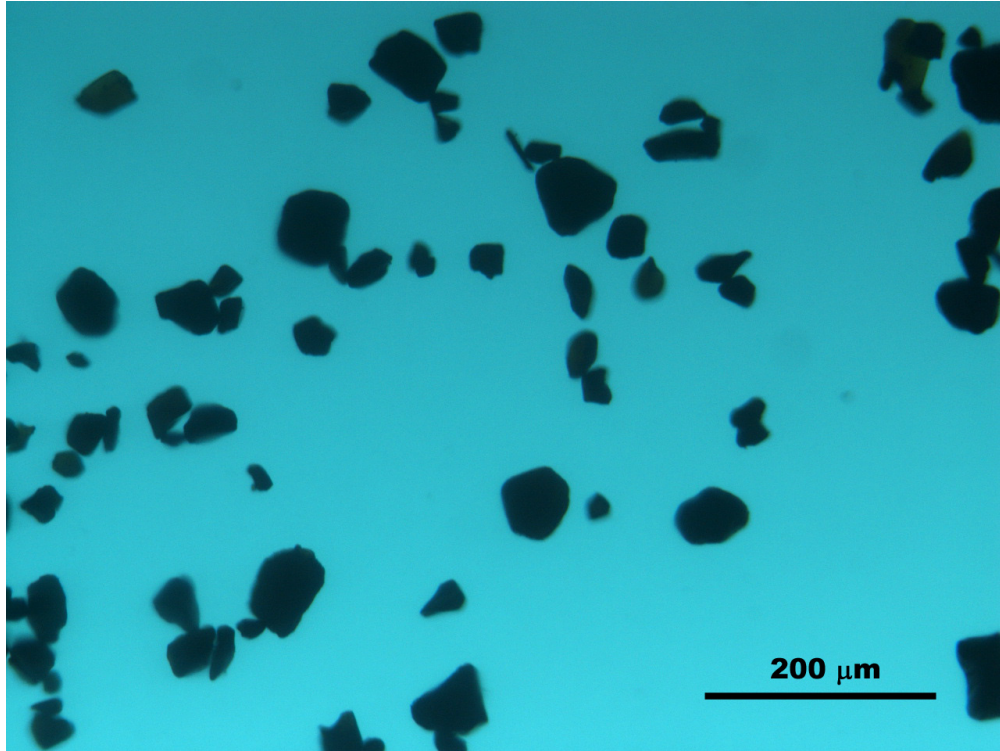


**Figure 35 – Porous silicon powder as seen under a light microscope. Dimensions of the particles range from 20 – 60  $\mu\text{m}$ . Scale: 200  $\mu\text{m}$ .**

### ***3.5.3. Pellet fabrication from silanised porous silicon powder***

Silanised porous silicon powder was first compacted without any additives. Lubrication was also required for the ejection of the pellet. Cod liver oil and stearic acid were used in the same fashion as described in **Section 3.5.2**.

## **3.6. Cell Culture Studies**

### ***3.6.1. Pellet composition used for cell culture studies***

All pellets used for cell culture studies contained 10% (w/w) glycine, 10% (w/w) stearic acid, 20% (w/w) starch and 60% (w/w) aminosilanised porous silicon powder. The

pellets were pressed at 35 kN for 5 mins. Pellets were heat treated by incubation at 160 °C for a minimum of 6 hours. Pellets were prepared for SEM by coating with a thin layer of platinum. Images were obtained using a Philips XL30 operating at 10 keV.

### **3.6.2. Pellet stabilisation after pressing**

#### **3.6.2.1. Glutaraldehyde and gelatin encapsulation**

For cell culture studies, pellets were tested for their stability in aqueous solutions by immersion in 4 ml of dH<sub>2</sub>O. The pellets were used without any further modification after pressing, and were shown to be stable for 2 days in water at room temperature. To further increase their stability, two methods were tested.

Firstly, as the pellets contained glycine and aminosilanised porous silicon, glutaraldehyde was added to the pellet as a cross-linking agent. Glutaraldehyde might bind the particles together by cross-linking amine groups. A 10% (v/v) glutaraldehyde solution in water was added to the pellet, but the pellet showed signs of disintegration immediately after immersion. Pre-treatment of the pellet by heat-treatment at 160 °C for 6 hours, allowed the pellet to maintain its structure when immersed in the glutaraldehyde solution for 1 minute. The pellet was then allowed to air dry completely.

The second stabilisation method tested was gelatin encapsulation. A 10% (w/v) solution of gelatin was made in MilliQ water. The solution was heated and stirred to dissolve the gelatin granules. Heat-treated (160 °C) pellets were dipped in the gelatin solution to provide an outer coating on the pellet. The pellets were then allowed to air dry completely.

### **3.6.2.2. Stability in cell culture medium**

The pellets made in **Section 3.6.2.1** were tested for their stability in cell culture medium. Heat-treated (160 °C) pellets, glutaraldehyde-linked pellets and gelatin-coated pellets were tested for their stability in DMEM containing 10% (v/v) FBS, 2 mM L-glutamine, 100 IU/ml penicillin and 100 µg/ml streptomycin. The pellets were incubated in 3 ml of cell culture medium for 24 hours at room temperature. Images were taken during this time period.

### **3.6.3. Cell culture on pellet**

Human lens epithelial cells were cultured on 160 °C heat-treated pellets (from **Section 3.6.1**) for 1 hour. One pellet was added to 1 ml of cell culture medium containing 100,000 cells/ml, another pellet had 100,000 cells/100µl spotted onto the surface of the pellet only. As a control, a glass coverslip was used. The cells were incubated at 37 °C for 1 hour.

For visualisation, an FDA stain was utilised and added to the samples at a concentration of 10 µg/ml in PBS. The samples were stained for 10 minutes at 37 °C, before the staining solution was removed to reduce background fluorescence. Due to the fragile nature of the pellets, extensive washing of the samples with PBS to remove background fluorescence could not be conducted. The cells were observed with a Leitz Laborlux II fluorescence microscope equipped with a Nikon DS-L1 digital camera.

## **3.7. Indirect Cell Viability Assay**

### **3.7.1. Indirect viability assay of pellet components**

To identify if any component within the pellet structure was reducing cellular viability, another indirect viability utilising each individual component within the pellet was conducted.

### *Chapter 3: Methods and Materials*

Starch, glycine, stearic and aminosilanised porous silicon powder were all incubated individually in 3 ml of cell culture medium at their corresponding amounts within the 100 mg pellet (**Section 3.6.1**). Therefore, 20 mg of starch, 10 mg of glycine, 10 mg of stearic acid and 60 mg of either aminosilanised porous silicon, untreated porous silicon or thermally oxidised (600°C for one hour) porous silicon were incubated with 3 ml of cell culture medium in separate containers overnight at 37 °C. The powders were all sterilised by dry heat at 160 °C overnight before their incubation. As a control, a piece of silicon wafer was used (3-6 Ω·cm, boron doped).

In a 24 well plate, human lens epithelial cells were seeded at a density of 50,000 cells/well. The cells were allowed to attach overnight and the cells were washed twice with sterile PBS before further use.

The 3 ml of medium that was incubated with the pellet components was centrifuged at 7000 g to pellet any remaining particles. 1 ml of the supernatant was then placed onto the cells and was incubated for 24 hours at 37 °C. After this incubation step, the medium was removed from the wells, the cells were washed with sterile PBS three times and a 10% (v/v) solution of Alamar Blue in fresh cell culture medium was placed in each well at a volume of 0.5 ml. The cells were incubated for 2 hours at 37 °C. 100 µl of each solution was removed and placed into a 96 well plate for spectrophotometric analysis at 570 nm and 600 nm.

### **3.8. Statistical Analysis**

Statistical analysis was conducted using KaleidaGraph software version 4.02 (Synergy Software, Reading, PA, USA). An independent *t*-test was performed on all samples against the positive control, considering  $p \leq 0.05$  as statistically significant.

## **Results and Discussion**

### **3.9. Silicon Powder**

The results of silicon pellet fabrication are shown in Figure 36. Pellets containing 10% (w/w) silicon powder and 90% (w/w) micronised silicon powder, were prepared at 25 kN, 30 kN, 35 kN and 40 kN. Pellets generated at these pressures were able to be manipulated using tweezers, indicating that the components within the pellet had bonded well together (Figure 36). For comparison, a pellet containing 100% silicon powder (non-micronised) was pressed at 35 kN. This pellet disintegrated upon handling, indicating that the smaller micronised particles were required to create a stable pellet. The micronised particles were able to fill the voids between the larger non-micronised powder during pressing and a denser pellet afforded better structural integrity.

For the pellets containing the mixture of silicon and micronised silicon components, some surface defects were observed after the pellet was ejected from the cast. Cracks could be seen across the surface of the pellet. This was initially attributed to end caps that were not completely cleaned of particulates. However, these defects continued to occur even after thorough cleaning of the end caps and it was hence determined that the material in the pellet was not binding well enough to form a stable pellet.

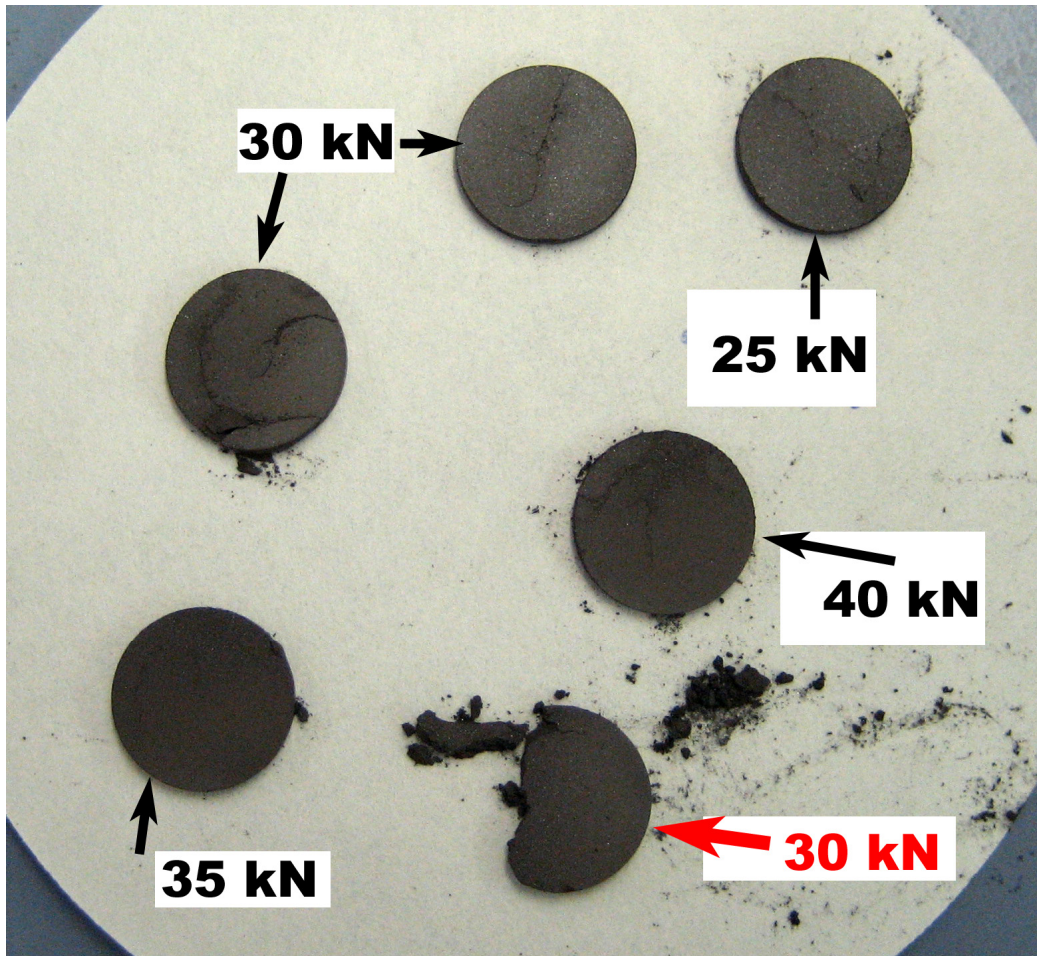


Figure 36 – Pellet containing 10% silicon powder and 90% micronised silicon powder pressed at 25 kN, 30 kN and 40 kN. The broken pellet marked in red was generated from 100% silicon powder and demonstrates the fragility of the pellet after it was handled with tweezers. All other pellets were able to be handled with tweezers without fracturing.

### 3.10. Pellets Made From Oxidised Porous Silicon Powder

Initial experiments involved the pressing of oxidised porous silicon powder without any additives. We used oxidised porous silicon powder as we have shown in **Chapter 1** that freshly etched or untreated porous silicon undergoes rapid degradation in aqueous solutions and hence was not conducive for the attachment of cells. We required the porous silicon powder to be stable in cell culture conditions. The oxidised powder was initially pressed at 20 kN for 5 mins. When the pellet was extracted, a layer of the pellet could be removed (Figure 37). Since the 20 kN force may not have been high

enough to cause particle bonding, the powder was subsequently pressed at 35 kN. When this pellet was extracted, a “popping” noise was audible. This was an indication that bonds were being broken and reformed. It is possible that silane gas was being produced, as porous silicon particles have been shown to release ppm concentrations of silane when exposed to air <sup>[157]</sup>. The 35 kN pellet also demonstrated laminations (Figure 37). This was attributed to friction between the pellet and the walls of the die cast <sup>[158]</sup>. Laminating effects can be reduced by using a lubricant, either as a component within the pellet or as a coating on the walls of the die cast <sup>[159]</sup>.

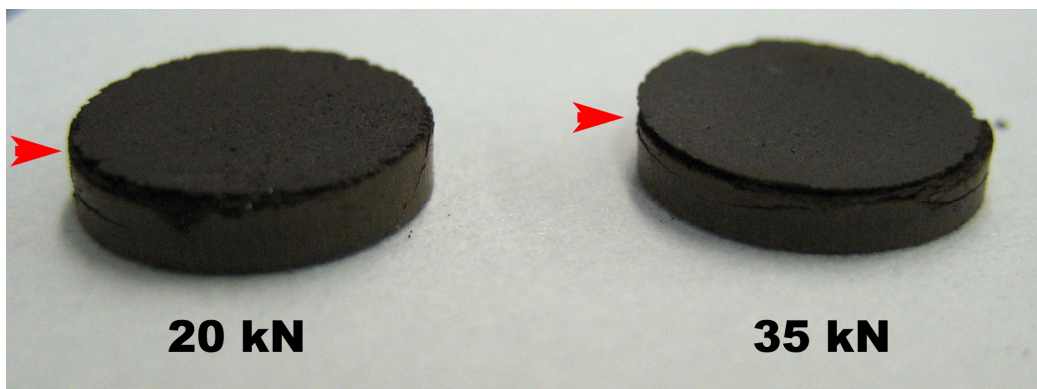
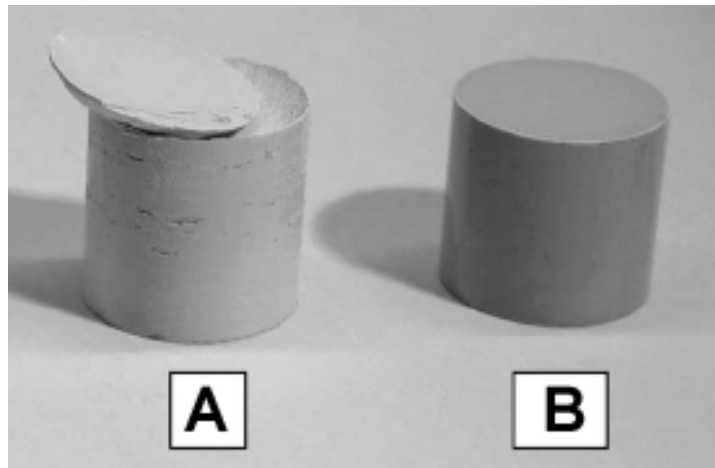


Figure 37 – Oxidised porous silicon powder pressed at 20 kN and 35 kN pressures without any additives. Laminating effects were observed in both pellets (red arrowheads).

### 3.11. Use of Lubricants During Pellet Fabrication

#### 3.11.1. Stearic acid as a lubricating agent

Stearic acid has been shown to be useful in reducing particle-particle and pellet-wall friction <sup>[158]</sup> in pellets comprised of silicon nitride (Figure 38). Laminating effects were observable in pellets that did not contain stearic acid as a component. Therefore, stearic acid was added to the oxidised porous silicon powder, in an attempt to reduce pellet-wall friction.



**Figure 38 – Pellets composed of silicon nitride pressed at the same pressure in the absence of a lubricating agent (A) and with 1% stearic acid added to the silicon nitride matrix (B). The laminating effect was reduced upon addition of the lubricating agent. Taken from Vieth *et al*, 2003 <sup>[159]</sup>.**

Stearic acid was added to oxidised porous silicon powder at 3% (w/w). The mixture was then pressed at 35 kN and 45 kN. The resultant pellets demonstrated that friction was still occurring, with laminations clearly evident (Figure 39), although the pellet pressed at 45 kN showed this to a lesser extent, suggesting that a higher pressure might be required to bind the components in a more stable fashion. Barraclough *et al* also found that silicon containing an oxidised layer did not compact well <sup>[157]</sup>, as it was the breaking and re-forming of hydrogen bonds that held the pellet components together.



**Figure 39 – Oxidised porous silicon powder containing 3% (w/w) stearic acid pressed at 35 kN and 45 kN. The 35 kN pellet clearly shows laminations, whereas in the 45 kN pellet, the effect is not so pronounced.**

### **3.12. Pellet Production from Aminosilanised Porous Silicon Powder**

Since we were unable to form pellets without surface defects or laminations using oxidised porous silicon powder, silanised porous silicon powder was tested. The reason for using aminosilanised porous silicon powder was because we showed in **Sections 2.7 and 2.9** that cells adhere and survive better on aminosilanised porous silicon, in comparison to oxidised porous silicon. Images of pellets formed using aminosilanised porous silicon powder are shown in Figure 40. We compressed silanised porous silicon powder and found that the laminating effects were still evident, indicating that there was friction against the die cast wall.

Two lubricating agents were tested, cod liver oil and stearic acid. Cod liver oil contains a variety of omega-3 or n-3 fatty acids, such as eicosapentaenoic acid and docosahexaenoic acid, and is often used as a dietary supplement <sup>[160, 161]</sup>. As a lubricating agent, cod liver oil is commonly coated on the walls of a cast to reduce pellet-wall friction and not incorporated into the pellet components. Stearic acid is used to prevent particle-particle friction and is incorporated into the powder mixture. We compared the effectiveness of the two lubricating agents.

A pellet was pressed in a die cast that had the inner chamber coated with cod liver oil. The resultant pellet showed many laminations (Figure 40B). To test the stearic acid, aminosilanised powder was mixed with 1% (w/w) stearic acid. The resultant pellet still showed some laminating effects (Figure 40C) but to a lesser extent than pellets pressed with cod liver oil. This demonstrated that cod liver oil was not as effective as stearic acid in reducing friction.



**Figure 40** – Thermally oxidised porous silicon powder silanised functionalised with 3-aminopropyltrimethoxysilane (aminosilanised powder). **A:** Pressed at 45 kN (no lubricant); **B:** Inner chamber coated with cod liver oil and pressed at 45 kN; **C:** Silanised powder mixed with 1% (w/w) stearic acid and pressed at 45 kN.

### **3.12.1. Use of starch as a binding agent during pellet formation**

Starch is a binder commonly used in pharmaceutical tablets for oral drug delivery. Drugs that have poor compression properties are often mixed with starch to form a stable tablet<sup>[162]</sup>. The starch used in this work was pregelatinised maize starch, which is composed of two long-chain polymers, linear amylose and branched amylopectin. Pregelatinisation refers to the heat treatment imposed upon the starch to break apart the two polymers into smaller semi-crytalline structures, giving the starch better binding characteristics by increasing its compaction capabilities. Recently, novel starch/polymer compounds have been investigated as a carrier in implantable drug delivery systems. An example is the use of methyl methacrylate or acrylic acid monomers polymerised with starch<sup>[163]</sup>. Starch provides structural strengths, enabling the polymer to be used as a biodegradable scaffold that can be handled easily. These scaffolds find applications in tissue engineering where cells can be cultured on the surface, which is then implanted into the body. Since the scaffold is biodegradable, its removal by human intervention is not required. The degradation products of starch are mainly fructose, maltose and lower molecular weight starch chains<sup>[164]</sup>. The biocompatibility of these starch-based compounds has been tested on fibroblast and osteoblast-like cell lines. For these cell lines, no cytotoxicity was apparent<sup>[164, 165]</sup>.

### Chapter 3: Results and Discussion

Starch was recently used to form a porous 3-dimensional matrix with the polymers poly(L-lactide) and polycaprolactone, two components commonly used in biodegradable sutures, which are known for their biocompatibility [166]. Starch and the polymer components were formed into scaffolds using a novel printing method. This printing method used repetitive deposition of layers aided by computer controlled equipment to form a large 3-dimensional structure that contained a porous microstructure (Figure 41).

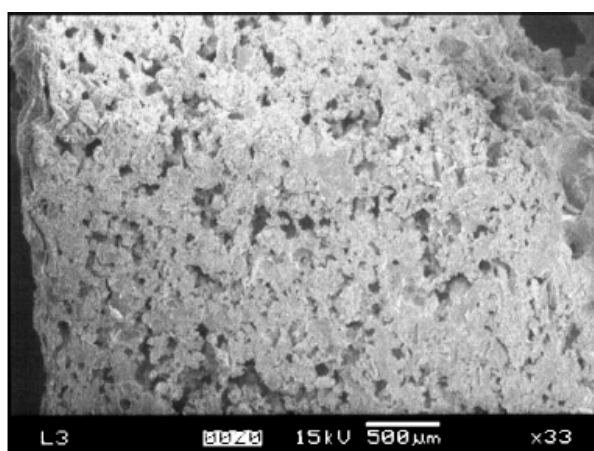


**Figure 41 - SEM image showing the microstructure of the printed starch scaffold. Taken from Lam *et al* (2002) [166].**

Starch was used as a binding agent for porous silicon powder. First a pellet was formed using 20% (w/w) starch with 5% (w/w) stearic acid (as a lubricant) and 70% (w/w) aminosilanised porous silicon pressed at 35 kN. The pellet had laminations, so a pellet was formed using the same components except the stearic acid component was increased to 10% (w/w). The resultant pellet was well-formed, free of laminations and mechanically stable, and could be manipulated easily (Figure 42).

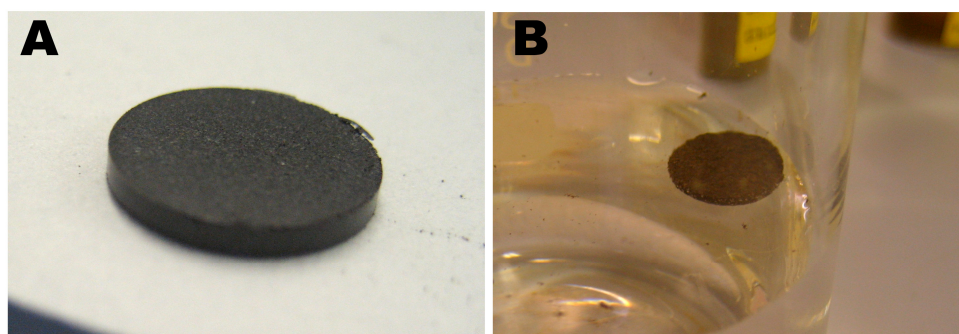


**Figure 42 – A: Porous silicon pellet formed by pressing 20% starch with 10% stearic acid and 70% aminosilanised porous silicon powder. B: the pellet placed into a beaker of water. Note that the pellet floats on the surface of the water.**

As stable pellets could be formed using starch, the wettability of the pellet was then tested. Cell adhesion on the pellet surface requires the pellet to be immersed or partially submerged in cell culture solution. When the pellet was placed into a beaker of water, it floated, indicating that the composite material contained air-filled voids that were not being wetted (Figure 42). The stearic acid was likely to have contributed to the reduced wettability of the pellet. As mentioned before, a lower concentration of stearic acid was also tested, but a 5% (w/w) stearic acid concentration resulted in observable laminations. This demonstrated that the stearic acid concentration could not be reduced. Further experiments were therefore carried out using 10% (w/w) stearic acid.

### **3.13. Increasing Pellet Wettability**

#### **3.13.1. Glucose as a wetting agent**

To increase the wettability of the pellet, glucose was added to the pellet composition. Glucose has previously been used in poly(L-lactide)-based polymer matrices to increase the wettability of the polymer surface<sup>[167]</sup>.

Glucose that was hand milled to a size ranging from  $> 45 \mu\text{m}$  to  $< 75 \mu\text{m}$  was mixed at a concentration of 10–30% (w/w) with starch, stearic acid and aminosilanised porous silicon powder. The concentrations of starch and stearic acid were maintained at 20% (w/w) and 10% (w/w), respectively, with the concentration of porous silicon changing

to accommodate the glucose. The pellets were pressed at 35 or 45 kN. The pellets formed broke easily upon handling. This indicated that glucose was not a good binding agent. The 45 kN pellet was less structurally sound than the 35 kN pellet. It has been shown that higher pressures can lead to the formation of cracks on the surface, partially due to frictional forces and non-uniform distribution of the force across the pellet face. This can be alleviated by the inclusion of lubricants and isostatic pressing<sup>[157]</sup>. We had already included stearic acid as a lubricant and considered that our equipment provided an isotatic pressure. We therefore concluded that with our facilities, a more stable pellet was formed at the lower pressure of 35 kN than at 45 kN.

### **3.13.2. Glycine as a wetting agent**

Glycine was also tested as an agent to increase the wettability of the pellet. Pellets containing glycine at 10%, 30% and 40% (w/w) were pressed at 35 kN, with starch and stearic acid maintained at 20% (w/w) and 10% (w/w), respectively. Aminosilanised porous silicon concentrations were changed accordingly.

All the pellets pressed with glycine were stable and well-formed without any defects. The pellets were then placed into 4 ml of distilled water to observe their wettability. Pellets containing glycine did not float immediately after immersion. This indicated that glycine increased the wettability of the pellet sufficiently to allow surface wetting. Glycine containing pellets were also more stable in water than pellets containing glucose. Figure 43 shows a comparison of the stability of pellets containing glucose or glycine when immersed in water. The glucose-containing pellet did not maintain its structure in water (Figure 43A) whereas the glycine-containing pellets retained their overall shape (Figure 43B-D).

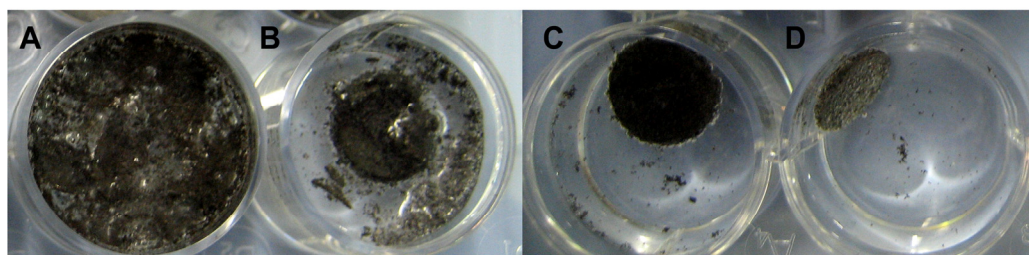


**Figure 43 – Structure of pellets after being placed into 4 ml of distilled water for 10 minutes. A: 30% of glucose, B: 10% glycine, C: 30% glycine, D: 40% glycine. All pellets contain 20% starch, 10% stearic acid and aminosilanised porous silicon. All pellets were pressed at 35 kN. Percentages are in (w/w).**

A scaffold supporting the growth of cells would be required to maintain its form when immersed in aqueous solution under cell culture conditions. These results indicated that glycine-containing pellets were stable in water. A 20% (w/w) glycine-containing pellet was also made and tested in water, and was shown to have similar stability to a 30% or 40% (w/w) glycine containing pellet. When these pellets were immersed in water, gas bubble evolution was evident and the pellets rose to the surface after one hour. This indicated that the porous silicon was degrading and in the process releasing hydrogen [129]. Hydrogen bubbles trapped within the pellet caused it to rise. This suggested that the wettability of the pellet was still not optimal, as the liquid was not able to penetrate to the centre of the pellet to release the hydrogen trapped within.

We chose a pellet containing 10% (w/w) glycine to continue further studies. Although this pellet did not show the best wettability, a higher concentration of glycine will still lead to a floating pellet after a period of time immersed in solution. Glycine is also easily dissolved in aqueous solution. A higher concentration of glycine may affect the stability and structure of the pellet. In this respect, glycine could also be used as a leaching agent, as it will dissolve more readily than the porous silicon component, leaving voids within the pellet structure.

### **3.14. Effect of Compaction Force on Pellet Stability**

The effect on the stability of the pellets created under different compaction forces was investigated. Pellets containing 10% (w/w) glycine, 10% (w/w) stearic acid, 20% (w/w) starch and 60% (w/w) aminosilanised porous silicon powder were pressed at 20 kN, 35 kN and at 45 kN. These pellets were placed into 4 ml of dH<sub>2</sub>O.

When the pellets were placed into solution, the pellets prepared at 20 kN and 45 kN showed signs of fast dissolution (Figure 44). A higher amount of gas evolution was observed on the 45 kN in comparison to the 20 kN and the 35 kN pellet. This resulted in the surface of the 45 kN pellet showing more degradation in comparison to the other pellets, observed as the pellet surface becoming rough and showing individual particles. The surface of the 25 kN pellet showed greater instability and roughness in comparison to the 35 kN, evident immediately after immersion, where fragments broke away from the 25 kN pellet. The 35 kN pellet showed the least fragmentation and surface roughening in comparison to the other pellets. This suggested that a pressure of 35 kN was appropriate for the formation of a pellet. One hour after immersion, the 20 kN and the 35 kN pellet floated to the surface.

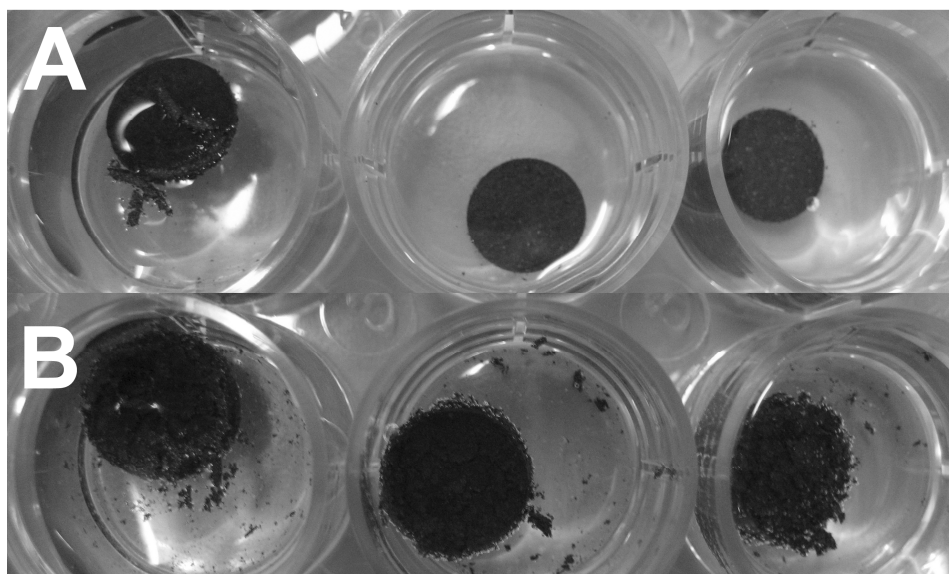


**Figure 44 – Pellets containing 10% glycine, 10% stearic acid, 20% starch and 60% aminosilanised porous silicon. Pellets were pressed at: Left wells: 20 kN; Centre wells: 35 kN; and Right wells: 45 kN. Pellets were placed into 4 ml of dH<sub>2</sub>O. A: immediately after immersion; B: after 1 hour immersion. Percentages are represented as (w/w).**

### **3.15. Heat Treatment of Pellets**

To be used as a cell support structure, a pellet should be capable of withstanding sterilisation procedures. We tested the ability of our pellets to withstand dry heat sterilisation at 160 °C for a minimum 6 hours, a common sterilisation method <sup>[168]</sup>. Pellets containing 10% (w/w) glycine, 20% (w/w) starch, 10% (w/w) stearic acid and 60% (w/w) aminosilanised porous silicon powder were fabricated at 35 kN.

We wanted to alleviate the issue of air trapped within the centre of pellet when immersed in liquid. A heat-sterilised pellet was dipped into water for 1 minute before being dried thoroughly. We anticipated that dipping the pellet would open up pores at the surface of the pellet and to allow any trapped gas to escape and hence prevent the pellet from floating. Dipping the pellet in water also served as a pre-treatment for cell culture; creating a structure with open pores that cells could potentially infiltrate. Pre-wetting of structures has been conducted for biological scaffolds, as it serves to ensure that all pores are accessible to fluid (and hence cells), especially in hydrophobic

### *Chapter 3: Results and Discussion*

scaffolds <sup>[169]</sup>. We wanted to test the feasibility of pre-wetting the pellet and to test the stability of the pre-wetted pellet in aqueous solutions. We allowed the pre-wetted pellet to dry completely before being immersed in 4 ml of dH<sub>2</sub>O. A pellet that was heat-treated only, was also placed into dH<sub>2</sub>O.

Upon drying, the pellet that was pre-wetted showed little observable change on the surface. By visual inspection, the pellet appeared to have a slightly rougher surface than the pellet that was not pre-wetted (Figure 45A & B). This indicated that some changes in the structure had occurred, due to the dissolution of the pellet components at the surface. This was further verified by SEM images (Figure 45E & F). Here it was shown that large pores were opened on the surface of the pellet upon short contact with the water and individual porous silicon powder granules could be identified.

When placed into 4 ml of water, the pre-wetted pellet floated to the surface of the water. Despite obvious surface changes, it was found that the pre-wetting process did not open sufficient pores within the pellet to remove air that was trapped during the pressing process. It is also possible that hydrogen release occurs from the degradation of porous silicon when it was wetted (**Section 1.2.2**), which would also provide the pellet buoyancy. The pre-wetted pellet was not stable and did not maintain its structure longer than 24 hours, therefore a pre-wetted pellet is not a suitable candidate for further investigation.

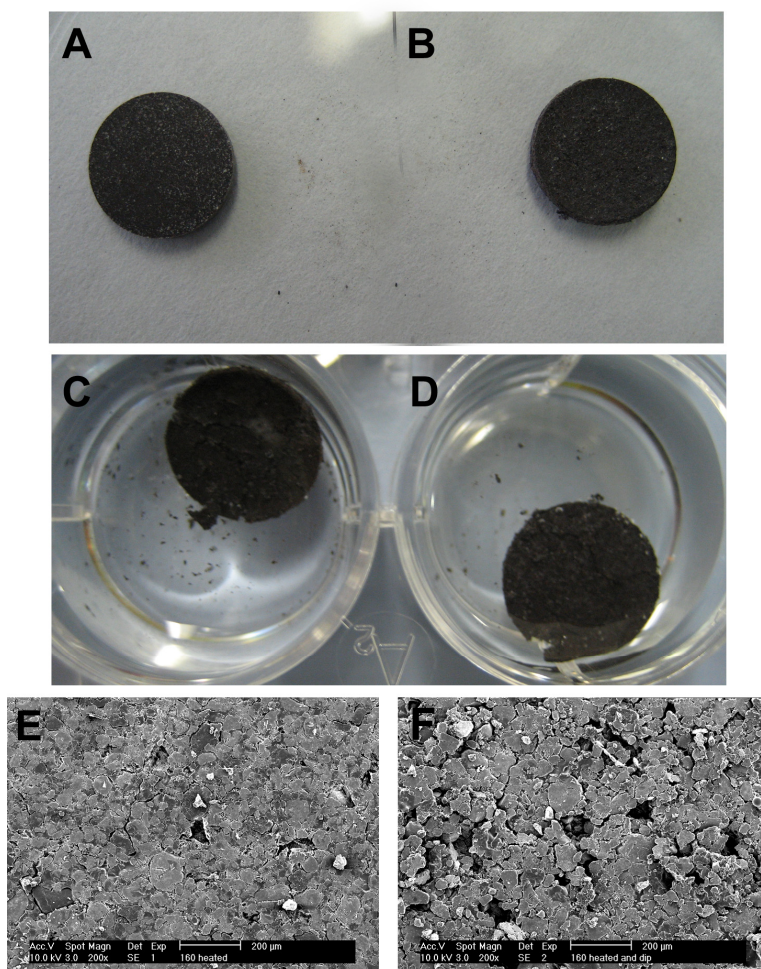


**Figure 45 – 10% (w/w) glycine containing pellets pressed at 35 kN. A, C and E: Pellets were heat-treated at 160 °C for a minimum of 6 hours. B, D and F: Heat-treated pellets were dipped into dH<sub>2</sub>O for 1 minute and allowed to dry completely (pre-wetted pellets). A & B: Pellets before immersion. C & D: Pellets after immersion in 4 ml dH<sub>2</sub>O for 24 hours. E & F: SEM images of the pellet surfaces.**

In comparison, a pellet that was heat-treated only showed less gas evolution than a pre-wetted pellet and a pellet that was not heat-treated. When the heat-treated pellet was placed into water, the pellet initially sank, but due to the gas formation, the pellet floated to the surface after 20 minutes of immersion. Then at 24 hours, the pellet became fully wetted and sank. The pellet was again observed after 2 days, and the pellet structure was still maintained, indicating good stability in solution (Figure 46).

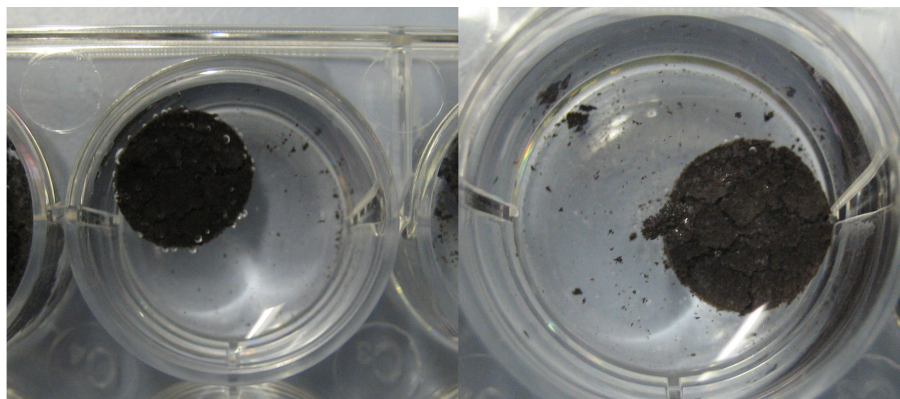


**Figure 46 – Pellets containing 10% glycine, 10% stearic acid, 20% starch and 50% (w/w) aminosilanised porous silicon powder and pressed at 35 kN. The pellets were heat sterilised at 160 °C for a minimum of 6 hours before being immersed in 4 ml of dH<sub>2</sub>O. Left panel: image of pellet immediately after immersion. Right panel: image of pellet after 2 days immersion in water.**

These data showed that dry heat sterilisation of a pellet after pressing created a pellet that was more stable than a pellet that was not dry heat-treated. In addition, it is possible that thermal bonding had occurred between porous silicon particles and the other components. The melting and recrystallisation upon cooling of stearic acid which has a melting point of approximately 70 °C may have helped to stabilise the pellet by filling voids in the structure.

Pre-wetting of a heat-treated pellet, on the other hand, destabilised the structure. The opening of pores may have swelled the pellet and broken particle bonds. Therefore, all further experiments were conducted on pellets that were dry heat-sterilised at 160 °C. These pellets contained 20% (w/w) starch, 10% (w/w) glycine, 10% (w/w) stearic acid and 60% (w/w) aminosilanised porous silicon without pre-wetting.

### **3.16. Cell Culture Studies**

The pellet used in the following cell culture studies contained 20% (w/w) starch, 10% (w/w) glycine, 10% (w/w) stearic acid and 60% (w/w) aminosilanised porous silicon.

### **3.16.1. Stability of pellets in cell culture medium**

Heat-treated pellets were treated with either a 10% (v/v) glutaraldehyde solution or with a 10 mg/ml gelatin coating. Glutaraldehyde was used as a cross-linker for the amine functionalities of the aminosilanised porous silicon and the glycine. Gelatin was used to coat the pellet surface. Both treatments were aimed at improving the stability of the pellet structure in solution.

The stabilities of the treated pellets were studied by immersion in cell culture medium and incubation at 37 °C over 24 hours. Images of the pellets residing in tissue culture wells were taken during the 24 hour time period. The results are shown in Figure 47.

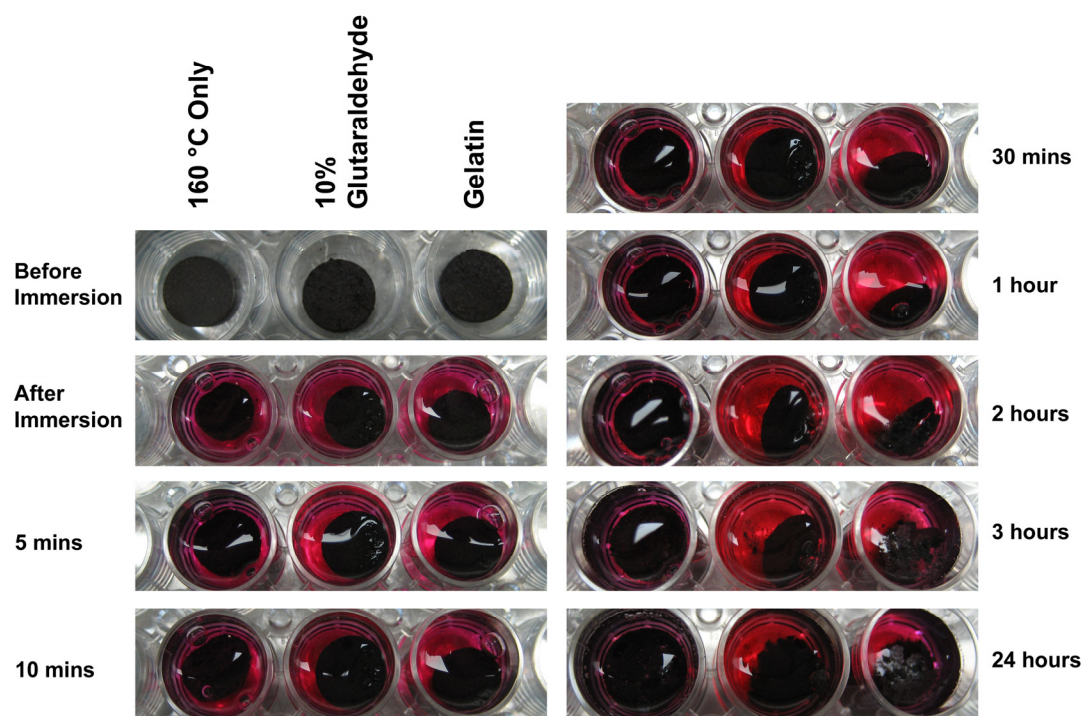


**Figure 47 – Time course images of treated pellets immersed in 2 ml cell culture medium. 160 °C Only: pellet was only heat treated at 160 °C. 10% Glutaraldehyde: 160 °C heat treated pellet was immersed in a 10% (v/v) glutaraldehyde solution for 1 minute before being allowed to air dry completely. Gelatin: 160 °C heat treated pellet was immersed in a 10 mg/ml gelatin solution before being allowed to air dry completely. At 1 hour, gelatin coated pellet showed signs of fragmentation. At 3 hours gelatin coated pellet had fragmented, and the glutaraldehyde treated pellet also showed signs of fragmentation. At 24 hours, both glutaraldehyde and gelatin pellet had lost structural integrity. Heat treated pellet had not fragmented, but had swollen due to the absorption of culture medium.**

The results indicated that only the 160 °C heat-treated pellet was stable in cell culture medium over a 24 hour period. Pellets that were pre-treated with either glutaraldehyde or gelatin were less durable and obvious fragmentation of the pellet could be seen as soon as 3 hours after immersion. These results demonstrated that wetting (and hence swelling) of the pellet during the glutaraldehyde or gelatin pre-treatment and then drying the pellet, reduced the stability of the overall structure. This was probably due to the breaking of the porous silicon-porous silicon particle bonds. These bonds were formed during the pressing process and were critical to maintaining the structure of the

pellet. When the pellet was wetted, the pellet again absorbed liquid and swelled. Due to the weakened structure, the pellet fragmented when it swelled again.

Significant swelling of the heat-treated pellet was also observed during the 24 hour incubation period, but it did not show signs of disintegration. This pellet did not float, whereas both the gelatin-encapsulated and glutaraldehyde-treated pellets started to float. This indicated that the gelatin coating or the glutaraldehyde-bonded particles on the surface were preventing the escape of gas and the lack of these additives allowed for the diffusion of gas from within the pellet to the medium and hence prevented the pellet from floating. Therefore the heat-treated pellet was shown to be the most stable structure in cell culture medium.

For further studies, all pellets were heat sterilised at 160 °C for a minimum of 6 hours before being used in cell culture experiments.

### **3.16.2. Cell culture on pellets**

As the 160 °C heat-treated pellet was the most stable in cell culture medium, a preliminary cell culture experiment was carried out with human lens epithelial cells cultured directly on the pellet surface. 100,000 cells were incubated with the pellet, either as a component of the cell culture medium in the well (100,000 cells/ml solution), or were spotted onto the surface of the pellet (100,000 cells in a 100µl solution). The results, presented in Figure 48, indicated that after 1 hour incubation, the cells had not started to spread on the surface (Figure 48A). The pellet that was immersed in cell culture medium containing cells, showed a large amount of background fluorescence, but individual cells could still be discerned (Figure 48B and C). Due to the fragility of the pellet, the dye could not be removed without disrupting the surface of the pellet and dislodging the cells.

On the pellet with the cell suspension spotted directly on the surface, few cells were observed on the surface (Figure 48C). This was surprising as more cells were expected

to be observed on this surface. Only viable cells are able to enzymatically cleave the acetate bond of FDA to release fluorescein, hence only live cells fluoresce. Possibly the majority of cells on this surface were no longer viable. The instability of the pellet in the cell culture medium should also be considered as it might have prevented the cells from attaching. Hence only a few cells could be observed on the surface. To determine if the lack of cell attachment to the pellet was due to the pellet instability or if it was due to any cytotoxic components within pellet, a different assay had to be used.

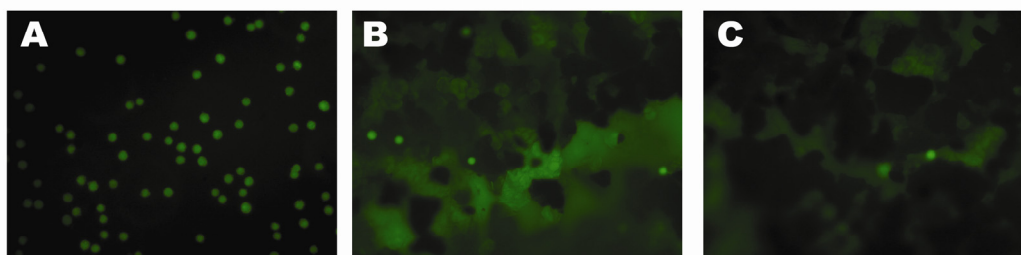


**Figure 48 – Human lens epithelial cells after 1 hour incubation, stained with FDA. A: glass coverslip, B: 160 °C heat treated pellet with 100,000 cells/ml/well and C: 160 °C heat treated pellet with 100,000 cells/100 µl spotted onto the surface of the pellet. Scale bar: 50 µm.**

### **3.17. Indirect Cell Viability Assay**

#### **3.17.1. Indirect cell viability assay on pellet components**

We used Alamar Blue in an indirect assay to determine cell viability. The Alamar Blue assay was not conducted in direct contact with the porous silicon as we showed in **Chapter 2** that porous silicon can reduce the reagent. Therefore an indirect assay allows us to determine if any toxic components are produced in cell culture medium. The mechanism in which Alamar Blue determines the viability of cells is described in **Chapter 2**.

Starch, glycine, stearic acid and aminosilanised porous silicon (thermally oxidised at 600 °C and aminosilanised) were incubated separately with cell culture medium which was then placed onto a confluent layer of human lens epithelial cells. Untreated porous

### *Chapter 3: Results and Discussion*

silicon powder (non-oxidised) and porous silicon powder that was thermally oxidised at 600 °C only were also included in this assay.

This experiment showed that cell viability for cells incubated with the glycine and starch medium was not significantly different to the positive control (glycine:  $p=0.73$ ; starch:  $p=0.47$ ), indicating cell viability was not compromised by these powders (Figure 49). The stearic acid medium induced a slight decrease in cell viability, but was not shown to be significantly different to the positive control ( $p=0.16$ ). It has been shown in the literature that a concentration of 300  $\mu\text{M}$  stearic acid is capable of inducing apoptosis in cells after 24 hours incubation<sup>[170]</sup>. The concentration of the stearic acid in the medium was 11.71 mM and we recorded a 20% loss in cell viability in comparison to the positive control.

More importantly, cells incubated with the aminosilanised porous silicon medium showed cell viability results that were comparable to the positive control ( $p=0.55$ ), indicating that the powder was not having an adverse effect upon cell survival. Porous silicon that was thermally oxidised induced a slight decrease in cell viability that was not significantly different from the control ( $p=0.32$ ).

Interestingly, it was the untreated porous silicon powder sample that showed a significantly different cell viability to the positive control ( $p=0.04$ ). This was an indication that the degree of porous silicon oxidation might have an influence upon cell survival. It has been suggested that non-oxidised or untreated porous silicon particles/powders have the ability to form free radicals by direct electron exchange with molecules adsorbed onto the surface of the particles<sup>[171]</sup>. Free radicals have cytotoxic effects upon cells<sup>[172]</sup>, which could explain the loss in cell viability observed with the untreated particles. Oxidised particles do not exhibit this property as the oxygen molecules within the porous silicon structure prevent or reduce the efficiency of this electron exchange<sup>[171, 173]</sup>. We did not pursue this interesting topic as it was never our intention to use untreated porous silicon for biomaterial purposes. The rapid dissolution

of the untreated form of porous silicon in aqueous medium was not suitable to support cell growth, and our focus remains on the use of thermally oxidised porous silicon.

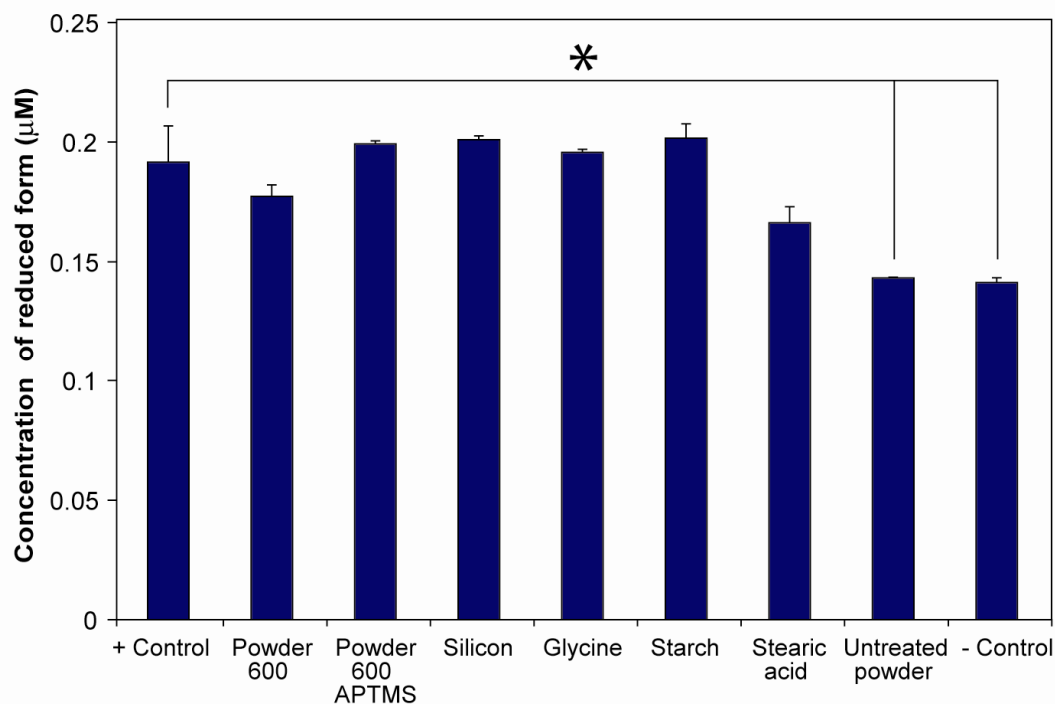


**Figure 49 – Indirect Alamar Blue cell viability assay results for human lens epithelial cells cultured with medium that had been in contact with porous silicon powders and with pellet components. Powder 600: porous silicon powder that was thermally oxidised at 600 °C for 1 hour; Powder 600 APTMS: porous silicon powder that was thermally oxidised and then aminosilanised; Silicon: silicon wafer; Glycine: glycine powder; Starch: starch powder; Stearic acid: stearic acid powder; Untreated powder: porous silicon powder that was not oxidised or silanised. + Control: Cells containing fresh medium; - Control: no cells containing fresh medium. Statistics were performed with a paired independent *t*-test. All *p* values are from comparisons made between the positive control and other samples. \* denotes significant difference ( $p \leq 0.05$ ). Error bars: standard deviation of the mean.**

The indirect viability assay had demonstrated that each component of the pellet did not cause a loss in cell viability. Therefore the pellet can be used for the culture of mammalian cells. The direct cell culture of cells on the pellet, as shown in **Section 3.16.2**, did not show a large number of cells attached to the structure. The evidence in this section has indicated that the lack of attached cells was not due to the pellet toxicity. The most likely explanation for the few attached cells is the stability of the

### *Chapter 3: Results and Discussion*

pellet in aqueous medium. We showed in **Section 3.16.1**, that the pellets displayed significant swelling and absorption of liquid after immersion in cell culture medium. This unstable surface may have prevented the cells from attaching to the pellet surface.

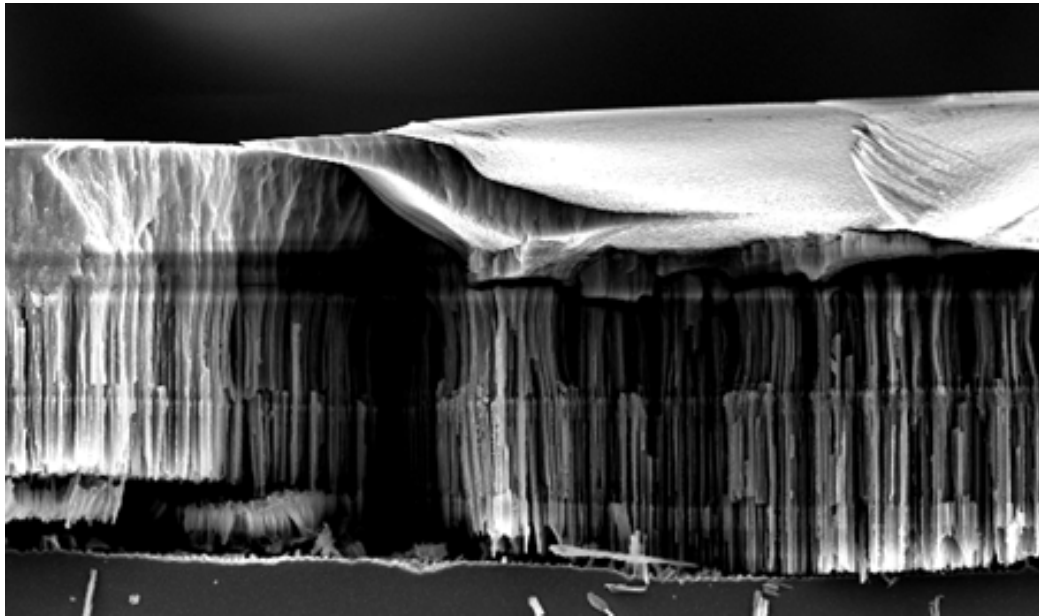
## **Conclusions**

We were able to generate a structurally sound pellet through the use of starch as a binding agent and stearic acid as a lubricating agent. This pellet could be easily manipulated and handled. When the pellet was immersed in an aqueous solution, the pellet became unstable and was unable to maintain its structure for more than 24 hours. We have shown through an indirect viability assay that starch, glycine and stearic acid were not toxic to human lens epithelial cells at the concentrations used in this section. Although the pellet was able to support the growth of cells, the pellet's instability in aqueous solution made it an unsuitable material for the propagation of cells or as a cell delivery scaffold. We may require the porous silicon scaffold to be able to support the growth of cells over a period of weeks, but we have shown that the pellets are not able to maintain their structure for longer than 24 hours. For our purposes in developing a potential ocular implant, the large dimension of the pellet (10 mm x 0.2 mm) made it an incongruous and uncomfortable material to be placed into the eye.

It was desirable to have a porous silicon platform that was able to support the growth of cells and could be manipulated with tweezers after a culture period with cells. As a potential implantable structure, the stability of the platform was important. To conduct this, we turned to other forms of porous silicon, such as porous silicon membranes.

## Chapter 4

### Primary cell culture and *in vivo* studies on porous silicon membranes



*Scanning electron micrograph of a porous silicon membrane that has undergone an incomplete electropolishing step*

## **Introduction**

Currently, the applications of porous silicon membranes have focused upon the development of drug release <sup>[174, 175]</sup>, biosensing <sup>[176]</sup> or filtration devices <sup>[177, 178]</sup>. Furthermore, porous silicon membranes have recently been developed for radiation cancer treatment <sup>[179]</sup>. In this last-mentioned application, membranes were loaded with the radionuclide <sup>32</sup>P and were then implanted into tumours, which resulted in a significant decrease in tumour size <sup>[179]</sup>. In a biomaterials study, particles derived from porous silicon membranes were mixed into a poly-caprolactone polymer matrix, onto which fibroblast cells were then cultured. This matrix composite did not show any adverse effect upon the proliferation of the cells <sup>[180]</sup>. Yet only 5% of this matrix consisted of the membrane particles, so it was unclear what effect the porous silicon alone has on the cells. Apart from this one study, in depth direct studies of cell culture on porous silicon membranes have not yet been conducted.

As an implant for the transplantation of cells into the eye or elsewhere, porous silicon membranes may offer advantages over a pellet consisting of porous silicon particles, as described in **Chapter 3**. The major benefit is size; the pellets measured 1 cm in diameter and 1.15 mm in height. This size is a key issue as it would be extremely difficult to place and secure such an object around the limbus region of the eye or in many other body sites. In contrast, the membranes are much thinner and can be easily manipulated with tweezers, even after extended exposure to culture conditions. As the membranes contain only the porous silicon layer, it is able to degrade completely, unlike the form of porous silicon studied in **Chapter 2** which was still attached to a flat silicon layer.

In this section, we investigate the suitability of using porous silicon membranes as a support for mammalian cell culture. Surface modification techniques used in **Chapter 2** were applied to the membranes, which were characterised by means of AFM and EDX. Subsequent cell culture studies of the cells on these surfaces were conducted. The degradation rate of porous silicon membranes was investigated using different

#### *Chapter 4: Introduction*

techniques than methods used **Section 2.4.4**, as we were trying to emulate fluid flow conditions found in the eye or in other body tissues. This chapter also introduces the culture of human primary cells (from a cornea) on these membranes.

The aim of the work presented in this chapter was to determine if porous silicon membranes are capable of supporting the growth of primary cells. In particular we wanted to culture limbal stem cells from human corneal rims, which contain limbal tissue, onto porous silicon membranes. We aimed to identify the cells cultured from this tissue using a set of antibodies that would allow us to distinguish between terminally differentiated cells and cells still containing some stem cell-like properties. We were also interested in the effect porous silicon had on cells in an *in vivo* environment. Our final goal was to establish that limbal cells cultured on a porous silicon membrane were able to migrate from the membrane into the surrounding tissue of a rat model.

In summary, the aims of this chapter were:

- to characterise the surface of porous silicon membranes;
- to culture human lens epithelial cells on the membranes;
- to observe the degradation of the membranes under different conditions;
- to culture human limbus-containing tissue to expand cell numbers;
- to identify the cell populations within the cells cultured from limbal tissue;
- to obtain cell outgrowths from limbal tissue on porous silicon membranes and observe the migration of cells from the membrane;
- to observe the host response to aminosilanised membranes when implanted into the eye;
- to track the movement of cells from the membrane into the surrounding tissue when implanted into the rat eye.

## **Methods and Materials**

### **4.1. Chemicals and Antibodies**

Ammonium molybdate tetrahydrate, sodium metasilicate pentahydrate, anhydrous sodium sulphite and calcium chloride were all obtained from Ajax Chemicals, Sydney, NSW, Australia. Sodium hydrogen carbonate, sodium chloride, potassium chloride, lactic acid and sodium dihydrogen phosphate were obtained from ChemSupply, Gillman, SA, Australia. MOPS (4-morpholinepropanesulfonic acid), insulin-transferrin-sodium selenite and eosin Y were purchased from the Sigma Chemical Company, St Louis, MO, USA. All solvents were of analytical grade and were purchased from ChemSupply. The dyes DiOC<sub>5</sub>(3) and Hoechst 33342 and L-glutamine were purchased from Molecular Probes, Invitrogen, Carlsbad, CA, USA. Dulbecco's modified Eagle's medium (DMEM), PKH26, normal horse serum and penicillin/streptomycin solution were obtained from Sigma Chemical Company, St Louis, MO, USA. Foetal Bovine Serum (FBS) was purchased from Bovogen Biologicals Ltd., Essenden, Vic, Australia.

Mouse anti-p63 was obtained from LabVision, Fremont, CA, USA and antibodies against CK3/12 and CK 19 were purchased from Chemicon, Billerica, MA, USA. GelMount™ was purchased from Biomedex, Foster City, CA, USA. DePeX mounting medium was obtained from Merck, Darmstadt, Germany.

### **4.2. Membrane Preparation**

Porous silicon membranes (BioSilicon™) were prepared by Dr Armando Loni at pSiMedica, Malvern, Worcestershire, UK. Membrane thickness was approximately 150 µm with porosity of approximately 68 – 70%.

The membranes were cut to size using a diamond scribe and thermally oxidised at 600 °C for 1 hour. The oxidised membranes were subsequently silanised with 50 mM 3-aminopropyltrimethoxysilane in toluene for 5 mins and then washed with methanol and

acetone before being dried in air. The thermally oxidised membranes, which were then aminosilanised, are henceforth referred to as **thermal APTMS**. Sterilisation was carried out by dry heat at 160 °C overnight before use in cell culture studies.

### **4.3. Pore Size and Surface Roughness**

Surface topography was determined by means of AFM on a Multimode Nanoscope IV operating under tapping mode in air. FESP cantilevers with a resonance frequency of ~ 75 kHz were used at a free oscillation amplitude of 2 V. Pore size and surface roughness of the porous silicon membranes were determined through offline analysis of images using Nanoscope 6.12r1 software.

### **4.4. Energy Dispersive X-Ray Spectroscopy (EDX)**

To determine the extent of oxidation and silanisation on the membranes, thermally oxidised and thermal APTMS membranes were snapped to reveal a cross section. The membranes were then mounted onto brass stubs with the exposed cross section facing the detector. The cross section surface was probed with an energy dispersive X-ray (EDX) spectroscope coupled to a Phillips XL30 scanning electron microscope operating at 10 keV at a working distance of 10 mm. X-ray analysis was obtained using an EDAX (Ametek, Paoli, PA, USA) thin film, standardless EDS detector. The cross section was probed at 1 µm, 2.5 µm, 5 µm, 10 µm, 20 µm, 30 µm and 60 µm distances from the top of the membrane. At least three different samples were used with a minimum of three sections on each sample probed.

### **4.5. Degradation Studies**

#### **4.5.1. Ammonium molybdate assay in Tris-HCl**

To determine the rate of porous silicon degradation, a colorimetric ammonium molybdate based assay <sup>[181-183]</sup> was adapted to the analysis of porous silicon membranes.

#### Chapter 4: Methods and Materials

The source of the silicic acid standard was from sodium metasilicate pentahydrate, diluted in Tris-HCl buffer (pH 7.2) to concentrations ranging from 0 to 0.1 mM. 60  $\mu$ l of this solution was placed into a 96 well plate to which reagents were added in the following order:

Reagent	Volume
0.25 M Tris-HCl (pH 7.2)	40 $\mu$ l
0.3 M HCl	40 $\mu$ l
42 mM Ammonium molybdate tetrahydrate	20 $\mu$ l - 10 min incubation
27 mM EDTA	20 $\mu$ l
1.35 M Sodium sulphite	40 $\mu$ l - 1 hour incubation

**Table 2 – Method for the colorimetric silicic acid assay in Tris-HCl. 60  $\mu$ l of sample was placed with the reagents in the order stated above. Yellow colour formation was observed upon the addition of ammonium molybdate and 10 minute incubation was required for that colour formation. Blue colour formation was observed upon the addition of sodium sulphite. 1 hour incubation was required for the colour formation. All reagents were diluted in MilliQ water.**

The plate was then placed into a plate reader for spectrophotometric analysis at 650 nm. Calibration curve samples were made in triplicate.

##### **4.5.1.1. Static assay in Tris-HCl**

Untreated and 600 °C thermally oxidised porous silicon membranes were used in a static degradation assay. As controls, a glass coverslip and a piece of a silicon wafer were used. The mass of the samples used are as shown below:

Sample	Mass (mg)
Thermally oxidised pSi	13.56
Untreated pSi	8.15
Glass	182.45
Silicon	77.41

The samples were placed into separate containers of 50 ml of Tris-HCl (pH, 7.2, 0.25 M). The samples were kept in the dark at room temperature on a wave shaker for 5 days. 60  $\mu$ l of solution was removed daily and placed into a 96 well plate and assayed

for silicic acid concentration as in **Section 4.5.1**. The plate was read on a plate reader at 650 nm.

#### **4.5.2. Silicic acid assay in artificial tear fluid (ATF)**

A modified artificial tear fluid (ATF) solution <sup>[184]</sup> was used for the remaining silicic acid release studies. The artificial tear fluid did not contain any proteins or lipids as the studies were conducted at room temperature and could not be kept sterile during the assay period

The artificial tear fluid was composed of: 11.3 mM sodium chloride, 23 mM potassium chloride, 16.3 mM sodium hydrogen carbonate, 3 mM lactic acid, 0.72 mM sodium dihydrogen phosphate, 20 mM MOPS (4-morpholinepropanesulfonic acid) buffer and 1.32 mM calcium chloride in MilliQ water. The solution was adjusted to pH 7.4 using either NaOH or HCl.

##### **4.5.2.1. Calibration curve in ATF**

A calibration curve of silicic acid in artificial tear fluid was made. The source of silicic acid was from sodium metasilicate pentahydrate diluted in ATF. The assay method was also changed slightly from the method in **Section 4.5.1**, and is shown in the table below (Table 3).

<b>Reagent</b>	<b>Volume</b>
Sample	100 µl
0.3 M HCl	40 µl
42 mM Ammonium molybdate tetrahydrate	20 µl - 10 min incubation
27 mM EDTA	20 µl
1.35 M Sodium sulphite	40 µl - 1 hour incubation

**Table 3 – Method for the ammonium molybdate assay to determine silicic acid concentration in artificial tear fluid. The reagents were added in the order shown above. The sample was read at 650 nm and at 700 nm.**

#### **4.5.2.2. Static assay in ATF**

0.63 mg of 600 °C thermal APTMS and 0.73 mg of untreated membranes were placed into 50 ml of ATF and kept at room temperature for 10 days. The membranes were placed into a fresh 50 ml solution of ATF daily. Samples were taken at the end of 10 days and used to determine the silicic acid content using the method described in Table 3.

#### **4.5.2.3. Flow through assay in ATF**

0.53 mg of 600 °C thermal APTMS and 0.53 mg of untreated membranes were placed into separate flow cells. ATF was introduced into the cell using a peristaltic pump at a flow rate of approximately 2 ml per hour. Daily fractions of approximately 50 ml were collected. Samples were taken from the fractions to determine the concentration of silicic acid released using the method described in Table 3.

### **4.6. Human Lens Epithelial Cells**

Human lens epithelial cells were cultured in DMEM supplemented with 5 mM L-glutamine, 100 IU/ml penicillin, 100 µg/ml streptomycin sulphate and 10% (v/v) FBS. The cells were maintained at 37 °C in 5% CO<sub>2</sub> in air.

#### **4.6.1. Human lens epithelial cell growth on porous silicon membranes**

Human lens epithelial cells were seeded onto thermal APTMS membranes at a density of 20,000 cells/well in a 12 well plate. A glass coverslip was used as a control surface. The cells were allowed to incubate overnight at 37 °C.

### **4.6.2. Fluorescence imaging**

Cells were stained with 4  $\mu$ l/ml of a 4 mM solution of DiOC<sub>5</sub>(3) for 2 hours. DiOC<sub>5</sub>(3) is a dye that stains the lipid membrane of cells [185, 186]. The cells were then rinsed in water before being wet mounted on a glass coverslip. The cells were observed using a Leitz Laborlux II microscope and images were obtained using a Nikon (DS-5M) digital CCD camera.

### **4.6.3. SEM preparation**

The cells cultured on the membranes and glass coverslips were washed with PBS to remove any remaining cell culture medium. The cells were fixed with a solution containing 4% (v/v) formaldehyde and 2.5% (v/v) glutaraldehyde for 10 mins at room temperature. The cells were washed twice with PBS to remove any remaining fixative. The samples were then dehydrated by sequential immersion in graded alcohol baths; starting from 50%, 70% 95% and two separate 100% (v/v) ethanol baths. A final dehydration bath of xylene was also used. The samples were then air dried and stored under vacuum before being coated with platinum for SEM imaging.

## **4.7. Human Corneal Rims**

Corneal rims containing the limbus that were left over from corneal transplantation surgery were used for the tissue expansion studies. Family consent was obtained for the donated tissue to be used for transplantation and for research. All donor tissue was stored in Optisol™ (Chiron Ophthalmics, Irvine, California) corneal storage medium. Following corneal transplantation, the rims were returned to the Optisol™ solution. The rims were used for expansion studies on the day that they were obtained. The experiments were performed with approval from the institutional Clinical Ethics Committee of Flinders Medical Centre.

### **4.7.1. Expansion of human corneal cells on glass coverslips**

The rims were removed from the Optisol™ and placed into sterile PBS. Excess conjunctival tissue was removed using a sterile blade. If the central corneal button was still present, the button was removed with the use of an 8 mm trephine. The endothelium was removed by scraping the tissue with a blade and washing off the removed endothelial cells with PBS. The rims were then segmented and placed epithelial side up onto glass coverslips in a 6 well plate. The tissue was allowed to attach to the coverslips for 10 mins under sterile air flow before 500 µl of medium was added to each well. In the following day, the volume of medium was brought up to 1 ml and the medium was replaced three times a week. Tissue that failed to attach to the surface after the overnight incubation was discarded. Cell outgrowths were visible after 1 week in culture.

The tissue was incubated in medium containing DMEM/F12, supplemented with 2 mM L-glutamine, 100 IU/ml penicillin, 100 µg/ml streptomycin, 5 µg/ml insulin, 5 µg/ml transferrin, 5 ng/ml sodium selenite, 5% (v/v) FBS and 5 ng/ml epidermal growth factor (EGF). The tissue was cultured at 37 °C in a humidified incubator with 5% CO<sub>2</sub> in air.

For fluorescence microscopy, human corneal cells were expanded onto 18 mm<sup>2</sup> diameter glass coverslips. The cells were cultured for 2 weeks before being stained with 4 µM DiOC<sub>5</sub>(3) for 2 hours. The cells were counterstained with 10 µg/ml Hoechst 33342 dye. Images were captured on an Olympus IX81 fluorescence microscope equipped with an F-view II digital camera and captured using AnalySIS LS Research v2.5 (Olympus, Soft Imaging System, Münster, Germany). Images were false coloured with Adobe Photoshop (Adobe Systems, San Jose, CA, USA).

### **4.7.2. Expansion of limbal tissue on membranes**

Limbal tissue was also expanded onto thermal APTMS membranes. The membranes were cut to approximately 2 mm x 3 mm before oxidation and silanisation as described

in **Section 4.2**. Membranes of these dimensions were used as we could only implant membranes of this size in our *in vivo* studies. Therefore to maintain consistency 2 mm x 3 mm size membranes were used. The surface-modified membranes were then sterilised by dry heat at 160 °C overnight and allowed to cool to room temperature before use. The limbal tissue was dissected as described in **Section 4.7.1**, and allowed to attach to the surface of a 6 well plate for 10 mins under sterile air flow. Pieces of the membranes were then placed around the explant, and sections of the membranes were placed partially under the explant to prevent them from moving when cell culture medium was added. As the epithelial cells do not migrate under the tissue explant, placing the membranes at the edge of the explant ensured that cellular outgrowths and cell migration would occur onto the membrane.

After 2 weeks in culture the cells were stained with 4 µM DiOC<sub>5</sub>(3) for 2 hours. Images were captured in a Leitz Laborlux II fluorescence microscope equipped with a Nikon (DS-5M) digital camera.

## **4.8. Identification of Cell Populations**

### **4.8.1. Immunohistochemistry**

Primary monoclonal antibodies against human p63, cytokeratin 3/12 and cytokeratin 19 were used to probe the cells. All antibodies were mouse based. The secondary detection antibody was an anti-mouse immunoglobulin conjugated to FITC (fluorescein isothiocyanate) for detection via fluorescence. As a negative control, supernatant from the X63 mouse myeloma cell was used. This supernatant contains IgG1 of no known specificity.

Cells were expanded onto 18 mm<sup>2</sup> diameter glass coverslips for 2 weeks as described in **Section 4.7.1**. The explant tissue was removed from the coverslip with a blade, whilst retaining the expanded cells on the glass coverslip. The cells were then fixed with 100% ice-cold methanol (for p63) or 2% (w/v) paraformaldehyde (for all other antibodies) in PBS for 10 mins.

#### *Chapter 4: Methods and Materials*

The cells were washed three times with PBS containing 0.05% Tween 20 (PBST) for 10 mins each. A 10% (v/v) solution of horse serum in PBS solution was used to block non-specific binding of the primary antibodies. The blocking solution was applied to the cells for 1 hour at room temperature before being washed three times with PBST for 10 mins each. The primary antibodies were all diluted in PBS at a dilution of 1:100 and added separately to the cells. The antibodies were incubated with the cells overnight at 4 °C in a humidified chamber. The cells were then washed three times with PBST for 10 mins each, before the addition of an anti-mouse-FITC conjugated secondary antibody. The antibody was diluted in PBS at 1:100 and incubated with the cells for 2 hours at room temperature in the dark to preserve fluorescence. The cells were counterstained with 10 µg/ml Hoechst 33342 (for cytokeratin 3/12 and 19) or 10 µg/ml of eosin Y (for p63) for 30 mins before being washed with PBST for 10 mins three times. The cells were rinsed in dH<sub>2</sub>O and mounted onto glass slides using GelMount™ before being examined with a Leica Laborlux II fluorescent microscope equipped with a Nikon (DS-5M) digital camera.

#### **4.9. MicroCT (X-ray Micro Computerised Tomography)**

Thermally oxidised and thermal APTMS membranes were placed into ATF for a period of 9 weeks. The membranes were then washed with MilliQ water and allowed to air dry completely. The membranes were examined via MicroCT, in a SkyScan-1072, high resolution desk-top microCT system. A control sample was an untreated membrane that was not subjected to the 9 week incubation in ATF.

#### **4.10. Animal Studies**

All animal studies adhered to the ARVO Statement for the Use of Animals in Ophthalmic and Vision Research and approval was obtained from the institutional animal welfare committee.

Inbred male Sprague Dawley rats were bred within our institution and were allowed unlimited access to food and water. All operative procedures were conducted under general anaesthesia using inhaled isoflurane in oxygen. Only the right eye was used for implantation, with the contralateral eye being used as a control.

#### **4.10.1. Surgical technique for the implantation of porous silicon membranes into the eye**

Samples of thermal APTMS membranes, measuring approximately 2 mm x 3 mm, were sterilised by dry heat at 160 °C overnight. The membranes were cooled to room temperature before use. Five animals were used for implantation.

Incisions were made in the conjunctiva to expose the subconjunctival space. The membranes were inserted into the space and the opening was closed using 10-0 Ethilon monofilament nylon sutures (Ethicon, Piscataway, NJ, USA). Implants were made in the superior, temporal and inferior regions of the eye. 1% chloramphenicol ointment (Parke Davis, Caringbah, NSW, Australia) was placed onto the eye at the end of surgery to prevent infection. The implanted eye was monitored under an operating microscope three times a week for four weeks and then once weekly. Images were captured using an Olympus E-330 digital camera. The animals were killed by an overdose of inhalational isoflurane six weeks after implantation. The eyes were then enucleated for histology.

#### **4.10.2. Histology**

##### **4.10.2.1. Fixation**

The enucleated eyes were fixed in 10% (v/v) buffered formalin for a minimum of 24 hours. Subsequently, the globes were placed in 70% (v/v) ethanol overnight and were then transferred through 80% (v/v) ethanol, 90% (v/v) ethanol, and 2 solutions of 100% (v/v) ethanol, each for one hour to dehydrate the tissue. They were left in 100% (v/v) chloroform on the second night. Eyes were then placed in molten paraffin wax at 60 °C

for one hour, then in fresh wax under a vacuum for two 45 minute periods, and finally embedded in fresh wax. 5 mm ocular cross-sections were cut by microtome, and mounted on glass slides which were air-dried before being stored at room temperature.

#### **4.10.2.2. Haematoxylin and eosin staining**

Paraffin-embedded sections were dewaxed by two consecutive 2 minute washes in 100% (v/v) xylene. They were then rehydrated by 2 minute washes in 100% (v/v), 100% (v/v), 90% (v/v) and 70% (v/v) ethanol, and finally water. The sections were stained with a modified Harris haematoxylin stain for 10 minutes, rinsed with water, dipped momentarily into acid alcohol, and again rinsed with water. After standing 2 minutes in 0.05% (w/v) lithium carbonate and rinsing in water, they were counter-stained for 2 minutes with eosin. The slides were finally rinsed in water, and dehydrated with three 30-second washes in 100% (v/v) alcohol, and two 1 minute washes in xylene before being cover-slipped with DePeX mounting medium.

The stained tissue was observed and imaged on a Leitz Laborlux II microscope equipped with a Nikon (DS-5M) digital camera.

#### **4.10.3. Membranes with Corneal Cell Outgrowths**

##### **4.10.3.1. Cell staining with cell tracker dye PKH26**

Thermal APTMS membranes were cultured with corneal rims (as described in **Section 4.7.2**). We wanted to determine if the cells on the membranes were able to be stained with the cell tracker dye PKH26 as this normally stains cells in suspension, rather than adherent cells.

The protocol for staining was modified from a method by Lee *et al* (2000) <sup>[187]</sup>. The cells and membranes were washed twice with sterile PBS to remove any traces of serum. A  $2 \times 10^{-6}$  mM solution (1:500 dilution) of the dye was made up in the

manufacturer-supplied dilution solution (Diluent C) to a volume of 500  $\mu\text{l}$ . The dye was made up immediately prior to the addition of cells. The cells were stained for 5 minutes at room temperature and were shielded from bright light and agitated occasionally to ensure even staining. After staining, 500  $\mu\text{l}$  of foetal bovine serum was added (equal to the volume of the staining solution) to stop the staining reaction, and incubated for a further 1 minute. The cells were then washed three times with cell culture medium containing 10% (v/v) FBS. As a comparison, human corneal outgrowths on glass coverslips were subjected to the same staining treatment. The stained cells were placed onto a glass slide and a coverslip was mounted using glycerol. The cells were imaged on a Leitz Laborlux II fluorescence microscope, equipped with a Nikon (DS-5M) digital camera.

#### **4.10.3.2.      *Implantation of membranes containing human corneal cells***

Thermal APTMS membranes containing human corneal cell outgrowths were stained with the cell tracker dye PKH26 as described in **Section 4.10.3.1**. The stained cells were incubated at 37 °C overnight before being implanted into the right eye of rats (as described in **Section 4.10.1**). To determine if the stained cells could still be observed when placed into the eye, one rat was killed immediately after implantation by an overdose of inhaled isoflurane.

The eye was enucleated and the cornea dissected. Radial cuts were made in between the implantation sites so the cornea could be mounted flat. A coverslip was mounted on the tissue using glycerol and a weight was placed above for 5 mins to flatten the tissue evenly. The flat-mounted corneas were imaged under an Olympus BX50 fluorescence microscope, equipped with a CoolSnap fx digital camera.

A further three animals were implanted with the membrane-containing cells. These animals were killed by an overdose of inhaled isoflurane after one week. Observations

*Chapter 4: Methods and Materials*

of the implanted eye were made during the week under an operating microscope. The implanted eyes were enucleated and prepared for microscopy as described above.

## Results and Discussion

### 4.11. Characterisation of Porous Silicon Membranes

#### 4.11.1. AFM analysis

AFM analysis indicated that the pores in the porous silicon membranes were approximately 40-60 nm in diameter (Figure 50). These were slightly larger than the pore sizes of the porous silicon used in **Chapter 2**, where pore sizes ranged from 10-20 nm. Area statistical rms roughness values for the membrane were approximately 0.71 nm, showing that the membrane had a rougher surface than the porous silicon samples used in **Chapter 2**, which had roughness values of approximately 0.16 nm.

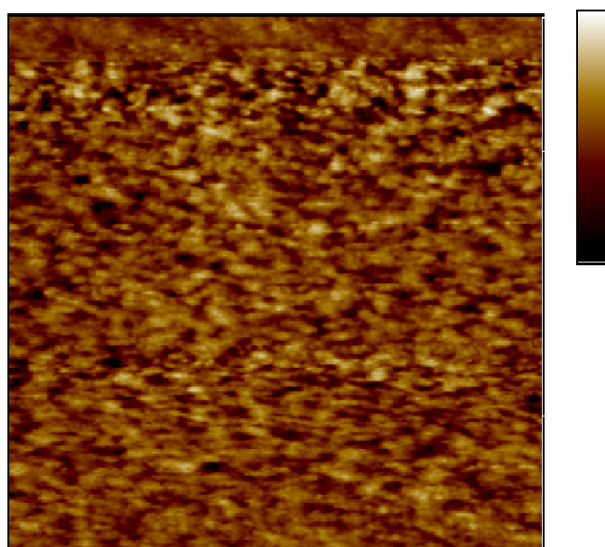


**Figure 50** – AFM image of porous silicon membrane taken under tapping mode. Scan size: 1  $\mu\text{m}$  x 1  $\mu\text{m}$ , height scale: 5 nm.

#### 4.11.2. Energy dispersive X-ray analysis

It was of interest to establish whether the oxidation by thermal treatment of the membrane at 600 °C for one hour would penetrate through to the centre of a membrane or whether the exterior regions would remain more heavily oxidised than the centre of

#### *Chapter 4: Results and Discussion*

the membrane. At the same time, we also wanted to determine the extent of silane penetration. Both the oxidation state and the extent of silane penetration might influence the stability of the membrane in aqueous solutions. A porous silicon membrane that was not completely silanised at the centre would be more susceptible to degradation occurring at the centre of the membrane.

The cross-section of thermally oxidised and thermal APTMS membranes was probed using EDX. The membranes were probed at specific distances from the surface up to 60  $\mu\text{m}$ , towards the centre. Since the membranes were approximately 145  $\mu\text{m}$  in diameter, a distance of 60  $\mu\text{m}$  from the surface was almost in the centre of the membrane.

In the thermally oxidised membrane, we expected a uniform amount of silicon and oxygen throughout the membrane. The EDX results confirmed this, indicating that the centre of the membrane was as oxidised as areas at the exterior of the membrane (Table 4). We were also expecting low amounts of carbon and nitrogen in this sample. Carbon values were low at approximately 2 atomic %, indicating low carbon contamination of the sample. Nitrogen values were also low at approximately 2.2 atomic %. This value was then used as the base value of nitrogen detected in any sample using EDX.

Distance from surface	Atomic Percentage (%) $\pm$ standard deviation							
	Carbon		Nitrogen		Oxygen		Silicon	
1 $\mu\text{m}$	1.46	$\pm 0.92$	2.21	$\pm 0.89$	41.61	$\pm 0.27$	54.72	$\pm 1.91$
2.5 $\mu\text{m}$	1.76	$\pm 0.58$	2.45	$\pm 0.92$	40.76	$\pm 0.79$	55.03	$\pm 0.91$
5 $\mu\text{m}$	1.38	$\pm 0.44$	0.79	$\pm 0.89$	42.20	$\pm 0.66$	55.63	$\pm 0.56$
10 $\mu\text{m}$	2.08	$\pm 1.02$	2.52	$\pm 0.35$	41.66	$\pm 1.14$	53.74	$\pm 0.78$
20 $\mu\text{m}$	1.75	$\pm 0.24$	2.12	$\pm 1.11$	41.93	$\pm 1.56$	54.18	$\pm 1.83$
30 $\mu\text{m}$	1.84	$\pm 0.69$	2.53	$\pm 0.66$	42.13	$\pm 1.23$	53.52	$\pm 1.05$
60 $\mu\text{m}$	2.10	$\pm 0.69$	2.45	$\pm 0.64$	42.21	$\pm 2.27$	53.25	$\pm 2.9$

**Table 4 – EDX results of the cross section of a 600 °C thermally oxidised porous silicon membrane. The cross section was probed at specific distances from the surface of the membrane towards the centre of the membrane. A minimum of 3 samples was used, with a minimum of 3 different locations being probed on each sample. The atomic % is presented as an average of the results.**

As expected, the thermal APTMS porous silicon membranes showed higher amounts of carbon and nitrogen (Table 5) than the thermally oxidised membranes. This was attributed to the 3-aminopropyltrimethoxysilane molecule having reacted with the porous silicon surface. It was expected that the carbon and nitrogen values would remain the same through the whole depth of the membrane, which would indicate good penetration of the silane. The results showed significantly higher amounts of carbon and nitrogen closer to the surface than in the centre of the membrane. Carbon values were 5.6 atomic % at 1  $\mu\text{m}$  below the surface and only 2.4 atomic % at the centre of the membrane. This trend was repeated for the nitrogen percentage: 3.4 atomic % at 1  $\mu\text{m}$  below the surface and 2.4 atomic % at the centre of the membrane. 60  $\mu\text{m}$  below the surface of the membrane, the carbon and nitrogen values were almost at base level. These results suggested that the centre of the membrane was poorly silanised.

Distance from surface	Atomic Percentage (%) $\pm$ standard deviation							
	Carbon		Nitrogen		Oxygen		Silicon	
1 $\mu\text{m}$	5.6	$\pm 2.23$	3.43	$\pm 0.75$	48.23	$\pm 1.92$	42.66	$\pm 3.52$
2.5 $\mu\text{m}$	4.05	$\pm 1.41$	3.02	$\pm 0.65$	47.46	$\pm 2.05$	45.47	$\pm 3.76$
5 $\mu\text{m}$	5.16	$\pm 1.06$	3.15	$\pm 0.87$	47.33	$\pm 2.44$	44.37	$\pm 2.93$
10 $\mu\text{m}$	4.71	$\pm 1.15$	2.90	$\pm 0.68$	47.52	$\pm 2.03$	44.86	$\pm 2.81$
20 $\mu\text{m}$	4.34	$\pm 1.23$	2.95	$\pm 0.92$	47.95	$\pm 2.66$	44.76	$\pm 3.23$
30 $\mu\text{m}$	3.22	$\pm 0.96$	2.54	$\pm 0.97$	47.57	$\pm 2.48$	46.67	$\pm 2.68$
60 $\mu\text{m}$	2.44	$\pm 0.69$	2.41	$\pm 0.64$	46.81	$\pm 2.27$	48.34	$\pm 2.90$

**Table 5 – EDX results of the cross section of a 600 °C thermally oxidised and APTMS silanised porous silicon membrane (thermal APTMS). The cross section was probed at specific distances from the surface of the membrane towards the centre of the membrane. A minimum of 3 samples was used, with a minimum of 3 different locations being probed on each sample. The atomic % is presented as an average of the results.**

We have shown that aminosilanised porous silicon membranes support cell growth and attachment. Thermally oxidising this membrane before silanisation provided protection against degradation in aqueous solutions. The EDX results demonstrated that thermal oxidation was able to fully oxidise a membrane under the methods used. On the other hand, the results showed that silanisation at the centre of the membrane was poor. This could possibly be attributed to the rate of diffusion of the silane into the membrane, where the time or the solvent used for silanisation did not allow the silane to diffuse completely across the whole membrane. This has been shown by other researchers, who they found that slow diffusion into the pores of porous substrates limited the amount of silanisation occurring <sup>[188]</sup>. This result was actually beneficial, with researchers generating DUAL ZONE™ silica based products, where the external surface had one functional group and the internal surface contained a different functional group <sup>[189]</sup>. For our use as a biomaterial, this property may be useful. As the centre of the membrane is poorly silanised, there is less protection against hydrolytic attack and the centre of the membrane could possibly undergo degradation faster than the surface, which is more heavily silanised. It is therefore possible that the centre of the membrane might undergo degradation, whilst cells might be cultured undisturbed on the relatively stable surface. On the other hand, the centre of the membrane may not be

sensitive to hydrolytic attack, as we have shown that the centre has been oxidised (Table 4), and we have shown that thermal oxidation is sufficient to protect the membrane against significant hydrolytic attack.

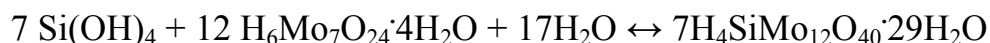
The EDX results have demonstrated that the silicon membranes are not as heavily oxidised and silanised at the centre of the membrane than at the surface. This may effect the degradation of the membranes, where degradation might occur preferentially at the centre, rather than at the surface.

## **4.12. Degradation Studies**

### **4.12.1. Ammonium molybdate assay**

As porous silicon degrades in aqueous solutions, silicic acid is released. We can measure the amount of silicic acid released over time. This enables us to determine the rate of degradation of a piece of porous silicon membrane.

Silicon in solution can occur in the monomeric  $\text{Si}(\text{OH})_4$  form or in polymeric forms. The silicic assay is based upon the formation of a coloured compound with  $\text{Si}(\text{OH})_4$  which can be measured spectrophotometrically. Molybdic acid reacts with  $\text{Si}(\text{OH})_4$  to produce the yellow silicomolybdic acid. The reaction for the formation of silicomolybdic acid is given as <sup>[190]</sup>:



Two forms of silicomolybdic acid complexes are formed; an  $\alpha$ -acid and a  $\beta$ -acid, and both are yellow in colour. The  $\beta$ -acid has twice the absorbance value of the  $\alpha$ -acid, and hence is more sensitive in an assay, and converts spontaneously to the  $\alpha$ -acid at higher pH values. The sample of silicic acid taken for the assay is acidified using HCl to firstly form monomeric  $\text{Si}(\text{OH})_4$  as only the monomeric form is able to react with ammonium molybdate <sup>[181]</sup>. The solution is kept acidified to maintain the formation of

the  $\beta$ -acid complex. The limit of detection of the  $\beta$ -acid yellow complex is 10 mM, which is insufficient for low concentration measurements<sup>[190]</sup>. The silicomolybdic acid complex can be reduced by sodium sulphite to form a molybdenum blue complex of which concentrations as low as 5  $\mu$ M can be detected<sup>[190]</sup>.

#### 4.12.2. Calibration curve in Tris-HCl

The method used for the ammonium molybdate assay was able to produce a detection limit of approximately 20  $\mu$ M of silicic acid. This was comparable to the limits reported by others<sup>[190]</sup>. At a zero concentration of silicic acid, there is a background absorbance value above the blank, indicating that a blue complex is forming in the absence of any silicic acid. It has been reported that the depth of colour formation is not directly proportional to the amount of silicic acid present<sup>[183]</sup>, therefore a calibration curve will not pass through the origin.

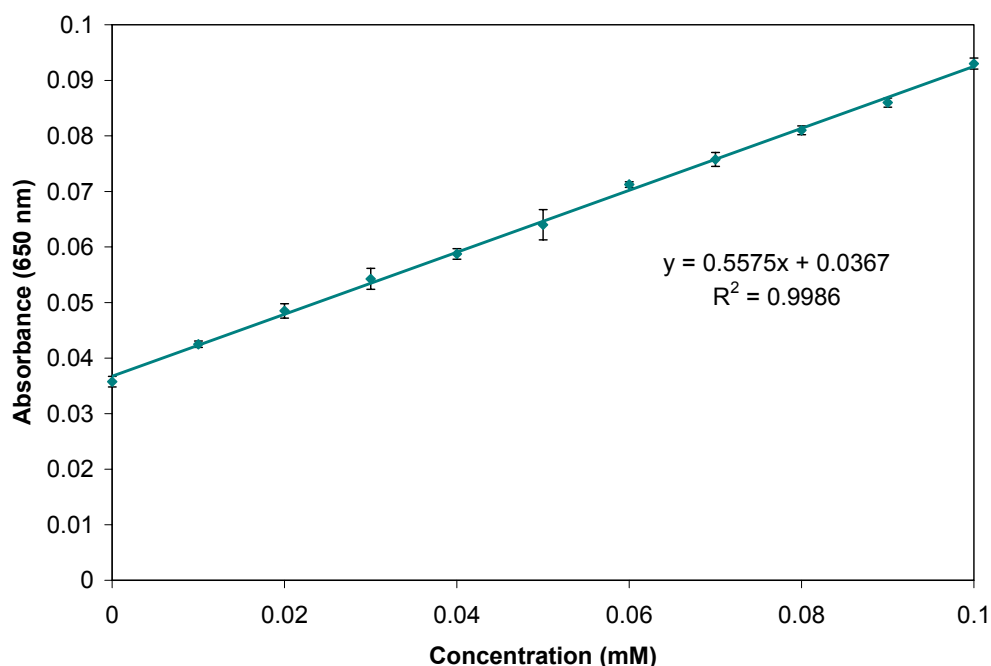


**Figure 51 – Standard curve of sodium metasilicate pentahydrate (silicic acid) in Tris-HCl. Bars represent standard deviation of the mean. Samples were made in triplicate**

#### **4.12.2.1. Static assay in Tris-HCl**

Untreated and thermally oxidised membranes were immersed in a Tris-HCl buffer for 5 days. As the membranes degraded, silicic acid was released into the buffer. The amount of the silicic acid was measured using the ammonium molybdate assay and the concentration calculated using a calibration curve (Figure 51). As the buffer was not changed over the 5 days, this was a static assay and the concentration of silicic acid accumulated over the incubation period (Figure 52). Samples of the buffer were taken daily.

The results demonstrated that untreated porous silicon showed a high release of silicic acid over the 5 days (Figure 52). Thermally oxidised porous silicon, which is protected from hydrolytic attack by the surface silicon oxide groups, also showed some release of silicic acid but at concentrations lower than the untreated porous silicon. This indicated that the thermally oxidised porous silicon was also degrading, though to a lesser extent than the untreated porous silicon samples. As expected, the controls, a glass coverslip and a silicon wafer did not exhibit any release of silicic acid.

At day 4, the amount of silicic acid release rate had decreased in both the thermally oxidised and untreated sample. This indicated that either the amount of silicic acid in the solution was nearing saturation point or that surface passivation had occurred, hence reducing the rate of degradation. As the amount of silicic acid released at the end of 5 days was different for both the untreated and thermally oxidised sample (5.51  $\mu\text{mol}$  and 2.65  $\mu\text{mol}$  per gram of sample, respectively) it indicated that the solution was not saturated. The membranes were still clearly visible at the end of the five day incubation. Therefore, this again suggests that the slowdown in silicic acid release was due to surface passivation. These results suggested that under static conditions, surface passivation occurred around days 4-5, which prevented further degradation from occurring.

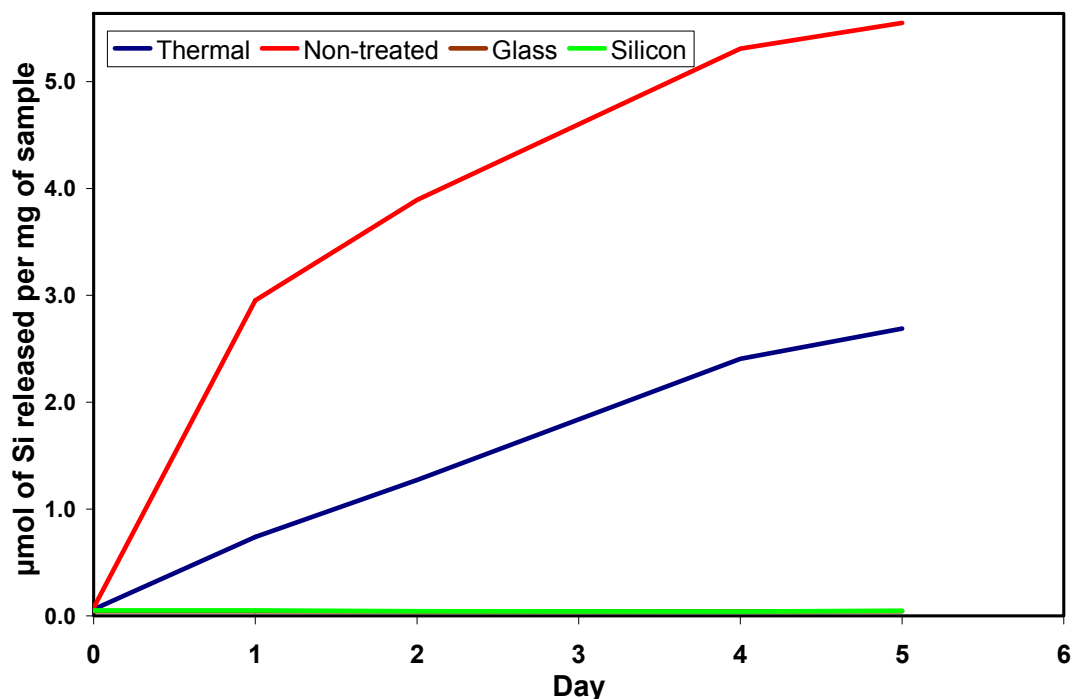


Figure 52 – Amount of silicic acid release over 5 days in static conditions. **Thermal:** 600 °C thermally oxidised porous silicon membrane; **Non-treated:** untreated porous silicon membrane; **Glass:** control glass coverslip and **Silicon:** control silicon wafer. Samples were placed into 50 ml of Tris-HCl and samples of the solution were taken daily. The solution was reacted with ammonium molybdate and the absorbance results were used to calculate the concentration of silicic acid in the solution using the calibration curve in Figure 51. Glass and Silicon samples recorded very low (almost baseline) amounts of silicic acid release over the 5 day period. The Thermally oxidised sample showed some release, whereas the Non-treated sample showed the greatest release of silicic acid over the 5 day period. Data are represented as  $\mu\text{mol}$  of silicic acid released per mg of sample used.

We can calculate and compare the amount of silicic acid released and the total amount of silicic acid expected from a porous silicon membrane (Table 6). The results show that the untreated porous silicon membrane released a greater amount of silicic acid per mg of porous silicon (15.5% release), in comparison to the thermally oxidised membrane (7.5%). These results demonstrate that thermal oxidation of a porous silicon membrane is capable of protecting the membrane from significant hydrolytic attack.

<b>Sample</b>	<b>Mass (mg)</b>	<b>Maximum expected Si amount (mmol)</b>	<b>Measured amount (mmol) at 5 days</b>
Thermally oxidised pSi	13.56	0.48	0.036
Untreated pSi	8.15	0.29	0.045
Glass	182.45	6.50	0.001
Silicon	77.41	2.76	0.000

**Table 6 – Mass of porous silicon and control samples (glass and silicon) used in the degradation assay. The samples were placed into 50ml of Tris-HCl for the assay. The maximum concentration of silicic acid that can be released can be calculated from the mass of the sample. The concentration of silicic measured at the end of 5 days showed that untreated porous silicon had released the greatest amount of silicic acid.**

#### **4.12.3. Artificial tear fluid (ATF)**

Since this porous silicon membrane is to be used as an ophthalmic implant, we opted to use artificial tear fluid to emulate conditions within the eye. We had established the feasibility of the ammonium molybdate assay in Tris-HCl buffer, and we now wanted to determine if this assay was able to be conducted in ATF. The salt composition of the ATF might change the absorbance values when used in the ammonium molybdate assay. Therefore, a calibration curve had to be obtained using sodium metasilicate diluted in ATF (Figure 53).

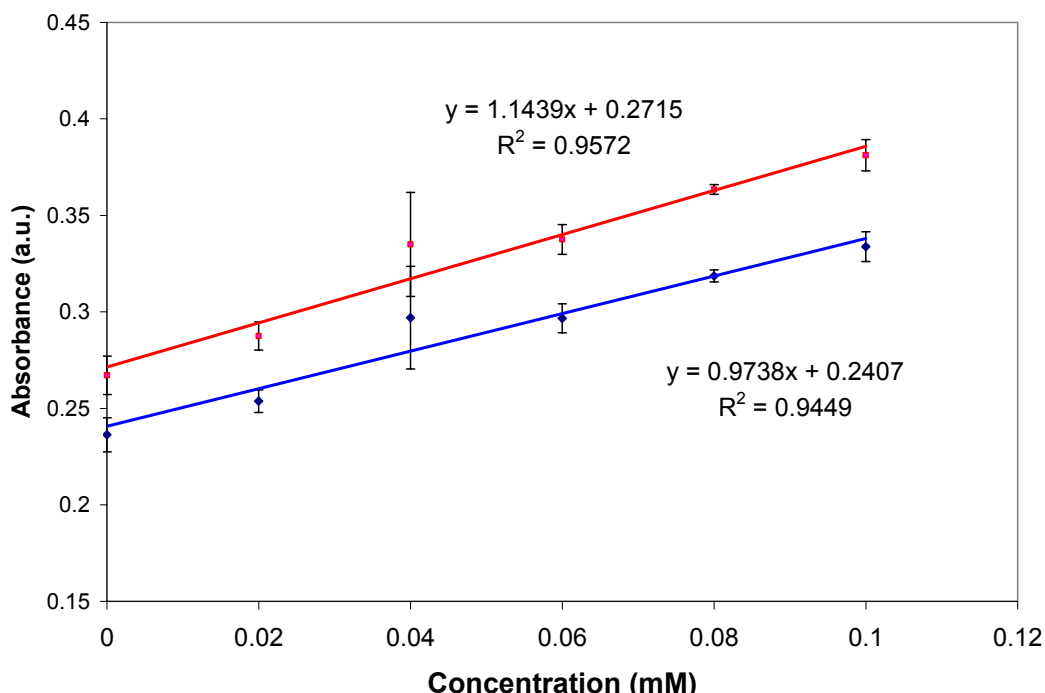


**Figure 53 – Calibration curve of silicic acid in ATF using the ammonium molybdate assay. Absorbance values were taken at 650 nm (blue) and at 700 nm (red). Error bars: standard deviation of the mean. Samples were made in triplicate.**

A linear result was obtained across concentrations ranging from 0-0.1 mM, but again a background absorbance was obtained at the zero concentration. This indicated that the assay reagents were reacting with the ATF components and it has been reported that certain salts can react with the ammonium molybdate reagent<sup>[190]</sup>. This did not seem to affect the slope of the graph, as a linear slope was obtained. A higher absorbance reading was obtained when read at 700 nm and a steeper slope at this absorbance enabled us to measure smaller differences in concentration. The assay was hence read at 700 nm.

#### **4.12.3.1. Static assay in ATF**

Thermal APTMS and untreated porous silicon membranes were placed into 50 ml of artificial tear fluid. The membranes were placed into a fresh 50 ml solution of ATF daily for 10 days. The concentration of silicic acid was measured in each daily fraction

*Chapter 4: Results and Discussion*

(Table 7). From this the amount of silicon being released from the porous silicon membranes was determined and the accumulated concentration calculated. The total amount of silicon released from the thermal APTMS porous silicon membrane was approximately 3  $\mu\text{mol}$  at the end of 10 days. The total mass of thermal APTMS porous silicon used in the assay was 0.63 mg. This showed that only a small amount of degradation occurred with this sample, approximately a 13.5% release. The sample was still visible at the end of the 10 days, further demonstrating that little degradation had occurred. For the untreated membrane, approximately 19  $\mu\text{mol}$  of silicon had been released at the end of the incubation period, approximately a 73% release, which is a significant amount. The silicic acid release rate decreased over time. This occurred with both samples, indicating that stabilisation of the surface by oxidation from the fluid was occurring, rather than solution saturation. The edges of the untreated membrane turned translucent, indicating degradation and surface passivation. The translucency of the membrane was probably due to the thinning of the porous silicon layer and conversion into silica <sup>[129]</sup>.

Day	Thermal APTMS		Untreated	
	Conc. (mM)	Accumulated release ( $\mu\text{mol}$ )	Conc. (mM)	Accumulated release ( $\mu\text{mol}$ )
1	0.002	0.117	0.077	3.851
2	0.006	0.429	0.054	6.555
3	0.018	1.345	0.096	11.372
4	0.010	1.823	0.036	13.172
5	0.006	2.126	0.008	13.568
6	0.002	2.235	0.023	14.712
7	N/D	2.235	0.010	15.231
8	0.011	2.780	0.030	16.748
9	N/D	2.780	0.043	18.890
10	0.006	3.060	0.004	19.090

**Table 7 – Static assay displaying the concentration of silicic acid and the corresponding accumulated amount of Si release from membranes in ATF as determined by the ammonium molybdate assay. Amount of Si release is the accumulated calculated mass of silica released over the 10 day period. Thermal APTMS: 0.63 mg of 600 °C thermally oxidised and aminosilanised porous silicon membrane. Untreated: 0.73 mg of non-treated porous silicon membrane. N/D: not detectable.**

#### **4.12.3.2. Flow-through assay in ATF**

We tried to emulate the conditions found in the eye by using a constant fluid flow of ATF over the membranes. This was expected to give us an indication of the degradation rate of the membranes when implanted in the eye. Normal tear fluid flow in the human eye is approximately 72  $\mu\text{l}/\text{hour}$  <sup>[191]</sup>. Our facilities enabled us to produce a minimum fluid flow of 2 ml/hour, sufficient to give us an indication of the degradation rate in a flow situation.

In the flow-through assay, the thermal APTMS porous silicon did not show any detectable release of silicic acid for the first few days and only a small amount could be detected over the 10 day period (Table 8). The overall release was calculated to be 10% of the original membrane and this demonstrated that very little degradation had occurred. The untreated membrane again showed a greater release of silicic acid, indicating a faster degradation rate, a 35% release over the 10 day period. Surface passivation occurred with the untreated membrane at day 6, at which time no recordable amount of silicic acid could be detected. This indicated that surface stabilisation had occurred and had stabilised the surface from further degradation.

Day	Thermal APTMS		Untreated	
	Conc. (mM)	Accumulated release ( $\mu\text{mol}$ )	Conc. (mM)	Accumulated release ( $\mu\text{mol}$ )
1	N/D	0.00	0.020	0.98
2	N/D	0.00	0.030	2.42
3	N/D	0.00	0.049	4.76
4	0.002	0.11	0.027	6.03
5	N/D	0.11	0.015	6.75
6	0.015	0.81	N/D	6.75
7	0.002	0.92	N/D	6.75
8	N/D	0.92	N/D	6.75
9	N/D	0.92	N/D	6.75
10	0.002	1.03	N/D	6.75

**Table 8 – Results of the flow through assay displaying the concentration of silicic acid and the corresponding accumulated amount of Si release from membranes in ATF when placed in a flow through system. Amount of Si release is the calculated accumulated amount of silica released over the 10 day period. A fluid flow of 2 ml/hour was used through the system and daily fractions of the effluent were collected over 10 days. Thermal APTMS: 0.53 mg of 600 °C thermally oxidised and aminosilanised porous silicon membrane. Untreated: 0.53 mg of non-treated porous silicon membrane. N/D: not detectable.**

Both the flow-through and the static assay results both confirmed that thermal APTMS membranes were more resistant to degradation in aqueous conditions than an untreated membrane. The membrane recorded a smaller release of silicic acid in the flow-through assay, although it is unclear why this would be the case. The membranes were placed into a custom-made Perspex holder for the flow-through assay. The presence of the membranes in the holder may have limited the flow and the diffusion of silicic acid from the membrane. This would have resulted in extremely low or undetectable amounts of silicic acid. The membranes were observed to be degrading by the production of gas (hydrogen gas as shown in **Section 1.2.2**). It was also observed that this gas was unable to escape the holder, generating hydrogen bubbles around the membrane and hence not coming into contact with the fluid. This was observed for both membranes, but more evident with the untreated membrane. This was due to the oxidation and silanisation of the thermal APTMS generating a more wettable surface, allowing the fluid to penetrate the membrane better (as we have shown in **Section 2.6.1**). We did not expect surface passivation to occur quickly, and the untreated

membrane only showed a decrease in silicic acid release after day 5, which was consistent with results obtained in the static assay.

### **4.13. Cell Culture Studies**

#### **4.13.1. Immortalized cells**

##### **4.13.1.1. Cell growth on porous silicon membranes**

Fluorescence microscopy was conducted on human lens epithelial cells cultured on thermal APTMS membranes. We used APTMS as a surface modification in **Chapter 2** and we had shown that APTMS-treated surfaces promoted cell attachment and proliferation of human lens epithelial cells. Here, our results showed that the cells adhered well and had a similar morphology to cells cultured on a glass coverslip (Figure 54). This result confirmed that aminosilanisation of porous silicon membranes created a surface that was conducive for cell attachment.

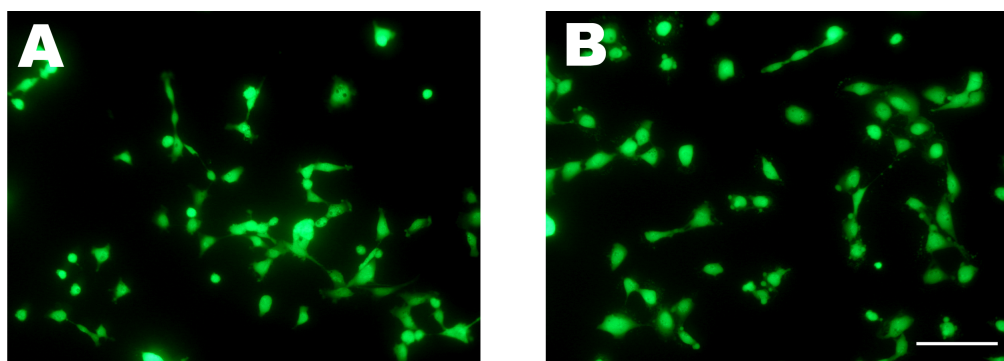


**Figure 54 – Human lens epithelial cells stained with FDA. Cells were cultured for 24 hours on A: thermal APTMS porous silicon membrane and B: control surface of a glass coverslip. Scale: 150  $\mu$ m.**

SEM allowed us to examine the cellular morphology in relation to the surface. On the thermal APTMS membrane, the cells spread across the surface, indicating good adhesion. A similar morphology was observed in cells cultured on glass (Figure 55).

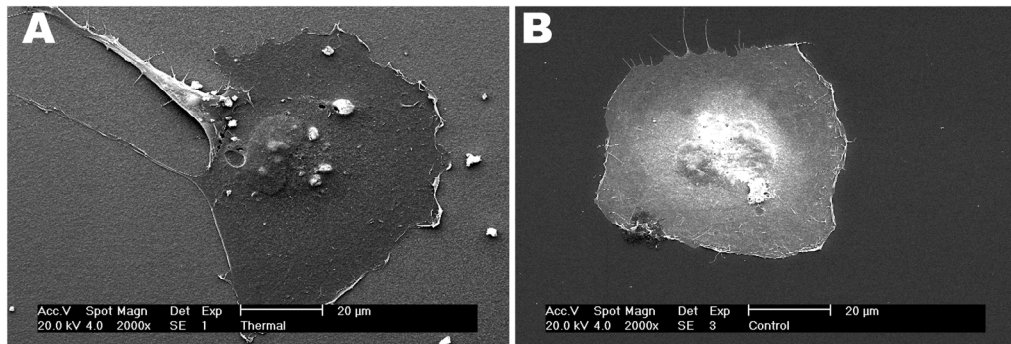


**Figure 55 – SEM images of human lens epithelial cells cultured on A: a thermal APTMS membrane, B: a glass coverslip. Cells on the membrane show similar morphology to the cells on the glass coverslip.**

### **4.13.2. Primary cell culture**

#### **4.13.2.1. Fluorescence images of corneal outgrowths**

Corneal rims were dissected and placed onto glass coverslips for the culture of cellular outgrowths. Rounded cells were observed at the edges of the tissue after 3 days in culture, indicating that some cell migration had occurred from the tissue. After one week, cells were observed as a monolayer sheet on the glass coverslip at the edges of the tissue. Observation of this cell sheet showed at least three distinct cell types: large flat cells, thin elongated cells and small cuboidal cells (Figure 56). The large cells have been reported to be terminally differentiated epithelial cells from the central cornea as they bear a resemblance to cells cultured from the central cornea (Figure 57A)<sup>[192]</sup>. As these cells do not replicate, they spread out along the surface, becoming large cells. It has been reported that these large cells do not survive longer than 2 weeks in culture<sup>[192]</sup>.

The thin elongated cells were probably fibroblasts<sup>[193]</sup>. In longer culture conditions (> 2 weeks), we observed these cells to show a swirl-like pattern on the surface of the plate, which is a characteristic of fibroblast behaviour at high cellular density<sup>[194]</sup>. The

*Chapter 4: Results and Discussion*

smaller cuboidal cells (Figure 57B) are thought to originate from the limbal region and have been shown to have higher mitotic rates than the larger cells <sup>[192, 195]</sup>.

When the outgrowths were cultured onto aminosilanised porous silicon membranes, a similar cellular population was observed (Figure 58). Large cells, fibroblasts and cuboidal cells were all present on the membranes. During culture, the migration of cells proceeded across the membrane. When the cells encountered the edge of the membrane, migration paused at this interface. Cells then migrated along the membrane edge until the increase in cell density caused the migration to continue across the interface.

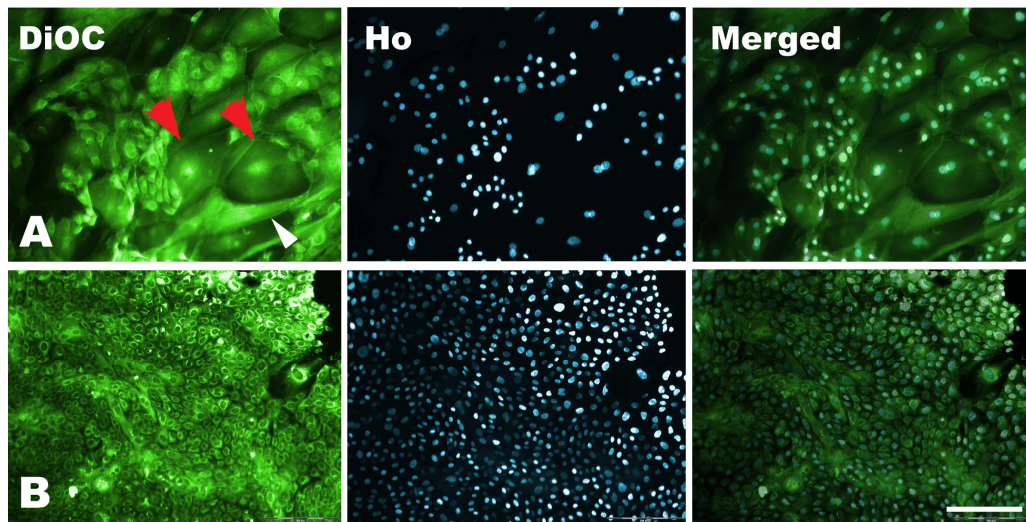


**Figure 56 – Limbal cell expansion on glass coverslips after a 2 week culture. Three distinct cell populations can be observed. A: large cells (red arrowheads) and thin elongated cells (white arrowhead), B: clusters of small cells. A single layer of cells were obtained as shown by the dual staining. DiOC: DiOC<sub>5</sub>(3) stained cells, Ho: Hoechst 33342 stained cells and Merged: merged image of the two stains. Scale: 200  $\mu$ m.**

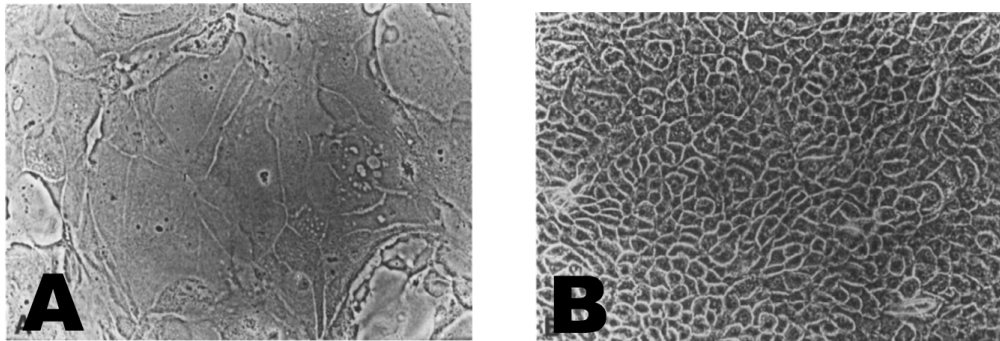


**Figure 57** – Light microscope images of cell outgrowths from corneal explants. **A:** cells from the central cornea and **B:** cells from the peripheral cornea. Reproduced from Ebato *et al* 1987 <sup>[192]</sup>.

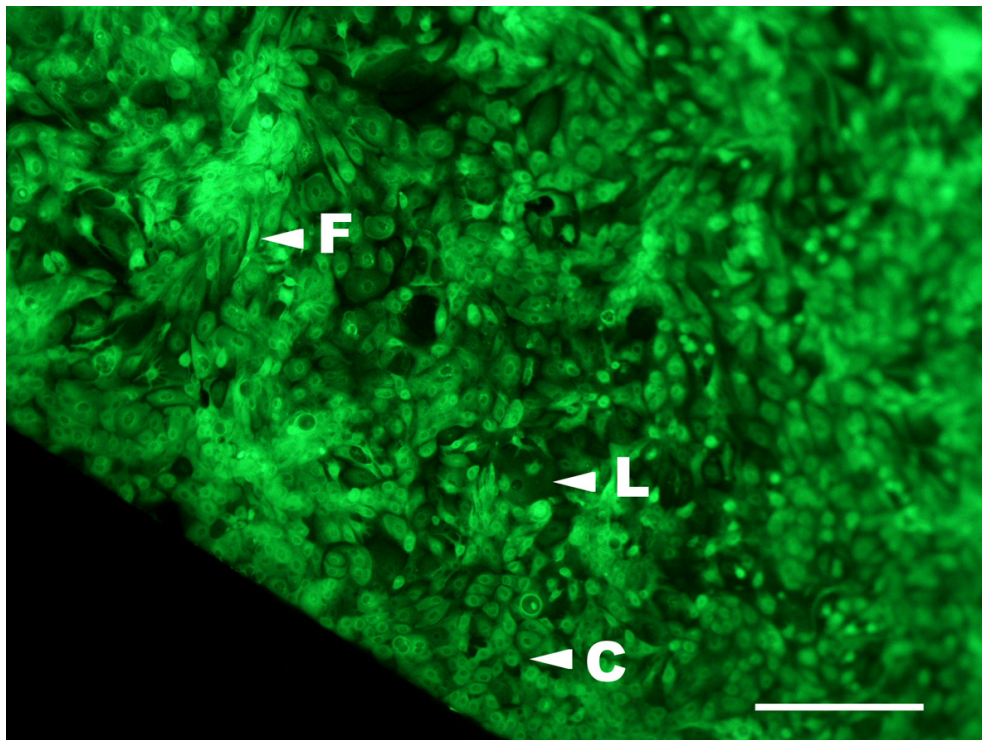


**Figure 58** – Cellular outgrowths from a corneal rim explant on thermal APTMS porous silicon membranes after a 2 week culture. Cell migration paused at the edge of the membrane, although at longer culture, cells migrated off the membrane. Large cells (L) were visible in the population, as well as cells with fibroblast (F) morphology and cuboidal (C) morphology. Cells were stained with DiOC<sub>5</sub>(3). Scale: 150  $\mu$ m.

#### **4.13.2.2. Immunohistochemistry of cultured cells**

The cellular outgrowths from the limbal tissue explants were cultured onto glass coverslips and known marker proteins were identified using a variety of antibodies.

Intermediate filaments have long been used to identify cellular origins. Cells can be classified according to the type of intermediate filament present; neuronal cells contain neurofilaments, muscle cells contain desmin, mesenchymal cells contain vimentin and epithelial cells are characterised by cytokeratin proteins<sup>[196]</sup>.

Human epithelial cells can be classified according to the cytokeratin protein (CK) expression. In the cornea, the epithelial cells have been shown to express CK3 and 12, and as they are often expressed together, the proteins are often referred to as CK 3/12<sup>[197]</sup>. CK 3/12 has been shown to be expressed in mature or terminally differentiated epithelial cells of the cornea<sup>[82]</sup>. Ubiquitous expression of CK 3/12 in the cellular outgrowths indicates that the cells are highly differentiated and theoretically do not contain any proliferative activity<sup>[104]</sup>. Our results showed that most cells in corneal rim explants expressed CK 3/12 (Figure 59).

Another cytokeratin expressed in the cornea is CK 19. This protein has been shown to be expressed in cells in the basal layer of the limbus<sup>[79, 84]</sup>, which do not co-express CK 3/12. Since these cells are present in the basal layer, they are expected to have undergone less differentiation than epithelial cells expressing CK 3/12. This suggests that CK 19 expressing cells may be capable of proliferation. When our cell outgrowths were probed for the presence of CK 19, we did not encounter any positive cells (Figure 60). This demonstrated that the cell outgrowths we obtained did not contain many cells with proliferative capabilities and contained mainly terminally differentiated cells.

We next probed the outgrowths against nuclear transcription factor p63. The expression of p63 has been shown to be essential for the development of normal epithelium<sup>[198]</sup> and has been associated with cells of stem cell phenotype<sup>[87]</sup>. To date there is no specific marker to identify the presence of limbal stem cells, although Pellegrini *et al*

#### *Chapter 4: Results and Discussion*

has shown that p63 is expressed in the basal cells of the limbus and has associated the proliferative capability of corneal cells with the expression of p63, where cells with lower proliferation capabilities express lower amounts of p63 [87]. When we probed for the presence of p63 in the cell outgrowths, we observed a few positive cells (Figure 61). As p63 is expressed in the nucleus, a non-nuclear counterstain was used, in this case, Eosin Y. The counterstain helped to identify the positive cells as some autofluorescence was observed. In all instances, the negative control using the X63 supernatant, did not yield any positively stained cells.

The presence of some positively stained cells in the outgrowths indicated that there were some cells that had some stem cell-like properties. However, the majority of cells in the outgrowths were terminally differentiated. The limbal tissue used to form cell outgrowths were from normal (non-damaged) eyes, and hence, limbal stem cells should be present in the tissue. The immunohistochemistry experiments were carried out on cell outgrowths that were cultured on glass coverslips. Therefore the porous silicon surface did not promote the differentiation of cells. This indicated that the culture conditions used for the explants were not conducive for the maintenance of poorly differentiated cells. Several other different methods of cell culture were tested, such as using the enzyme dispase to obtain epithelial cells. Dispase acts upon the basement membrane, thereby allowing an epithelial cell sheet to be lifted off the basement membrane [199]. The epithelial cells could then be treated with trypsin to form a single cell suspension [200]. When we tested these methods, few cells were obtained using the dispase method and these cells did not attach to a glass or TCPS surface when cultured further to expand the cell population. As we were testing the use of porous silicon as a biomaterial, we required the cells to have attachment capabilities. The method described in this thesis was a method that was able to promote the formation of cell outgrowths onto glass, TCPS and porous silicon surfaces.

In the future, changes to cell culture components may reduce the amount of differentiation during culture. For example, cholera toxin has been added to the medium of limbal cultures by some researchers [195, 201]. Cholera toxin has been shown

#### Chapter 4: Results and Discussion

to have an immunosuppressive effect and hence prevents the release of certain cytokines [202, 203]. Cytokines are expressed by the fibroblast cells in the limbus and it has been postulated that these cytokines, such as keratinocyte growth factor, may play a role in promoting the differentiation of the stem cells [204]. In this respect, hydrocortisone is another component that has been added to the medium of some *in vitro* limbal cell cultures [195, 201, 205]. Hydrocortisone is a hormone and has been shown to promote the binding of epidermal growth factor (EGF) to cells [206] and to maintain the clonal growth of keratinocytes [207, 208]. The addition of cholera toxin, cytokines and hydrocortisone at appropriate concentrations to the medium might help maintain the undifferentiated state of the cells.

Cells from the limbus region have been cultivated on several surfaces by others. As mentioned previously, the use of inactivated mouse 3T3 feeder cell layers have often been used to culture cells from the limbus [209-211]. Outgrowths on human amniotic membrane have also been shown to maintain the differentiation state of the outgrowth cells [100, 195]. This has been attributed to the presence of specific collagen sub-chains and laminin proteins in the human amniotic membrane [212]. It has also been shown that on human amniotic membrane, limbal cell outgrowths proliferate faster [101], demonstrating that the membrane promotes the growth of cells without inducing the differentiation of cells.

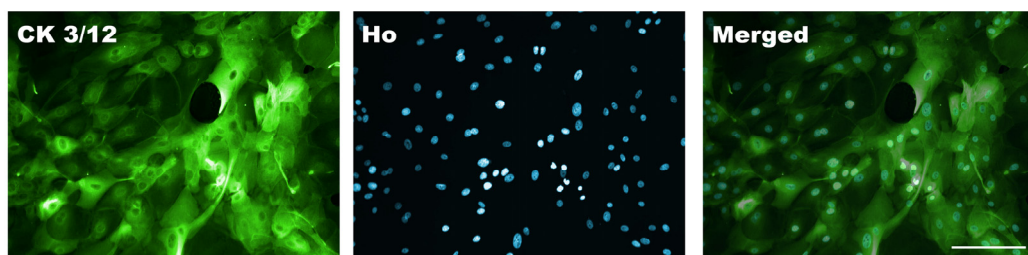


**Figure 59 – Expression of CK 3/12 in 2 week old cell outgrowths from corneal rim explants (CK 3/12). The nuclear Hoechst 33342 (Ho) was used as a counterstain to mark the position of cells. The majority of cells are positive for CK 3/12. Scale: 100  $\mu$ m.**



**Figure 60 – Expression of CK 19 in 2 week old cell outgrowths from corneal rim explants (CK 19). The nuclear stain Hoechst 33342 (Ho) was used as a counterstain to mark the position of cells. We did not detect the presence of any positive cells. Scale: 100  $\mu$ m.**

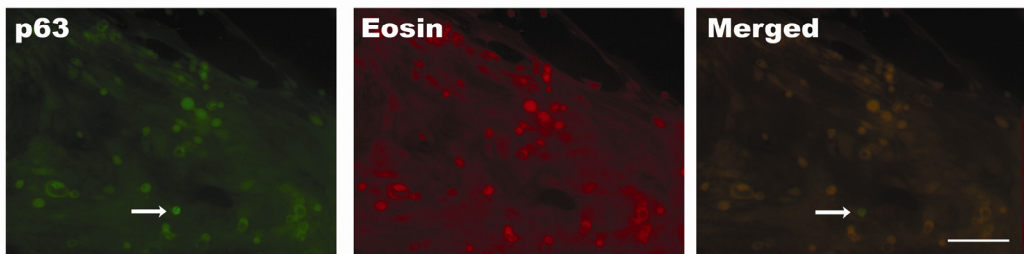


**Figure 61 – Cell outgrowths from a corneal rim explant probed against the presence of p63. The cells were counterstained with eosin Y to mark the position of cells. Only a few cells positive to p63 could be seen in the cell outgrowths (white arrows). Scale: 100  $\mu$ m.**

Cells from corneal rim tissue have been successfully cultured on surfaces without the need of feeder layers or human amniotic membrane [192, 193, 213]. The efficacy of human amniotic membrane (containing cultured cells) in facilitating the wound healing of the eye has been demonstrated by several researchers [90, 105, 214, 215]. However, amniotic membrane is a harvested human product which will lead to batch to batch variability. It would be beneficial to have a non-human and a non-animal product that is highly controlled but has the valuable properties of amniotic membrane.

We wanted to use porous silicon membranes as a support for stem cell delivery into the eye. Although experiments involving the cell outgrowths onto the porous silicon membrane have shown that the population of stem cell-like cells was rare, cells remained viable on the surface. In addition, we showed that it was possible to obtain outgrowths on the porous silicon membranes.

## **4.14. Animal Studies**

### **4.14.1. Implantation of thermal APTMS membranes into the eye**

We wanted to determine the biocompatibility of the porous silicon membranes. We did this by implanting thermal APTMS porous silicon membranes into the subconjunctival space of a rat eye. Previous results have shown that this porous silicon surface modification supported the growth and viability of cells on its surface *in vitro*. By implanting the membrane only, we expected to observe any response generated by the host against the implant. If the implant showed signs of bioincompatibility, we would observe necrosis, inflammation and vascularisation around the implant. For this study, we implanted pieces of thermal APTMS membranes into five animals. In each animal, three pieces were implanted into the right eye at the superior, temporal and inferior regions of the eye (Figure 62).

The animals were observed over a period of 9 weeks or until the pieces of porous silicon were no longer visible under the operating microscope (Figure 63 and Figure 64). We looked for signs of implant rejection as well as for the presence of the porous silicon implant. In all animals, we observed in the first week that the tissue was swollen around the implant and sutures. The swelling became less evident after the first week indicating that the swelling was an inflammatory response to the injury caused during implantation <sup>[216]</sup>. We observed some signs of vascularisation but this seemed to be confined to the suture site. It has been shown that a nylon suture by itself, causes fibrin deposition around the material <sup>[217, 218]</sup>. We did not observe signs of inflammation or vascularisation around the porous silicon membrane, suggesting that the membranes did not invoke an observable immune response and were well tolerated by the host. This was also confirmed by the histology results presented in **Section 4.14.2**.

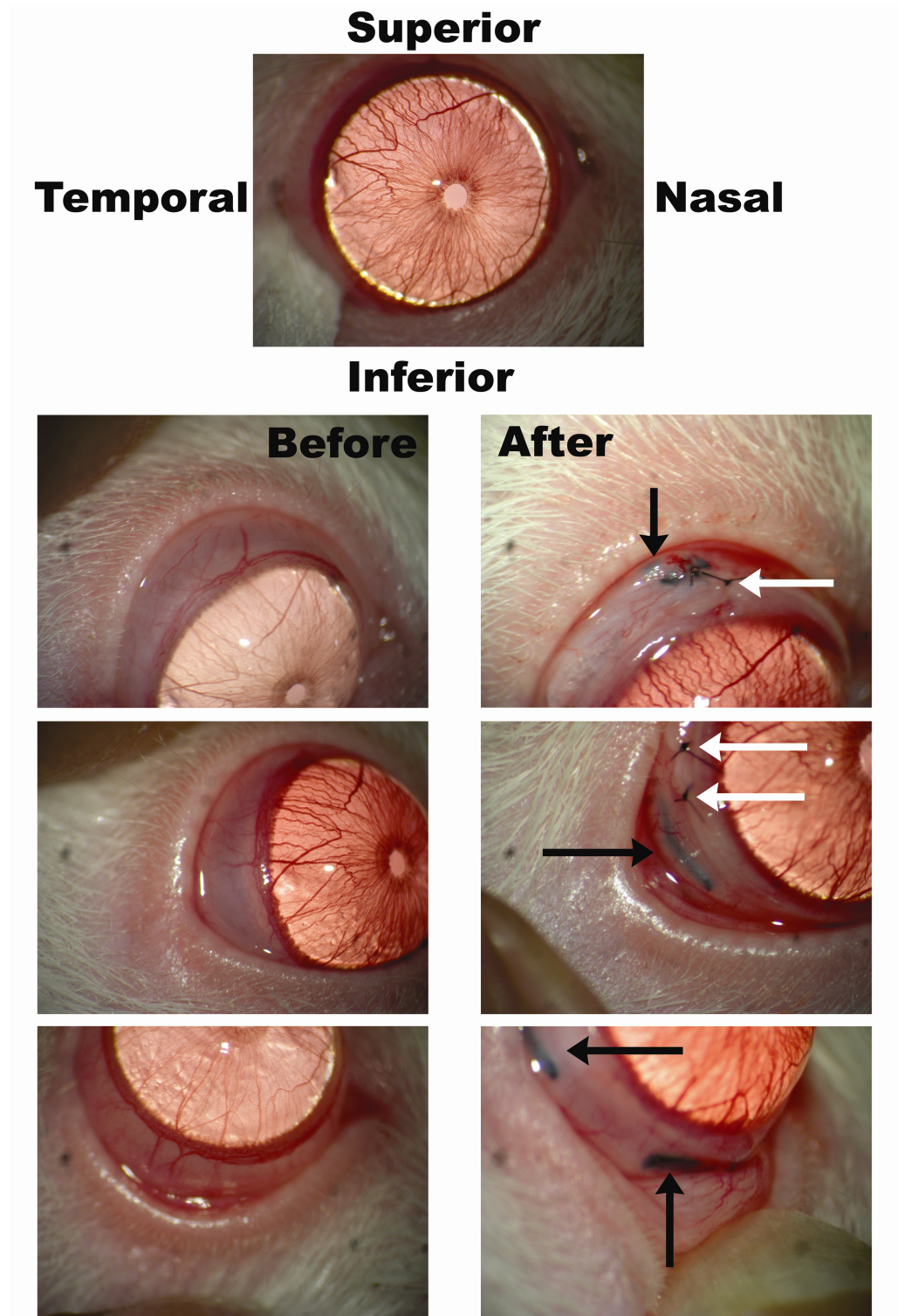
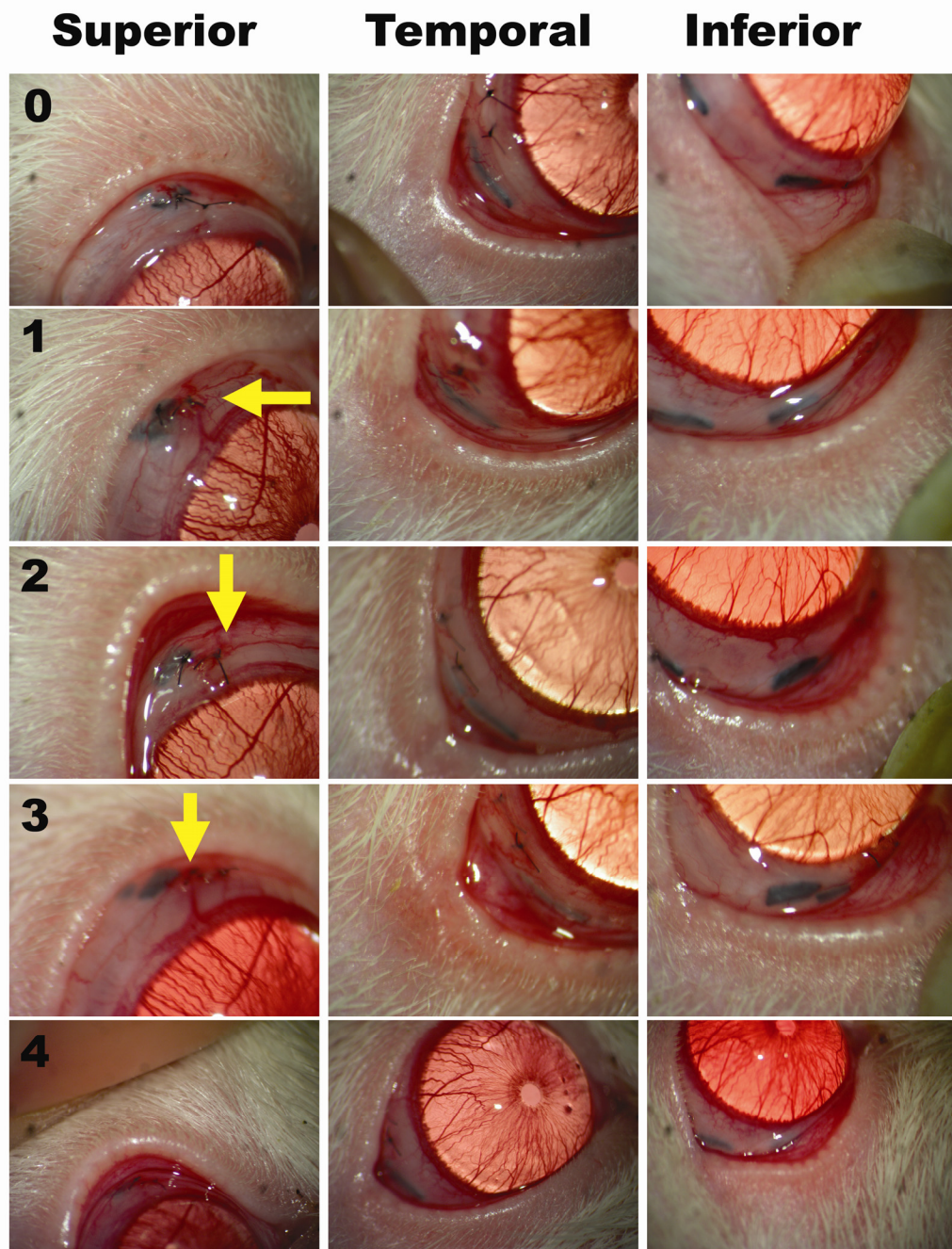


Figure 62 – Images of the rat eye before and immediately after implantation with thermal APTMS porous silicon membranes in the superior, temporal and inferior regions (black arrows). Monofilament nylon sutures were used to seal the incision site (white arrows).



**Figure 63 – Photographs of thermal APTMS porous silicon implants at the superior, temporal and inferior sites as viewed through as operating microscope. Photographs were taken from immediately after implantation and week 0 to week 4. There was no observable change in the implanted membranes within this 4 week period. Vascularisation can be seen in the superior implant at the sutures sites (arrows). Photographs are continued in Figure 64.**

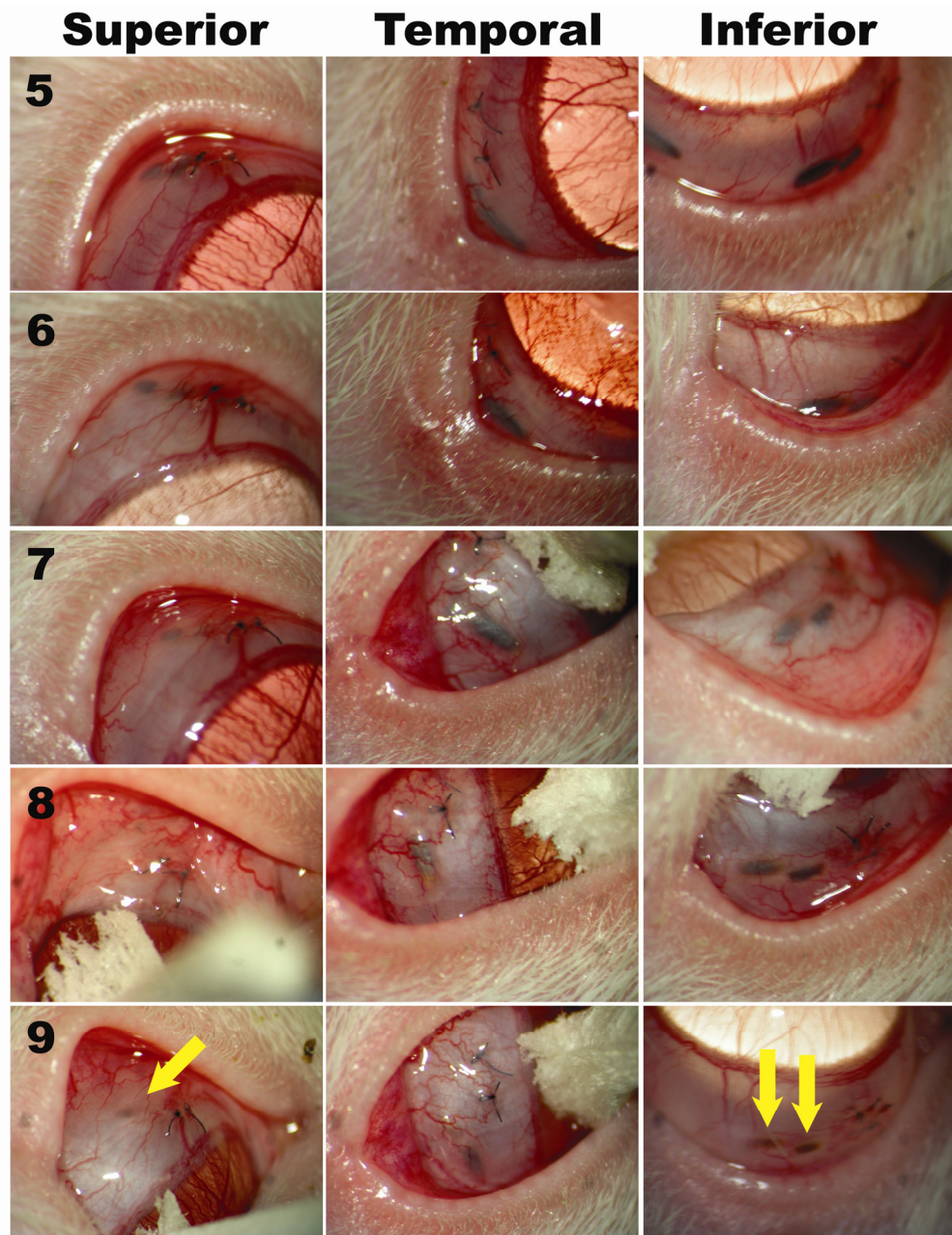


Figure 64 – Photographs of thermal APTMS porous silicon membranes in the superior, temporal and inferior sites of the eye, continued from Figure 63. Photographs were taken from week 5 to week 9. The implanted porous silicon showed signs of dissolution during this period. At week 9 the implanted porous silicon pieces (arrows) had significantly reduced in size in comparison to the implants at week 1. The superior implant could barely be discerned at week 9.

In three animals, we could still observe the porous silicon membranes after a period of 6½ weeks. In a fourth animal, the membranes were no longer observable under the operating microscope after 2 weeks, and in the fifth animal, after 3 weeks. Upon enucleation of the eyes, the membranes could be observed, but had turned translucent, making observation difficult in the live animal. This indicated that the membranes had undergone degradation and oxidation. This was verified by histology.

#### **4.14.2. Histology of eyes implanted with porous silicon membranes**

The eyes containing the porous silicon implants were enucleated, sectioned and stained with a haematoxylin and eosin stain (H&E). Haematoxylin is a basic dye and stains the nuclei of cells a blue/purple colour <sup>[219]</sup> whilst eosin is an acidic dye that stains basic structures such as the cytoplasm of cells, a red colour <sup>[220]</sup>. Figure 65 is a photographic montage of a H&E stained section of a rat eye showing a region around a porous silicon membrane implant.

When a foreign material is inserted into host tissue, the host initiates a foreign body response to the implant <sup>[216]</sup>. The degree of response and reactions by the host is determined by the material inserted, and is related to its biocompatibility. A biocompatible material will induce a small host response <sup>[216]</sup>. Inflammation will occur in response to a tissue injury in order to heal the injured site. Therefore we expected some inflammation to occur at the implant site. Generally speaking, an inflammation response is initiated by lymphocytes, granulocytes and monocytes, which differentiate to form macrophages <sup>[221]</sup>. In the case of an implant, a response is initiated when macrophages come into contact with the material <sup>[222]</sup>. At the material surface, the macrophages releases chemical signals to attract other macrophage cells to the material. These cells can combine to form multinuclear giant cells. These cells are often observed surrounding implanted materials <sup>[222]</sup>. In an H&E stain, immune cells are generally seen as dark cells surrounding an implant or foreign body. Lymphocytes are observed as cells with little cytoplasm and a dominating nucleus, and macrophages are

large cells with a large nucleus. The macrophages and giant cells have been observed to persist throughout the lifetime of an implant, although it is unclear if these cells remain in an activated state or become dormant [222].

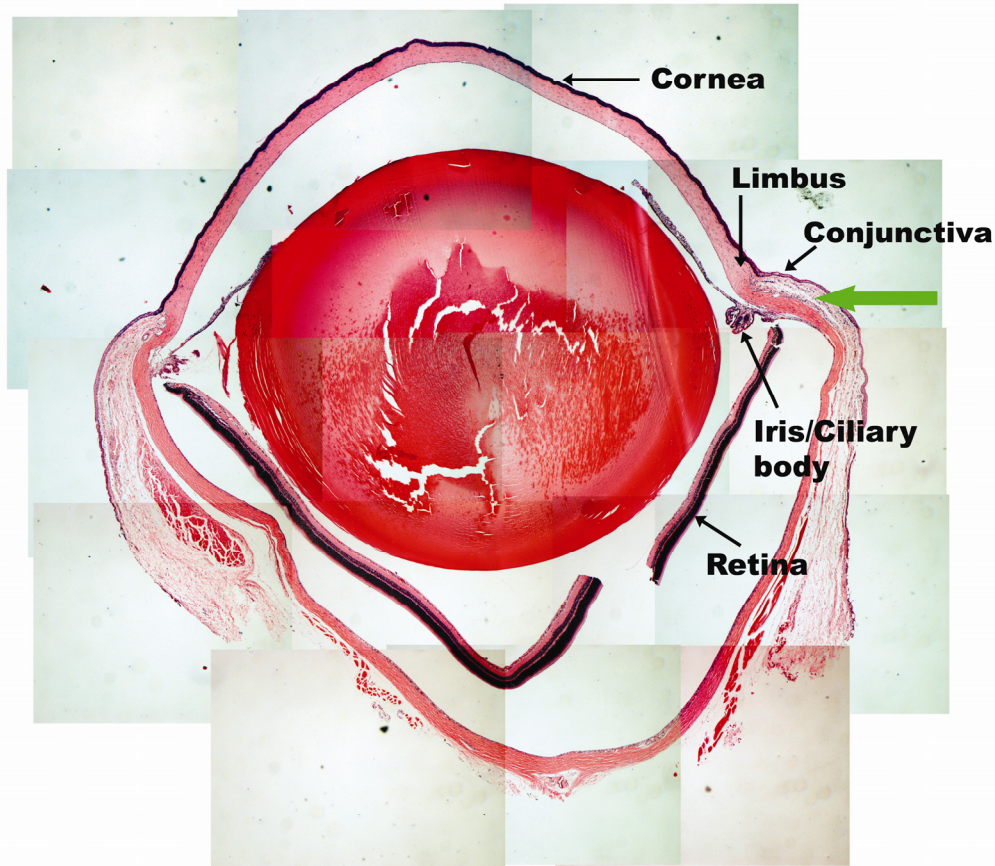


**Figure 65 – Photographic montage of an H&E stained tissue section of the rat eye. In this section the retina has detached from the back of the eye. The green arrow represents the region in which a piece of porous silicon membrane was implanted.**

A secondary response to an implant is the formation of fibrous tissue surrounding the implant. This phenomenon isolates the implant from the surrounding tissue and is formed by fibroblasts at the implant site. The fibroblasts generate a thick layer of protein, which has shown to be mainly Type III collagen [216]. In an H&E stained section, this is observed as pink tissue surrounding the implant or foreign body. Angiogenesis may also occur around the implant site, depending upon signals released by the activated macrophages [223]. In an H&E stain, the presence of blood cells can be

#### *Chapter 4: Results and Discussion*

observed as red cells without a nucleus. The presence of a cluster of blood cells can indicate a blood vessel.

In Figure 66 and Figure 67, a porous silicon membrane surrounded by few inflammatory cells is visible after being implanted for 9 weeks. The porous silicon is observed as the brown object in the section. In Figure 66, small fractures in the membrane can be observed, whilst in Figure 67, it appears that the membrane has fragmented. As the membranes are brittle, this was most likely generated during the sectioning process as voids between the tissue and membrane are observed, indicating that the membrane was pulled away from the tissue due to the mechanical forces during sectioning. The membrane in Figure 66 has also thinned significantly. Originally, the membranes were approximately 150  $\mu\text{m}$  thick. In Figure 66, the membrane is now measured to be approximately 70  $\mu\text{m}$  thick. Parts of the membrane are observed as pink, seen at the ends and through the central fracture in Figure 66, and in half of the membrane in Figure 67. It is possible that the porous silicon has taken up some of the eosin stain, turning the porous silicon pink. It is also possible that the membrane has absorbed protein, which is stained pink by eosin.

In Figure 66, the cells infiltrating the large fracture through the centre are mainly lymphocytes and macrophages, as assessed by morphology, and these cells are also concentrated at the ends of the membrane. It is unclear why cells have infiltrated the membrane. It is possible that the porous silicon had started to degrade in the centre of the membrane. We showed previously through the use of EDX that the central region of the membrane was not as highly silanised as the exterior regions (**Section 4.11.2**). Therefore, the central regions of the membrane may be more susceptible to degradation, allowing the infiltration of cells into the membrane. We briefly investigated this through the use of X-ray micro computerised tomography (microCT). Samples of thermally oxidised and thermal APTMS membranes were placed into artificial tear fluid for a period of 9 weeks (the same length of time that the membrane, shown in Figure 66, was implanted for). The membranes were subjected to microCT to observe the internal structure. A control sample of an untreated porous silicon membrane (that was

#### *Chapter 4: Results and Discussion*

not incubated in artificial tear fluid) was also observed under microCT. The microCT results were rather inconclusive and showed no observable differences between all three samples. Another method to determine if degradation occurs preferentially at the centre of the membrane is to implant the membranes into the rat eye and remove the membrane after a period of 9 weeks. The membrane could then be scrutinised via microCT or snapped to reveal the cross section and examined via SEM. Voids within the membrane would indicate that degradation does occur at the centre. However, we cannot exclude that the fractures within the membranes are artefacts formed during the sectioning and staining process. Some cells are also observed within the empty space near the fractured membrane (Figure 67), but it is difficult to determine if the cells had indeed migrated to the membrane region or if it is a sectioning artefact.

We suspect that lymphocytes and macrophages were located at the ends of the membrane due to the sharp edges of the membrane potentially causing injury to the adjacent tissue. A fibrous capsule was also noted, and is observed as the pink band surrounding the membrane, which, as mentioned above, is formed in a response to a foreign object. These results indicated that there was a small tissue response to the presence of the membrane when implanted into the eye. This was in line with the gross observations of the implanted eye at the operating microscope.

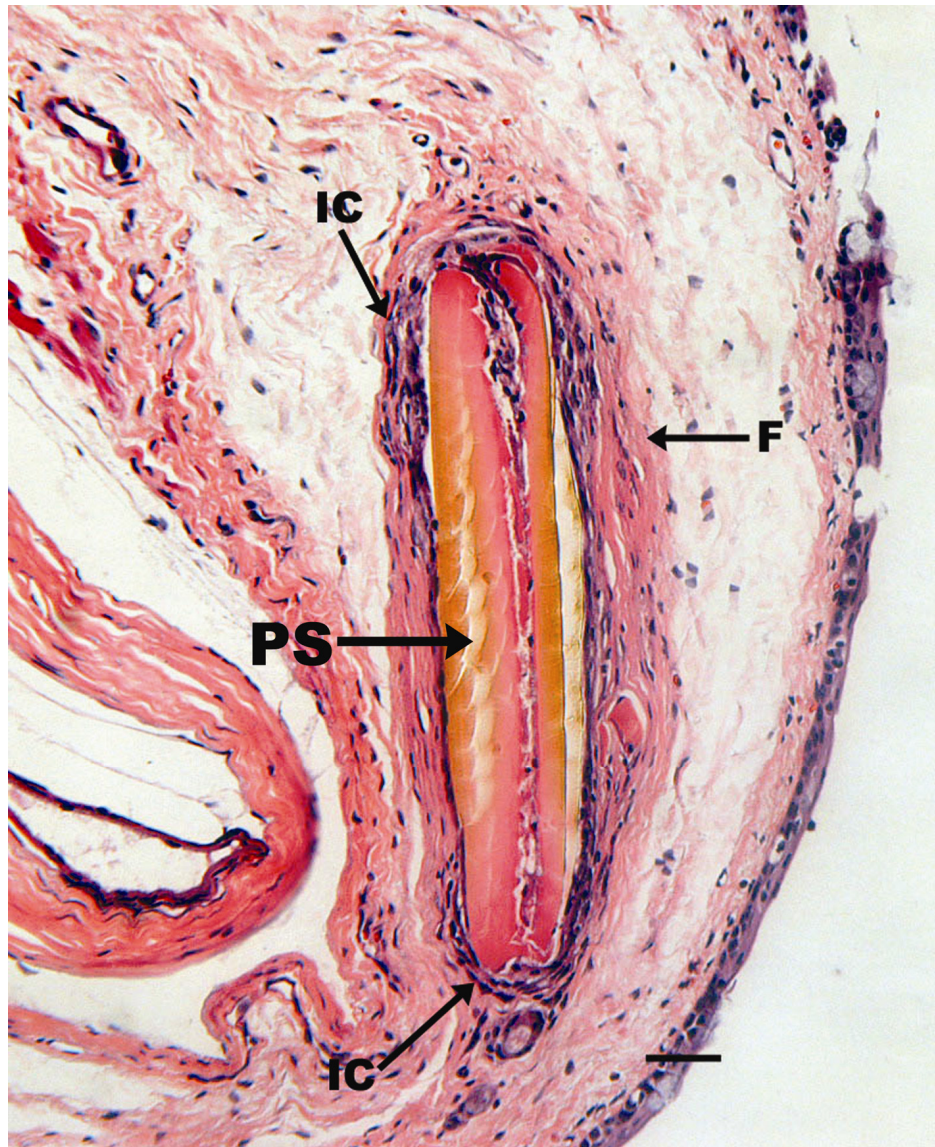


**Figure 66 – H&E stained section of the eye containing the remains of a thermal APTMS porous silicon membrane. The membrane was implanted in the subconjunctival space of the eye for a period of 9 weeks before fixation and sectioning for histology. The porous silicon membrane (PS) can be easily discerned by its brown colour, though parts of it have been stained with eosin. Inflammatory cells (IC) were seen at either end of the membrane and only a thin layer of cells was observed around the membrane. A fibrous capsule (F) was seen surrounding the membrane. This stained pink and is expected to consist mainly of collagen. Scale: 50  $\mu\text{m}$ .**



**Figure 67 - H&E stained section of the eye containing the remains of a thermal APTMS porous silicon membrane. The membrane was implanted in the subconjunctival space of the eye for a period of 9 weeks before fixation and sectioning for histology. The porous silicon membrane (PS) in this section was fragmented. It was unclear if this was due to the sectioning process or occurred *in vivo*. There was a small layer of inflammatory cells (IC) around the membrane and a fibrous layer (F) was observed surrounding the membrane. Cells are also observed within the fractured membrane (green arrow). It is unknown if these cells had migrated to this region or if the cells were an artefact generated from the sectioning process. Scale: 50  $\mu\text{m}$ .**

#### *Chapter 4: Results and Discussion*

We compared the amount of inflammation observed around a porous silicon implant to the tissue response to the 10-0 monofilament nylon sutures used to seal the incision site. Figure 68 shows an H&E section of a monofilament nylon suture that was implanted in the eye for a period of 9 weeks. The suture is surrounded by a thick layer of inflammatory cells, approximately 5-6 cells deep. This inflammatory cell layer is much thicker than the cells around the porous silicon implant (Figure 66 & Figure 67), which only had 2-3 layers of inflammatory cells. We also observed red blood cells close to the suture and the presence of a blood vessel, suggesting vascularisation around the suture. Vascularisation was not observed around the porous silicon membranes. These results indicated that in comparison to a nylon suture, porous silicon membranes invoked a less intense inflammatory response.

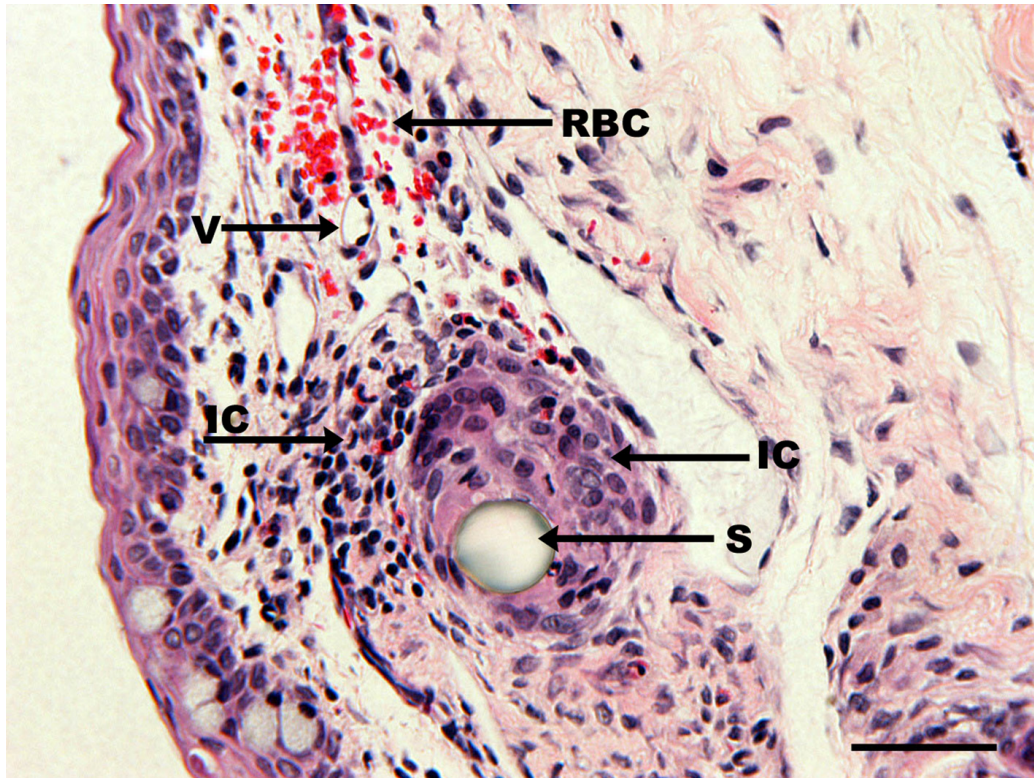


Figure 68 – H&E stained section containing a 10-0 monofilament nylon suture (S). The suture was surrounded by inflammatory cells (IC) of macrophages and lymphocytes. There was also evidence of vascularisation near the suture with vessels observed above the suture (V). Blood cells (RBC), observed as bright red cells without a nucleus, are seen, indicating vascularisation. This section demonstrated that inflammation is more severe around the suture than around a porous silicon membrane. Scale: 50  $\mu$ m.

#### *Chapter 4: Results and Discussion*

In one of the animals, the porous silicon membrane was no longer visible under the operating microscope after a period of 2 weeks. In Figure 69 and Figure 70, a section of the eye at the region in which the membrane was implanted is shown. The characteristic brown translucent membrane was no longer visible. Instead we saw a region that stained with eosin with small voids and some cells. This could either indicate that the porous silicon had absorbed the eosin dye or the porous silicon had completely degraded, leaving behind the fibrous protein layer, which cells were able to migrate into. In Figure 69, the small voids within the stained region were not typical of fractures observed in porous silicon. Porous silicon will break according to its crystalline alignment, resulting in straight edges (as seen in Figure 66 and Figure 67). The small voids in Figure 69 were not straight and showed curved edges. This observation is an indication that the porous silicon had degraded, leaving behind a protein layer.

Figure 69 also shows the inflammatory cells around a suture knot. There was a thick layer of cells around the suture and there was again evidence of vascularisation around the suture. Figure 70 shows a small layer of cells around the remains of the fibrous layer that encapsulated a porous silicon membrane. A giant cell has formed at one end of the fibrous capsule. Macrophage and lymphocyte cells migrate to surround a foreign body in an initial inflammatory response. The formation of a giant cell is usually an indication of a more severe form of inflammation <sup>[216]</sup>, although in comparison to the tissue response around a suture, the immune response was still considered to be low.

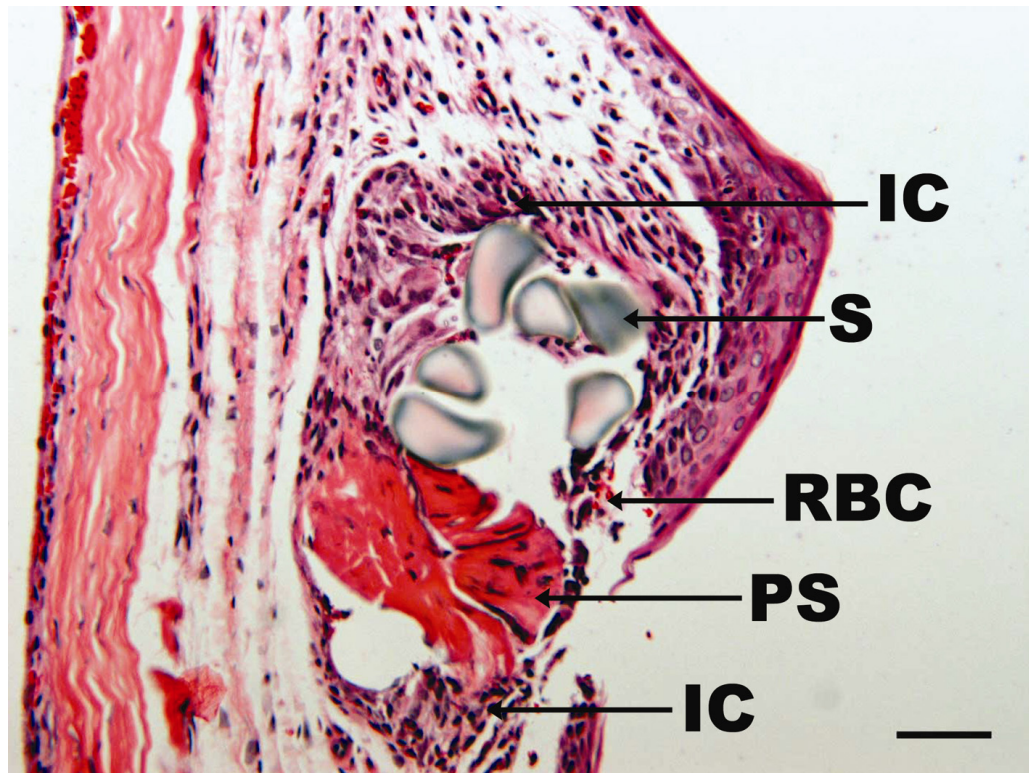
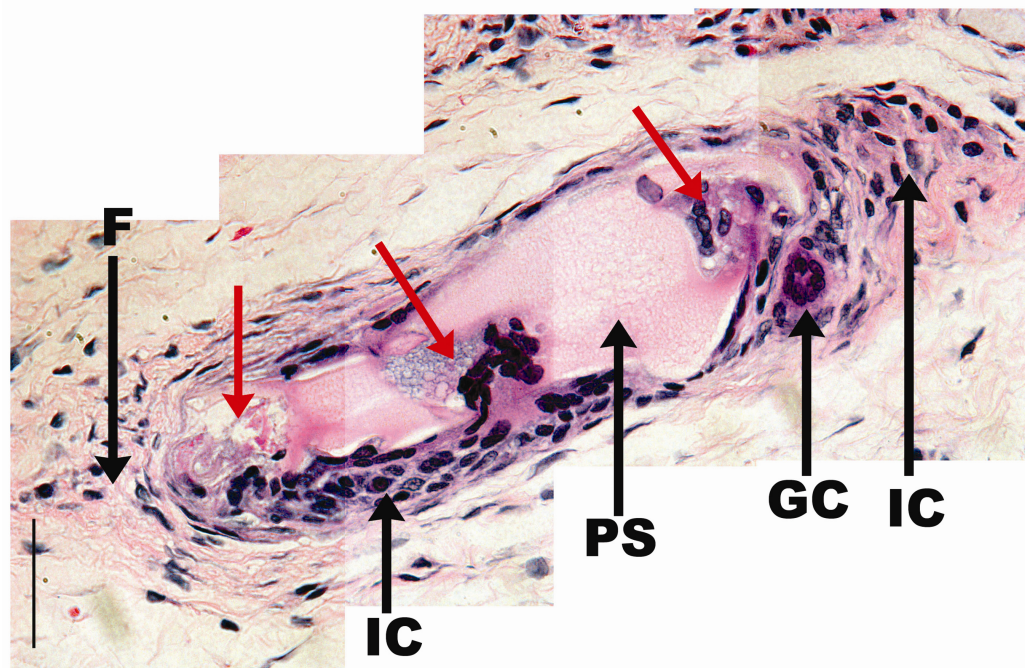


Figure 69 – H&E stained section containing suture and the possible remains of a thermal APTMS porous silicon membrane. Gross observation of the membrane was no longer evident after 2 weeks implantation. The possible remains of a porous silicon membrane (PS), the porous silicon had either taken up the eosin stain or the porous silicon had degraded completely and only the fibrous capsule remained. Evidence points to fibrosis as cells have infiltrated the structure. Inflammatory cells (IC) were observed surrounding the sutures and the porous silicon membrane. Blood cells (RBC) were evident around 10-0 monofilament nylon sutures (S), indicating vascularisation around the sutures. Scale: 50  $\mu$ m.



**Figure 70 – H&E stained section of the possible remains of a thermal APTMS porous silicon membrane that was implanted into the eye for a period of 2 weeks. It was possible that the porous silicon (PS) had degraded completely and only the protein surrounding the fibrous protein capsule remained (F). Macrophages can coalesce to form giant cells (GC). Other inflammatory cells were seen around the implant site (IC). Some cells had infiltrated the former implant site (red arrows). Scale: 50  $\mu$ m.**

#### *Chapter 4: Results and Discussion*

Figure 71 shows images of a porous silicon membrane that was implanted into the eye for 6 weeks. The membrane was still partly visible at the end of the 6 weeks, showing characteristic straight edges and the brown colouration, particularly along the lower edge of the membrane. This section showed the membrane in close proximity to the remains of some sutures and a comparison in the inflammatory response between the two objects can be easily made. Many inflammatory cells were observed surrounding the sutures, whereas only a small layer of inflammatory cells were seen around the porous silicon. Red blood cells were evident around the sutures and at the ends of the membrane. The sharp edges of the membrane may have caused continuous injury to the surrounding tissue, hence vascularisation to that area. The inflammatory cells around the membrane were localised around the ends of the membrane, again suggesting that the sharp edges of the membrane may have caused some localised injury.

The porous silicon membrane is also observed to have a void at the centre. As mentioned previously, this could be due to degradation occurring more rapidly at the centre of the membrane in comparison to the external regions, or is an artefact generated by the sectioning process.

These results have so far demonstrated that porous silicon membranes that have been thermally oxidised and then aminosilanised (thermal APTMS), invoke a relatively low inflammatory response in host tissue. This suggests that porous silicon membranes have good biocompatibility. Therefore, we next wanted to determine whether the membranes were able to be used as a cell delivery platform.

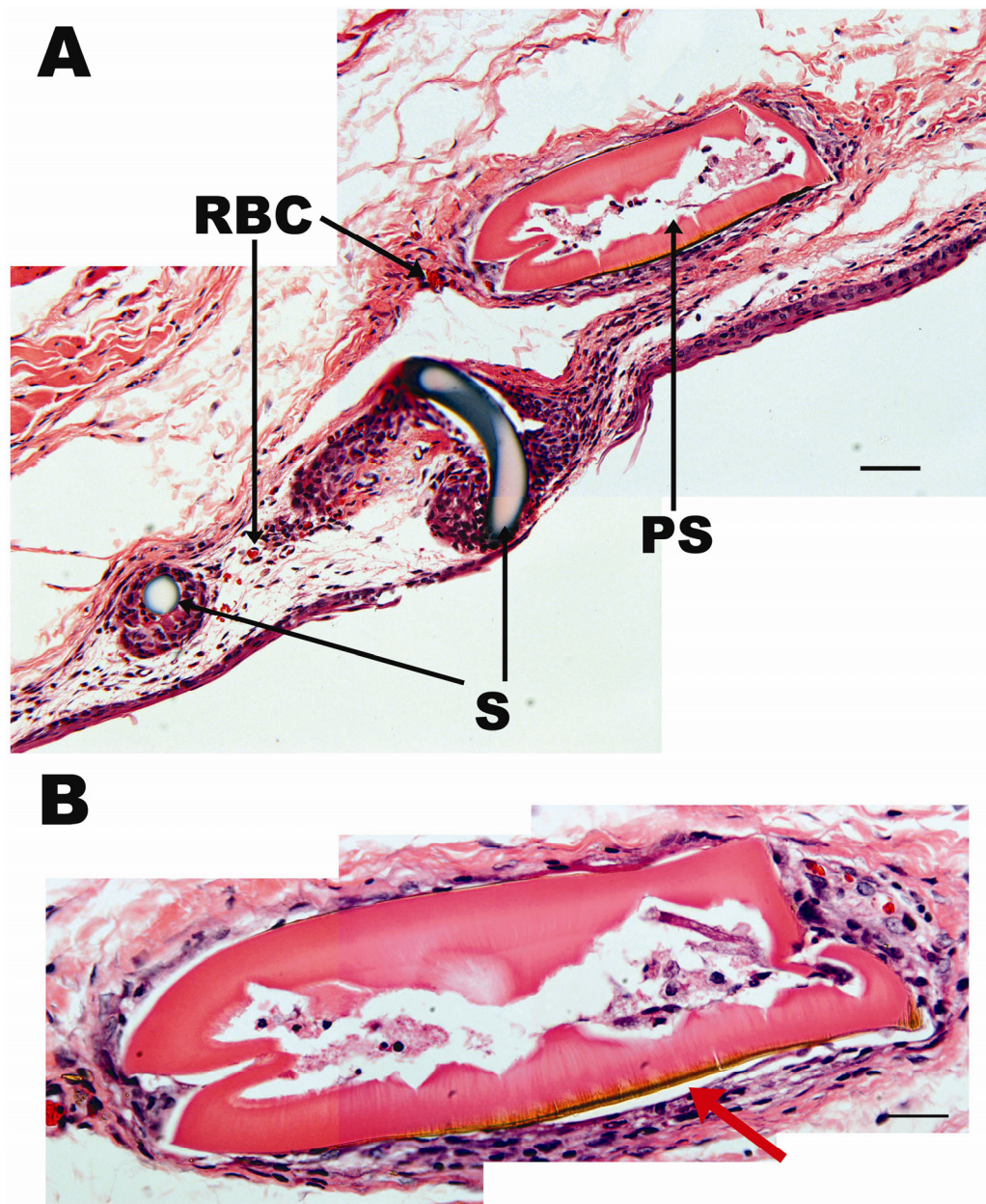


**Figure 71 - H&E stained sections of A: a thermal APTMS porous silicon membrane (PS) with nearby 10-0 monofilament nylon sutures (S) that were implanted into the eye for a period of 6 weeks; and B: Magnified image of the porous silicon membrane, some of the characteristic brown translucent colour is still visible (red arrow). Red blood cells (RBC) were observed around the sutures and around the ends of the membranes. Scale: 50  $\mu$ m.**

#### **4.15. Implantation of Membranes Containing Cultured Primary Cells**

Cell outgrowths from corneal rims were cultured onto thermal APTMS porous silicon membranes for a period of 2 weeks. The approximate sizes of the membranes were 2 mm x 3 mm, a similar size to the membranes implanted previously. The cells were then stained with PKH26, a dye that is incorporated into the lipid membranes of the cells [224]. The dye was used to track the movement of the cells from the membrane into the surrounding tissue.

We first had to determine if PKH26 was capable of staining cells that were attached to the membranes. This dye is commonly used to stain cells in suspension. We tested the suitability of the dye following a protocol for staining adherent cells from Lee *et al* [187]. This protocol was able to stain the cells on membranes, although the stain did not penetrate evenly throughout the cell. The staining was patchy and was as expected for adherent cells [187] (Figure 72).

The membranes with the cultured and PKH26-stained cells were then implanted into the sub-conjunctival space of a rat eye in the superior, temporal and inferior regions. The membranes were held in place with 10-0 monofilament nylon sutures. To determine if we could still observe the stained cells once implanted into the eye before proceeding with more animal experiments, one animal was sacrificed immediately after implantation. The eye was enucleated and the cornea was flat-mounted. Figure 73 shows representative images of cells observed through the conjunctiva of the flat mounted cornea. The outline of the membrane was clearly defined (Figure 73A) and cells were observed on the surface of the membrane and a few single cells were seen in the surrounding tissue to the left of the membrane. These cells were probably dislodged from the membrane during implantation. Cells were still able to be identified on the membrane surface when viewed through the conjunctiva.

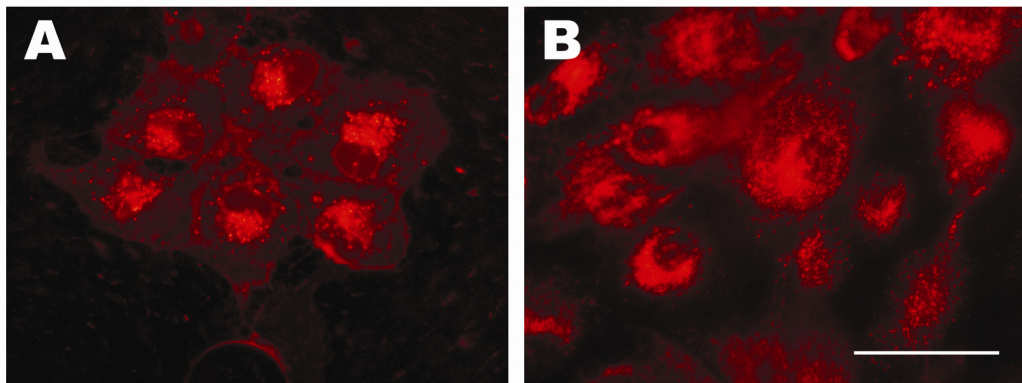


**Figure 72** – Human corneal cells, from corneal outgrowths, stained with PKH26 dye on **A**: glass coverslip and **B**: thermal APTMS porous silicon membranes. Cell staining was patchy on both surfaces, but individual cells could be discerned. Scale: 50  $\mu\text{m}$ .

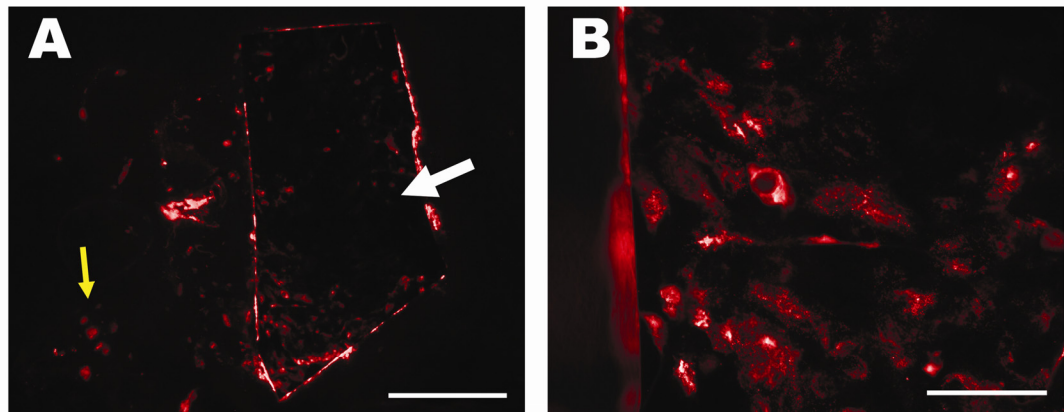


**Figure 73** – Images of human corneal cells, from corneal outgrowths, on thermal APTMS porous silicon membranes in a flat mounted cornea. The membranes were implanted into the sub-conjunctival space of a rat. Immediately after implantation, the rat was killed and the cornea flat mounted. **A**: image of membrane (white arrow) and cells. Some cells were observed to the left of the membrane and were dislodged from the membrane during implantation (yellow arrow), scale: 200  $\mu\text{m}$ . **B**: High magnification image of cells on the membrane surface. Individual cells could still be identified. Scale: 50  $\mu\text{m}$ .

#### *Chapter 4: Results and Discussion*

A further three rats were then implanted with membranes containing cultured human corneal cells that were stained with PKH26. This was to determine if the cultured cells were able to migrate from the membrane into the surrounding tissue. Human limbal rims, used to form the cell outgrowths, were remnants of corneal transplantation surgery and would normally be discarded. The size of the human limbal rims made them easier to handle and dissect than rat limbal tissue. Additionally, we had established culture conditions for human corneal rims. Therefore we implanted membranes containing human cells into the eyes of rats. Since human cells were placed into a rat host, an immune response to the foreign human cells was expected. Therefore the implants were left in place for one week before the animals were killed. For the short-term culture to determine if cells are able to migrate from the membrane, the human cells were deemed to be appropriate.

The animals were monitored during the week, where some vascularisation and inflammation was observed around the sutures and to some of the implants. In the animals that were implanted with the membranes only (**Section 4.14.1**), inflammation was generally observed around the sutures and not around the membrane.

Figure 74 shows representative images of the membranes containing cultured cells that were implanted into the eyes of three rats. The low magnification images show the cells in relation to the membrane. These images show bands of cells migrating off the membranes into the surrounding tissue. Higher magnification images show that these are indeed cells, and staining intensity decreases in the cells that have migrated the furthest away from the membrane (Figure 74a and Figure 74c), due to the dilution of the stain as the cells divide and proliferate.

These results demonstrate that it is possible to use porous silicon membranes as a support for the culture of primary cells. When the membranes were implanted into the eyes, cells were able to migrate off the membrane surface into the surrounding tissue. This provides strong evidence that porous silicon membranes can be used as a cell scaffold to deliver cells into tissue.

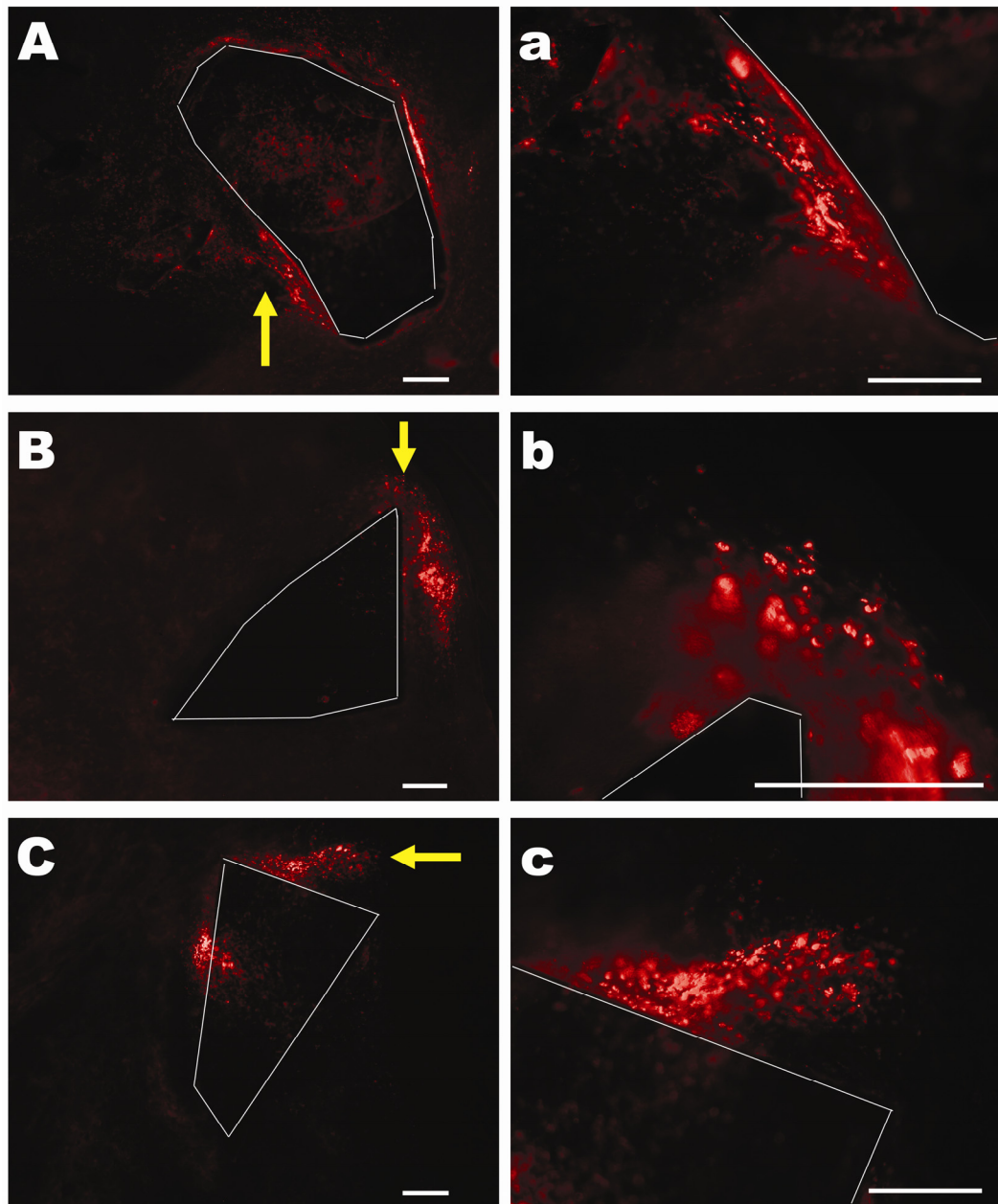


**Figure 74** – Representative images of human corneal cells migrating (yellow arrows) from thermal APTMS porous silicon membranes (white outlines) implanted into the sub-conjunctival space of the eye for one week. Cells were pre-stained with PKH26 before implantation. **A, B & C:** low magnification images showing the cells in relation to the membranes; **a, b & c:** higher magnification of the cells that have migrated from the membrane surface into the surrounding tissue. Scale: 200  $\mu\text{m}$ .

## Conclusions

We have shown that untreated porous silicon is unstable in aqueous solutions and quickly undergoes degradation. We previously demonstrated this indirectly by showing a decrease in the effective optical thickness of the porous silicon layer through interferometric reflectance spectroscopy (**Chapter 2**). In the experiments described here, we chose a direct detection method, measuring degradation of the porous silicon membranes by detecting silicic acid in solution. The ammonium molybdate method allowed us to measure the degradation rate of small pieces of membranes and we could effectively measure silicic acid concentrations as low as 0.002 mM. We showed that thermal oxidation stabilised the membrane surface significantly. Aminosilanisation further prevented degradation of the membrane. In static and flow-through assays, the results suggested that surface passivation, by the formation of an oxide layer <sup>[225]</sup>, occurred approximately after 5 days in solution, which decreased the rate of degradation after this time. In our animal studies, we were still able to observe a membrane that was implanted into the eye of a rat after 9 weeks, whereas in other animals, the membrane was no longer observable after 3 weeks. This may have been partly due to the uncontrolled environment. It is unknown if slight differences in protein or enzyme concentrations in the eyes of the animals used or rubbing of the eye might have hastened the degradation rate of the porous silicon. Therefore, more study has to be done on the degradation of porous silicon membranes *in vivo*.

The EDX results demonstrated that the membranes were more heavily silanised on the external regions than in the centre of the membrane. This characteristic of the membrane may also have had an effect upon the degradation rate of the membranes. The EDX and histology results implied that degradation might be occurring faster at the more susceptible membrane centre than at the external regions. This was manifested as fractures or voids within the membranes. MicroCT results suggested that degradation was not progressing faster at the centre of the membrane and hence it cannot be excluded that the voids and fractures were artefacts produced during the sectioning and staining process.

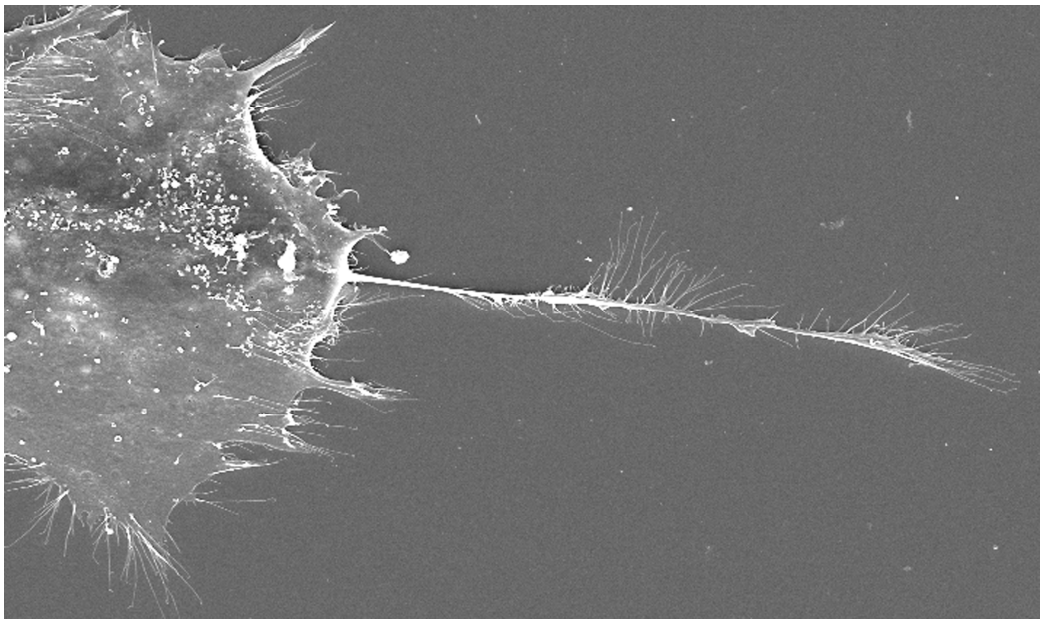
#### *Chapter 4: Conclusions*

We had previously demonstrated that aminosilanisation created a surface that was suitable for cell attachment on porous silicon attached to bulk silicon. We have now shown that this surface modification on membranes also facilitates the growth of human lens epithelial cells as well as the growth of primary cells from human corneal tissue (corneal outgrowths). We were able to culture cells from limbal tissue, although immunohistochemical results demonstrated that the majority of cells on this surface were terminally differentiated cells. We identified a few cells that were positive for p63, a transcription factor found in cells with a stem cell phenotype. This indicated that there were still some cells in our cell outgrowth population that maintained some stem cell-like properties.

The animal studies showed that aminosilanised porous silicon membranes were biocompatible and did not invoke a large immune response to the membrane when it was implanted into the eye. Some protein encapsulation was observed around the membranes but the lack of significant inflammatory response led us to believe that the implant would not be rejected. We also saw evidence of membranes that had degraded completely, retaining only the protein capsule layer. We then implanted pieces of membranes containing cells cultured from limbal tissue into the eye. We were able to observe cells moving away from the implant into the surrounding tissue. This is evidence that porous silicon membranes can be used as a surface that is biodegradable and biocompatible to deliver cells into the eye.

## Chapter 5

### Overall Findings and Conclusions



*Scanning electron micrograph of a PC12 cell displaying a neurite, cultured on a porous silicon membrane*

## **Overall findings**

Our goal was to generate a porous silicon-based biomaterial for the delivery of stem cells into a diseased eye. Firstly we established the suitability of using porous silicon as a scaffold for cell culture, and then we had to determine the most suitable form of porous silicon to be used as a cell delivery device. The main findings from this thesis are outlined below.

### **APTMS-modified porous silicon surface best for mammalian cell attachment**

At the beginning, we used analytical techniques to determine the fundamental characteristics of surface-modified porous silicon. Porous silicon was generated by anodically etching a silicon wafer in hydrofluoric acid. The subsequent porous silicon surface was modified by oxidation, silanisation and protein coatings. The presence of the various surface modifications was confirmed through the use of FTIR. The topographies of these surfaces was characterised through the use of AFM techniques. AFM studies showed that there was little observable difference between untreated (freshly etched), ozone oxidised and silanised samples. The deposits of collagen and foetal bovine serum proteins used to coat the porous silicon could be clearly observed with AFM.

In our degradation studies, we found that simple ozone oxidation of the porous silicon surface was able to slow down hydrolytic attack in aqueous medium (**Section 2.6.3**). Of great interest was the finding that silanisation further protected the surface and in later studies, we found that thermal oxidation gave the most protection against hydrolytic attack and thermally oxidised samples showed the slowest degradation rate of all the samples investigated (**Section 2.8**).

The various surface modifications were chosen to promote the attachment of mammalian cells to the porous silicon surface. The porous silicon was first oxidised to stabilise the surface and to provide hydroxyl groups for the silanisation reactions. We used two different silanes: an aminosilane (APTMS) and a PEG-containing silane

## *Chapter 5: Overall Findings and Conclusions*

(PEGS). APTMS has been used in other applications to promote cell adhesion [113, 115]. PEGS on the other hand, contains polyethylene glycol chains that are commonly used to prevent non-specific cell and protein attachment [118, 119]. Collagen and foetal bovine serum proteins were also used to coat the surface of oxidised porous silicon surfaces. Collagen is an extracellular matrix protein and is well-known for promoting cell attachment [226, 227]. Foetal bovine serum is a protein source often used in cell culture medium, which also contains factors that promote cell attachment [228].

Two different mammalian cell lines were cultured on these surfaces: human lens epithelial cells and PC12, a rat cell line with neuronal-like properties. Both cell lines were shown to attach poorly to freshly etched, oxidised and PEGS-modified porous silicon surfaces (**Section 2.7**). We suspect that cells did not attach to the freshly etched surface due to its instability, as this surface degraded completely within a matter of hours. Contact angle measurements showed that the oxidised surface was extremely hydrophilic, with contact angles below 5 °. In normal cell culture conditions, proteins first adsorb to a surface, the cells then attach to these proteins. Proteins do not adsorb well to extremely hydrophilic surfaces [113], hence only a few cells were observed to attach to the ozone oxidised surface.

In contrast, APTMS surfaces had contact angles of 56 degrees. This made the surface moderately wettable and as a result, more proteins were able to be adsorbed to the surface [113]. As a consequence we observed a large number of cells attached to the surface. We were also able to silanise the surface using PEGS, and we showed that we were able to prevent cell attachment through the use of this method. In the future, this method could be used for patterning devices such as live-cell microarrays [229, 230], where we can specify regions on which we require cell attachment and regions on which cell attachment is not desired.

Coatings with collagen and serum deposited a thick protein layer onto the porous silicon surface (as shown through AFM, **Section 2.6.1**). Cells attached to these coated surfaces, but collagen-coated surfaces displayed a higher number of attached cells,

where approximately 20% more cells were observed on the collagen-coated surface than on the serum-coated surface (**Section 2.9**).

Of all the surfaces tested, it was determined that an APTMS-modified porous silicon surface showed good stability, slow degradation and showed the largest number of attached cells. We also found that thermally oxidised surfaces were the most stable in aqueous solutions. The APTMS was covalently bonded to the surface, and not adsorbed (as with the protein coating), and did not require the use of any animal or human products (both collagen and foetal bovine serum are animal-derived products), factors which are always favoured for biomaterials. It was therefore decided that APTMS-modified surfaces that were previously thermally oxidised, would be the best surface to be used for cell culture.

### **The cell viability reagent, Alamar Blue, is reduced by the porous silicon surface**

To determine which surface would promote cell attachment, cell viability assays were initially used. Alamar Blue was used as it formed the basis of a quick and non-toxic assay that could be read colorimetrically <sup>[138]</sup>. Cells were cultured on the surface-modified porous silicon surfaces, and after the appropriate culture period, any non-attached cells were washed off. Alamar Blue was then applied to determine the number of attached cells. The Alamar Blue assay indicated that all surfaces had a similar number of cells attached. This was a confusing result, as microscopy images of each surface clearly showed that certain surfaces, such as the ozone oxidised and the PEGS surface, did not contain any cells. When the porous silicon surface was incubated with the Alamar Blue reagent in the absence of cells, we found that the reagent was being reduced from the blue form into the red form, hence giving a positive result (**Section 2.8.1**). It was porous silicon that caused the reduction of Alamar Blue, as when we incubated the reagent with a piece of silicon wafer, we did not observe a colour change. Alamar Blue is a redox-active dye that is reduced by enzymes contained in live cells <sup>[138]</sup>. Our study shows that an intermediate product formed during porous silicon dissolution is able to act as a reducing agent for Alamar Blue, generating false positive

results. Recently, authors have also demonstrated this ability for porous silicon to reduce XTT, another redox active viability assay, supporting our conclusions <sup>[150]</sup>. Therefore all redox-sensitive viability reagents such as Alamar Blue, MTT and XTT <sup>[153, 155]</sup>, should be used with caution when used in direct contact with porous silicon.

### **The cell viability reagent, neutral red, can become trapped in the pores of porous silicon**

As redox-sensitive cell viability assays could not be used, a neutral red assay was chosen as a different method to measure cell viability. The neutral red assay operates by live cells actively taking up the dye, whereas dead cells exclude the dye <sup>[231]</sup>. After the appropriate culture time, the cells are washed to remove excess dye and a lysis solution added to release the incorporated dye from the cells. The number of live cells is proportional to the intensity of the solution, which can be determined spectrophotometrically. In this instance, we found that the dye was being absorbed into the pores of the surface. A piece of porous silicon (without cells) was incubated with the neutral red solution and a buffered salt solution (PBS) was used to wash the porous silicon. When the lysis solution, which contained ethanol, was added to the porous silicon, the solution turned red, indicating the presence of the neutral red dye. This indicated that the dye was becoming trapped in the pores and the PBS solution was unable to penetrate into the pores to remove the dye, whereas the lysis solution was able to do this, thus creating a false positive result (**Section 2.8.2**). The dye may not be incorporated into pores of different sizes and dimensions. We only tested neutral red with porous silicon which had pore dimensions between 10-20 nm. It is possible that the dye could be removed from porous silicon with larger pores sizes by simple washing, where the PBS solution would be able to penetrate the pores better. Different lysis solutions not containing ethanol might also be investigated, such as commercial cell lysis solutions or detergent-based lysis solutions. Therefore when using colorimetric cell viability assays, the user must bear in mind that the dye may become trapped in the pores of the porous silicon surface.

### **Processing porous silicon particles to a pellet form did not yield a suitable structure for culturing cells**

The form of porous silicon that was used in **Chapter 2** was not feasible for a biomaterial application. Only a thin porous layer was formed, which was still attached to the bulk silicon beneath. As a biomaterial, only the porous silicon layer is able to degrade and hence only the porous silicon layer was desired.

We set out to generate a three dimensional scaffold, consisting of porous silicon micro particles. Incorporated into this scaffold would be crystals of leaching agents, that would dissolve easily in aqueous solution to reveal large macropores, into which cells could infiltrate.

As it was previously determined that APTMS-modified surfaces promoted cell attachment, the porous silicon particles were aminosilanised. Before silanisation, the particles were also thermally oxidised, as we had previously shown that this method of oxidation created the most stable surface and prevented significant degradation from occurring. It was discovered that modified particles could not be compacted on their own to form a stable pellet, and a binder had to be included into the formulation. Starch was chosen, as this is commonly added to pharmaceutical tablets <sup>[162]</sup> and has been shown to have low cellular toxicity <sup>[164, 165]</sup>. We found that it was also necessary to add a lubricating agent in the form of stearic acid, to relieve friction between the pellet and the wall of the cast. When the resultant pellet was tested for its stability in aqueous solution, the pellet was hydrophobic and could not be immersed in solution. Glycine was added as a wetting agent, because as an amino acid, glycine was not considered to be toxic for cells.

Overall, a pellet consisting of modified porous silicon particles, starch, stearic acid and glycine, was stable enough to be handled and manipulated with tweezers. We found that when immersed in cell culture solution, this pellet lost its structure within 24 hours (**Section 3.16.1**), which explains why cells could not be successfully cultured on the pellet. It may be worth investigating different methods for pressing the pellet. An

example might be the addition of cross-linkers to the porous silicon particles before being placed into the press. We tried adding cross-linkers (glutaraldehyde) after the pellet was formed, which did not help maintain the pellet structure. Mixing the cross-linker with the particles before pressing, might ensure even distribution of the cross-linker amongst the particles and might assist in binding the pellet together. Overall, the instability of the pellet prevented the attachment of cells to the pellet surface, and for our purpose in the development of a biomaterial that is stable over a period of weeks, the pellet was not a suitable material.

### **Primary cells can be cultured on thermal APTMS membranes**

Porous silicon layers that have been removed from the supporting silicon base are referred to as membranes. Porous silicon membranes were thermally oxidised as this was shown in **Section 2.8.1** and **Section 4.5** to stabilise the surface significantly and decrease degradation rates. The oxidised surface was then silanised with APTMS, which was shown in **Section 2.9** to promote cell attachment. The resultant membrane is referred to as thermal APTMS. The membranes could be easily manipulated with tweezers. Porous silicon particles were not used in primary cell culture studies, due to the potential toxic effects as discussed above.

It was expected that cells that migrated from the human corneal rims onto the thermal APTMS membranes would contain a population of adult stem cells. Immunohistochemical results of the cells expanded on the glass coverslips showed that the majority of the cells were terminally differentiated, although a few cells were marked as p63 positive, a cellular marker for cells that have retained some stem cell-like characteristics <sup>[87]</sup>. This indicates a need to review the culture techniques and reagents used in this thesis, to generate culture conditions that will promote the growth of p63-positive cells.

A variety of cells could be distinguished in the population of cells expanded from the human corneal rims, as expected for cells cultured from tissue. There was no observable difference in the cell types (as determined by morphology) when they were

## *Chapter 5: Overall Findings and Conclusions*

allowed to grow on glass coverslips or onto membranes. The cells were seen in similar proportions when cultured on both surfaces (**Section 4.13.2.1**). This demonstrated that the membranes do not have an influence on the proliferation and migration of cells, and that cellular morphology is maintained on the membranes. Cells were also observed to migrate across the membrane surface. Therefore it was shown that primary cells can be successfully cultured and grown on thermal APTMS membranes.

### **The eye can be used as a model to test biocompatibility of materials**

We discovered that the eye was a satisfactory model to test the biocompatibility of potential biomaterials. Due to the lack of pigmentation in the conjunctiva of the albino strain of rat used, occurrences of vascularisation could be easily observed with an operating microscope (**Section 4.14.1**). This reduced the need for invasive procedures and the use of imaging equipment. The lack of invasive procedures allowed us to observe the same eye over a period of weeks, which reduced that number of animals we had to use. Inflammation around the biomaterial could also be easily discerned. For use with translucent biomaterials, the eye model may not be as suitable since it may be harder to identify the material whilst in the tissue.

### **Porous silicon membranes show good biocompatibility in the eye**

The thermal APTMS membranes had been shown to support the growth of cell lines and primary cells (**Section 4.13**). The membrane was then tested for its biocompatibility in the rat eye. Small pieces of thermal APTMS membranes were placed into the sub-conjunctival space of the rat eye. A total of 5 animals were used and the implanted eye of each animal was monitored under an operating microscope until the implanted membranes could no longer be clearly observed. The durations in which the membranes could be observed in the eye varied from animal to animal. In the first animal, the membranes were no longer observable after 2 weeks, in the second, the membranes had diminished significantly in size, but were still observable after 9 weeks. In the third animal, the membranes could no longer be seen clearly after 3 weeks and in the remaining animals, the membranes were still observable after 6½ weeks, at this time the animals were euthanased and the implanted eyes were taken for

## *Chapter 5: Overall Findings and Conclusions*

histology (**Section 4.14.1**). This inconsistency in degradation rates of the membranes could be partially explained by slight variations in the membrane size, where it was difficult to obtain membranes of the exact same dimensions. The eye environment may also have caused the differences observed. It is unknown if slight variations in protein or enzymes present within the eyes of the different animals can cause a change in the degradation rate of the membranes. A larger sample number of animals could be used to provide a more information on the membrane degradation rate in the eye.

The implanted eyes were not only monitored to determine the degradation rate of the membranes, but also to observe any inflammatory responses. Observations under the operating microscope showed that inflammation occurred around the implant site 24 hours after surgery, which subsided over the week. By the second week, it was observed in all animals, that tissue inflammation was confined to areas around the nylon sutures used to seal the incision site. This was an indication that the porous silicon membranes were well tolerated in the rat eye. For further clarification that this was the case, these implanted eyes were subjected to histology.

The histology results were encouraging. At least twice, or even three times as many, inflammatory cells were observed around the nylon sutures in comparison to the membranes (**Section 4.14.2**). 10-0 monofilament nylon sutures are known for inducing what is considered only a slight inflammatory response in the eye <sup>[218]</sup>, hence their common use in ophthalmic surgery. The noticeably smaller inflammatory response observed around the membranes indicate that porous silicon membranes have good biocompatibility in the eye.

There has only been one other reported occurrence of testing porous silicon biocompatibility *in vivo*. Rosengren *et al* <sup>[63]</sup> implanted pieces of porous silicon into the abdominal wall of rats. They stated that a fibrous protein capsule formed around the porous silicon, which we also observed. The researchers compared the foreign-body response to the porous silicon against other biomaterials, such as titanium, and determined that the inflammatory response to porous silicon was similar to the other

## *Chapter 5: Overall Findings and Conclusions*

biomaterials. We have shown that porous silicon membranes invoke a smaller foreign body response in comparison to a material that is commonly used in the eye (nylon sutures), thus suggesting that porous silicon membranes have good biocompatibility. The low inflammatory response to porous silicon in the eye can be extrapolated to other tissues. It should be possible to use porous silicon in a variety of other places within the body, such as skin or muscle, without inducing a large inflammatory response. In other areas of the body, the membranes can be used as a biodegradable drug delivery material or as a cell delivery device, as we have shown in this thesis.

### **Porous silicon membranes can deliver cells into the eye**

Our main goal was to develop a porous silicon-based biomaterial that was biocompatible and biodegradable, for the delivery of cells into the eye. As mentioned above, we were able to successfully culture primary cells onto thermal APTMS membranes and we demonstrated that the membranes showed good biocompatibility when placed into the eye. Through the use of ammonium molybdate assays, it was found that the membranes did degrade over time. Surface passivation by the formation of an oxide layer occurred approximately after 5 days immersion in an aqueous solution, at which point the degradation rate slowed down (**Sections 4.12.3.1 and 4.12.3.2**). The histology of rat eyes implanted with membranes suggested that the membranes are capable of complete degradation, as the only residue found at the implant site was fibrous material that had formed around the implanted membrane (**Section 4.14.2**). Longer term assays (over weeks, rather than the 10 days that we tested) using the ammonium molybdate method are required to determine conclusively that the membranes are able to show complete degradation.

Primary cells cultured from human corneal rims were used as the cells to be delivered into the eye. The cells were stained with a tracker dye before being implanted into the sub-conjunctival space of the eye. As we expected an immune response from the rat to the human cells on the membrane, the animal was killed after only one week. When the eye was examined, we found evidence of cell migration from the membrane into the surrounding tissue (**Section 4.15**). The cells also showed a loss in staining intensity, the

## *Chapter 5: Overall Findings and Conclusions*

further they were away from the membrane. As the staining intensity is reduced each time the cell divides <sup>[224]</sup>, this was evidence that the cells cultured on the membrane were not only migrating, but continued to proliferate.

Culturing primary rat cells from rat corneal rims onto porous silicon membranes would allow us to implant these membranes into the eyes of rats for a longer period, as a lesser immune response would be invoked against cells of the same species. We decided to culture primary human cells onto the membranes instead. There are several reasons for this decision. First, we were able to obtain human corneal rims that were left over from corneal transplantation surgery. These rims would otherwise be discarded. We have also established culture conditions for inducing the cells in the human corneal rim to expand onto the membranes (**Sections 4.7.2 and 4.13.1.1**) and lastly, since the penultimate application was human regenerative medicine, we wanted to show that human cells can be cultured on this biomaterial successfully.

If these studies are to be taken further, it would be interesting to see if the human cells delivered by the porous silicon, are able to migrate across the rat cornea in a similar fashion to the rat corneal epithelial cells. For this experiment, it would be preferable if the cultured human cells from the corneal rim contained a more refined population of stem cells. This would have to be achieved by fine-tuning tissue culture and dissection conditions. These stem cells would have better proliferative capability than the terminally differentiated cells that we were able to culture on the porous silicon membranes. If these stem cells are able to be cultured on porous silicon, they could then be delivered into the rat eye via porous silicon membranes. The centre of the cornea could then be injured to stimulate proliferation <sup>[77]</sup>, and the implanted human stem cells might be induced to proliferate as well. To follow the migration of the cells, the use of a cell tracker dye (as used in this thesis) might not be sufficient, as each time the cell divides, the dye is split evenly amongst the daughter cells <sup>[224]</sup>. Therefore in subsequent generations of cells, the dye intensity would be reduced to the point where they may no longer be visible.

## *Chapter 5: Overall Findings and Conclusions*

Another possible method for tracking the migration of cells and taking advantage of using human stem cells in a rat eye is using DNA markers specific to human cells. Alu elements are found in high numbers specifically in human DNA and contain the sequence for the restriction enzyme *AluI* <sup>[232, 233]</sup>, and these elements can be used to detect a population of human cells amongst the rat cells of the cornea. Impression cytology could be taken of the central cornea and a polymerase chain reaction could be conducted to detect the presence of the Alu elements <sup>[234, 235]</sup>. It could then be determined if the human cells have been able to migrate towards the central cornea. This would bring us one step closer to being able to use stem cells with the aim of healing a diseased eye.

### **Overall conclusions**

APTMS-modified porous silicon surfaces promoted the cellular attachment of cell lines and primary cells. Coupled with thermal oxidation (thermal APTMS), this surface was also resistant to hydrolytic attack when placed in aqueous solution, hence has slow degradability in aqueous medium. Cells were successfully cultured from human corneal rims onto thermal APTMS membranes, although immunohistochemistry results demonstrated that the majority of cells cultured were mature epithelial cells. Thermal APTMS membranes demonstrated good biocompatibility when placed into an eye. Histological analysis of the implanted membranes showed that a minimal inflammatory response was observed around the membranes. This response was smaller than the inflammation observed around monofilament nylon sutures, which are commonly used in ophthalmic surgery. To this date, the biocompatibility of porous silicon *in vivo* has not been shown in this amount of detail before. This thesis has demonstrated that porous silicon membranes can be successfully used as a biomaterial and as a scaffold for the delivery of cultured cells into tissue, with a minimal risk of implant rejection occurring.

## References

1. R. G. Ham (1965) Clonal growth of mammalian cells in a chemically defined, synthetic medium. *Proceedings of the National Academy of Sciences of the United States of America*. **53**(2):288-293
2. J. Black (1999) *Biological performance of materials: Fundamentals of biocompatibility*, Third Edition, Marcel Dekker, New York
3. D. Byrom (1991) *Biomaterials*, Stockton Press, New York
4. M. R. Scott, R. Will, J. Ironside, H.-O. B. Nguyen, P. Tremblay, S. J. DeArmond and S. B. Prusiner (1999) Compelling transgenic evidence for transmission of bovine spongiform encephalopathy prions to humans. *Proceedings of the National Academy of Sciences of the United States of America*. **96**(26):15137-15142
5. H. Ohgushi, Y. Dohi, T. Katuda, S. Tamai, S. Tabata and Y. Suwa (1996) *In vitro* bone formation by rat marrow cell culture. *Journal of Biomedical Materials Research*. **32**:333-340
6. A. Okumura, M. Goto, T. Goto, Y. Masao, S. Masuko, T. Katsuki and T. Tanaka (2001) Substrate affects the initial attachment and subsequent behaviour of human osteoblastic cells (Saos-2). *Biomaterials*. **22**:2263-2271
7. K. Søballe, E. S. Hansen, H. Brockstedt-Rasmussen and C. Bünger (1992) Hydroxyapatite coating converts fibrous tissue to bone around loaded implants. *Journal of Bone and Joint Surgery*. **75**(B):270-278
8. M. P. Lutolf, F. E. Weber, H. G. Schmoekel, J. C. Schense, T. Kohler, R. Müller and J. A. Hubbell (2003) Repair of bone defects using synthetic mimetics of collagenous extracellular matrices. *Nature Biotechnology*. **21**:513-518
9. M. Shen and T. A. Horbett (2001) The effects of surface chemistry and adsorbed proteins on monocyte/macrophage adhesion to chemically modified polystyrene surfaces. *Journal of Biomedical Materials Research*. **57**:336-345
10. A. Curtis and C. Wilkinson (1997) Topographical control of cells. *Biomaterials*. **18**(24):1573-1583
11. J. Fitton, B. Dalton, G. Beumer, G. Johnson, H. J. Griesser and J. G. Steele (1998) Surface topography can interfere with epithelial tissue migration. *Journal of Biomedical Materials Research, Part A*. **42**:245-257

## References

12. Y. H. Bae, P. A. Johnson, C. A. Florek, J. Kohn and P. Moghe (2006) Minute changes in composition of polymer substrates produce amplified differences in cell adhesion and motility via optimal ligand conditioning. *Acta Biomaterialia* **2**. (473-482)
13. C. Streuli (1999) Extracellular matrix remodelling and cellular differentiation. *Current Opinion in Cell Biology*. **11**:634-640
14. E. Cukierman, R. Pankov, D. R. Stevens and K. M. Yamada (2001) Taking cell-matrix adhesions to the third dimension. *Science*. **294**:1708-1712
15. E. Cukierman, R. Pankov and K. M. Yamada (2002) Cell interactions with three-dimensional matrices. *Current Opinion in Cell Biology*. **14**:633-639
16. P. Friedl and E.-B. Bröcker (2000) The biology of cell locomotion within three-dimensional extracellular matrix. *Cellular and Molecular Life Sciences*. **57**:41-44
17. M. Ahmad, D. Gawronski, J. Blum, J. Goldberg and G. Gronowicz (1999) Differential response of human osteoblast-like cells to commercially pure (cp) titanium grades 1 and 4. *Journal of Biomedical Materials Research*. **46**:121-131
18. J. M. Wozney and R. H. Li (2003) Engineering what comes naturally. *Nature Biotechnology*. **21**:506-508
19. A. W. Llyod, R. G. A. RFaragher and S. P. Denyer (2001) Ocular biomaterials and implants. *Biomaterials*. **22**:769-785
20. M. R. O'Neal, K. A. Polse and M. D. Sarver (1984) Corneal response to rigid and hydrogel lenses during eye closure. *Invest. Ophthalmol. Vis. Sci*. **25**(7):837-842
21. N. A. Brennan, N. Efron and B. A. Holden (1986) Oxygen permeability of hard gas permeable contact lens materials. *Clinical and Experimental Optometry*. **69**(3):82-89
22. E.-S. Visser (1997) The silicone rubber contact lens: clinical indications and fitting technique. *Contact Lens and Anterior Eye*. **20**(Supplement 1):S19-S25
23. A. López-Alemany, V. Compañ and M. F. Refojo (2002) Porous structure of Purevision™ versus Focus® Night&Day™ and conventional hydrogel contact lenses. *Journal of Biomedical Materials Research*. **63**(3):319-325
24. C. M. Weikart, Y. Matsuzawa, L. Winterton and H. K. Yasuda (2001) Evaluation of plasma polymer-coated contact lenses by electrochemical

## References

- impedance spectroscopy. *Journal of Biomedical Materials Research*. **54**(4):597-607
25. H. Ridley (1960) Intra-ocular acrylic lenses 10 years' development. *British Journal of Ophthalmology*. **44**(12):705-712
  26. M. Pekna, R. Larsson, B. Formgren, U. R. Nilsson and B. Nilsson (1993) Complement activation by polymethyl methacrylate minimized by end-point heparin attachment. *Biomaterials*. **14**(3):189-192
  27. M. Chehade and M. J. Elder (1997) Intraocular lens materials and styles: A review. *Australian and New Zealand Journal of Ophthalmology*. **25**:255-263
  28. C.-H. Hong, A. Arosemena, D. Zurakowski and R. S. Ayyala (2005) Glaucoma drainage devices: A systematic literature review of current controversies. *Survey of Ophthalmology*. **50**(1):48-60
  29. V. B. Kompella, V. Sangwan, A. Bansal, P. Garg, M. K. Aasuri and G. N. Rao (2002) Ophthalmic complications and management of Stevens-Johnson syndrome at a tertiary eye care centre in South India. *Indian Journal of Ophthalmology*. **50**(4):283-286
  30. D. Duan, B. Klenkler and H. Sheardown (2006) Progress in the development of a corneal replacement: keratoprotheses and tissue-engineered corneas. *Expert Review of Medical Devices*. **3**(1):59-72
  31. B. F. Kahn, E. J. Dudenhofer and C. H. Dohlman (2001) Keratoprosthesis: An update. *Current Opinion in Ophthalmology*. **12**:282-287
  32. J.-M. Legeais and G. Renard (1998) A second generation of artificial cornea (Biokpro II). *Biomaterials*. **19**(16):1517-1522
  33. S. Burkert, T. Schmidt, U. Gohs, I. Mönch and K.-F. Arndt (2007) Patterning of thin poly(*N*-vinyl pyrrolidone) films on silicon substrates by electron beam lithography. *Journal of Applied Polymer Science*. **106**(1):534-539
  34. A. Brecht and G. Gauglitz (1995) Optical probes and transducers. *Biosensors & Bioelectronics*. **10**:923-936
  35. V. S.-Y. Lin, K. Motesharej, K.-P. S. Dancil, M. J. Sailor and M. R. Ghadiri (1997) A porous silicon-based optical interferometric biosensor. *Science*. **278**(5339):840-843
  36. M. J. Sailor and E. J. Lee (1997) Surface chemistry of luminescent silicon nanocrystals. *Advanced Materials*. **9**(10):783-793

## References

37. L. T. Canham (1990) Silicon quantum wire array fabrication by electrochemical and chemical dissolution of wafers. *Applied Physics Letters*. **57**(10):1046-1048
38. L. T. Canham, M. R. Houlton, W. Y. Leong, C. Pickering and J. M. Keen (1991) Atmospheric impregnation of porous silicon at room temperature. *Journal of Applied Physics*. **70**(1):422-431
39. J. Dian, T. Holec, I. Jelinek, J. Jindrich, J. Valenta and I. Pelant (2000) Time evolution of photoluminescence response from porous silicon in hydrocarbon gas sensing. *Physica Status Solidi A: Applied Research*. **182**:485-488
40. S. E. Letant, B. R. Hart, S. R. Kane, M. Z. Hadi, S. J. Shields and J. G. Reynolds (2004) Enzyme immobilization on porous silicon surfaces. *Advanced Materials*. **16**(8):689-693
41. L. Karlsson, P. Tengvall, I. Lundstrom and H. Arwin (2003) Penetration and loading of human serum albumin in porous silicon layers with different pore sizes and thicknesses. *Journal of Colloid and Interface Science*. **266**:40-47
42. X. Li, J. St John, J. L. Coffey, Y. Chen, R. F. Pinizzotto, J. P. Newey, C. L. Reeves and L. T. Canham (2000) Porosified silicon wafer structures impregnated with platinum anti-tumor compounds: Fabrication, characterization, and diffusion studies. *Biomedical Microdevices*. **2**(4):265-272
43. J. Sarathy, S. Shih, K. Jung, C. Tsai, K.-H. Li, D.-L. Kwong and J. C. Campbell (1992) Demonstration of photoluminescence in nonanodized silicon. *Applied Physics Letters*. **60**(13):1532-1534
44. R. Smith and S. Collins (1992) Porous silicon formation mechanisms. *Journal of Applied Physics*. **71**(8):R1-R22
45. O. Bisi, S. Ossicini and L. Pavesi (2000) Porous silicon: A quantum sponge structure for silicon based optoelectronics. *Surface Science Reports*. **38**:1-126
46. V. Lehmann and U. Gosele (1991) Porous silicon formation: A quantum wire effect. *Applied Physics Letters*. **58**(8):856-858
47. P. Allongue, C. Henry de Villeneuve, M. Bernard, J. Peou and A. Boutry-Forveille (1997) Relationship between porous silicon formation and hydrogen incorporation. *Thin Solid Films*. **297**:1-4
48. M. I. J. Beale, N. G. Chew, M. J. Uren, A. G. Cullis and J. D. Benjamin (1985) Microstructure and formation mechanism of porous silicon. *Applied Physics Letters*. **46**(1):86-88

## References

49. D. Soares, O. Teschke and M. dos Santos (1996) Dynamics of the hydrogen oxidation and silicon dissolution reactions in the formation of porous silicon. *Langmuir*. **12**(12):2875-2877
50. L. T. Canham, C. L. Reeves, J. P. Newey, M. R. Houlton, T. I. Cox, J. M. Buriak and M. P. Stewart (1999) Derivatized mesoporous silicon with dramatically improved stability in simulated human blood plasma. *Advanced Materials*. **11**(18):1505-1507
51. P. Allongue, V. Costa-Kieling and H. Gerischer (1993) Etching of silicon in NaOH solutions. *Journal of the Electrochemical Society*. **140**(4):1018-1026
52. X. Xia, C. Ashruf, P. French, J. Rappich and J. Kelly (2001) Etching and passivation of silicon in alkaline solution: A coupled chemical/electrochemical system. *Journal of Physical Chemistry*. **105**:5722-5729
53. L. T. Canham (1995) Bioactive silicon structure fabrication through nanoetching techniques. *Advanced Materials*. **7**(12):1033-1037
54. S. H. C. Anderson, H. Elliot, D. J. Wallis, L. T. Canham and J. J. Powell (2003) Dissolution of different forms of partially porous silicon wafers under simulated physiological conditions. *Physica Status Solidi A: Applied Research*. **197**(2):331-335
55. J. P. Bellia, J. Birchall and N. Roberts (1994) Beer: a dietary source of silicon. *Lancet*. **343**:235
56. E. M. Carlisle (1972) Silicon: An essential element for the chick. *Science*. **178**(4061):619-621
57. R. Jugdaohsingh, D. M. Reffit, C. Oldham, J. P. Day, L. K. Fifield, R. P. Thompson and J. J. Powell (2000) Oligomeric but not monomeric silica prevents aluminium absorption in humans. *American Journal of Clinical Nutrition*. **71**:944-9
58. M. Desouky, R. Jugdaohsingh, C. R. McCrohan, K. N. White and J. J. Powell (2002) Aluminium-dependent regulation of intracellular silicon in the aquatic invertebrate *Lymnaea stagnalis*. *Proceedings of the National Academy of Sciences of the United States of America*. **99**(6):3394-3399
59. D. M. Reffit, R. Jugdaohsingh, R. P. Thompson and J. J. Powell (1999) Silicic acid: its gastrointestinal uptake and urinary excretion in man and effects on aluminium excretion. *Journal of Inorganic Biochemistry*. **76**:141-147

## References

60. S. C. Bayliss, P. Harris, L. D. Buckberry and C. Rousseau (1997) Phosphate and cell growth on nanostructured semiconductors. *Journal of Materials Science Letters*. **16**:737-740
61. S. C. Bayliss, R. Heald, D. I. Fletcher and L. D. Buckberry (1999) The culture of mammalian cells on nanostructured silicon. *Advanced Materials*. **11**(4):318-321
62. S. Ben-Tabou de Leon, A. Sa'ar, R. Oren, M. E. Spira and S. Yitzchaik (2004) Neurons culturing and biophotonic sensing using porous silicon. *Applied Physics Letters*. **84**(22):4361-4363
63. A. Rosengren, L. Wallman, M. Bengtsson, T. Laurell, N. Danielsen and L. M. Bjursten (2000) Tissue reactions to porous silicon: A comparative biomaterial study. *Physica Status Solidi A: Applied Research*. **182**:527-531
64. T. V. Chirila (2001) An overview of the development of artificial corneas with porous skirts and the use of PHEMA for such an application. *Biomaterials*. **22**:3311-3317
65. R. A. Thoft and J. Friend (1983) The x, y, z hypothesis of corneal epithelial maintenance. *Investigative Ophthalmology and Visual Science*. **24**(10):1442-1443
66. Y. S. Rabinowitz (1998) Keratoconus. *Survey of Ophthalmology*. **42**(4):297-319
67. N. A. Afshari, A. B. Pittard, A. Siddiqui and G. K. Klintworth (2006) Clinical study of Fuchs corneal endothelial dystrophy leading to penetrating keratoplasty: A 30-year experience. *Archives of Ophthalmology*. **124**(6):777-780
68. T. A. Casey and D. J. Mayer (1984) *Corneal grafting: Principles and practice*, 1st Edition, W.B. Saunders, Philadelphia
69. A. Waldock and S. D. Cook (2000) Corneal transplantation: how successful are we? *British Journal of Ophthalmology*. **84**(8):813-815
70. M. Davenger and A. Evensen (1971) Role of the pericorneal papillary structure in renewal of corneal epithelium. *Nature*. **229**:560-561
71. K. Y. Chee, A. Kicic and S. J. Wiffen (2006) Limbal stem cells: the search for a marker. *Clinical and Experimental Ophthalmology*. **34**:64-73
72. S. Kinoshita, T. C. Kiorpes, J. Friend and R. A. Thoft (1982) Limbal epithelium in ocular surface wound healing. *Investigative Ophthalmology and Visual Science*. **23**(1):73-80

## References

73. R. C. Buck (1985) Measurement of centripetal migration of normal corneal epithelial cells in the mouse. *Investigative Ophthalmology and Visual Science*. **26**(9):1296-1299
74. T. Nagasaki and J. Zhao (2003) Centripetal movement of corneal epithelial cells in the normal adult mouse. *Investigative Ophthalmology and Visual Science*. **44**(2):558-566
75. I. Jalbert, F. Stapleton, E. Papas, D. F. Sweeney and M. Coroneo (2003) In vivo confocal microscopy of the human cornea. *British Journal of Ophthalmology*. **87**:225-236
76. M. S. Lehrer, T.-T. Sun and R. M. Lavker (1998) Strategies of epithelial repair: modulation of stem cell and transit amplifying cell proliferation. *Journal of Cell Science*. **111**:2867-2875
77. G. Cotsarelis, S.-Z. Cheng, G. Dong, T.-T. Sun and R. M. Lavker (1989) Existence of slow-cycling limbal epithelial basal cells that can be preferentially stimulated to proliferate: Implications on epithelial stem cells. *Cell*. **57**:201-209
78. S. Kinoshita, J. Friend and R. A. Throft (1983) Biphasic cell proliferation in transdifferentiation of conjunctival to corneal epithelium in rabbits. *Investigative Ophthalmology and Visual Science*. **24**(8):1008-1014
79. B. Lauweryns, J. J. v. d. Oord, R. D. Vos and L. Missotten (1993) A new epithelial cell type in the human cornea. *Investigative Ophthalmology and Visual Science*. **34**(6):1983-1990
80. F. E. Kruse (1994) Stem cells and corneal epithelial regeneration. *Eye*. **8**:170-183
81. F. E. Kruse and H. E. Volcker (1997) Stem cells, wound healing, growth factors, and angiogenesis in the cornea. *Current Opinion in Ophthalmology*. **8**(4):46-54
82. A. Schermer, S. Galvin and T.-T. Sun (1986) Differentiation-related expression of a major 64K corneal keratin in vivo and in culture suggests limbal location of corneal epithelial stem cells. *Journal of Cell Biology*. **103**:49-62
83. Z. Chen, C. S. de Paiva, L. Luo, F. L. Kretzer, S. C. Pflugfelder and D.-Q. Li (2004) Characterization of putative stem cell phenotype in human limbal epithelia. *Stem Cells*. **22**:355-366
84. Z. Barnard, A. G. J. Apel and D. Harkin (2001) Phenotypic analyses of limbal epithelial cell cultures derived from donor corneoscleral rims. *Clinical and Experimental Ophthalmology*. **29**:138-142

## References

85. J. D. Zieske, G. Bukusoglu and M. A. Yankauckas (1992) Characterization of a potential marker of corneal epithelial stem cells. *Investigative Ophthalmology and Visual Science*. **33**(1):143-152
86. E.-H. Chung, P. G. DeGregorio, M. Wasson and J. D. Zieske (1995) Epithelial regeneration after limbus-to-limbus debridement. Expression of  $\alpha$ -enolase in stem and transient amplifying cells. *Investigative Ophthalmology and Visual Science*. **36**:1336-1343
87. G. Pellegrini, E. Dellambra, O. Golisano, E. Martinelli, I. Fantozzi, S. Bondanza, D. Ponzin, F. McKeon and M. De Luca (2001) p63 identifies keratinocyte stem cells. *Proceedings of the National Academy of Sciences of the United States of America*. **98**(6):3156-3161
88. K. R. Kenyon and S. C. Tseng (1989) Limbal autograft transplantation for ocular surface disorders. *Ophthalmology*. **96**:709-723
89. C. Tsai, T.-T. Sun and S. C. Tseng (1990) Comparison of limbal and conjunctival autograft transplantation in corneal surface reconstruction in rabbits. *Ophthalmology*. **97**:446-455
90. R. J.-F. Tsai, L.-M. Li and J.-K. Chen (2000) Reconstruction of damaged corneas by transplantation of autologous limbal epithelial cells. *New England Journal of Medicine*. **343**:86-93
91. R. A. Thoft (1977) Conjunctival Transplantation. *Archives of Ophthalmology*. **95**:1425-1427
92. K. Tsubota, Y. Satake, M. Kaido, N. Shinozaki, S. Shimmura, H. Bissen-Miyajima and J. Shimazaki (1999) Treatment of severe ocular-surface disorders with corneal epithelial stem-cell transplantation. *New England Journal of Medicine*. **340**(22):1697-1703
93. R. J.-F. Tsai and S. C. Tseng (1994) Human allograft limbal transplantation for corneal surface reconstruction. *Cornea*. **13**(5):389-400
94. R. A. Mills, D. J. Coster and K. A. Williams (2002) Effect of immunosuppression on outcome measures in a model of rat limbal transplantation. *Investigative Ophthalmology and Visual Science*. **43**:647-655
95. D. Tan, L. Ficker and R. Buckley (1996) Limbal transplantation. *Ophthalmology*. **103**(1):29-36
96. S. C. Tseng (2001) Amniotic membrane transplantation for ocular surface reconstruction. *Bioscience Reports*. **21**(4):481-489

## References

97. D. Meller and S. C. Tseng (1999) Conjunctival epithelial cell differentiation on amniotic membrane. *Investigative Ophthalmology and Visual Science*. **40**(5):878-886
98. S. C. Tseng, P. Prabhasawat, K. Barton, T. Gray and D. Meller (1998) Amniotic membrane transplantation with or without limbal allograft for corneal surface reconstruction in patients with limbal stem cell deficiency. *Archives of Ophthalmology*. **116**:431-441
99. N. Koizumi, T. Inatomi, A. J. Quantock, N. J. Fullwood, A. Dota and S. Kinoshita (2000) Amniotic membrane as a substrate for cultivating limbal corneal epithelial cells for autologous transplantation in rabbits. *Cornea*. **19**(1):65-71
100. Y. Du, J. Chen, J. L. Funderburgh, X. Zhu and L. Li (2003) Functional reconstruction of rabbit corneal epithelium by human limbal cells cultured on amniotic membrane. *Molecular Vision*. **9**:635-43
101. N. Koizumi, N. J. Fullwood, G. Bairaktaris, T. Inatomi, S. Kinoshita and A. J. Quantock (2000) Cultivation of corneal epithelial cells on intact and denuded human amniotic membrane. *Investigative Ophthalmology and Visual Science*. **41**:2506-2513
102. H. S. Dua (1999) Amniotic membrane transplantation. *British Journal of Ophthalmology*. **83**:748-752
103. S. C. Tseng, F. E. Kruse, J. Merrit and D.-Q. Li (1996) Comparison between serum-free and fibroblast-cocultured single-cell clonal culture systems: evidence showing that epithelial anti-apoptotic activity is present in 3T3 fibroblast-conditioned media. *Current Eye Research*. **15**(9):973-984
104. D. Harkin, Z. Barnard, P. Gillies, S. Ainscough and A. G. J. Apel (2004) Analysis of p63 and cytokeratin expression in a cultivated limbal autograft used in the treatment of limbal stem cell deficiency. *British Journal of Ophthalmology*. **88**:1154-1158
105. N. Koizumi, T. Inatomi, T. Suzuki, C. Sotozono and S. Kinoshita (2001) Cultivated corneal epithelial stem cell transplantation in ocular surface disorders. *American Academy of Ophthalmology*. **108**(1569-1574)
106. H. Geggel, J. Friend and R. A. Thoft (1985) Collagen gel for ocular surface. *Investigative Ophthalmology and Visual Science*. **26**(6):901-905
107. P. Rama, S. Bonini, A. Lambiase, O. Golisano, P. Paterna, M. De Luca and G. Pellegrini (2001) Autologous fibrin-cultured limbal stem cells permanently

## References

- restore the corneal surface of patients with total limbal stem cell deficiency. *Transplantation*. **72**(9):1478-1485
108. S. C. Bayliss, L. D. Buckberry, P. Harris and C. Rousseau (1997) Nanostructured semiconductors: compatibility with biomaterials. *Thin Solid Films*. **297**:308-310
109. S. C. Bayliss, L. D. Buckberry, P. Harris and M. Tobin (2000) Nature of the silicon-animal cell interface. *Journal of Porous Materials*. **7**:191-195
110. A. H. Mayne, S. C. Bayliss, P. Barr, M. Tobin and L. D. Buckberry (2000) Biologically interfaced porous silicon devices. *Physica Status Solidi A: Applied Research*. **182**:505-513
111. A. V. Sapelkin, S. C. Bayliss, B. Unal and A. Charalambou (2006) Interaction of B50 rat hippocampal cells with stain-etched porous silicon. *Biomaterials*. **27**(6):842-846
112. V. Chin, B. E. Collins, M. J. Sailor and S. N. Bhatia (2001) Compatibility of primary hepatocytes with oxidised nanoporous silicon. *Advanced Materials*. **13**(24):1877-1880
113. N. Faucheux, R. Schweiss, K. Lutzow, C. Werner and T. Groth (2004) Self-assembled monolayers with different terminating groups as model substrates for cell adhesion studies. *Biomaterials*. **25**:2721-2730
114. M. Franco, P. F. Nealy, S. Campbell, A. I. Teixeira and C. J. Murphy (2000) Adhesion and proliferation of corneal epithelial cells on self-assembled monolayers. *Journal of Biomedical Materials Research*. **52**:261-269
115. T. Groth and G. Altankov (1996) Studies on cell-biomaterial interaction: role of tyrosine phosphorylation during fibroblast spreading on surfaces varying in wettability. *Biomaterials*. **17**:1227-1234
116. I. Yanagisawa, H. Sakuma, M. Shimura, Y. Wakamatsu, S. Yanagisawa and E. Sairenji (1989) The effects of "wettability" of biomaterials on culture cells. *Journal of Oral Implantology*. **15**(3):168-177
117. K. Webb, V. Hlady and P. A. Tresco (2000) Relationships among cell attachment, spreading, cytoskeletal organization, and migration rate for anchorage-dependent cells on model surfaces. *Journal of Biomedical Materials Research*. **49**:362-368
118. N. A. Alcantar, E. S. Aydil and J. N. Israelachvili (2000) Polyethylene glycol-coated biocompatible surfaces. *Journal of Biomedical Materials Research*. **51**:343-351

## References

119. A. Papra, N. Gadegaard and N. B. Larsen (2001) Characterization of ultrathin poly(ethylene glycol) monolayers on silicon substrates. *Langmuir*. **17**:1457-1460
120. C. A. Buck and A. F. Horwitz (1987) Cell surface receptors for extracellular matrix molecules. *Annual Review of Cell Biology*. **3**:179-205
121. A. Pascual, J. Fernández, C. Sánchez, S. Manotas and F. Agulló-Rueda (2002) Structural characteristics of p-type porous silicon and their relation to the nucleation and growth of pores. *Journal of Porous Materials*. **9**:57-66
122. L. A. Greene and A. S. Tischler (1976) Establishment of a noradrenergic clonal line of rat adrenal pheochromocytoma cells which respond to nerve growth factor. *Proceedings of the National Academy of Sciences of the United States of America*. **73**(7):2424-2428
123. N. Ibaraki, S.-C. Chen, L.-R. Lin, H. Okamoto, J. M. Pipas and V. N. Reddy (1998) Human lens epithelial cell line. *Experimental Eye Research*. **67**:577-585
124. G. Altankov, F. Grinnell and T. Groth (1996) Studies on the biocompatibility of materials: Fibroblast reorganization of substratum-bound fibronectin on surfaces varying in wettability. *Journal of Biomedical Materials Research*. **30**:385-391
125. C. R. Jenny, K. M. DeFife, E. Colton and J. M. Anderson (1998) Human monocyte/macrophage adhesion, macrophage motility, and IL-4-induced foreign body giant cell formation on silane-modified surfaces *in vitro*. *Journal of Biomedical Materials Research*. **41**:171-184
126. H. Li, A.-P. Fu, D. Xu, G. Guo, L. Gui and Y.-Q. Tang (2002) In situ silanization reaction on the surface of freshly prepared porous silicon. *Langmuir*. **18**:3198-3202
127. D. Xu, L. Sun, H. Li, L. Zhange, G. Guo, X. Zhao and L. Gui (2003) Hydrolysis and silanization of the hydrosilicon surface of freshly prepared porous silicon by an amine catalytic reaction. *New Journal of Chemistry*. **27**:300-306
128. A. Janshoff, K.-P. S. Dancil, C. Steinem, D. P. Greiner, V. S.-Y. Lin, C. Gurtner, K. Motesharei, M. J. Sailor and M. R. Ghadiri (1998) Macroporous p-type silicon Fabry-Perot layers. Fabrication, characterization, and applications in biosensing. *Journal of the American Chemical Society*. **120**:12108-12116
129. C. Steinem, A. Janshoff, V. S.-Y. Lin, H. E. Volcker and M. R. Ghadiri (2004) DNA hybridization-enhanced porous silicon corrosion: mechanistic investigations and prospect for optical interferometric biosensing. *Tetrahedron*. **60**:11259-11267

## References

130. J. M. Buriak and M. J. Allen (1998) Lewis acid mediated functionalization of porous silicon with substituted alkenes and alkynes. *Journal of the American Chemical Society*. **120**:1339-1340
131. H. Oharazawa, N. Ibaraki, L.-R. Lin and V. N. Reddy (1999) The effects of extracellular matrix on cell attachment, proliferation and migration in a human lens epithelial cell line. *Experimental Eye Research*. **69**:603-610
132. D. K. Fujii, S. L. Massoglia, N. Savion and D. Gospodarowicz (1982) Neurite outgrowth and protein synthesis by PC12 cells as a function of substratum and nerve growth factor. *Journal of Neuroscience*. **2**(8):1157-1175
133. Y. Ito (1999) Surface micropatterning to regulate cell functions. *Biomaterials*. **20**:2333-2342
134. K. Webb, V. Hlady and P. A. Tresco (1998) Relative importance of surface wettability and charged functional groups on NIH 3T3 fibroblast attachment, spreading, and cytoskeletal organization. *Journal of Biomedical Materials Research*. **41**(3):422-430
135. S. Saneinejad and M. S. Shoichet (1998) Patterned glass surfaces direct cell adhesion and process outgrowth of primary neurons of the central nervous system. *Journal of Biomedical Materials Research*. **42**:13-19
136. S. R. Sheth and D. Leckband (1997) Measurements of attractive forces between proteins and end-grafted poly(ethylene glycol) chains. *Proceedings of the National Academy of Sciences of the United States of America*. **94**:8399-8404
137. H. Shau and J. Dawson (1984) The role of the lysosome in natural killing: inhibition by lysosomotropic vital dyes. *Immunology*. **53**(4):745-751
138. J. O'Brien, I. Wilson, T. Orton and F. Pognan (2000) Investigation of the Alamar Blue (resazurin) fluorescent dye for the assessment of mammalian cell cytotoxicity. *European Journal of Biochemistry*. **267**:5421-5426
139. L. Benati, G. Bencivenni, R. Leardini, M. Minozzi, D. Nanni, R. Scialpi, P. Spagnolo and G. Zanardi (2006) Radical reduction of aromatic azides to amines with triethylsilane. *Journal of Organic Chemistry*. **71**:5822-5825
140. A. V. Malkov, M. Figlus, S. Stončius and P. Kočovský (2007) Organocatalysis with a fluorous tag: Asymmetric reduction of imines with trichlorosilane catalyzed by amino acid-derived formamides. *Journal of Organic Chemistry*. **72**:1315-1325
141. C. Chatgililoglu (1995) Structural and chemical properties of silyl radicals. *Chemical Reviews*. **95**:1229-1251

## References

142. M. Rocchia, E. Garrone, F. Geobaldo, L. Boarino and M. J. Sailor (2003) Sensing CO<sub>2</sub> in a chemically modified porous silicon film. *Physica Status Solidi A: Applied Research*. **197**(2):365-369
143. D.-Q. Yang, M. Meunier and E. Sacher (2005) Photoacoustic Fourier transform infrared spectroscopy of nanoporous SiO<sub>x</sub>/Si thin films with varying porosities. *Journal of Applied Physics*. **98**:114310-114316
144. K.-P. S. Dancil, D. P. Greiner and M. J. Sailor (1999) A porous silicon optical biosensor: Detection of reversible binding of IgG to a protein A-modified surface. *Journal of the American Chemical Society*. **121**:7925-7930
145. M. Morita, T. Ohmi, E. Hasegawa, M. Kawakami and M. Ohwada (1990) Growth of native oxide on a silicon surface. *Journal of Applied Physics*. **68**(3):1272-1281
146. M. Morita, T. Ohmi, E. Hasegawa, M. Kawakami and K. Suma (1989) Control factor of native oxide growth on silicon in air or in ultrapure water. *Applied Physics Letters*. **55**(6):562-564
147. H. Ogawa, K. Ishikawa, C. Inomata and S. Fujimura (1996) Initial stage of native oxide growth on hydrogen terminated silicon (111) surfaces. *Journal of Applied Physics*. **79**(1):472-477
148. G. Vázquez, E. Alvarez and J. M. Navaza (1995) Surface tension of alcohol + water from 20 to 50 °C. *Journal of Chemical and Engineering Data*. **40**(3):611-614
149. I. Coulthard, R. Sammynaiken, S. Naftel, P. Zhang and T. Sham (2000) Porous silicon: A template for the preparation of nanophase metals and bimetallic aggregates. *Physica Status Solidi A: Applied Research*. **182**:157-162
150. T. Laaksonen, H. Santos, H. Vihola, J. Salonen, J. Riikonen, T. Heikkilä, L. Peltonen, N. Kumar, D. Murzin, V. Lehto and J. Hirvonen (2007) Failure of MTT as a toxicity testing agent for mesoporous silicon microparticles. *Chemical Research in Toxicology*. **20**(12):1913-1918
151. T. Mosmann (1983) Rapid colorimetric assay for cellular growth and survival: application to proliferation and cytotoxicity assays. *Journal of Immunological Methods*. **65**:55-63
152. R. J. Gonzalez and J. B. Tarloff (2001) Evaluation of hepatic subcellular fractions for Alamar blue and MTT reductase activity. *Toxicology In Vitro*. **15**:257-259

## References

153. S. Kasugai, N. Hasegawa and H. Ogura (1990) A simple in vitro cytotoxicity test using the MTT (3-(4,5)-dimethylthiazol-2-yl)-2,5-diphenyl tetrazolium bromide) colorimetric assay: Analysis of eugenol toxicity on dental pulp cells (RPC-C2A). *Japanese Journal of Pharmacology*. **52**:95-100
154. C. J. Goodwin, S. J. Holt, S. Downes and N. J. Marshall (1995) Microculture tetrazolium assays: a comparison between two new tetrazolium salts, XTT and MTS. *Journal of Immunological Methods*. **179**:95-103
155. N. W. Roehm, G. H. Rodgers, S. M. Hatfield and A. L. Glasebrook (1991) An improved colorimetric assay for cell proliferation and viability utilizing the tetrazolium salt XTT. *Journal of Immunological Methods*. **142**:257-265
156. T. Elsdale and J. Bard (1972) Collagen substrata for studies on cell behaviour. *Journal of Cell Biology*. **54**:626-637
157. K. Barraclough, A. Loni, E. Caffull and L. T. Canham (2007) Compaction of silicon powders without a binding agent. *Materials Letters*. **61**:485-487
158. S. Vieth, M. Uhlmann, U. Klemm and F.-D. Börner (2005) The influence of lubricants on uniaxial dry pressing of silanised silicon nitride powder. *Journal of the European Ceramic Society*. **25**:3509-3515
159. S. Vieth, M. Uhlmann, D. Linke, U. Klemm, D. Sobek and F.-D. Börner (2003) Effect of surface silanisation on the dry pressing behaviour of silicon nitride powder. *Journal of the European Ceramic Society*. **23**:1997-2004
160. P. Herold and J. Kinsella (1986) Fish oil consumption and decreased risk of cardiovascular disease: A comparison of findings from animal and human feeding trials. *American Journal of Clinical Nutrition*. **43**:566-598
161. N. Stone (1996) Fish consumption, fish oil, lipids, and coronary heart disease. *Circulation Journal*. **94**:2337-2340
162. G. Alebiowu and O. A. Itiola (2003) The effects of starches on mechanical properties of paracetamol tablet formulations. I. Pregelatinization of starch binders. *Acta Pharmaceutica* **53**:231-237
163. C. Pereira, A. Cunha and R. Reis (1998) New starch-based thermoplastic hydrogels for use as bone cements or drug-delivery carriers. *Journal of Materials Science: Materials in Medicine*. **9**:825-833
164. M. Gomes, R. Reis, A. Cunha, C. Blitterswijk and J. Bruijn (2001) Cytocompatibility and response of osteoblastic-like cells to starch-based

## References

- polymers: effect of several additives and processing conditions. *Biomaterials*. **22**:1911-1917
165. A. Marques, R. Reis and J. Hunt (2002) The biocompatibility of novel starch-based polymers and composites: in vitro studies. *Biomaterials*. **23**:1471-1478
166. C. Lam, X. Mo, S. Teoh and D. Hutmacher (2002) Scaffold development using 3D printing with a starch-based polymer. *Materials Science & Engineering, C: Biomimetic and Supramolecular Systems*. **20**:49-56
167. T. Ouchi, T. Uchida and Y. Ohya (2001) Synthesis of Poly(L-lactide) with one terminal D-Glucose residue and wettability of its film surface. *Macromolecular Bioscience*. **1**:371-375
168. C. Bruch (1964) Some biological and physical factors in dry heat sterilization: A general review. *Life Sciences and Space Research*. **2**:357-371
169. L. Wu and J. Ding (2004) In vitro degradation of three dimensional poly(D,L-lactide-co-glycolide) scaffolds for tissue engineering. *Biomaterials*. **25**(27):5821-5830
170. Y.-M. Mu, T. Yanase, Y. Nishi, A. Tanaka, M. Saito, C.-H. Jin, C. Mukasa, T. Okabe, M. Nomura, K. Goto and H. Nawata (2001) Saturated FFAs, palmitic acid and stearic acid, induce apoptosis in human granulosa cells. *Endocrinology*. **142**(8):3590-3597
171. E. Gross, D. Kovalev, N. Künzner, J. Diener, F. Koch, V. Y. Timoshenko and M. Fujii (2003) Spectrally resolved electronic energy transfer from silicon nanocrystals to molecular oxygen mediated by direct electron exchange. *Physical Review B: Condensed Matter*. **68**:1154051-11540511
172. I. Ohsawa, M. Ishikawa, K. Takahashi, M. Watanabe, K. Nishimaki, K. Yamagata, K.-i. Katsura, Y. Katayama, S. Asoh and S. Ohta (2007) Hydrogen acts as a therapeutic antioxidant by selectively reducing cytotoxic oxygen radicals. *Nature Medicine*. **13**(6):688-694
173. M. Fujii, N. Nishimura, H. Fumon, S. Hayashi, D. Kovalev, B. Goller and J. Diener (2006) Dynamics of photosensitized formation of singlet oxygen by porous silicon in aqueous solution. *Journal of Applied Physics*. **100**(12):124302-5
174. E. J. Anglin, M. P. Schwartz, V. P. Ng, L. A. Perelman and M. J. Sailor (2004) Engineering the chemistry and nanostructure of porous silicon Fabry-Perot films for loading and release of a steroid. *Langmuir*. **20**(25):11264-11269

## References

175. A. B. Foraker, R. J. Walczak, M. H. Cohen, T. A. Boiarski, C. Grove and P. Swaan (2003) Microfabricated porous silicon particles enhance paracellular delivery of insulin across intestinal Caco-2 cell monolayers. *Pharmaceutical Research*. **20**(1):110-116
176. M. Archer, M. Christophersen and P. M. Fauchet (2004) Macroporous silicon electrical sensor for DNA hybridization detection. *Biomedical Microdevices*. **6**(3):203-211
177. A. Rosenbloom, D. Sipe, Y. Shishkin, Y. Ke, R. Devaty and W. Choyke (2004) Nanoporous SiC: A candidate semi-permeable material for biomedical applications. *Biomedical Microdevices*. **6**(4):261-267
178. C. C. Striemer, T. R. Gaborski, J. L. McGrath and P. M. Fauchet (2007) Charge- and size-based separation of macromolecules using ultrathin silicon membranes. *Nature*. **445**:749-753
179. K. Zhang, S. L. E. Loong, S. Connor, S. W. K. Yu, S.-Y. Tan, R. Ng, T. H. K. M. Lee, L. T. Canham and P. K. H. Chow (2005) Complete tumor response following intratumoral <sup>32</sup>P BioSilicon on human hepatocellular and pancreatic carcinoma xenografts in nude mice. *Clinical Cancer Research*. **11**(20):7532-7537
180. J. L. Coffey, M. A. Whitehead, D. K. Nagasha, P. Mukherjee, G. Akkaraju, M. Totolici, R. S. Saffie and L. T. Canham (2005) Porous silicon-based scaffolds for tissue engineering and other biomedical applications. *Physica Status Solidi A: Applied Research*. **202**(8):1451-1455
181. G. Govett (1961) Critical factors in the colorimetric determination of silica. *Analytica Chimica Acta*. **25**:69-80
182. R. K. Iler (1979) *The chemistry of silica. Solubility, polymerization, colloid and surface properties, and biochemistry*, Wiley-Interscience,
183. E. J. King and H. Stantial (1933) The biochemistry of silicic acid: Micro-determination of silica. *Biochemical Journal*. **27**(4):990-1001
184. D. Mirejovsky, A. Patel, D. Rodriguez and T. Hunt (1991) Lipid adsorption onto hydrogel contact lens materials. Advantages of Nile Red over Oil Red O in visualization of lipids. *Optometry and Vision Science*. **68**(11):858-864
185. G. Carbrini and A. Verkman (1986) Potential-sensitive response mechanism of diS-C3-(5) in biological membranes. *Journal of Membrane Biology*. **92**(2):171-182

## References

186. H. Crissman, M. Hofland, A. Stevenson, M. Wilder and R. Tobey (1990) Supravital staining with Hoechst and DiOC<sub>5</sub>(3). *Methods in Cell Biology*. **33**:89-95
187. G. M. Lee, S. Fong, K. Francis, D. J. Oh and B. Palsson (2000) In situ labeling of adherent cells with PKH26. *In Vitro Cellular and Developmental Biology. Animal*. **36**(1):4-6
188. M. Owen and D. Williams (1991) Surface modification by fluoroalkyl-functional surfaces: A review. *Journal of Adhesion Science and Technology*. **5**(4):307-320
189. D. Williams and P. M. Kabra (1990) Extended life for blood serum analysis columns using Dual Zone chromatographic materials. *Analytical Chemistry*. **62**(8):807-810
190. T. Coradin, D. Eglin and J. Livage (2004) The silicomolybdic acid spectrophotometric method and its application to silicate/biopolymer interaction studies. *Spectroscopy*. **18**(4):567-576
191. S. Mishima, A. Gasset, S. D. Klyce and J. L. Baum (1966) Determination of tear volume and tear flow. *Investigative Ophthalmology and Visual Science*. **5**(3):264-276
192. B. Ebato, J. Friend and R. A. Thoft (1987) Comparison of central and peripheral human corneal epithelium in tissue culture. *investigative Ophthalmology and Visual Science*. **28**:1450-1456
193. L. P. K. Ang, D. T. H. Tan, C. J. Y. Seah and R. W. Beuerman (2005) The use of human serum in supporting the *in vitro* and *in vivo* proliferation of human conjunctival epithelial cells. *British Journal of Ophthalmology*. **89**:748-752
194. K. Arvidson, M. Cottler-Fox, E. Hammarlund and U. Friberg (1987) Cytotoxic effects of cobalt-chromium alloys on fibroblasts derived from human gingiva. *European Journal of Oral Sciences*. **95**(4):356-363
195. D. Meller, R. T. F. Pires and S. C. Tseng (2002) *Ex vivo* preservation and expansion of human limbal epithelial stem cells on amniotic membrane cultures. *British Journal of Ophthalmology*. **86**:463-471
196. M. Osborn (1983) Intermediate filaments as histologic markers: an overview. *Journal of Investigative Dermatology*. **81**(Supplement 1S):104-109
197. W. W. Franke, D. L. Schiller, R. Moll, S. Winter, E. Schmid, I. Engelbrecht, H. Denk, R. Krepler and B. Platzer (1981) Diversity of cytokeratins: Differentiation

## References

- specific expression of cytokeratin polypeptides in epithelial cells and tissues. *Journal of Molecular Biology*. **153**(4):933-959
198. A. Yang, R. Schweitzer, D. Sun, M. Kaghad, N. Walker, R. T. Bronson, C. Tabin, A. Sharpe, D. Caput, C. Crum and F. McKeon (1999) p63 is essential for regenerative proliferation in limb, craniofacial and epithelial development. *Nature*. **398**:714-718
199. I. K. Gipson and S. M. Grill (1982) A technique for obtaining sheets of intact rabbit corneal epithelium. *Investigative Ophthalmology and Visual Science*. **23**(2):269-273
200. N. Koizumi, L. J. Cooper, N. J. Fullwood, T. Nakamura, K. Inoki, M. Tsuzuki and S. Kinoshita (2002) An evaluation of cultivated corneal limbal epithelial cells, using cell-suspension culture. *Investigative Ophthalmology and Visual Science*. **43**(7):2114-2121
201. H.-S. Kim, X. Song, C. S. de Paiva, Z. Chen, S. C. Pflugfelder and D.-Q. Li (2004) Phenotypic characterization of human corneal epithelial cells expanded ex vivo from limbal explant and single cell cultures. *Experimental Eye Research*. **79**(1):41-49
202. M. C. Braun, J. He, C.-Y. Wu and B. L. Kelsall (1999) Cholera toxin suppresses interleukin (IL)-12 production and IL-12 receptor  $\beta$ 1 and  $\beta$ 2 chain expression. *Journal of Experimental Medicine*. **189**(3):541-552
203. K. Saito, J. Shoji, N. Inada, Y. Iwasaki and M. Sawa (2001) Immunosuppressive effect of cholera toxin B on allergic conjunctivitis model in guinea pig. *Japanese Journal of Ophthalmology*. **45**:332-338
204. D.-Q. Li and S. C. Tseng (1997) Differential regulation of keratinocyte growth factor and hepatocyte growth factor/scatter factor by different cytokines in human corneal and limbal fibroblasts. *Journal of Cellular Physiology*. **172**:361-372
205. M. Grueterich, E. M. Espana and S. C. Tseng (2003) Modulation of keratin and connexin expression in limbal epithelium expanded on denuded amniotic membrane with and without a 3T3 fibroblast feeder layer. *Investigative Ophthalmology and Visual Science*. **44**(10):4230-4236
206. R. Wu, R. Wolfe and G. Sato (1981) Distinctive effects of hydrocortisone on the modulation of EGF binding and cell growth in hela cells grown in defined medium. *Journal of Cellular Physiology*. **108**(1):83

## References

207. S. T. Boyce and R. G. Ham (1983) Calcium-regulated differentiation of normal human epidermal keratinocytes in chemically defined clonal culture and serum-free culture. *Journal of Investigative Dermatology*. **81**:33s-40s
208. F. E. Kruse and S. C. Tseng (1991) A serum-free clonal growth assay for limbal, peripheral, and central corneal epithelium. *Investigative Ophthalmology and Visual Science*. **32**(7):2086-2095
209. F. Castro-Munozledo (1994) Development of a spontaneous permanent cell line of rabbit corneal epithelial cells that undergoes sequential stages of differentiation in cell culture. *Journal of Cell Science*. **107**:2343-2351
210. Y. Hayashida, K. Nishida, M. Yamato, K. Watanabe, N. Maeda, H. Watanabe, A. Kikuchi, T. Okano and Y. Tano (2005) Ocular surface reconstruction using autologous rabbit oral mucosal epithelial sheets fabricated *ex vivo* on a temperature-responsive culture surface. *Investigative Ophthalmology and Visual Science*. **46**(5):1632-1639
211. K. Nishida, M. Yamato, Y. Hayashida, K. Watanabe, N. Maeda, H. Watanabe, K. Yamamoto, S. Nagai, A. Kikuchi, Y. Tano and T. Okano (2004) Functional bioengineered corneal epithelial sheet grafts from corneal stem cells expanded *ex vivo* on a temperature-responsive cell culture surface. *Transplantation*. **77**(3):379-385
212. K. Fukuda, T. Chikama, M. Makamura and T. Nishida (1999) Differential distribution of subchains of the basement membrane components type IV collagen and laminin among the amniotic membrane, cornea, and conjunctiva. *Cornea*. **18**:73-79
213. A. Kiritoshi, N. SundarRaj and R. A. Thoft (1991) Differentiation in cultured limbal epithelium as defined by keratin expression. *Investigative Ophthalmology and Visual Science*. **32**(12):3073-3077
214. I. Schwab, M. Reyes and R. Isseroff (2000) Successful transplantation of bioengineered tissue replacements in patients with ocular surface disease. *Cornea*. **19**:421-426
215. J. Shimazaki, M. Aibu, E. Goto, N. Kato, S. Shimmura and K. Tsubota (2002) Transplantation of human limbal epithelium cultivated on amniotic membrane for the treatment of severe ocular surface disorders. *American Academy of Ophthalmology*. **109**:1285-1290
216. B. D. Ratner, A. S. Hoffman, F. J. Schoen and J. E. Lemons (2004) *Biomaterials science: An introduction to materials in medicine*, 2nd Edition, Academic Press, New York

## References

217. P. Beauchamp, D. Guzick, B. Held and W. Schmidt (1988) Histologic response to microsuture materials. *Journal of Reproductive Medicine*. **33**(7):615-623
218. J. Faulborn, G. MAckensen, K. Beyer and J. Moringlane (1975) Studies on the tolerance of silk, nylon, dacron and collagen suture material in the cornea of the rabbit. *Advances in Ophthalmology*. **30**:50-54
219. M. Titford (2005) The long history of hematoxylin. *Biotechnic and Histochemistry*. **80**(2):73-78
220. D. Wittekind (2003) Traditional staining for routine diagnostic pathology including the role of tannic acid. 1. Value and limitations of the hematoxylin-eosin stain. *Biotechnic and Histochemistry*. **78**(5):261-270
221. J. M. Anderson, A. Rodriguez and D. T. Chang (2008) Foreign body reaction to biomaterials. *Seminars in Immunology*. **20**(2):86-100
222. J. M. Anderson (2001) Biological responses to materials. *Annual Review of Materials Research*. **31**:81-110
223. C. Sunderkötter, K. Steinbrink, M. Goebeler, R. Bhardwaj and C. Sorg (1994) Macrophages and angiogenesis. *Journal of Leukocyte Biology*. **55**:410-422
224. P. Horan and S. Slezak (1989) Stable cell membrane labelling. *Nature*. **340**:167-168
225. Y. Ogata, H. Niki, T. Sakka and M. Iwasaki (1995) Oxidation of porous silicon under water vapor environment. *Journal of the Electrochemical Society*. **142**(5):1595-1601
226. A. Yamamoto, S. Mixhima, N. Maruyama and M. Sumita (2000) Quantitative evaluation of cell attachment to glass, polystyrene, and fibronectin- or collagen-coated polystyrene by measurement of cell adhesive shear force and cell detachment energy. *Journal of Biomedical Materials Research*. **50**:114-124
227. S. Yashiki, R. Umegaki, M. Kino-Oka and M. Taya (2001) Evaluation of attachment and growth of anchorage-dependent cells on culture surfaces with Type I collagen coating. *Journal of Bioscience and Bioengineering*. **92**(4):385-388
228. R. I. Freshney (2005) *Culture of animal cells: A manual of basic technique*, Fifth Edition, John Wiley & Sons,
229. B. Kannan, K. Castelino, F. Chen and A. Majumdar (2006) Lithographic techniques and surface chemistries for the fabrication of PEG-passivated protein microarrays. *Biosensors & Bioelectronics*. **21**(10):1960-1967

## References

230. J. Lee, C. Jones, M. Zern and A. Revzin (2006) Analysis of local tissue-specific gene expression in cellular micropatterns. *Analytical Chemistry*. **78**(24):8305-8312
231. A. Bulychev, A. Trouet and P. Tulkens (1978) Uptake and intracellular distribution of neutral red in cultured cells. *Experimental Cell Research*. **115**(2):343-355
232. M. A. Batzer and P. L. Deininger (2002) Alu repeats and human genomic diversity. *Nature Reviews Genetics*. **3**:370-380
233. J. A. Walker, G. E. Kilroy, J. Xing, J. Shewale, S. Sinha and M. A. Batzer (2003) Human DNA quantitation using *Alu* element-based polymerase chain reaction. *Analytical Biochemistry*. **315**:122-128
234. J. K. G. Dart (1997) Impression cytology of the ocular surface-research tool or routine clinical investigation? *British Journal of Ophthalmology*. **81**:930
235. K. Williams, H. Brereton, R. Aggarwal, P. Sykes, D. Turner, G. Russ and D. Coster (1995) Use of DNA polymorphisms and the polymerase chain reaction to examine the survival of a human limbal stem cell allograft. *American Journal of Ophthalmology*. **120**(3):342-350